

eman ta zabal zazu



Universidad  
del País Vasco

Euskal Herriko  
Unibertsitatea

# **Natural killer cell subset reconstitution after autologous hematopoietic stem cell transplantation in multiple myeloma patients.**

TESIS DOCTORAL PRESENTADA POR:

**Ane Orrantia Robles**

DIRECTORES:

**Francisco Borrego Rabasco**

**Olatz Zenarruzabeitia Belaustegi**

Leioa, 2022

## INDEX

INTRODUCTION.....	6
1. Natural Killer cells .....	7
1.1 Innate lymphoid cells .....	7
1.2 NK cell subset diversity .....	7
1.3 Human NK cell receptors .....	10
1.4 NK cell effector functions .....	12
1.5 NK cell development and differentiation .....	13
2. Hematopoietic stem cell transplantation .....	15
2.1 Types and indications.....	15
2.2 Factors affecting outcome after autologous hematopoietic stem cell transplantation.	16
2.3 Immune reconstitution after autologous hematopoietic stem cell transplantation .....	17
3. NK cells in autologous hematopoietic stem cell transplantation.....	18
3.1 KIRs and HLA class I ligands.....	18
3.2 Other phenotypic characteristics and NK cell subsets .....	19
HYPOTHESIS AND OBJECTIVE .....	22
CHAPTER I .....	23
INTRODUCTION.....	24
METHODS .....	26
RESULTS .....	30
DISCUSSION .....	35
CHAPTER II.....	39
INTRODUCTION.....	40
METHODS .....	42
RESULTS .....	46
DISCUSSION .....	53
CHAPTER III.....	58
INTRODUCTION.....	59
METHODS .....	61
RESULTS .....	65
DISCUSSION .....	71
DISCUSSION .....	75
CONCLUSIONS.....	80
REFERENCES.....	81
FIGURES AND TABLES .....	107



## ABBREVIATIONS

**A-ALC:** autograft absolute lymphocyte count

**ADCC:** antibody-dependent cell-mediated cytotoxicity

**AILC:** activation-induced C-type lectin

**ALC:** absolute lymphocyte count

**ALC-15:** day 15 absolute lymphocyte count

**alloHSCT:** allogenic hematopoietic stem cell transplantation

**AML:** acute myeloid leukemia

**autoHSCT:** autologous hematopoietic stem cell transplantation

**bnAbs:** broadly-neutralizing antibodies

**BSA:** bovine serum albumin

**cART:** combined antiretroviral therapy

**CB:** cord blood

**cDNA:** complementary DNA

**CMV:** cytomegalovirus

**CR:** complete remission

**Ct:** cycle threshold

**DCs:** dendritic cells

**DEGs:** differentially expressed genes

**DMSO:** dimethylsulfoxide

**dNK:** decidual natural killer

**Eomes:** eomesodermin

**FasL:** Fas ligand

**FBS:** fetal bovine serum

**Fc:** fragment crystallizable region

**FcεRγ:** Fc epsilon receptor gamma chain

**G-CSF:** granulocyte colony-stimulating factor

**GM-CSF:** granulocyte-macrophage colony stimulating factor

**GSEA:** gene set enrichment analysis

**GvHD:** graft-versus-host disease

**GvT :** graft-versus-tumor

**HCV:** hepatitis C virus

**HD:** healthy donor

**HIV:** human immunodeficiency virus

**HLA:** human leukocyte antigen

**HSCs:** hematopoietic stem cells

**HSCT:** hematopoietic stem cell transplantation

**IFNγ:** interferon gamma

**IL:** interleukin

**ILCs:** innate lymphoid cells

**KEGG:** Kyoto Encyclopedia of Genes and Genomes

**KIRs:** killer cell immunoglobulin-like receptors

**mAbs:** monoclonal antibodies

**MFI:** median fluorescence intensity

**MHC:** major histocompatibility complex

**MICA:** major histocompatibility complex class I chain-related molecule A

**MICB:** major histocompatibility complex class I chain-related molecule B

**MIP-1 $\beta$ /- $\alpha$ :** macrophage inflammatory protein-1beta/-1alpha.

**MM:** multiple myeloma

**MRD:** minimal residual disease

**NCR:** natural cytotoxicity receptors

**NGS:** next-generation sequencing

**NHL:** non-Hodgkin lymphoma

**NK:** natural killer

**NK-15:** day 15 NK cell count

**NKG2DLs:** NKG2D ligands

**NSCLC:** non-small cell lung cancer

**ORA:** over representation analysis

**OS:** overall survival

**PBMCs:** peripheral blood mononuclear cells

**PBS:** phosphate buffered saline

**pDCs:** plasmacytoid dendritic cells

**PFA:** paraformaldehyde

**PFS:** progression-free survival

**PLGF:** placental growth factor

**PLZF:** promyelocytic leukemia zinc finger

**PMA:** phorbol myristate acetate

**pNK:** peripheral blood natural killer

**PR:** partial response

**qPCR:** quantitative PCR

**rh:** recombinant human

**RNA-seq:** RNA sequencing

**RT:** room temperature

**scRNA-seq:** single-cell RNA sequencing

**SD:** standard deviation

**SEM:** standard error of the mean

**SLT:** secondary lymphoid tissues

**TGF- $\beta$ :** transforming growth factor beta

**TINK:** tumor infiltrating NK

**TNF:** tumor necrosis factor

**TRAIL:** TNF-related apoptosis-inducing ligand

**trNK:** tissue-resident natural killer

**TTNT:** time to next treatment

**VEGF:** vascular endothelial growth factor

**VGPR:** very good partial response

**VIM:** vimentin

## SUMMARY

Natural killer (NK) cells are phenotypically and functionally diverse lymphocytes that constitute an essential part of the innate immune system. NK cells have the ability to recognize and eliminate malignant cells without prior sensitization, thus playing a relevant role in tumor immunosurveillance. Autologous hematopoietic stem cell transplantation (autoHSCT) is an established treatment option worldwide for many hematologic malignancies, including multiple myeloma (MM). For years, several publications have highlighted the importance of early lymphocyte recovery for prolonged survival of patients undergoing autoHSCT. Notably, NK cells constitute the major subset of peripheral blood lymphocytes in the first week after autoHSCT and a rapid recovery of NK cell counts has been associated with a better prognosis. Therefore, the main objective of this doctoral thesis was to study the reconstitution of the NK cell subset after autoHSCT in MM patients.

It is very important to correctly phenotype the different immune cell populations. Our results showed that, NKp80 is a more accurate marker than the traditionally used CD16 to identify the CD56<sup>neg</sup> NK cell subset in cryopreserved samples. Furthermore, we observed that the effector functions of CD56<sup>neg</sup> NK cells are not as diminished as previously described. Analysis of NK cell reconstitution after autoHSCT revealed that there is extensive redistribution of NK cell subsets shortly after autoHSCT and that NK cells undergo a profound phenotypic change characterized, among other things, by their immature phenotype and proliferative capacity. In addition, we have documented significantly elevated plasma IL-15 levels early after autoHSCT that correlate with the number, proliferative capacity and cytotoxic potential of NK cells. We have also found an association between the maturation stage of NK cells and the outcome of MM patients undergoing autoHSCT. Finally, we have analyzed the transcriptome of NK cells and found that the gene expression profile of NK cells changes dramatically immediately after autoHSCT and they acquire a decidual NK cell-like phenotype with different effector functions compared to conventional NK cells.

In conclusion, our data provide new insights into the NK cell biology and reconstitution of NK cell subsets after autoHSCT.

# INTRODUCTION

Parts of this chapter have been published in:

Orrantia A, Terrén I, Astarloa-Pando G, Zenarruzabeitia O, Borrego F. Human NK Cells in Autologous Hematopoietic Stem Cell Transplantation for Cancer Treatment. *Cancers* (Basel). 2021 Mar 30;13(7):1589. doi: 10.3390/cancers13071589.

## 1. Natural Killer cells

Natural killer (NK) cells are phenotypically and functionally diverse lymphocytes with the ability to recognize and kill malignant cells without prior sensitization, and therefore, they are very relevant in tumor immunosurveillance. Although the role that NK cells play in allogeneic hematopoietic stem cell transplantation (alloHSCT) settings has been well documented for years, their significance and favorable effects associated with the outcome after autologous HSCT (autoHSCT) have been much less studied. For that reason, the following doctoral thesis has been focused on the study of the NK cell pool reconstitution after autoHSCT to gain a better understanding of the impact that this cell type could have in disease progression after autoHSCT.

### 1.1 Innate lymphoid cells

NK cells constitute a crucial part of the innate immune system and probably are the best-known members of the heterogeneous family of the innate lymphoid cells (ILCs). In contrast to T and B lymphocytes, ILCs lack rearranged antigen-specific receptors and act early in the immune response [1]. Currently, ILCs are classified based on their functional and transcriptional profile into five different subsets: ILC1, ILC2, ILC3, lymphoid tissue-inducer cells, and NK cells [2]. Moreover, ILCs can be grouped into non-cytotoxic “helper” ILCs and cytotoxic ILCs. NK cells represent the classic cytotoxic population of ILCs [3,4]. As ILC1s, NK cells also produce the pro-inflammatory cytokine interferon gamma (IFN $\gamma$ ) but are dependent on both T-bet and eomesodermin (Eomes) transcription factors to develop, while ILC1s only depend on T-bet [5,6]. Even though, generally grouped into the above mentioned five subsets, several studies have also demonstrated that ILCs can transdifferentiate into other ILC subsets depending on the cytokine milieu, evidencing the plasticity and the heterogeneity of these cells [7–10].

### 1.2 NK cell subset diversity

Traditionally, according to the differential expression of CD56 and CD16, human NK cells are divided in two major subsets known as CD56<sup>bright</sup>CD16<sup>low/-</sup> and CD56<sup>dim</sup>CD16<sup>+</sup> (hereafter referred to as CD56<sup>bright</sup> and CD56<sup>dim</sup>, respectively) [11]. Although both subsets express similar levels of several surface receptors such as NKp80



and the common interleukin (IL)-2 and IL-15 receptor beta chain (IL-2/15R $\beta$ ), there are some distinct phenotypical and functional features between them [12]. For instance, CD56<sup>bright</sup> NK cells express CD94/NKG2A (hereafter NKG2A) but lack the expression of killer cell immunoglobulin-like receptors (KIRs). They also show low expression of perforin and granzymes A and B and low or undetectable expression of CD16. In addition, they produce large amounts of immunomodulatory cytokines and chemokines in response to cytokines but are poor mediators of natural cytotoxicity and antibody-dependent cell-mediated cytotoxicity (ADCC) [11,13,14]. However, it has been also demonstrated that after cytokine activation they become more cytotoxic, as e.g., upon priming with IL-15 and after expansion with irradiated K562-feeder cells engineered to express membrane-bound IL-21, the CD56<sup>superbright</sup>CD16+ NK cells exhibit increased degranulation after target recognition [15,16]. Conversely, CD56<sup>dim</sup> NK cells are characterized by lower expression of NKG2A and high expression of CD16, perforin, granzymes, and KIRs. Moreover, CD56<sup>dim</sup> NK cells are highly cytotoxic but produce lower amounts of cytokines in response to monocyte-derived cytokines [11,13]. Nevertheless, they can produce significant amounts of cytokines upon target cell recognition [17,18]. Apart from conventional CD56<sup>bright</sup> and CD56<sup>dim</sup> NK cells, CD56<sup>dim</sup> NK cells that lack CD16 expression have also been shown to be expanded in patients undergoing haploidentical HSCT. Due to their transcriptional profile, these cells, also known as unconventional CD56<sup>dim</sup> NK cells, are considered an intermediate stage between CD56<sup>bright</sup> and CD56<sup>dim</sup> NK cells [19]. Finally, CD56<sup>bright</sup> and CD56<sup>dim</sup> NK cells also exhibit different expression patterns of chemokine and homing receptors, which are linked to their tissue localization [20]. While CD56<sup>bright</sup> are the major NK cell subset in secondary lymphoid tissues (SLT), CD56<sup>dim</sup> are the predominant subset in the peripheral blood, approximately 95% of total NK cells [11,13].

However, thanks to the development of pioneering experimental technologies, results published over the last years have revealed that human NK cells are much more diverse than just CD56<sup>bright</sup> and CD56<sup>dim</sup> NK cell subsets (Figure 1). Some years ago, a study using mass cytometry that simultaneously analyzed more than 30 parameters, revealed that, within an individual, there may be 6,000–30,000 phenotypically distinct peripheral blood NK (pNK) cell subsets, highlighting the existing NK cell diversity [21]. Furthermore, the diversity of pNK cells has also been revealed by single-cell RNA sequencing (scRNA-seq) analysis [22]. This phenotypic diversity is mainly influenced by

both genetics and environmental factors. Genetics strongly influence the combinatorial expression patterns of KIRs, which are expressed by NK cells and recognize human leukocyte antigen (HLA) class I molecules. Moreover, different environmental factors influence the expression of other receptors, such as activating and costimulatory receptors [21,23]. For example, HLA-DR expression varies in response to activation [24,25], the expression of CD117 differs during differentiation [26] and the expression of 2B4 could be regulated in response to viral infection [27]. Furthermore, diverse tissue-resident NK (trNK) cell subpopulations have been identified in different peripheral tissues, such as human liver, uterus, spleen, kidney, intestine and salivary gland, showing that local tissue environment also contributes to NK cell diversity [23,28]. These trNK cells are in general CD56<sup>bright</sup>, express tissue-residency markers (e.g., CD49a, CD69, and CD103), which are involved in retaining lymphocytes in tissues, and present unique transcriptional signatures distinct from pNK cells [13,29]. One example of trNK cells are decidual NK (dNK) cells, which are a specialized type of trNK cells found at the endometrial decidual tissue and regulate key developmental processes, such as trophoblast invasion and angiogenesis during pregnancy [30,31]. dNK cells account over 70% of lymphocytes in the uterine decidua and they display a CD56<sup>bright</sup> phenotype, express NKG2A, lack expression of CD16, but highly express KIRs, although KIR repertoire is distinct from pNK cells [32]. Moreover, the vast majority express CD9 which is a characteristic marker of this subset [33]. Although they possess large quantities of cytotoxic granules, unlike pNK cells, they are poorly cytotoxic as they are unable to polarize those granules to the immune synapse [34]. However, they are able to produce a wide range of cytokines (eg. IFN $\gamma$ , tumor necrosis factor (TNF), IL-10, granulocyte-macrophage colony stimulating factor (GM-CSF)), chemokines (eg. IL-8, macrophage inflammatory protein-1beta (MIP-1 $\beta$ ), MIP-1alpha (MIP-1 $\alpha$ )) and angiogenic factors (platelet growth factor (PLGF), vascular endothelial growth factor (VEGF)), at least in vitro after IL-2 and IL-15 stimulation [30,32].

Infections by different pathogens also contribute to NK cell diversity. For instance, infection with human cytomegalovirus (CMV), a DNA virus that belongs to the herpesvirus family, is associated with important changes in the configuration of the NK cell repertoire [35]. Increased numbers of CD94/NKG2C<sup>+</sup> (hereafter NKG2C<sup>+</sup>) NK cells, commonly known as adaptive NK cells, have been observed following CMV infection or reactivation in different clinical settings [36–38]. These adaptive NK cells

exhibit certain memory-like properties such as increased CD16-triggered responses [39]. CMV infection is also associated with an increase in CD57 expression on NK cells [40]. Although NKG2C<sup>+</sup> NK cells expansion has also been observed in patients infected by other viruses, it mostly occurs in individuals who have been previously infected with CMV, suggesting that the expansion of these cells might be specific to human CMV [35,39]. Apart from expressing NKG2C, high expression of KIRs, reduced expression of NKG2A and lack of promyelocytic leukemia zinc finger (PLZF) protein, SYK and EAT2 expression have been described as hallmarks of CMV-infection induced adaptive NK cells [41]. Moreover, adaptive NK cells subsets that lack expression of the fragment crystallizable region (Fc) epsilon receptor gamma chain (FcεRγ) have been described to be expanded in CMV infection, although they can be found in CMV seronegative individuals as well [39,42]. Furthermore, even though the lack of FcεRγ is often associated with NKG2C expression, both markers may appear disassociated, suggesting the existence of distinct human adaptive NK cell subsets [43,44].

Additionally, other viral infections (e.g., human immunodeficiency virus (HIV)-1) and also aging, alter NK cell subsets repertoire. An expansion of CD56<sup>neg</sup>CD16<sup>+</sup> NK cell subset (hereafter CD56<sup>neg</sup>) has been described in both situations [40,45,46]. CD56<sup>neg</sup> NK cells are very scarce in the peripheral blood of healthy individuals and their expansion occurs primarily at the expenses of CD56<sup>dim</sup> NK cells [47]. Proteome analysis of CD56<sup>neg</sup> NK cells from healthy individuals revealed that this subset has an overall CD56<sup>dim</sup>-like phenotype [48] and other studies have described this NK cell subset as dysfunctional [49]. More age-related alterations have also been described such as a reduced frequency of CD56<sup>bright</sup> NK cells in elderly individuals and decreased expression of receptors such as NKp30, NKp46, and DNAM-1 on CD56<sup>dim</sup> NK cells. Furthermore, aging affects NK cell cytotoxicity against classic NK cell targets while ADCC is maintained [50]. Lastly, compared to children, adults exhibit lower developmental markers diversity on NK cells [51].

### **1.3 Human NK cell receptors**

The capacity to recognize and spontaneously eliminate virus-infected and tumor cells is one of the key functions of NK cells. This function is tightly regulated by a wide range of receptors expressed at the cell surface of NK cells [52]. One type of receptors expressed on the surface of NK cells are inhibitory receptors, which can be divided in

several groups. A first group comprise KIRs, which signal upon binding to HLA class I molecules HLA-A, -B, and -C (Table 1) [53]. A second group comprise the C-type lectin-like heterodimeric receptor NKG2A (and its isoform NKG2B) which recognize the non-classical HLA class I molecule HLA-E [54,55]. Via these inhibitory receptors, NK cells are able to detect the absence of self-molecules, specifically eliminating cells that have downregulated HLA class I molecules, a frequent event in cancer cells (Figure 2A). This is known as the missing-self recognition [56]. Moreover, NK cells may exert anti-tumor effect due to KIR-HLA class I mismatch. As demonstrated in acute myeloid leukemia (AML) patients undergoing HLA-mismatched alloHSCT, HLA class I-binding receptors of donor NK cells do not engage with their cognate ligand on recipient cells and thus, sense the missing expression of self-HLA class I molecules [57–59]. In this scenario, the inhibitory signal mediated by inhibitory receptors upon engagement with their ligands will be absent, thus allowing the killing of the target cells by donor NK cells. Also, and to avoid NK cell activation against self-healthy cells and at the same time to acquire a cytotoxic and cytokine production potential, during development, most NK cells randomly express at least one inhibitory receptor matching the own HLA class I molecules in a process known as NK cell “education” or “licensing”. Otherwise, NK cells that are not “licensed” or “educated” become somehow anergic [60,61]. NK cells can also express other additional constitutive or inducible inhibitory receptors that serve as immune checkpoints for cell activation, (e.g., PD-1, TIGIT, CD96, CD300a, etc.). Upon interaction with their ligands, these receptors hamper NK cell IFN $\gamma$  production and NK cell-mediated cytotoxicity [62,63].

However, some situations cannot be explained by the abovementioned missing-self hypothesis. For example, cells lacking HLA class I expression, such as human erythrocytes, are not eliminated by NK cells. Moreover, under some circumstances, NK cells are able to eliminate HLA class I-expressing tumor cells. This is because NK cells also have the capability to detect stress-induced ligands present on transformed cells, leading to the postulation of the “induced-self” model [64]. The recognition of those inducible ligands is mediated by a broad spectrum of activating receptors on the surface of NK cells. Natural cytotoxicity receptors (NCR) are one of the family of activating receptors. These NCRs include NKp46, NKp30, and NKp44, being the last one only expressed after activation of NK cells, while NKp46 and NKp30 are constitutively expressed [65]. Ligands for this family of receptors have been detected not only on many

tumor cells but also in some healthy tissues [66]. Other well-studied and particularly important activating receptor is the C-type lectin-like receptor NKG2D, which is expressed as a homodimer in virtually all NK cells. In humans, two families of NKG2D ligands (NKG2DLs) have been described: the major histocompatibility complex (MHC) class I chain-related molecules A and B (MICA and MICB) and the UL16-binding proteins. NKG2DLs are, in general, not expressed on healthy tissues, instead their expression is induced by cellular stress [67]. Other activating receptors expressed by NK cells are NKG2C that interacts with HLA-E [55], and DNAM-1, which compete with TIGIT and CD96 for binding to its ligands Poliovirus Receptor (CD155) and Nectin-2 (CD112) [63]. NK cells also express activating KIRs which ligands are HLA class I molecules (Table 1) [53]. Moreover, the function of these activating receptors can be enhanced by a second family of activating co-receptors (e.g., 2B4 and NKp80) whose action requires the co-engagement of the main activating receptors [68].

#### **1.4 NK cell effector functions**

The intricate balance between activating and inhibitory signals transmitted by the surface receptors mentioned above determines if NK cells will be activated and, consequently, what will be the outcome of the encounter with the potential target cell. Healthy cells expressing self-HLA class I molecules and none or few activating ligands will not be attacked by NK cells (tolerance), while transformed cells that present a reduced expression or mismatched expression of HLA class I molecules (missing-self) and/or an increased expression of activating ligands (induced-self) will be eliminated (Figure 2A) [69]. Moreover, NK cells are also strongly activated via CD16 surface receptor that recognize the Fc portion of IgG antibodies, and thus can kill antibody-coated cells via ADCC (Figure 2B). Apart from activating and inhibitory receptors, NK cell activation is also regulated by cytokines secreted by other cells, via the engagement of cytokine receptors present on the surface of NK cells (Figure 2B). Particularly, IL-15 is a critical cytokine for NK cell differentiation [70]. Moreover, IL-2 and IL-15 are needed for NK cell survival and proliferation [71]. Furthermore, cooperative effect of IL-2 and IL-15 and other cytokines such as IL-12 and IL-18 induce high IFN $\gamma$  production by NK cells [72].

Once activated, NK cells can mediate different effector mechanisms to eliminate both normal and transformed (tumor and virus-infected) cells [73]. On the one hand, NK cells may release cytolytic granules to the immunological synapse leading to the killing of

target cells. These granules are composed of perforin and granzymes. Perforin is a pore-forming molecule that facilitates granzymes to enter into the target cells [74]. Then, granzymes initiate target cell apoptosis by different pathways. For instance, granzyme B can cleave pro-caspases into active caspases inducing caspase-dependent cell death or can activate mitochondrial death pathway [73,75]. In addition to the perforin/granzyme pathway, NK cells also express Fas ligand (FasL) and TNF-related apoptosis-inducing ligand (TRAIL), which are ligands for tumor-cells expressing Fas and TRAIL receptors, members of the TNF receptor superfamily (Figure 2B). The engagement of these death receptors with their corresponding ligands also contributes to NK cell cytotoxicity by activating the caspase enzymatic cascade that causes the apoptosis of the target cell [73,76,77]. Moreover, the anti-tumor and anti-viral activity of NK cells also involves the secretion of cytokines, as, e.g.,  $\text{IFN}\gamma$ , which act on tumor and virus-infected cells [78]. Finally, NK cells through their cytotoxic activity and secretion of cytokines and chemokines also have a very important role in shaping the innate and adaptive immune responses [79].

### **1.5 NK cell development and differentiation**

The development of NK cells, as it occurs with other leukocytes, comprise a succession of coordinated differentiation steps that lead to commitment toward NK cell lineage and to the acquisition of functional competency. Traditionally, bone marrow has been considered the major site of NK cell generation and differentiation. However, studies carried out over the last years describing the presence of different NK cell progenitors in tissues other than bone marrow evidence that NK cell development also occurs in extra-medullary sites [80]. Thus, it is now well accepted that NK cells can also migrate, develop and mature in SLT, as it is the case of lymphoid nodes [81,82].

Due to obvious experimental limitations, a detailed picture of human NK cell development has been difficult to obtain. Moreover, the classical developmental model in where hematopoietic stem cells (HSCs) bifurcate into common myeloid progenitors and common lymphoid progenitor was challenged by the discovery of a lymphoid-primed multipotent progenitor that sustains lymphoid and myeloid potential [83]. The definition of a lineage-restricted NK cell progenitor has been also difficult to achieve given the complexity and plasticity of early hematopoiesis and lineage commitment. Nevertheless, phenotypically distinct progenitors that give rise to NK cells have been described [84–

90]. Years ago, a step forward in the characterization of the human NK cell developmental pathway was done by Caligiuri and colleagues, by defining a five-stage model of human NK cell development in SLT [91,92]. In this study, and based on the differential expression of CD34, CD117, CD94, and CD16, five human NK cell developmental stages were defined (Figure 3) [93]. In this model, cells comprising stages 1 and 2 are capable to differentiate into dendritic cells (DCs), T cells and NK cells, while stage 3 cells can give rise to NK cells but not to DCs or T cells. Thus, stage 3 cells are considered lineage-restricted NK cell precursors. The acquisition of CD122 (IL-2/15 receptor  $\beta$ -chain) marks an important step towards NK cell differentiation as the trans-presentation of soluble IL-15 is essential for mature NK cell survival [70,71,94]. However, functional maturity is not acquired until stage 4, as stage 3 cells are characterized by the lack of key mature NK cell features, such as IFN $\gamma$  production and perforin-mediated cytotoxicity [93,95].

Subsequent studies have described additional differentiation steps of this model. For instance, using 10-parameters flow cytometry, Eissen et al. defined 7 human NK cell developmental stages in the bone marrow, adding a layer of complexity [80]. In addition, Scoville et al. proposed that SLT stage 2 cells can be divided in two functionally distinct subsets [96,97]. Furthermore, two different steps of stage 4 have been described also in SLT, differing in the C-type lectin-like activating receptor NKp80 expression. Stage 4a subset was NKp80- and characterized by ILC3-associated features and not significant effector functions, while stage 4b subset was NKp80+ and cells produced IFN $\gamma$  and mediated perforin-dependent cytotoxicity [95]. These stage 4b cells are thought to represent CD56<sup>bright</sup> NK cells, whereas stage 5 cells represent the CD56<sup>dim</sup> NK cell subset. Thus, according to this linear model of NK cell development, there is a transition from CD56<sup>bright</sup> to CD56<sup>dim</sup> NK cells [84,98]. However, this step is considered somehow controversial, as the existence of CD56<sup>dim</sup> NK cells was reported in primary immunodeficiency patients that lack CD56<sup>bright</sup> NK cells [99]. Nevertheless, the generation of CD56<sup>dim</sup> NK cells from CD56<sup>bright</sup> NK cells when human HSCs are engrafted in humanized mice [70], the fact that CD56<sup>bright</sup> NK cells display longer telomeres [100] and that CD56<sup>bright</sup> NK cells are the predominant population immediately after HSCT [101], among others, supports the hypothesis for a developmental relationship between CD56<sup>bright</sup> and CD56<sup>dim</sup> NK cells.

CD56<sup>dim</sup> NK cells are a very heterogeneous population and are further differentiated until stage 6, defined by the acquisition of CD57 (Figure 3), thus being considered terminally

differentiated NK cells [102,103]. Through the final differentiation steps, CD56<sup>dim</sup> NK cells lose NKG2A expression and sequentially acquire KIRs and CD57. CD57 expression increases with the expression of KIRs and correlates inversely with the expression of NKG2A. Moreover, they experience a gradual decline in proliferative capacity, along with different expression patterns of homing molecules [104,105]. Terminally differentiated NK cells are less responsive to stimulation by cytokines but produce IFN $\gamma$  and have a potent lytic activity when stimulated via CD16, evidencing a gradual shift in functionality during differentiation [103].

Although these NK cell developmental steps are well accepted, NK cell development is a more intricate process. For instance, different studies have revealed the existence of multiple cellular intermediates, such as unconventional CD56<sup>dim</sup>CD16<sup>-</sup> NK cells [19,81] and CD56<sup>bright</sup>CD16<sup>+</sup> NK cells [106]. Moreover, although in lower frequencies, it is possible to find all combinations of NKG2A and KIR expression in either CD57<sup>+</sup> or CD57<sup>-</sup> CD56<sup>dim</sup> NK cells [104]. Thus, it is obvious that the linear model of NK cell development is only an oversimplification of what really happens. Finally, little is known about the developmental origin of other NK cell subsets, such as adaptive NK cells [107] or CD56<sup>neg</sup> NK cells, opening the possibility of yet not explored differentiation pathways.

## **2. Hematopoietic stem cell transplantation**

HSCT is a worldwide-established treatment option for many hematological disorders. In this type of cell immunotherapy, after the administration of an appropriate conditioning regimen that will ablate the recipient's own bone marrow and induce sufficient immunosuppression to allow engraftment, HSCs are infused to replace the recipient's unhealthy native bone marrow cells and immune system.

### **2.1 Types and indications**

HSCT can be classified in different types based on the relationship between donor and recipient and the source of the graft. Thus, HSCT can be classified as autoHSCT, when the patient's own stem cells are collected and reinfused at a later time, or alloHSCT, when HSCs come from another individual. In this latter scenario, donors can be related or unrelated HLA-matched. Moreover, when such donor cannot be found, a related half-matched donor, also known as haploidentical transplantation, in which only one of the two HLA haplotypes is matched, can be used. On the other hand, according to the source,



HSCs can be obtained from bone marrow, peripheral blood or umbilical cord blood (CB). Although HSCs were first harvested from bone marrow, nowadays, and due to the development of mobilization procedures, such as the use of granulocyte colony-stimulating factor (G-CSF), peripheral blood is the main source of precursors [108,109].

In 2012, a total of 68,146 HSCTs were reported worldwide. Among them, 47% were allogenic and 53% autologous [110]. Moreover, in 2018, 47,468 transplants were reported only in Europe. Of these, 41% were allogenic and 59% autologous. In Europe, the main indications for alloHSCT are myeloid malignancies, being AML the largest indication, while the main indications for autoHSCT are lymphoid malignancies, being multiple myeloma (MM) and non-Hodgkin lymphoma (NHL) the largest indications [111]. In Spain, according to the National Transplant Organization, in 2020, 3375 transplant were reported, from which 2049 were autologous and 1326 were allogenic. Also, 51% of the autoHSCT performed in Spain in 2020 were indicated to treat MM patients.

## **2.2 Factors affecting outcome after autologous hematopoietic stem cell transplantation**

The benefits of alloHSCT go beyond the recovery from bone marrow aplasia after conditioning regimen, as immune cells in the graft might recognize and eliminate residual malignant cells, which is known as graft-versus-tumor (GvT) effect [112]. Conversely, for years, autoHSCT has only been seen as a form for bone marrow rescue, necessary for hematologic engraftment, and its antitumor effect has been thought to rely on the conditioning regimen. Nevertheless, studies carried out in the last 15–20 years pointed out that a GvT effect might also be possible in autoHSCT setting [113]. As in alloHSCT, early immune recovery after autoHSCT has been associated with prolonged survival in a wide range of hematological malignancies [114–117]. Particularly, day 15 absolute lymphocyte count (ALC-15) of  $\geq 500$  cells/ $\mu\text{L}$  after autoHSCT was reported as an independent prognostic indicator for overall survival (OS) and progression-free survival (PFS) in MM and NHL patients [115]. Moreover, while different studies have not found any correlation between CD34+ cells dose and ALC recovery [118–120], a strong correlation was identified between the number of passively infused lymphocytes in the peripheral blood autograft (A-ALC) and ALC-15, being A-ALC higher in patients achieving an ALC-15 of  $\geq 500$  cells/ $\mu\text{L}$  [121]. The amount of passively transferred lymphocytes correlated inversely with the time to achieve a lymphocyte count of  $0.5 \times$

$10^9$  cells/L [119]. Furthermore, A-ALC was reported to be an independent prognostic factor for OS and PFS in NHL patients [121]. T cells and NK cells were the main lymphocyte subsets identified in the autograft, and among them, a strong correlation was found between NK cells absolute numbers from the apheresis product and ALC-15 [118]. Subsequently, NK cells were identified as the key lymphocyte subset in ALC-15 that impacted the outcome after autoHSCT. Thus, NHL patients with NK cell count at day 15 (NK-15) of  $\geq 80$  cells/ $\mu$ L experienced superior 3-year OS and PFS [122] and MM patients with NK cell count at 1 month of  $\geq 100$  cells/ $\mu$ L experienced prolonged PFS [123] than patients with lower counts. In addition, NHL patients with IL-15 levels  $\geq 76.5$  pg/mL at day 15 post-autoHSCT experienced superior 3-year OS and PFS compared with those patients with lower IL-15 levels. However, this survival benefit was reported to be most likely mediated by enhanced NK cell recovery after transplant [124]. Although all these are circumstantial evidences, and thus do not prove causality, they all suggest that the infusion of autograft lymphocytes does impact not only on immune reconstitution but also on the clinical outcome after autoHSCT (Table 2). Residual disease progression may be controlled by an early immune reconstitution and passively infused lymphocytes, opening the possibility for an autologous GvT effect [125,126].

### **2.3 Immune reconstitution after autologous hematopoietic stem cell transplantation**

After HSCT, clinical engraftment is commonly considered when achieving a peripheral blood neutrophil count of  $>0.5 \times 10^9$ /L [127]. However, this does not mean that complete immune reconstitution occurs at this point. Reconstitution of immunologically competent cells occurs very gradually and more than a year may be needed to restore normal humoral and cellular immunity. Of note, B cells are barely detectable during the first 2–3 months post-HSCT, and the recovery of normal B cell numbers and functions can take up to 18 months [126,128]. Moreover, T cell recovery is also delayed, being CD8+ T cells restoration faster than CD4+ T cells, as the latter may fully reconstitute after 1-year post-HSCT. Thus, an inverted CD4/CD8 ratio is reported after HSCT [126].

In contrast, NK cells have been reported to be the first lymphocyte subset to return to normal levels, being the counts and functionality of NK cells restored as early as day 14 post-HSCT [126,129].

### 3. NK cells in autologous hematopoietic stem cell transplantation

Considering that NK cells play a role in immune surveillance and recover early after HSCT, the study of the reconstitution of this cell subset in autoHSCT settings and their impact on outcome is of utmost interest.

#### 3.1 KIRs and HLA class I ligands

In alloHSCT, the GvT effect exerted by NK cells mainly relies in a mismatch between KIRs expressed by donor NK cells and the HLA class I ligands expressed on the recipient's tumor cells [130,131]. As genes that encode KIRs and their HLA class I ligands segregate independently, expression of inhibitory KIRs but not its corresponding ligands, and vice versa, may happen. Although NK cells expressing inhibitory KIRs for non-self HLA class I molecules are hyporesponsive in steady state, in certain situations like inflammation, they may become responsive and play biologically important roles [132,133]. Thus, even though far less reported and studied, inhibitory KIR-HLA receptor-ligand mismatch can also occur in autoHSCT and affects patient's outcome (Table 2).

In lymphoma patients undergoing autoHSCT, *HLA-Cw8* was reported to be an independent risk factor for poor outcome [134]. Moreover, lower risk of relapse was found when inhibitory KIR-HLA receptor ligand mismatch occur in a cohort of patients undergoing autoHSCT for solid tumor and lymphoma [135]. A similar outcome was also seen in patients undergoing autoHSCT for high-risk neuroblastoma. Particularly, patients lacking HLA-C1, the ligand for KIR2DL2/KIR2DL3, have the highest 3-years survival rate [136]. However, Stern and colleagues were not able to show that missing KIR-ligand effect in their autoHSCT cohort [137]. This is probably due to the fact that, in contrast to Leung et al. [135], they grouped patients exclusively based on the presence or absence of KIR ligands and do not take into account inhibitory KIRs expression. In a cohort of AML patients treated with autoHSCT, those with *KIR* and *HLA* genotypes predictive of low-affinity interactions (*KIR3DL1+* and *HLA-Bw4-80Thr+*, *HLA-Bw4-80Ile-* genotype) had lower incidence of relapse than patients with genotypes predictive of high-affinity interactions (*KIR3DL1+* and *HLA-Bw4-80Ile+* genotype), and this effect was also influenced by *HLA-Bw4* copy number [138]. This can be explained because HLA-Bw4-80Thr molecules bind KIR3DL1 with lower affinity than HLA-Bw4-80Ile, endowing lower responsiveness but weaker NK cell inhibition [138,139]. Finally, MM patients who

were KIR3DS1+ (activating KIR encoding gene) experienced shorter PFS after autoHSCT and this was more evident in patients that were at complete or partial remission at transplantation and who lacked the ligand for the inhibitory KIR3DL1, i.e., HLA-Bw4 [140]. Although the mechanism by which KIR3DS1 affects patient's survival is not well understood, one possible explanation for its negative impact could be that KIR3DS1+ NK clones may exert an immunomodulatory effect of antitumor responses by the production of anti-inflammatory cytokines [140]. On the other hand, it has been suggested that KIR3DS1 accomplishes a protective role in other human diseases, for example for the development of hepatocellular carcinoma in patients chronically infected with the hepatitis C virus (HCV) [141]. Thus, this KIR might have either detrimental or beneficial effect depending on the type of disease.

### **3.2 Other phenotypic characteristics and NK cell subsets**

As KIRs are just a minor part of the complex NK cell receptor repertoire, the study of further receptors, as well as the reconstitution of different NK cell subsets that might be implicated in the survival of patients undergoing autoHSCT is of great importance. In this sense, recently, whether a particular immune signature was associated with long-term complete response in MM patients was investigated. The authors found that, even if the frequency of NK cells within total lymphocytes was similar in patients and healthy donors, higher frequency of the inhibitory receptor KIR2DL1-expressing NK cells, higher frequency of NKG2A+ NK cells and lower frequency of NKp46+ NK cells were observed in MM patients in long-term complete response. Thus, a particular redistribution of NK cell activating and inhibitory receptors occurs in these patients [142]. In another recent study, Bhutani et al. examined the differences in NK cell numbers and phenotype between MM patients with minimal residual disease (MRD) positive status and MRD negative status after autoHSCT. These authors found that absolute numbers of NK cells were lower in patients with MRD positive response. In addition, and although the differences were not statistically significant, these patients have a higher frequency of KIR2DS4+ NK cells and a lower frequency of NKG2A+ NK cells compared to patients with MRD-negative response [143].

Moreover, a few years ago, a comprehensive study of different NK cell subsets, their phenotype, and their function at three different time points, i.e., before autoHSCT (T1), after leukocyte regeneration (1000 leukocytes/ $\mu$ l) (T2), and after 2 weeks of leukocyte

recovery (T3), in patients undergoing autoHSCT was carried out (Figure 4) [144]. In this study, authors found that the frequency of NK cells within the leukocyte population significantly decreases from T1 to T2 but then reached pre-autoHSCT levels at T3. Furthermore, the fold change ratio T2/T1 of the NK cell percentage was different between patients having a period time of  $\leq 11$  days between autoHSCT and T2 and those having a period of  $> 11$  days and also in patients with recurrent or refractory disease at 1 year after autoHSCT and those without. Focusing on NK cell subsets, they observed that CD56<sup>dim</sup> (CD56+CD16++) subset was the main population at T1 and T3. However, NK cell subsets redistribution was observed at T2, in which the frequency of CD56<sup>dim</sup> decreased, while the two populations of CD56<sup>bright</sup> that they distinguished (CD56++CD16- and CD56++CD16+) significantly increased, being the percentage of CD56<sup>bright</sup>CD16+ subset similar to the one of CD56<sup>dim</sup> subset. The NK cell subset distribution at T3, although similar to the one observed at T1, was not the same. In addition, they studied the expression of NKG2A, CD57, and KIRs, i.e., markers related to NK cell differentiation and education. They found that on total NK cells, the frequency of NKG2A+ NK cells increased from T1 to T2 and was maintained elevated at T3. Furthermore, the expression of CD57 also increased from T1 to T2 but then returned to the initial levels at T3. A similar pattern of expression was also observed when the three subsets were separately analyzed. Particularly, the expression of CD57 at T2 in both CD56<sup>bright</sup> subsets was surprising, as CD57 is considered a marker of terminally differentiation and CD56<sup>bright</sup> are thought to be immature NK cells. In contrast, the frequency of KIR-expressing NK cells remains constant during NK cell reconstitution, even though the percentage of KIR+ cells in both CD56<sup>bright</sup> subsets increased at T2 and maintained elevated at T3 (Figure 4). Finally, when effector functions of NK cells were assessed, Jacobs et al. reported that NK cells were able to degranulate (CD107a) and to produce cytokines (IFN $\gamma$ ) and chemokines (MIP1 $\beta$ ) upon target cell recognition early after autoHSCT [144]. As the cohort of patients analyzed in this study is quite heterogeneous in terms of the type of cancer, it must be elucidated whether the NK cell subsets distribution, their phenotype and functionality during NK cell reconstitution will be the same in a particular hematological malignancy. In this sense, Jacobs et al. also found some differences regarding the CD56<sup>dim</sup>/CD56<sup>bright</sup> ratio and the frequency of CD56<sup>bright</sup>NKG2A+ cells at T2 between MM and lymphoma patients undergoing autoHSCT [144].

Analysis of different NK cell subsets distribution was also carried out in a cohort of MM undergoing autoHSCT. In this case, the authors found that a population of CD56<sup>dim</sup>CD16<sup>low</sup> was expanded after 2 weeks post-transplant and returned to initial levels after a month post-HSCT. They also described that this subset displayed the highest capacity to degranulate in vitro against K562 and MM cell lines [145]. As in alloHSCT, adaptive NK cell expansion after autoHSCT has been associated with lower relapse (Table 2)[146–148]. Finally, an expansion of CD56<sup>neg</sup> NK cells after different HSCT settings, others than autoHSCT, have been described [149–151]. Specifically, in T cell-depleted haploidentical HSCT, CD56<sup>neg</sup> appear to be functional and capable of GvT effect [151].

All the above mentioned data highlights that not only NK cell counts after autoHSCT have an impact on patient's outcome but also the reconstitution of different NK cells subsets and their phenotype may be of great importance. For this reason, the study of other NK cells subsets rather than the conventional CD56<sup>bright</sup> and CD56<sup>dim</sup> subpopulations, in addition to other aspects of NK cells phenotype will contribute to a better understanding of NK cell reconstitution after autoHSCT. These studies may also help in the search of new biomarkers that may predict autoHSCT outcome, allowing patient individualization and further improving this therapy.

## **HYPOTHESIS AND OBJECTIVE**

NK cells counts after autoHSCT has been defined as a prognostic indicator in NHL and MM patients. We hypothesize that not only a rapid reconstitution of the NK cells pool, but also an adequate grade of maturation, expression of specific receptors and the distribution of different NK cell subsets have a significant impact on the outcome of patients undergoing an autoHSCT. In addition, we also predict that, among others, the cytokine milieu modulates the expression of NK cell receptors and the functionality of these cells. Finally, we postulate that NK cells undergo a drastic alteration in their gene expression profile during their reconstitution after autoHSCT.

Therefore, the main purpose of this project was to investigate changes in the peripheral NK cell pool during the immune reconstitution after autoHSCT in MM patients. For that, we have established the following objectives:

1. To determine an alternative surface marker to CD16 to better identify the CD56<sup>neg</sup> NK cell subset.
2. To phenotypically and functionally characterize NK cells during the immune reconstitution after autoHSCT in MM patients.
3. To study alterations in the NK cell transcriptome after autoHSCT in MM patients.

## **CHAPTER I**

### **Flow cytometry-based strategy for the correct identification of CD56<sup>neg</sup> NK cells.**

Parts of this chapter have been published in:

Orrantia A, Terrén I, Izquierdo-Lafuente A, Alonso-Cabrera JA, Sandá V, Vitallé J, Moreno S, Tasia M, Uranga A, González C, Mateos JJ, García-Ruiz JC, Zenarruzabeitia O, Borrego F. A NKp80-Based Identification Strategy Reveals that CD56<sup>neg</sup> NK Cells Are Not Completely Dysfunctional in Health and Disease. *iScience*. 2020 Jul 24;23(7):101298. doi: 10.1016/j.isci.2020.101298.



## INTRODUCTION

As mentioned in the introduction section, NK cells are classified within the ILCs family which main characteristic is the absence of rearranged antigen receptors. Although the cell subsets that conform the ILCs family are distinguish based on their effector functions, the cytokine pattern they secrete and the transcription factors they need to develop and differentiate, especially the distinction between ILC1 and NK cells could be problematic since they express similar cell surface markers [2,152–154]. Nevertheless, in humans the NKp80 cell surface receptor is expressed on NK cells and seems to be a NK-cell specific marker among human ILCs [13,95]. Furthermore, NK cells express both T-bet and Eomes transcription factors, while ILC1 only express T-bet [2,152,153,155–157].

Commonly, due to the lack of a cell-surface-specific receptor that leads to NK cell identification within peripheral blood mononuclear cells (PBMCs), they are usually identified by the absence of other lineage markers, such as those that are specific for T cells (CD3), B cells (CD19) and monocytes (CD14). Furthermore, CD56 in combination with CD16, the low-affinity Fc gamma receptor IIIa, are generally used to distinguish the different NK cell subsets: CD56<sup>bright</sup>, CD56<sup>dim</sup>, unconventional CD56<sup>dim</sup> and CD56<sup>neg</sup> [13,158]. However, none of these markers is specific to NK cells. For instance, although all ILCs are mostly negative for the above mentioned lineage markers [2,153,154], CD56 is expressed by a subset of ILC3, known as NCR+ ILC3 and which, like NK cells, expresses NCR NKp30, NKp44, NKp46 [2,153,154,159]. On the other hand, although CD16 is widely accepted to be a NK cell-specific marker among ILCs [2,6,154], it is known that CD16 could be downregulated following target cell activation [160–164] and cryopreservation [165]. Therefore, the lack of marker specificity makes the process of identifying NK cells quite challenging and highlights the need to start using other set of cell surface markers.

The CD56<sup>neg</sup> subset expresses NK cell-associated surface markers, such as CD16, CD94 and NKp46, in addition to the transcription factors Eomes and T-bet [48,166]. As mentioned before, in healthy individuals, the presence of CD56<sup>neg</sup> NK cells in blood is very rare [40,47,167]. However, years ago, in patients with chronic HIV-1 infection, a significant expansion of CD56<sup>neg</sup> NK cells was reported [45,46], which was associated with high HIV-1 viral load [49,168,169]. Indeed, long term non-progressors and patients who successfully suppress viral load after highly active antiretroviral therapy have

CD56<sup>neg</sup> NK cell levels comparable to the ones found in non-infected subjects [168,170]. However, patients who fail to suppress viral load upon treatment, have similar CD56<sup>neg</sup> numbers to those untreated patients with persistent viremia [168]. In addition, in chronically HIV-1-infected individuals who developed broadly-neutralizing antibodies (bnAbs), a high proportion of NK cells have a CD56<sup>neg</sup> phenotype, while in patients that do not have bnAbs the proportion of CD56<sup>neg</sup> NK cells was lower, although still high when compared to HIV-1 seronegative subjects [171]. Elevated frequencies of the CD56<sup>neg</sup> subset has also been described in HCV-monoinfected and HCV/HIV-1-coinfected people [172,173]. Furthermore, the abnormal expansion of these cells correlated with monoinfected patient's ability to respond to pegylated-IFN $\alpha$  and ribavirin treatment [172]. Moreover, treatments that suppress HCV replication, decreases CD56<sup>neg</sup> NK cells number in HCV/HIV-1-coinfected patients [173]. On the other hand, it has been described that aging and CMV status has an effect on the frequency and distribution of NK cell subsets, increasing the percentage of CD56<sup>neg</sup> NK cells [40,167].

Studies performed with similar cohorts of patients differ in the frequency, functionality and phenotype of the CD56<sup>neg</sup> NK cell subset, which could be due to different gating strategies used for the identification of this NK cell subset [47,49,174,175]. In those publications, this NK cell subset has been identified as CD56<sup>neg</sup>CD16+, and depending on the studies, they have or have not included an exclusion channel in the gating strategy for the exclusion of T cells, B cells and/or monocytes. As indicated above, CD16 has an unstable expression in some situations, and hence, the usage of this marker could lead to an inaccurate identification of CD56<sup>neg</sup> NK cells and inconsistent results.

Therefore, in this first chapter, we have explored the possibility of using NKp80 as an alternative surface marker to CD16 to better identify CD56<sup>neg</sup> NK cells. NKp80, the product of the *KLRF1* gene, is an activating receptor expressed by virtually all mature human NK cells [176]. It marks a critical step in NK cell development, as it defines functionally mature NK cells [95] and is a NK cell-specific marker among human innate lymphoid cells (ILCs) [2].

## METHODS

### Subjects and Samples

For this study, buffy coats from 24 healthy adult donors and cryopreserved PBMCs from 9 MM patients were collected through the Basque Biobank for Research (<http://www.biobancovasco.org>), which complies with the quality management, traceability and biosecurity, set out in the Spanish Law 14/2007 of Biomedical Research and in the Royal Decree 1716/2011. The study was approved by the Basque Ethics Committee for Clinical Research (PI2014017 and PI+CES+INC-BIOEF 2017-03). All subjects provided written and signed informed consent in accordance with the Declaration of Helsinki. In addition, cryopreserved PBMCs from healthy donors (n=5), untreated HIV-1 infected subjects (n=9) and patients under combined antiretroviral therapy (cART) (n=8) were provided by the HIV BioBank integrated in the Spanish AIDS Research Network (RIS). Samples were processed following current procedures and frozen immediately after their reception. All patients participating in the study gave their informed consent and protocols were approved by institutional ethical committees.

All HIV-1 infected patients were asymptomatic when the sample was collected, were not co-infected with HCV, had more than 200 CD4+ T cells/mm<sup>3</sup> and they had never been diagnosed with acquired immunodeficiency syndrome. Untreated HIV-1 infected subjects had detectable viremia (>10,000 HIV-RNA copies/ml) and they had never been treated with cART, while patients under cART had undetectable viremia and had been treated at least for 6 months. Clinical data of HIV-1 infected patients were obtained from the RIS database. Clinical data are shown in Table 3.

### Antibodies and Reagents

For flow cytometry-based procedures, the following fluorochrome-conjugated anti-human monoclonal antibodies (mAbs) were used: BV421 anti-CD56 (clone NCAM 16.2), BV510 anti-CD3 (UCHT1), BV510 anti-CD14 (MΦP9), BV510 anti-CD19 (SJ25C1), BV510 anti-CD123 (9F5), PE anti-CD123 (9F5), PE anti-CD7 (M-T701) and PerCP-Cy5.5 anti-IFN $\gamma$  (B27) from BD Biosciences; FITC anti-CD16 (B73.1) and APC anti-TNF (MAb11) from BioLegend; PE anti-CD300a (E59.126) and PE anti-2B4 (clone C1.7) from Beckman Coulter; PE anti-CD107a (REA792) and PE-Vio770 anti-NKp80 (4A4.D10) from Miltenyi Biotec; eFluor660 anti-Eomes (WD1928) from Invitrogen.

Dead cells were excluded by using the LIVE/DEAD™ Fixable Aqua Dead Cell Stain Kit for 405nm excitation from Invitrogen, following manufacturer's protocol.

The following reagents were also used: Foxp3/Transcription Factor Staining Buffer Set from eBioscience; Brilliant Stain Buffer, BD GolgiStop™ Protein Transport Inhibitor (monensin), BD GolgiPlug™ Protein Transport Inhibitor (brefeldin A) and BD Perm/Wash™ Buffer from BD Bioscience; and paraformaldehyde (PFA) from Sigma-Aldrich/Merck.

### **PBMCs Isolation from buffy coats**

Fresh PBMCs from healthy donors were obtained from buffy coats by Ficoll (GE Healthcare) density gradient centrifugation (x800g 20-25 minutes) without braking. The PBMC layer was collected and washed twice. Finally, PBMCs were cryopreserved in Fetal Bovine Serum (FBS) (GE Healthcare Hyclone) with 10% dimethylsulfoxide (DMSO) (Thermo Scientific Scientific).

### **Phenotypic Analysis**

For phenotypical studies, fresh and cryopreserved PBMCs from healthy donors, HIV-1-infected subjects and MM patients were used. Cryopreserved PBMCs were thawed at 37°C and washed twice with RPMI 1640 medium with L-Glutamine (Lonza). Then, cells were incubated for 1 hour at 37°C with 10U DNase (Roche) in R10 medium (RPMI 1640 medium containing GlutaMAX from Thermo Fisher Scientific, 10% FBS and 1% Penicillin-Streptomycin from Thermo Fisher Scientific). Afterwards, cells were counted and washed with Phosphate Buffered Saline (PBS) (Gibco, Thermo Fisher Scientific). Then, dead cells were excluded by using the LIVE/DEAD reagent (Invitrogen, Thermo Fisher Scientific). For the staining of NK cell surface markers, cells were first washed with PBS containing 2.5% of Bovine Serum Albumin (BSA) (Millipore) and then incubated for 30 minutes at 4°C with fluorochrome-conjugated mAbs. To identify NK cells, viable cells that were negative for CD3, CD14 and CD19 were electronically gated, and then, by using the anti-CD56 mAb in combination with mAbs against CD16, NKp80, CD300a, 2B4 and/or CD7, CD56<sup>neg</sup> NK cells were selected (Figure 5). After this, cells were washed again with 2.5% BSA in PBS and fixed and permeabilized with Foxp3/Transcription Factor Staining Buffer Set (eBioscience, Thermo Fisher Scientific) following manufacturer's recommendations. Finally, cells were stained using anti-Eomes

mAb for 30 minutes at room temperature (RT) and washed with Permeabilization Buffer 1x (eBioscience). Sample acquisition was carried out in a MACSQuant Analyzer 10 flow cytometer (Miltenyi Biotec). Flow cytometry panels used to study NK cell phenotype are shown in Table 4.

### **Functional Assays**

For functional assays, after DNase treatment, PBMCs from HIV-1-infected subjects and healthy donors were counted and plated at  $0.5 \times 10^6$  cells/well in 48 well plates in NK cell culture medium (RPMI 1640 medium with GlutaMAX, 10% FBS, 1% penicillin streptomycin, 1% non-essential amino acids and 1% Sodium-Pyruvate). PBMCs were then primed with recombinant human (rh) IL-15 (10 ng/mL) and cultured for 20 hours. For cytokine stimulation, rhIL-12 (10ng/mL) and rhIL-18 (50 ng/mL) were also added to plated PBMCs. For target cell stimulation, K562 or 721.221 cells were added after the 20 hours of culture in IL-15 at Effector:Target (E:T) 1:1 ratio ( $0.5 \times 10^6$  PBMCs and  $0.5 \times 10^6$  K562 or 721.221 cells). Then, IL-12+IL-18 stimulated and K562 or 721.221 stimulated PBCMs were cultured for 6 hours. CD107a was added at the start of the co-culture period and protein transport inhibitors (monensin and brefeldin A) were added after 1 hour for the rest of the incubation time following manufacturer's protocol. Afterwards, viability and surface marker staining was performed as explained in the Phenotypic Analysis section. For intracellular staining, cells were fixed with 4% PFA for 15 minutes on ice and then washed twice with 2.5% BSA in PBS. After this, cells were permeabilized with BD Perm/Wash Buffer 1X for 15 minutes at RT. Finally, the corresponding mAbs were added for 30 minute and cells were washed with BD Perm/Wash Buffer 1X before acquisition in the MACSQuant Analyzer 10 flow cytometer (Miltenyi Biotec). Flow cytometry panel used to study NK cell functionality is shown in Table 4. The percentage of positive cells for CD107a, IFN $\gamma$  and TNF was calculated after subtracting the non-stimulus condition.

For redirected killing assay showed in Figure 11D, cryopreserved PBMCs were thawed at 37°C, washed twice with RPMI 1640 medium, plated at  $2 \times 10^6$  cell/mL in 6 well plates and incubated overnight at 37°C in R10 medium. Next day, PBMCs and P815 cells were co-incubated at Effector:Target (E:T) 1:1 ratio ( $0.5 \times 10^6$  PBMCs and  $0.5 \times 10^6$  P815 cells) in R10 medium in U-bottom 96 well plates. Then, 0.5 mg/mL unconjugated IgG isotype control (clone MOPC21) from BioLegend or 0.5 mg/mL unconjugated anti-CD16

mAb (Clone 3G8) from BD Bioscience were added and cells were cultured at 37°C for 6h.

K562, 721.221 and P815 cell line were cultured in NK cell medium supplemented with 5 µg/mL Plasmocin (InvivoGen). All cell lines were routinely tested for mycoplasma infection with Venor GeM Classic detection kit (Minerva Biolabs).

### **Quantification and Statistical Analysis.**

Data were analyzed using FlowJo™ v10.4.1. GraphPad Prism v8.01 software was used for graphical representation and statistical analysis. As specified in all figure legends, each dot in the graphs represents a donor. Data were represented showing means ± standard error of the mean (SEM) or median as indicated in the figure legend. Prior to statistical analyses, data were tested for normal distribution with Kolmogórov-Smirnov normality test. In the case of MM patients, an outlier was identified and removed using Grubb test (alpha=0.05). If data were normally distributed, t test for paired values was used to determine significant differences. Non-normal distributed data were compared with Wilcoxon matched-pairs signed rank test. Kruskal-Wallis test was used for multiple comparisons of non-normal data. \*p<0.05, \*\*p<0.01, \*\*\*p<0.001, \*\*\*\*p<0.0001, ns: not significant.

## RESULTS

### **The NKp80 receptor is superior to CD16 for the identification of circulating CD56<sup>neg</sup> NK cell subset in healthy donors**

CD16 receptor has traditionally been used, in combination with CD56, to identify the circulating NK cell subsets, with CD56<sup>neg</sup> NK cells defined as CD56<sup>neg</sup>CD16<sup>+</sup> [47]. However, CD16 show unstable expression. It is well known that CD16 is downregulated in some situations, such as cryopreservation, after target cell stimulation or activation via different compounds, cell surface receptors and cytokines [160–165]. CD16 is shed from the cell surface as a consequence of matrix metalloproteinases activation, such as MT6 (also known as MMP25) and ADAM17 [161–164].

With the aim to identify a more accurate marker with a more stable expression, we first compared CD16 with NKp80 receptor to identify CD56<sup>neg</sup> NK cells in healthy donors. Our gating strategy included an exclusion channel (viability, CD3, CD14 and CD19) that allowed us to specifically study non-T, non-B and non-monocytes viable cells (Figure 5). As previously described [165], CD16 expression was clearly downregulated in cryopreserved samples as seen in both pseudocolor dot plot graphs and histograms showing the median fluorescence intensity (MFI) (Figure 6). However, the expression of NKp80 was not significantly altered after cell freezing (Figure 6), suggesting that this receptor is more suitable for the detection of CD56<sup>neg</sup> NK cells when it concerns to frozen cells. Very importantly, although no differences were seen regarding the percentage of CD56<sup>neg</sup> NK cells selected using both markers (Figure 7A), there was a significantly higher frequency of Eomes<sup>+</sup> cells in the CD56<sup>neg</sup>NKp80<sup>+</sup> subpopulation than in CD56<sup>neg</sup>CD16<sup>+</sup> cells (Figure 7B). As explained above, Eomes expression is a specific intracellular marker for the detection of NK cells within the ILCs, given that it is a T-box transcription factor needed for the development and function of NK cells, while for example, ILC1 do not express Eomes [2,152,153,155–157]. For this reason, we used Eomes as a standard marker for NK cell identification.

As the percentage of Eomes<sup>+</sup> cells within the CD56<sup>neg</sup>CD16<sup>+</sup> subset was low (Figure 7B), we considered the possibility that other CD16<sup>+</sup> non-NK cells could have been included using this gating strategy. This hypothesis was strengthened by the fact that within the CD56<sup>neg</sup>CD16<sup>+</sup> population, the Eomes<sup>-</sup> cells had larger size than Eomes<sup>+</sup> cells (Figure 7C). Thus, we studied the expression of CD123 receptor ( $\alpha$ -chain of the

interleukin 3 receptor) expressed, among others, in plasmacytoid dendritic cells (pDCs) and basophils, which are characterized by a larger size and granularity [177–181]. Results showed that CD56<sup>neg</sup>CD16+Eomes<sup>-</sup> cells expressed CD123, in contrast to CD56<sup>neg</sup>NKp80+Eomes<sup>-</sup> cells that barely did (Figure 7D). Furthermore, the addition of an anti-CD123 mAb to the exclusion channel revealed that the frequency of CD56<sup>neg</sup>CD16+Eomes<sup>+</sup> cells significantly increased, but still tended to be lower compared with CD56<sup>neg</sup>NKp80+Eomes<sup>+</sup> cells (Figure 7E). These results suggested that the inaccuracy in the identification of the CD56<sup>neg</sup> NK cell subset using the CD16 marker in the gating strategy is due to the selection of Eomes<sup>-</sup> cells that, at least partially, could be pDCs and/or basophils, which are characterized by the expression of CD123.

Given that there are no significant differences in the frequency of CD56<sup>neg</sup>CD16+ and CD56<sup>neg</sup>NKp80+ cells (Figure 7A), but the latter expressed significantly higher levels of Eomes (Figure 7B), we analyzed if NKp80 is inclusive of the CD56<sup>neg</sup>CD16+ subset. Results showed no significant differences in the frequency of CD16+NKp80<sup>-</sup>, CD16-NKp80+ and CD16+NKp80+ subsets within the CD56<sup>neg</sup> cells, and that half of the CD56<sup>neg</sup>NKp80+ NK cells also co-express CD16 (Figure 8A). Importantly, when the expression of Eomes was analyzed within these three subsets, we found that the frequency of Eomes<sup>+</sup> cells was very low in CD16+NKp80<sup>-</sup> cells and significantly higher in both CD16-NKp80+ and CD16+NKp80+ cells (Figure 8B). Moreover, while CD16+NKp80<sup>-</sup> cells included a significant frequency of CD123+ cells (50%), both CD16-NKp80+ and CD16+NKp80+ subsets comprised negligible levels of CD123+ cells (Figure 8C). Altogether, these results suggest that although CD16 and NKp80 do not completely identify the same CD56<sup>neg</sup> cells, NKp80 is more precise for the identification of CD56<sup>neg</sup> NK cells.

Years ago, it was shown that including CD7 as an additional marker to CD56 and CD16 was an effective method to accurately identify CD56<sup>neg</sup> NK cells [175,182]. Therefore, we compared the frequency of Eomes<sup>+</sup> cells using CD7 or NKp80 markers to identify the CD56<sup>neg</sup> NK cell subpopulation. There were no significant differences between CD7+CD56<sup>neg</sup>CD16+ and CD56<sup>neg</sup>NKp80+ cells in terms of Eomes expression, indicating that both strategies were equally effective for the identification of CD56<sup>neg</sup> cells in these specific experimental settings. However, when we only used the CD7 marker instead of using it in combination with CD16, the frequency of Eomes<sup>+</sup> cells in



the CD7+CD56<sup>neg</sup> population was much lower than in both CD7+CD56<sup>neg</sup>CD16+ and CD56<sup>neg</sup>NKp80+ cells (Figure 9A).

Next, we studied CD300a [62,183,184] and 2B4 (CD244) [185] receptors that are also expressed in NK cells, although not exclusively, as markers for the identification of the CD56<sup>neg</sup> NK cells. Results showed a lower frequency of Eomes+ cells both in CD56<sup>neg</sup>CD300a+ and in CD56<sup>neg</sup>2B4+ cells compared with CD56<sup>neg</sup>NKp80+ cells (Figure 9B, 9C). Moreover, the addition of an anti-CD123 mAb to the exclusion channel minimally increased the frequency of Eomes+ cells (Figure 9D). Altogether, our results demonstrate that NKp80 is the best cell surface marker to identify the CD56<sup>neg</sup> NK cell subset with a very high certainty and accuracy.

**CD56<sup>neg</sup>NKp80+ cells are expanded in HIV-infected people and patients with multiple myeloma.**

As CD56<sup>neg</sup> NK cells are infrequent in the peripheral blood of healthy donors, we next evaluated the accuracy of the NKp80 receptor to identify the expanded CD56<sup>neg</sup> NK cells in pathological conditions, such as HIV infection and MM. Although not always statistically significant, we observed a tendency to a higher frequency of both CD56<sup>neg</sup>CD16+ and CD56<sup>neg</sup>NKp80+ NK cells in HIV-infected subjects and MM patients compared to healthy donors (Figure 10A). No significant differences were noticed in the frequency of Eomes+ cells between CD56<sup>neg</sup>CD16+ and CD56<sup>neg</sup>NKp80+ subpopulations in untreated HIV-1 infected subjects. However, the frequency of Eomes+ cells was significantly higher in CD56<sup>neg</sup>NKp80+ than in CD56<sup>neg</sup>CD16+ cells in HIV-1 infected subjects under cART (Figure 10B). In addition, a higher frequency of Eomes+ cells within CD56<sup>neg</sup>NKp80+ cells in comparison with CD56<sup>neg</sup>CD16+ cells was also noticeable in MM patients (Figure 10C), in which CD56<sup>neg</sup> NK cell expansion is more similar to the one of HIV-1 infected subjects under cART (Figure 10A). Furthermore, we also studied the CD7 marker to identify CD56<sup>neg</sup> NK cells in HIV-1 infected subjects and we observed similar results to those obtained when we analyzed samples from healthy donors (Figure 9A, Figure 10B). These findings suggest that NKp80, as demonstrated in healthy donors, is a noteworthy alternative to CD16 as a marker to identify CD56<sup>neg</sup> NK cells also in disease.

**CD56<sup>neg</sup>NKp80+ cells showed increased effector functions than CD56<sup>neg</sup>CD16+ cells**

Although surface receptor profiling and proteomic analyses indicate that CD56<sup>neg</sup> NK cells have a phenotypic relationship to CD56<sup>dim</sup> ones [48], CD56<sup>neg</sup> NK cells have been described as functionally impaired compared to CD56<sup>dim</sup> NK cells [47,49,168,175]. However, others have proposed that these cells are skewed rather than dysfunctional [174]. These differences may be due to inaccurate identification of CD56<sup>neg</sup> NK cells using the CD16 marker. Therefore, we studied the effector functions of CD56<sup>neg</sup>CD16+ and CD56<sup>neg</sup>NKp80+ cells from healthy donors and HIV-1 infected subjects, by measuring degranulation (CD107a) [186] and production of TNF and IFN $\gamma$  after cytokines and K562 target cell stimulations [187].

First, we wanted to compare CD16 and NKp80 expression downregulation after NK cell stimulation. As observed in both pseudocolor dot plot graphs and histograms showing MFI, NKp80 was not significantly downregulated after K562 cell line and cytokine stimulation, while CD16 expression significantly decreased, mainly after stimulation with K562 cell line (Figure 11A, 11B). However, when NK cells were stimulated with the 721.221 cell line, we observed downregulation of both NKp80 and CD16 (Figure 11C). Moreover, we also performed a redirected lysis assay using the Fc receptor-bearing cell line P815. CD16 from NK cells were triggered by specific mAb and MOPC-21 isotype control was utilized as a negative control [62]. In this situation, NKp80 was not significantly downregulated, between stimulated and non-stimulated cells (Figure 11D).

In terms of functionality, we observed that CD56<sup>neg</sup>NKp80+ cells exhibited higher production of TNF and IFN $\gamma$  than CD56<sup>neg</sup>CD16+ cells in HIV-1 infected subjects under cART and that they showed a tendency to a higher production of both cytokines in untreated subjects (Figure 12A). Furthermore, in healthy donors, both cytokine production and the degranulation capability tended to be higher in the CD56<sup>neg</sup>NKp80+ cells than in CD56<sup>neg</sup>CD16+ cells (Figure 12B).

Finally, we compared the functionality of CD56<sup>dim</sup> and CD56<sup>neg</sup> NK cells. Very importantly, our results showed that, although CD56<sup>neg</sup> NK cells have lower effector functions than CD56<sup>dim</sup> NK cells (Figure 12C) in healthy donors and HIV-infected people, their functionality is much lower when we used the CD16-based gating strategy to identify CD56<sup>neg</sup> NK cells than when we used the NKp80-based gating strategy. Altogether, our results indicate that CD56<sup>neg</sup> NK cells, defined as viable CD3-CD19-

CD14-CD56<sup>neg</sup>NKp80+ cells, are significantly less dysfunctional than previously thought.

## DISCUSSION

It is of the utmost importance to correctly phenotype the different subpopulations of immune cells not only in healthy people, but also in disease situations. In the latter, variations in the frequency of cells subsets and in their effector functions, in comparison to healthy state, are frequently observed. These variations can help to understand the pathogenesis of diseases, and moreover, these changes can serve as biomarkers for the diagnosis, prognosis and/or to determine the efficacy of the treatment.

Some immune cell types are characterized by the expression of specific lineage cell surface markers. For example, T cells are CD3<sup>+</sup> while other cell types do not express CD3. However, a specific NK cell surface marker has not been described yet. In general terms, the minimum requirement to define circulating human NK cells is based in the expression of CD56 and the absence of the CD3 marker, since an important subpopulation of T cells expresses CD56 [188]. However, there are other cells, such as ILC3, which can also express CD56 [2,153,155,159]. On the other hand, according to the expression of CD56 and CD16, NK cells have been classified into four subpopulations: CD56<sup>bright</sup>, CD56<sup>dim</sup>, unconventional CD56<sup>dim</sup> and CD56<sup>neg</sup>[13,19,46,81,158]. Finally, although the Eomes transcription factor is also expressed in CD4<sup>+</sup> and CD8<sup>+</sup> T cells [189,190], it is used as a specific intracellular marker of NK cells within the ILCs.

CD56<sup>neg</sup> cells represent a very low percentage of NK cells in peripheral blood from healthy people [40,47,167]. However, in certain diseases there is a very significant expansion of this cell subpopulation [45,46,49,168,169,191]. To our knowledge, in previous publications, the expression of the CD16 marker have so far being used in all the gating strategies to identify the CD56<sup>neg</sup> NK cell subset. Some authors have made use of a strategy based on only three markers (CD3, CD56 and CD16) [40,150,168,169,192–194]. This strategy poses the risk of including other cell types that are not NK cells in the CD56<sup>neg</sup> subpopulation, such as non-classical monocytes, which express high levels of CD16 [195,196]. Other authors have used an exclusion channel that includes other lineage markers in addition to CD3 (T cells), such as CD19 (B cells), CD14 (monocytes) and CD4 (T cells and monocytes), so these cell types will not be included within the CD56<sup>neg</sup> cells [171–174,197–201]. However, even using these exclusion channels for the identification of the CD56<sup>neg</sup> subpopulation, other cells that are not NK cells could be included, such as basophils and pDCs, that are characterized, among others, by the

expression of CD123 [177–180]. In fact, our results demonstrate that adding an anti-CD123 mAb to the exclusion channel significantly increases the number of NK cells (Eomes+) within the CD56<sup>neg</sup> subpopulation (Figure 7E). Importantly, we observed differences in the percentage of Eomes+ cells within CD56<sup>neg</sup>CD16+ NK cells between HIV-1 infected subjects and HIV-1 infected subjects under cART, as in the latter the frequency of CD56<sup>neg</sup>CD16+ cells was lower (Figure 10B). The differences between patients groups could be explained because the relative frequency of CD56<sup>neg</sup>CD16+ non-NK cells (Eomes-) is lower in untreated patients due to a higher expansion of the CD56<sup>neg</sup>CD16+ NK cells (Eomes+) [49,168,169]. Thus, CD16 could only serve to identify CD56<sup>neg</sup> NK cells in certain pathological conditions in which this subset is very highly expanded.

A progress to better identify CD56<sup>neg</sup> NK cells consists in a gating strategy that, in addition to the exclusion channel (CD3, CD14 and CD19), includes the lymphocyte specific marker CD7, which among other things, showed a high Eomes expression [48,167,175,182]. However, it is important to note that CD7 is also expressed and used to identify ILC2 [202]. Very significantly, our data demonstrate that the percentage of NK cells (Eomes+) is the same in CD7+CD56<sup>neg</sup>CD16+ cells and in CD56<sup>neg</sup>NKp80+ cells (Figure 9A). However, combining the CD7 and CD16 markers to identify the CD56<sup>neg</sup> NK cell subset could be an obstacle in certain situations, especially due to the unstable expression of the CD16 receptor after cryopreservation and cell stimulation. Also, there is a need for an additional antibody included in the panel and an extra flow cytometer detector, which can be very relevant in many laboratories that do not have such advanced and sophisticated equipment.

The cryopreservation of biological samples is very advantageous in certain circumstances, such as when the samples are collected in locations far from the place where cytometry studies are performed. Cryopreservation also provides an additional benefit, since samples can be analyzed in large batches, minimizing overall analytical variability. This is especially important for studies in which the collection occurs over a long period of time or a large number of samples are obtained. However, cryopreservation also has drawbacks. It is well known that the expression of certain receptors, including CD16, is downregulated with freezing [165] (Figure 6). Therefore, when frozen samples are used, the gating strategy for the identification of CD56<sup>neg</sup> NK cells based on CD16 expression is probably not the most appropriate, thus, the results obtained on studies that

have been conducted with cryopreserved samples [40,167,199,201,203] should be carefully considered. Following this, we have shown that the expression of NKp80 is not significantly modulated during cryopreservation (Figure 6). Therefore, NKp80 is a suitable marker for the study of CD56<sup>neg</sup> NK cells in frozen samples. However, NKp80 is not a specific marker of NK cells. In fact, a minor subset of CD8+ T cells also express it [204]. Nevertheless, using an exclusion channel that includes CD3, such as the one we used in this study, these NKp80+CD8+ T cells will be not selected within the CD56<sup>neg</sup> NK cell subset.

Finally, it has been documented for a long time that CD16 expression is downregulated after activation of NK cells with cytokines, target cells, ADCC and after stimulation with compounds such as phorbol myristate acetate (PMA) [160,162–164]. Therefore, a gating strategy based on CD16 expression to analyze the effector functions of the CD56<sup>neg</sup> NK cells is not very appropriate. Especially, in those situations when the stimuli, such as PMA and ADCC, induce a very deep downmodulation of CD16 [160,162,164,205]. Thus, the results of functional studies of CD56<sup>neg</sup> NK cells identified with a CD16-based strategy should also be carefully considered [168,174,175,199]. Related to NKp80, Klimosch et al. have described that NK cells stimulated with PMA or IL-2+IL-12+IL-18 induced the downregulation of this receptor after 24 hours of stimulation [206]. However, in our hands, and in response to stimulation with K562 target cells and IL-12+IL-18, the expression of NKp80 is not significantly altered (Figure 11). This difference could be due to, among others, the different cell stimulation protocols used in both studies. Of note, the expression of NKp80 is significantly downregulated after 721.221 cell line stimulation (Figure 11). The activation-induced C-type lectin (AICL) is a myeloid-specific receptor expressed by monocytes, macrophages and granulocytes, and has been identified as ligand of NKp80. However, AICL surface expression was not detectable on the 721.11 and K562 cell lines [207]. Thus, we propose NKp80 as a suitable marker for the study of the effector functions of CD56<sup>neg</sup> NK cells. In fact, our results show that when we use NKp80 in the gating strategy, CD56<sup>neg</sup> cells have greater effector functions compared with CD56<sup>neg</sup> cells identified with CD16 (Figure 12).

In conclusion, in this study we have demonstrated that NKp80 is a more precise marker than CD16 in order to identify CD56<sup>neg</sup> NK cells and that it is not downregulated after sample cryopreservation or cell activation. Importantly, using the NKp80 marker for the identification, we have demonstrated that the effector functions of CD56<sup>neg</sup> NK cells are

not as diminished as previously thought. Thus, an NKp80-based strategy for the better identification and re-characterization of this NK cell subset could help to clarify its function and relevance in health and disease.

## **CHAPTER II**

### **NK cell reconstitution after autologous hematopoietic stem cell transplantation in multiple myeloma patients**

Parts of this chapter have been published in:

Orrantia A, Terrén I, Astarloa-Pando G, González C, Uranga A, Mateos-Mazón JJ, García-Ruiz JC, Riñón M, Rey M, Pérez-Fernandez S, Zenarruzabeitia O, Borrego F. NK Cell Reconstitution After Autologous Hematopoietic Stem Cell Transplantation: Association Between NK Cell Maturation Stage and Outcome in Multiple Myeloma. *Front Immunol.* 2021 Oct 5;12:748207. doi: 10.3389/fimmu.2021.748207



## INTRODUCTION

Once we developed the strategy that leads to proper identification of not only CD56<sup>bright</sup> and CD56<sup>dim</sup> NK cells, but also the CD56<sup>neg</sup> NK cell subset, we were able to study the NK cell pool reconstitution after autoHSCT in MM patients.

As explained before, autoHSCT is a worldwide-established treatment option for a diverse group of hematological malignances, including MM. In fact, high-dose chemotherapy followed by autoHSCT is considered the standard of care for transplant-eligible MM patients. MM is a treatable but incurable plasma cell disorder characterized by an uncontrollable proliferation of these cells that accumulate in the bone marrow and secrete either an entire immunoglobulin (usually IgG or IgA) and light chain (kappa or lambda) or only immunoglobulin light chains. MM is known to arise from an asymptomatic pre-malignant stage termed monoclonal gammopathy of undetermined significance or MGUS [208]. Moreover, MM is a heterogeneous disease whose major clinical manifestations are bone lesions, anemia, hypercalcemia, renal failure, and an increased risk of infections [209].

In general, the treatment procedure for MM patients eligible for autoHSCT consists in induction, conditioning, transplant and post-transplant consolidation and maintenance therapies. During induction therapy, immunomodulatory drugs (e.g lenalidomide (R), thalidomide (T) and cyclophosphamide (C)) and proteasome inhibitors (e.g bortezomib (V) and carfilzomib (K)) are used along with steroids (e.g. dexamethasone (D)) to reduce tumor burden. Then, HSC are harvested prior to conditioning regimen for which high-dose melphalan is usually used. After autoHSCT is completed, consolidation regimen to further deepen the response and improve long-term outcomes and maintenance regimen to prevent relapse and prolong survival can be administered [208–211].

As mentioned in the introduction section, an early lymphocyte recovery, and more importantly, a rapid reconstitution of NK cells affect the outcome of MM patients that undergo autoHSCT (Table 2) [115,123]. In alloHSCT, NK cells play a key role mediating GvT effect due to KIR-HLA class I mismatch [212]. Moreover, CMV reactivation after alloHSCT is followed by an expansion of adaptive NK cells [213], which in turn has an impact in patients outcome. Some years ago, it was observed that higher expansion of CD3–CD56<sup>dim</sup>CD57+EAT-2– adaptive NK cells was associated with better disease-free survival in patients with different hematological malignances transplanted with HLA

matched CMV negative umbilical cord blood units [147]. In a study conducted previously by the same group, they found that in alloHSCT recipients, CD56<sup>dim</sup>CD57+NKG2C+ NK cells preferentially expanded after CMV reactivation and that expansion of this subset at 6 months post-transplant was directly associated with lower 2-year relapse rates [148]. Very recently, it was also observed that an early expansion of CD56<sup>dim</sup>CD57+NKG2C+ adaptive NK cells was associated with lower relapse in MM but not in lymphoma patients undergoing autoHSCT [146]. In this case, the adaptive NK cell expansion occurred despite the absence of clinical CMV reactivation, which is a rare event in autoHSCT settings.

As extensively described in the introduction section, several groups had performed analysis of NK cell subsets and their phenotype after autoHSCT in different cohorts of patients [142–144]. However, apart from the aforementioned study on CD56<sup>dim</sup>CD57+NKG2C+ adaptive NK cells and the role of KIR-HLA class I mismatch, there is few data regarding the influence of other NK cell subsets and other aspects of NK cells phenotype and function in the outcome after autoHSCT. For that reason, in this second chapter, using multiparametric flow cytometry-based procedures we performed an extensive phenotypic and functional analysis of different NK cell subsets during their reconstitution after autoHSCT in MM patients. In addition, we examined the impact of the frequency of the different NK cell subsets and their phenotype on post-transplant outcomes.

## **METHODS**

### **Patients' characteristics and study design**

54 patients from Cruces University Hospital and Donostia University Hospital, who suffered from MM and received autoHSCT were included in the study. Clinical data of the patients can be found in Table 5. Blood samples were taken from patients at six different time points. Sample 1 (S1) was collected the day before the start of the conditioning treatment; sample 2 (S2) was collected after leukocyte recovery (>1000 leukocytes/ $\mu$ L) (median: 13 days after autoHSCT, range: 10-25 days); sample 3 (S3) was collected 30 days after cell infusion; sample 4 (S4) was collected 100 days after cell infusion; sample 5 (S5) was collected 180 days after cell infusion and sample 6 (S6) was collected 365 days after cell infusion. Sample collection was carried out through the Basque Biobank for Research (<http://www.biobancovasco.org>), which complies with the quality management, traceability and biosecurity, set out in the Spanish Law 14/2007 of Biomedical Research and in the Royal Decree 1716/2011. The study was approved by the Basque Ethics Committee for Clinical Research (BIO14/TP/003 and PI+CES+INC-BIOEF 2017-03). All subjects provided written and signed informed consent in accordance with the Declaration of Helsinki.

### **Sample preparation**

PBMCs were obtained from blood samples. PBMCs were isolated by Ficoll (GE Healthcare) density gradient centrifugation, cryopreserved in heat-inactivated FBS (GE Healthcare Hyclone) containing 10% DMSO (Thermo Scientific Scientific) and stored in liquid nitrogen until they were used. Plasma samples were stored at  $-80^{\circ}\text{C}$  until they were used.

Prior to flow cytometry experiments, cryopreserved PBMCs were thawed at  $37^{\circ}\text{C}$  in a water bath and washed twice with RPMI 1640 medium supplemented with L-Glutamine (Lonza). Then, cells were incubated for 1 hour at  $37^{\circ}\text{C}$  and 5%  $\text{CO}_2$  with 10U DNase (Roche) in R10 medium (RPMI 1640 medium containing GlutaMAX from Thermo Fisher Scientific, 10% FBS and 1% Penicillin-Streptomycin from Thermo Fisher Scientific). Afterwards, cells were washed once, resuspended in NK cell culture medium (RPMI 1640 medium containing GlutaMAX, 10% FBS, 1% Penicillin-Streptomycin, 1%

MEM Non-Essential Amino Acids Solution and 1% Sodium Pyruvate, both from Thermo Fisher Scientific), filtered using 70µm cell strainers and counted just before further used.

### **NK cell absolute number determination**

The absolute number of NK cells was measured in each blood sample at the Immunology Services of Cruces University Hospital and Donostia University Hospital. NK cells were defined as CD45+, CD3-, CD56+ and/or CD16+. The following clinical grade fluorochrome conjugated mAbs were used: FITC anti-CD16 (CLB/FcGran1), PE anti-CD56 (MY31), PerCP-Cy5.5 anti-CD3 (SK7) and V450 anti-CD45 (2D1) from BD Biosciences. The absolute number per µL of blood was calculated based on the following formula: (percentage of NK cells within lymphocyte gate X absolute number of lymphocytes) / 100. The absolute number of lymphocytes was obtained from the full blood count analysis.

### **Phenotypic analysis**

PBMCs were first stained with LIVE/DEAD Fixable Aqua Dead Cell Stain Kit (Invitrogen) reagent to exclude dead cells, following manufacturer's recommendations. Afterwards, cells were washed with PBS containing 2.5% BSA (Sigma-Aldrich) and extracellular staining was performed. For that, cells were incubated for 30 minutes on ice in the dark with the following fluorochrome conjugated mAbs: BV421 anti-CD56 (NCAM 16.2), BV510 anti-CD3 (UCHT1), BV510 anti-CD14 (MφP9), BV510 anti-CD19 (SJ25C1) from BD Bioscience; PE anti-NKG2C (134591) from R&D Systems; PE-Vio770 anti-NKp80 (4A4.D10), APC-Vio770 anti-CD57 (REA769) and APC-Vio770 anti-CD69 (REA824) from Miltenyi Biotec and APC anti-NKG2A (Z199) from Beckman Coulter. Cells were then washed again with PBS containing 2.5% BSA and fixed and permeabilized prior to intracellular staining. Two different intracellular staining protocols were used. For "phenotype panel 1" (Table 6), PBMCs were fixed by incubating them with 4% PFA (Sigma-Aldrich/Merck) for 15 minutes on ice. Next, cells were washed twice with PBS containing 2.5% BSA and permeabilized by incubating with 1x BD Perm/Wash Buffer (BD Bioscience) for 15 minutes at RT. Then, cells were incubated for 30 minutes on ice with FITC anti-FcεRIγ (Merck) antibody. On the other hand, for "phenotype panel 2" (Table 6), cells were fixed and permeabilized with Foxp3/Transcription Factor Staining Buffer Set (eBioscience) following manufacturer's

recommendations. Then, cells were incubated for 30 minutes at RT with the following mAbs: FITC anti-Ki67 (20Raj1, Invitrogen) and PE anti-Granzyme B (GB11, BD Bioscience). In both intracellular staining protocols, after the incubation with the corresponding antibodies, cells were washed with the corresponding permeabilization buffer and resuspended in PBS. Samples were then acquired in a MACSQuant Analyzer 10 flow cytometer (Miltenyi Biotec). Flow cytometry panels used to study NK cell phenotype are shown in Table 6.

### **Functional assay**

After thawing and counting the cryopreserved PBMCs, cells in NK cell culture medium were plated at  $0.5 \times 10^6$  cells/well in 48-well plates. PBMCs were then primed with 10 ng/mL of rhIL-15 (Miltenyi Biotec) and cultured for 20-21 hours. Then, for cytokine stimulation, 10 ng/mL of rhIL-12 (Miltenyi Biotec) and 50 ng/mL of rhIL-18 (MBL International) were also added in addition to rhIL-15. For target cell stimulation, 721.221 cells were added after the 20-21 hours of culture with rhIL-15 at Effector:Target (E:T) 1:1 ratio ( $0.5 \times 10^6$  PBMCs and  $0.5 \times 10^6$  721.221 cells). Then, IL-12+IL-18 and 721.221 stimulated PBMCs were cultured for 5 additional hours. PE anti-CD107a (REA792, Miltenyi Biotec) was added at the start of the co-culture period to all the conditions and GolgiStop (monensin) and GolgiPlug (brefeldin A) protein transport inhibitors (BD Biosciences) were added after 1 hour for the rest of the incubation time following manufacturer's protocol. Afterwards, viability and extracellular staining was performed as explained in the phenotypic analysis section. Next, cells were fixed with 4% PFA and permeabilized using 1x BD Perm/Wash Buffer. Then, cells were incubated for 30 minutes on ice with PerCP-Cy5.5 anti-IFN $\gamma$  (B27, BD Biosciences) and APC anti-TNF (MAb11, BioLegend). Samples were acquired in a MACSQuant Analyzer 10 flow cytometer. The flow cytometry panel used to study NK cell functionality is shown in Table 6. The percentage of NK cells positive for CD107a, IFN $\gamma$  and TNF was calculated after subtracting the non-stimulus condition. 721.221 cell line was cultured in NK cell medium supplemented with 5  $\mu$ g/mL of Plasmocin (InvivoGen). 721.221 cell line was routinely tested for mycoplasma infection with Venor GeM Classic detection kit (Minerva Biolabs).

### Measurement of IL-15 levels

For the measurement of IL-15 plasma levels, the Human IL-15 Quantikine ELISA Kit (R&D Systems) was used, following manufacturer's recommendations. IL-15 plasma levels were measured in S1, S2, S3 and S4 patients' samples. The optical density was determined using Varioskan Flash fluorimeter (Thermo Fisher Scientific) set to 450nm.

### Statistics

Flow cytometry data were analyzed using FlowLogic v.7.3 (Inivai Technologies) software. GraphPad Prism v.9 was used for graphical representation and statistical analysis. Data were tested for normal distribution with Shapiro-Wilk normality test. If data were normally distributed, Student's t test for paired values was used to determine significant differences. Non-normal distributed data were compared with Wilcoxon matched-pairs signed rank test. Statistical analysis were done by comparing S2 with the rest of the samples. Data were represented as boxplots with the median and 25–75th percentiles, as violin plots with the median and quartiles or as bar plots as mentioned in each figure legend.

For bivariate analysis, normality of continuous variables was tested with Shapiro-Wilks test. Mean and standard deviation (SD) was presented when the variable followed a normal distribution or median interquartile range otherwise. The Student's t test or Mann-Whitney U test were used to compare continuous variables between groups. Qualitative variables were compared using the Chi-square or Fisher exact test. Correlation plots between variables were calculated and visualized as correlograms. Spearman's Rank Correlation coefficient was indicated by square size and heat scale. Bivariate analysis was performed using Cox proportional hazard regression models. Survival curves were estimated with Kaplan-Meier method and compared by log-rank test. All the analysis were performed with R (version 4.0.4): A language and environment for statistical computing. R Foundation for Statistical Computing, Vienna, Austria.

Data from ELISA experiments were processed following manufacturer's recommendations. GraphPad Prism software was used to fit the standard curve with nonlinear regression and log-log line model.

## RESULTS

### **NK cells recovery is achieved 30 days after autoHSCT.**

We first studied NK cell recovery of 54 MM patients after autoHSCT. Although not significant, a decrease in the absolute number of NK cells was noticed from S1 to S2 (median S1: 108.2 cell/ $\mu$ l (range: 1 – 406 cell/ $\mu$ l) vs S2: 69.00 cell/ $\mu$ l (range: 4 - 806.5 cell/ $\mu$ l)). Afterward, a significant increase was observed at S3, followed by a decrease at S4. The absolute number of NK cells was maintained at the same levels after that; although, the values were significantly higher than what was observed in S1 and S2 (Figure 13A). In contrast to previous studies [122,123], no association was found between the absolute number of NK cells at S2 and the patients' OS and PFS (Figure 13B). Moreover, no differences were observed in the absolute number of NK cells at S2 if the sample was collected <13 days or  $\geq$ 13 days after the autoHSCT (Figure 13C). Thus, these results suggest that the recovery of NK cells is not completely achieved until 30 days after autoHSCT (S3).

### **NK cell subset distribution is altered at leukocyte recovery.**

We next studied the distribution of different NK cell subsets. NK cells were identified, based on the gating strategy developed in Chapter I, as viable CD3-/CD14-/CD19-/NKp80+ cells. Then, based on the expression of the CD56 marker, two major NK cell subsets were defined: CD56<sup>bright</sup> and CD56<sup>dim</sup> (Figure 14A). CD56<sup>dim</sup> NK cells were the main subset at all time points. However, their frequency significantly decreased at S2, while the frequency of CD56<sup>bright</sup> greatly increased. Nevertheless, this redistribution of NK cell subsets was not maintained over time (Figure 13D). We observed no differences in terms of the frequency of CD56<sup>bright</sup> and CD56<sup>dim</sup> NK cells at S2 between patients having a leukocyte recovery time period of <13 days vs  $\geq$ 13 days suggesting that subset redistribution was independent of the time needed for leukocyte recovery (Figure 13E). In addition, we studied the distribution of CD56<sup>neg</sup> NK cells. As shown in Chapter I, this subset was expanded in MM patients (Figure 10C). In the autoHSCT setting, the frequency of CD56<sup>neg</sup> NK cells significantly dropped at S2 and showed variations over the studied period (Figure 13D). These results suggest that NK cell subset distribution is altered at leukocyte recovery (S2) but, in general, resembles pre-transplant distribution 30 days after autoHSCT (S3).

We next used CD57, NKG2C and FcεRγ markers to study the different adaptive subpopulations within CD56<sup>dim</sup> NK cells and within CD56<sup>dim</sup>CD57<sup>+</sup> NK cells (Figure 14B). Of note, 88.9% of patients were CMV<sup>+</sup> prior to autoHSCT (Table 5). First, we determine the frequencies of FcεRγ<sup>-</sup> and NKG2C<sup>+</sup> (Figure 15A) and CD57<sup>+</sup>FcεRγ<sup>-</sup>, and CD57<sup>+</sup>NKG2C<sup>+</sup> (Figure 15B) adaptive NK cell subpopulations. Results showed that adaptive NK cells lacking the expression of FcεRγ were more abundant than the NKG2C<sup>+</sup> subset (Figure 15A, B). In addition, the percentage of FcεRγ<sup>-</sup> adaptive cells significantly decreased at S2 and it was maintained over time after that (Figure 15A, B). In contrast, no significant differences in the frequency of NKG2C<sup>+</sup> NK cells were noticed from S1 to S3. However, an expansion of these subsets was observed at S4 and their frequency continued elevated thereafter (Figure 15A, B). Next, we analyzed the co-expression of NKG2C and FcεRγ markers identifying four different populations as it can be seen in Figure 14 B. NKG2C-FcεRγ<sup>+</sup> population represents conventional NK cells and was not included in the analysis. Regardless CD57 expression, the main population at all time points were those with the NKG2C-FcεRγ<sup>-</sup> phenotype. Moreover, the frequency of both CD57<sup>+</sup>NKG2C-FcεRγ<sup>-</sup> and NKG2C-FcεRγ<sup>-</sup> populations was reduced at S2 and it maintained low after that (Figure 15C). In contrast, the frequency of NKG2C<sup>+</sup>FcεRγ<sup>+</sup> and CD57<sup>+</sup>NKG2C<sup>+</sup>FcεRγ<sup>+</sup> was not significantly altered immediately after autoHSCT (S2), while the frequency of NKG2C<sup>+</sup>FcεRγ<sup>-</sup> and CD57<sup>+</sup>NKG2C<sup>+</sup>FcεRγ<sup>-</sup> was reduced at S2 and expanded at S4 (Figure 15C). These results suggest a different reconstitution pattern among adaptive NK cell populations after autoHSCT.

**NK cells exhibit an immature phenotype at leukocyte recovery that last for more than 30 days after autoHSCT.**

As the frequency of CD56<sup>bright</sup> NK cells notably increases at leukocyte recovery, and these cells are considered more immature than CD56<sup>dim</sup> NK cells [84], we next studied the NK cell differentiation and maturation status using NKG2A and CD57 markers. As explained in the Introduction section, while CD57 has been described to be expressed by terminally differentiated NK cells, NKG2A is expressed in earlier differentiation stages (Figure 3) [103–105]. As others have previously reported [144], the frequency of NKG2A<sup>+</sup> NK cells increased from S1 to S2, decreased at S3 and reached pre-transplant levels at S4 (Figure 16A). In contrast, CD57<sup>+</sup> NK cells behave the opposite way: their frequency decreased at S2, and is maintained low at S3 and increased again at S4 (Figure 16B). The variations observed in the frequency of NKG2A<sup>+</sup> and CD57<sup>+</sup> cells were mainly due to an increment



in the frequency of CD56<sup>dim</sup>NKG2A<sup>+</sup> and CD56<sup>neg</sup>NKG2A<sup>+</sup> NK cells, and a decrease in the frequency of CD56<sup>dim</sup>CD57<sup>+</sup> NK cells respectively (Figure 16A, B). Surprisingly, an expansion of CD56<sup>bright</sup> NK cells expressing CD57 was observed at leukocyte recovery (S2) (Figure 16B). As CD57 expression is linked to cellular maturity in NK cells, CD56<sup>bright</sup> NK cells are not expected to express CD57 [103].

During the final steps of differentiation, NK cells lose the expression of NKG2A while acquire CD57 (Figure 3) [104]. Therefore, we analyzed the co-expression of both markers after autoHSCT identifying four different populations. We found that NKG2A<sup>+</sup>CD57<sup>-</sup> NK cells were the main subset at S2, but over time, the frequency of NKG2A<sup>+</sup>CD57<sup>+</sup> NK cells gradually increased, turning out to be the predominant subset after day 180 post-autoHSCT (S5). Moreover, the percentage of NKG2A<sup>-</sup>CD57<sup>+</sup> NK cells also gradually augmented after the initial decrease at S2 (Figure 16C). When CD56<sup>bright</sup>, CD56<sup>dim</sup> and CD56<sup>neg</sup> NK cell subsets were separately analyzed, we found that while within CD56<sup>bright</sup> NK cells, NKG2A<sup>+</sup>CD57<sup>-</sup> cells were the most abundant subset at all time points, CD56<sup>dim</sup> NK cells were mostly NKG2A<sup>+</sup>CD57<sup>-</sup> at leukocyte recovery (S2) and NKG2A<sup>+</sup>CD57<sup>+</sup> after day 100 post-autoHSCT (S4). In contrast, the majority of CD56<sup>neg</sup> NK cells were NKG2A<sup>-</sup>CD57<sup>-</sup> during all the studied period (Figure 16C). Together, these data reveal that NK cells have a more immature phenotype at leukocyte recovery (S2), as demonstrated by the increment in the frequency of NKG2A<sup>+</sup>CD57<sup>-</sup> cells, and that this phenotype last for more than 30 days after autoHSCT (S3) (% of NKG2A<sup>+</sup> cells in S1 vs S3: p<0.0001; S1 vs S4: ns; S1 vs S5: ns; and S1 vs S6: ns; % of CD57<sup>+</sup> cells in S1 vs S3: p = 0.0468; S1 vs S4: ns; S1 vs S5: ns; and S1 vs S6: p = 0.0139; % of NKG2A<sup>+</sup>CD57<sup>-</sup> cells in S1 vs S3: p<0.0001; S1 vs S4: ns; S1 vs S5: ns; and S1 vs S6: p = 0.0072; % of NKG2A<sup>+</sup>CD57<sup>+</sup> cells in S1 vs S3: ns; S1 vs S4: ns; S1 vs S5: ns; and S1 vs S6: p = 0.0088; % of NKG2A<sup>-</sup>CD57<sup>+</sup> cells in S1 vs S3: p <0.0001; S1 vs S4: ns; S1 vs S5: ns; and S1 vs S6: ns; % of NKG2A<sup>-</sup>CD57<sup>-</sup> cells in S1 vs S3: p <0.0001; S1 vs S4: p = 0.0487; S1 vs S5: ns; and S1 vs S6: ns).

### **NK cell activation, cytotoxic potential and proliferation are modulated during NK cell reconstitution and differ among NK cell subsets.**

Next, we further analyzed the phenotype of NK cells during cell reconstitution after autoHSCT. For that, we studied the activation status and the cytotoxic potential of NK cells. The analysis of the expression of CD69, an early activation marker [214], showed

that the frequency of CD69+ NK cells slightly decreased at leukocyte recovery (S2), and not significant differences were noticed after that (Figure 17A). This decrease might be principally due to a lower percentage of CD56<sup>bright</sup> NK cells expressing CD69 at S2 as we did not observed any significant difference in the percentage of CD56<sup>dim</sup>CD69+ and CD56<sup>neg</sup>CD69+ cells immediately after autoHSCT (S2) (Figure 17A). On the other hand, we evaluated the cytotoxic potential of NK cells after autoHSCT by assessing the expression of granzyme B. The expression of this marker, measured as MFI, did not differ on total NK cells from S1 to S2, but it was significantly incremented at S3. When the three NK cell subsets were separately analyzed, we observed that the levels of granzyme B on CD56<sup>bright</sup> NK cells were greatly increased at S2, maintained elevated at S3 and gradually reduced thereafter. Conversely, CD56<sup>dim</sup> NK cells expressed less granzyme B at S2 than at S1, but the expression increased again at S3 been higher than at pre-autoHSCT. In the case of CD56<sup>neg</sup> NK cells, a reduced expression was also observed at S2, and the expression was gradually incremented after that (Figure 17B). These data suggest that the activation status and the cytotoxic potential is different among the three studied NK cell subsets during NK cell reconstitution. Moreover, these data showed that the cytotoxic potential of CD56<sup>bright</sup> NK cells is incremented after autoHSCT.

Finally, we used the Ki67 nuclear protein, which is expressed during cell cycle but is absent when cells exit cell cycle and enter into quiescence, as a marker to study NK cell proliferation [215]. Results showed that there was a dramatic increase in the frequency of Ki67+ NK cells at leukocyte recovery (S2) that was not found at other time point. Moreover, CD56<sup>bright</sup>, CD56<sup>dim</sup> and CD56<sup>neg</sup> NK cell subsets also exhibited an increase in the percentage of Ki67+ cells at S2 (Figure 17C). However, the frequency of cells positive for the Ki67 marker significantly decreased thereafter, although CD56<sup>neg</sup> NK cells showed an elevated percentage of Ki67+ at S3. Therefore, these data suggest that NK cells exhibit a high proliferation rate immediately after autoHSCT (S2) while the majority of them enter into a quiescent state 30 days after autoHSCT (S3).

### **NK cells are functional after autoHSCT.**

Once phenotypic features of NK cells during their reconstitution after autoHSCT were analyzed, we next studied their functional capacities. For that, we examined degranulation and cytokine production by measuring CD107a and TNF, respectively, after stimulation with the 721.221 cell line and IFN $\gamma$  production after IL-12+IL-18 stimulation. Due to the

low number of cells we had from each patient, especially at S2, complete functional analysis of all the samples was only possible in one patient. However, for our analysis, we also included patients in which functional analysis was carried out at least in the first three samples (S1, S2, S3) as there were the most interesting time points (n=5). Results revealed that, in comparison to CD56<sup>dim</sup> NK cells, CD56<sup>bright</sup> NK cells exhibited a trend towards an increase in both cytokine production and degranulation in all time points (Figure 18A). When total NK cells were analyzed, no statistically significant differences were observed in the effector functions during NK cell reconstitution. Furthermore, similar results were obtained when CD56<sup>bright</sup> and CD56<sup>dim</sup> NK cells were separately analyzed (Figure 18B). Thus, as others have previously described [126,144], these data suggest that the effector functions of NK cells were recovered early after autoHSCT.

**Elevated IL-15 plasma levels at leukocyte recovery correlates with the number, proliferation capacity and the cytotoxic potential of NK cells after autoHSCT.**

IL-15 is a cytokine that plays an important role not only in proliferation, cytotoxic activity and cytokine production of NK cells, but also in their development and differentiation [70,216]. Some years ago, Porrata et al. showed that IL-15 levels were highly incremented after autoHSCT and that IL-15 levels at day 15 after autoHSCT affect survival of NHL patients through NK cell recovery [124]. For this reason, we determined plasma levels of IL-15 at different time points (S1, S2, S3 and S4) in our cohort of MM patients and tried to correlate them with patient's outcome after autoHSCT. As expected, results showed a large increment of IL-15 levels at S2 (Figure 19A). Moreover, patients with  $\leq 13$  days between autoHSCT and S2 showed significantly higher levels of IL-15 at S2 than those with  $> 13$  days (Figure 19B). Nevertheless, we were unable to find an association between IL-15 levels at S2 and OS and PFS of these patients (Figure 19C).

The expression of NK cell receptors is modulated by different environmental factors and thus, the singular cytokine milieu after autoHSCT may affect NK cell phenotype. For this reason, we performed correlation analysis between IL-15 levels at different time points and all variables studied by flow cytometry to try to find an association between IL-15 plasma levels and the phenotype of NK cells (Figure 20A). Interestingly, we found that IL-15 levels at S2 negatively correlated with absolute number of NK cells at S2. However, a positive association was observed at S2 between IL-15 levels and the percentage of Ki67+ NK cells and CD69+ NK cells. On the other hand, we found a negative correlation

between IL-15 levels and the expression of granzyme B on NK cells at S2 (Figure 20A-E). Then, we categorized the patients in two groups based on their IL-15 plasma levels at S2 (median: 17.45pg/mL, range: 3.96-52.83pg/mL): patients having IL-15 plasma levels of  $\leq 17.44$  pg/mL and patients with  $>17.45$  pg/mL of IL-15 in plasma. As expected, we observed that patients that had higher IL-15 plasma levels showed significantly lower NK cell absolute numbers, significantly higher frequency of Ki67+ NK cells and expressed less granzyme B in NK cells at S2 (Figure 20F). However, no significant differences were noticed in the percentage of CD69+ cells between groups (Figure 20F). Therefore, these results suggest that IL-15 play a major role in NK cell proliferation capacity and also affect the cytotoxic potential and NK cell numbers after autoHSCT.

**The differentiation and maturation status of NK cells at 30 and 100 days after autoHSCT associates with the clinical outcome of multiple myeloma patients.**

As NK cell count at 15 days post-autoHSCT has been defined as an independent predictor for survival after autoHSCT [122], we finally investigated whether a specific NK cell phenotype was associated with the clinical outcome of MM patients after autoHSCT. As shown in Table 5, at the time of the autoHSCT, 24.1% of MM patients were in complete remission (CR), 31.5% were in partial response (PR) and 40.7% were in very good partial response (VGPR). Moreover, at 100 days post-autoHSCT (S4), 46.3% of MM patients were in CR, 16.7% were in PR and 35.2% were in VGPR, and 53.7% received maintenance or conditioning regimen after autoHSCT. From the 54 patients included in this study, 29 patients experience disease progression (53.7%) and 9 patients died (16.7%) during the studied period (60 months). Thus, we performed bivariate analysis for PFS and OS and the phenotypic data generated in the present study. Moreover, as MM is an incurable disease, we also performed analysis regarding the time to next treatment (TTNT). However, we did not find any association between the phenotypic data and OS, PFS or TTNT in the bivariate analysis (data not shown). Each phenotypic variable was then dichotomized into high ( $>66^{\text{th}}$  percentile) and middle/low ( $\leq 66^{\text{th}}$  percentile) groups for further analysis. However, we did not obtain any significant result when bivariate analysis was done with dichotomized variables (data not shown).

Next, we carried out survival analysis with the dichotomized phenotypic variables and we observed statistically significant differences in terms of PFS when the frequency of terminally differentiated NKG2A-CD57+ NK cells at S3 and S4 was taken into account.

In addition, we also observed differences in terms of TTNT when the frequency of NKG2A-CD57+ NK cells at S4 was analyzed. Specifically, we noticed higher PFS in patients in the middle/low percentile group vs high percentile group of NKG2A-CD57+ NK cells at S3 and at S4: median PFS 44.4 vs 26.6 months in both S3 (HR=0.45; 95% CI=0.20-0.99; p=0.042), (Figure 21A) and S4 (HR=0.36; 95% CI=0.15-0.86; p=0.016) (Figure 21B). Furthermore, patients in the middle/low percentile group of NKG2A-CD57+ NK cells also exhibited a longer TTNT at S4; median TTNT 49.2 vs 37.2 months (HR=0.41; 95% CI=0.17-0.98; p=0.039) (Figure 21C). Therefore, these data suggest that the differentiation and maturation stage of NK cells at +30 (S3) and +100 (S4) days after autoHSCT affects the clinical outcome of MM patients and that a lower frequency of mature and terminally differentiated NK cells is associated with protection against disease progression after autoHSCT in these patients.

## DISCUSSION

In this second chapter, we have examined the reconstitution of the NK cell repertoire in patients with MM who had undergone autoHSCT by analyzing different NK cell subsets, their phenotype and functionality, in order to determine an association with the clinical outcome post-autoHSCT of these patients. We have demonstrated that there is a redistribution of NK cell subsets and that NK cells express an immature phenotype early after transplantation (S2). Moreover, NK cells seem to be completely functional and present an elevated proliferation capacity. We have documented significantly elevated IL-15 plasma levels when patients reached  $>1000$  leucocytes, that correlate with the number, proliferation capacity and cytotoxic potential of NK cells at this time point. Importantly, to our knowledge, we have revealed a previously undescribed association between the differentiation degree of NK cells at 30 and 100 days after autoHSCT and the clinical outcome of MM patients.

NK cells have been described to be the first lymphocyte subset reaching normal blood cell counts and functionality after autoHSCT. One month after transplantation NK cell count increases, reaching healthy donor levels, but then decreases again until 6 months after autoHSCT [123]. Moreover, a fast NK cell recovery at 1 month after autoHSCT has been associated with a prolonged PFS in MM patients [123]. In addition, a decrease of the NK cell percentage within the leukocyte population from pre-transplant to leukocyte regeneration was described in a cohort of patients suffering from hematological malignances that received autoHSCT. Two weeks after leukocyte regeneration the percentage of NK cell within the leukocyte population returned to initial values [144]. Although not statistically significant, we also noticed a slightly decrease in the absolute number of NK cells at S2 and a significantly increase at S3 in our cohort of patients. However, we were unable to see any association between NK cell counts and the PFS after autoHSCT in MM patients (Figure 13B).

In line with previous studies, both in autoHSCT and alloHSCT settings [19,144,217], our data points out to a redistribution of NK cell subsets during their reconstitution after autoHSCT, as observed by a higher frequency of CD56<sup>bright</sup> NK cells and a lower frequency of CD56<sup>dim</sup> NK cells, shortly after leukocyte reconstitution (S2) (Figure 13 D). This is also in accordance with the proposed linear model of NK cell development, in which CD56<sup>dim</sup> are generated from CD56<sup>bright</sup> NK cells [84]. When adaptive NK cells

were analyzed, we found that FcεRγ- NK cells were more abundant than the ones expressing NKG2C and that there were differences between the reconstitution of both cell subsets (Figure 15). As explained before, the expansion of adaptive NK cells expressing the activating receptor NKG2C has been largely associated with CMV infection or reactivation [35] and with the clinical outcome after autoHSCT and alloHSCT [146,147]. Moreover, expansion of FcεRγ- adaptive NK cells following CMV infection has also been described [42]. Nevertheless, although the lack of FcεRγ is often associated with NKG2C expression, occasionally, these markers may appear disassociated [43,44] and FcεRγ- NK cells have been found in CMV seronegative individual as well [42,218]. Thus, the expansion of NKG2C+ NK cells might be more specific to human CMV infection or reactivation than the expansion of FcεRγ- NK cells [219]. It is important to note that 88.9% of the patients in our cohort were CMV+ prior to autoHSCT and that the determination of the CMV serostatus of MM patients could be sometimes controversial. The treatment that these patients receive leads to a depletion of plasma cells and therefore, a significant number of them exhibit different degrees of hypogammaglobulinemia [220]. It may be possible that some patients that are catalogued as CMV negative could be false negatives because of the hypogammaglobulinemia. Moreover, it is also important to mention that, the incidence of CMV reactivation in autoHSCT is extremely low [221,222]. Furthermore, no patient in our cohort had clinical manifestations of CMV infection or reactivation following autoHSCT. In autoHSCT, as the infused cells come from the same patient, the possibility of infection after transplantation due to mismatch of CMV serostatus between donor and recipient is not possible. In addition, another common reason for CMV reactivation in alloHSCT is the immunosuppression status of the patients after transplantation. In our study, although some of the MM patients undergoing autoHSCT received maintenance regimen (with lenalidomide for example) (Table 5), they are not immunocompromised, or at least not to the same extent as patients undergoing alloHSCT. Therefore, the notion of adaptive NK cells as a heterogeneous population of cells [41,44] may explain the dissimilarities that the different subsets exhibited regarding their frequency and reconstitution-time after autoHSCT.

Consistent with the increment in the percentage of the less differentiated NK cell subset (CD56<sup>bright</sup> NK cells), we also observed an increase in the frequency of NKG2A+ cells and a decrease in the frequency of cells expressing CD57 at leukocyte recovery (Figure

16). This shift in the maturation status of NK cells is maintained for up to 3 months after autoHSCT (S4), when pre-transplant levels are restored. Although our data differ from the increment of the percentage of CD57+ NK cells at leucocyte recovery that Jacobs et al. have previously described [144], they are in accordance with the linear model of NK cell development and how the expression of NKG2A and CD57 is modulated during NK cell maturation (Figure 3) [13,104]. In addition, as Jacobs and colleagues observed in their study [144], we also found a surprising expression of CD57 in CD56<sup>bright</sup> NK cells shortly after autoHSCT that was not observed at any other time point. It is known that CD56<sup>dim</sup> NK cells are able to upregulate CD56 upon IL-15 stimulation [223] and, as we demonstrated, the IL-15 plasma levels are highly increased at leucocyte recovery (Figure 19A). Thus, it is possible that these cells are CD56<sup>dim</sup> NK cells that have upregulated CD56. Clearly, more studies are required to shed light on the biology of this interesting CD56<sup>bright</sup>CD57+ NK cells subset.

Our data demonstrate an important and previously undescribed association between the NK cell degree of differentiation and the clinical outcome after autoHSCT of MM patients, as observed by the detrimental effect that higher frequency of NKG2A-CD57+ NK cells at +30 days and +100 days post-autoHSCT have in the PFS and TTNT of these patients (Figure 21). Although it is well known that CD57+ NK cells exhibit a more mature phenotype and a higher CD16 induced-cytotoxic capacity, they also display a decreased responsiveness to IL-12 and IL-18 stimulation and a reduced proliferative capacity compared to NK cells lacking CD57 expression [103,104]. High frequencies of tumor infiltrating CD57+ NK cells have been associated with better clinical outcomes in different types of cancer patients [224], probably due to their enhanced cytotoxicity. However, in our study we look at circulating NK cells instead of intratumoral NK cells, which may explain differences in the results. In line with our data, an inverse correlation between circulating CD57+ and tumor-infiltrating NK cells numbers was described in breast cancer patients. These authors also found that patients with higher numbers of circulating CD57+ NK cells have lower pathological complete response rates to early treatment with anti-HER2 therapeutic antibodies [225]. In a similar manner, other studies have described an accumulation of CD57+CD8+ T cells in patients with different types of cancers and also an association between high frequencies of circulating CD57+CD8+ terminally differentiated T cells and poor prognosis [224,226,227]. On the other hand, it is known that CD57+ NK cells have a lower expression than CD57- NK cells of the



CXCR4 chemokine receptor, which is involved in the homing to the bone marrow [104]. Therefore, this could also be another mechanism contributing to the poor prognosis of patients with a higher frequency of circulating terminally differentiated NK cells, where less NK cells home to the bone marrow. Nevertheless, the above mentioned studies did not analyze the co-expression of NKG2A and CD57, and thus within those CD57+ NK cells there would be NKG2A+ and NKG2A- NK cells that might have different functional and proliferative capacities. Therefore, our results, in which we identified an association between the NKG2A-CD57+ NK cell subset and disease progression, adds new information about a specific NK cell subset with an important role in MM patients undergoing autoHSCT.

IL-15 is a critical cytokine for NK cell differentiation, survival and proliferation [70,71]. Monocytes and dendritic cells have been described as a source of this cytokine [228]. As explained above, in NHL patients, IL-15 has been proposed to influence clinical outcome through NK cell recovery after autoHSCT [124]. In contrast to Porrata et al., not only we did not observe any association between IL-15 plasma levels and clinical outcome (Figure 19C), but we also found a statistically significant negative correlation between IL-15 plasma levels at S2 and absolute NK cell numbers (Figure 20B). However, our cohort is composed of MM patients whereas Porrata et al. described those results in NHL patients. On the other hand, and similar to our results, a strong inverse correlation between NK cell numbers and plasma IL-15 levels at 2 weeks post-transplantation was observed in allo-HSCT [223]. The elevated plasma levels found early after autoHSCT (S2) might be related to transplant-regimen induced depletion of lymphoid cells that consume circulating IL-15. Considering that IL-15 production is tightly regulated [228], it is tempting to speculate that in those situations with high plasma IL-15 levels, this is due to the existence of a low number of this cytokine-consuming cells, among which are NK cells. When the number of these cells increase, the plasma levels of IL-15 decrease to almost undetectable levels.

Our data showed that NK cells experience a shift in terms of, among others, cytotoxic potential and proliferation capacity at leucocyte recovery (Figure 17). The percentage of Ki67+ cells is dramatically increased in the three NK cell subsets and the expression of granzyme B is incremented in CD56<sup>bright</sup> NK cells. It is very likely that these changes are due to the particular cytokine milieu that is present at that specific time. The role of IL-15 in upregulating Ki67 expression on NK cells has been previously described [229,230].

Moreover, induction of the expression of Ki67 occurs in NK cells after IL-15 infusion in patients with cancer [229]. On the other hand, while at rest CD56<sup>bright</sup> NK cells display a low expression of granzyme B, after an IL-15 priming granzyme B protein levels significantly increase in this subset [15].

To our knowledge, this is the first study that performed such extended analysis of NK cell phenotype in MM patients after autoHSCT and that includes other unconventional NK cell subsets, such as, CD56<sup>neg</sup> and several adaptive NK cell subsets. Furthermore, unlike previous studies in autoHSCT in which NK cells were only examined up to 1 month after autoHSCT [144], our analysis goes further by analyzing samples up to 1 year after transplantation (S6). In conclusion, in this second chapter we were able to demonstrate that there is a redistribution of NK cells subsets and a shift in NK cells phenotype shortly after autoHSCT. Importantly, we observed that MM patients with lower frequency of mature NK cells, identified by the NKG2A-CD57+ phenotype, showed better clinical outcomes after autoHSCT. Even though, further studies in a larger cohort of patients are needed to validate these results, the data presented in this chapter provide new insight into the importance of NK cell reconstitution and their degree of differentiation that could help to understand the outcome after autoHSCT in MM patients.

## **CHAPTER III**

### **Transcriptome analysis of NK cells in autologous hematopoietic stem cell transplantation.**

## INTRODUCTION

As observed in Chapter II, NK cell phenotype is drastically altered immediately after autoHSCT. Moreover, NK cell maturation stage impacts the outcome of MM patients after autoHSCT. Therefore, to obtain a more complete picture of changes occurring during this process and to try to comprehend in depth NK cell biology, we were interested in further study these cells during their reconstitution after autoHSCT.

Since their development, next-generation sequencing (NGS) technologies have been extensively used in biomedical research for multiple applications. Their use provides a large and complex dataset, so these technologies afford the possibility of answering complex biological questions. Gene expression is not a static process and is among others, time-, cell-type- and stimulus-dependent. One of the most used methods to study alterations in gene expression is RNA-sequencing (RNA-seq) [231,232]. This method offers the possibility to study the cellular transcriptome by quantifying the abundance or the relative changes of an mRNA in different conditions. Moreover, RNA-seq also provides the opportunity of investigating alternative splicing patterns, gene fusion, mutations, small RNAs, etc. [231,232]. In contrast to flow cytometry-based procedures, this technology is not limited to the study of selected markers, and therefore, a more complete information and a global non-biased picture of complex systems is obtained. Furthermore, the development of scRNA-seq technology provides a new powerful approach to study transcriptome at a single cell level and to explore cellular heterogeneity [233].

The study of gene expression profile of NK cells in different settings have generated extremely valuable data regarding NK cell activation, development, functions and NK cells subsets both in human and mouse. Differences in terms of gene expression between CD56<sup>bright</sup> and CD56<sup>dim</sup> have been widely study by different groups [33,234,235]. Recently, pNK cell subsets diversity has been depicted [236] and distinct NK cell populations in human bone marrow and blood have been identified by scRNAseq [237]. Genomic profiling has also been used to study differences between pNK and dNK, showing that these cells express a distinct repertoire of surface receptors, cytokines, chemokines and different transcription factors profile [33]. Microarray analysis, a hybridization based technique that quantifies the genes relative abundance, has also been used to investigate the transcriptional profile of dNK in terms of secreted cytokines,

growth factors and chemokines [30], to identify different responses generated by dNK when KIR2DS1 vs KIR2DL1 binds their ligand HLA-C2, which may impact placentation [238] and to study dNK cells from gravid uteri vs the cycling endometrium showing the existence of different NK cell subsets [239]. The existence of three different dNK cell subsets was also described by scRNAseq [240]. As expected, the heterogeneity of other trNK cells (e. g. liver, spleen) have been also largely investigated [29,241].

Apart from studying NK cell diversity, gene expression profiling has also been used to investigate alterations induced by NK cell activation, which led to a better understanding of NK cell-function and the molecular mediators underlying NK-cell responses. Examples of these studies are those comparing gene expression after cytokine stimulation (e.g IL-2 activated NK cells) [234,242], stimulation via activating receptors (e.g. using a soluble anti-KIR2DL4 agonist mAb) [243] and alterations induced by viral infections, such as CMV infection [41].

NK cells are a key component of the antitumor immune response. However, tumor cells have developed ways of subverting NK cell function [244,245]. Genomic profiling of NK cells from the tumor microenvironment has shed light on the suppression mechanisms used by tumors and results from these studies may help to improve NK cell antitumoral functions during tumor immunosurveillance [246]. For example, analysis of tumor infiltrating NK (TINK) cells had been conducted in non-small cell lung cancer (NSCLC) patients, revealing modification on gene expression profile induced by tumor microenvironment [247]. Study of TINK cells compared to circulating NK cells was also done in melanoma patients [248]. Moreover, the gene profile of circulating NK cells from AML [249], head and neck squamous cell carcinoma [250] and colorectal cancer [251] patients has been compared to healthy controls. All the data obtained in these and many others studies show the potential of using transcriptome analysis to discover biomarkers and provides new insight on the NK cell response against tumors. Therefore, in this third chapter, we have studied changes occurring during the NK cell pool reconstitution after autoHSCT by the analysis of the NK cell transcriptome using RNA-seq and validated the results by quantitative PCR (qPCR). We also have tried to correlate NK cell gene profile with patient's outcome with the objective of finding a valuable biomarker.

## METHODS

### Patients' characteristics and study design

Blood samples from 16 patients who suffered from MM and received autoHSCT were used in the study. From them, samples from 10 patients were used for RNA-seq experiments, 3 samples were used for qPCR experiments and 3 samples were used for flow cytometry experiments. Samples were obtained at three different time points: T1 was collected the day before starting with the conditioning treatment; T2 was collected after leukocyte recovery ( $>1000$  leukocytes/ $\mu\text{L}$ ) and T3 was collected 30 days after cell infusion. Patients' clinical data can be found in Table 7. Sample collection was carried out through the Basque Biobank for Research (<http://www.biobancovasco.org>), which complies with the quality management, traceability and biosecurity, set out in the Spanish Law 14/2007 of Biomedical Research and in the Royal Decree 1716/2011. The study was approved by the Basque Ethics Committee for Clinical Research (BIO14/TP/003 and PI+CES+INC-BIOEF 2017-03). All subjects provided written and signed informed consent in accordance with the Declaration of Helsinki.

### Sample preparation

PBMCs were isolated from blood samples by Ficoll (GE Healthcare) density gradient centrifugation and cryopreserved in heat-inactivated FBS (GE Healthcare Hyclone) containing 10% Dimethylsulfoxide (DMSO) (Thermo Scientific Scientific).

### NK cell isolation

Cryopreserved PBMCs were thawed at  $37^{\circ}\text{C}$  in a water bath, washed with PBS (Lonza), filtered using  $70\mu\text{m}$  cell strainers and counted. Next, PBMCs were stained with LIVE/DEAD Fixable Green Cell Stain Kit (Invitrogen) to exclude dead cells, following manufacturer's recommendations. Then, cells were washed with PBS containing 2.5% BSA (Sigma Aldrich). Extracellular staining was carried out by incubating PBMCs for 30 minutes on ice in the dark with the following fluorochrome conjugated monoclonal antibodies: PE anti-CD3 (UCHT1), PE anti-CD14 (M $\phi$ P9), PE anti-CD19 (HIB19) and PE-Cy5 anti-CD56 (B159) from BD Bioscience and PEVio770 anti-NKp80 (4A4.D10) from Miltenyi Biotec. NK cells were identified based on the gating strategy developed in Chapter I, as viable CD3-/CD14-/CD19-/NKp80+/CD56+/- cells and sorted using a BD

FACSJazz cell sorter (Figure 22). NK cell isolation was performed at the Cell Analysis Facility of the Achucarro Basque Neuroscience Center.

### **RNA extraction and sequencing**

Total RNA was isolated from sorted NK cells using RNeasy Plus Micro Kit (Qiagen) following manufacturer's recommendations. Quality and integrity of each RNA sample was checked using both a Bioanalyzer and Nanodrop before proceeding to the RNA sequencing (RNA-seq) protocol. 0.5 ng of total RNA were used to generate barcoded RNA-seq libraries using the NEBNext Single Cell/Low Input RNA Library Prep Kit for Illumina (New England Biolabs). Briefly, poly A+ RNA was purified using poly-T oligo-attached magnetic beads followed by fragmentation and then, first and second complementary DNA (cDNA) strand synthesis. Next, cDNA 3' ends were adenylated and the adapters were ligated and performed an uracil excision from the adaptor followed by PCR amplification. The size of the libraries was checked using the Agilent 2100 Bioanalyzer High Sensitivity DNA chip and their concentration was determined using the Qubit® fluorometer (ThermoFisher Scientific). Libraries were sequenced on a HiSeq4000 (Illumina) to generate 60 bases single reads. FastQ files for each sample were obtained using bcl2fastq 2.20 software (Illumina). Nine samples per time were finally sequenced. RNA Quality Control, library preparation and sequencing was performed in the Genomic Unit of the "Centro Nacional de Investigaciones Cardiovasculares" (CNIC).

### **RNA-seq data analysis**

Sequencing reads were aligned to the human reference transcriptome (GRCh38 v91) and quantified with RSEM v1.3.1 [252]. Raw counts were normalized with Transcripts per Million and Trimmed Mean of M-values methods, transformed into log<sub>2</sub> expression ( $\log_2(\text{rawCount}+1)$ ) and compared to calculate fold-change and corrected p value. Only those genes expressed with at least 1 count in 8 samples equal were taken into account. As expected, we had intra-group variability so, although we calculated the Benjamini and Hochberg correction procedure for all genes, we considered for functional analysis genes with  $|\text{Log}_2\text{FC}| > 0.58$  and unadjusted pValue  $< 0.05$ . One samples from T1 and one sample from T2 were not analyzed as they expressed a totally different gene expression profile, very probably due to technical problems during sample preparation prior to sequencing.

Heatmaps were generated with Morpheus online tool from Broad Institute (<https://software.broadinstitute.org/morpheus>). For functional analysis, we used clusterProfiler, ReactomePA and pathview R packages [253–255].

### **Reverse transcription reaction**

cDNA was synthesized from 3 ng of total RNA using SuperScript IV VILO Master Mix with ezDNase enzyme (ThermoFisher Scientific) following manufacturer's recommendations. A DNA removal step was performed using ezDNase before the reverse transcription.

### **Real time qPCR**

Real time qPCR was performed using Brilliant III Ultra-Fast SYBR Green qPCR Master Mix (Agilent Technologies) following manufacturer's recommendation on an Agilent AriaMX instrument (Agilent Technologies). In each reaction, 2  $\mu$ L of (1:10) diluted cDNA of each sample was loaded in triplicates into MicroAmp Fast 96-well reaction plates (Applied Biosystems). In addition, 18  $\mu$ L of qPCR master mix was added, which included Brilliant III Ultra-Fast SYBR Green qPCR Master Mix (10  $\mu$ L), housekeeping gene/probe gen primers (600nM of each primer, except for vimentin (VIM) in which 100nM of each primer were used), and nuclease free diethylpyrocarbonate-treated water (Fisher Scientific). Negative controls (no cDNA) were included to verify the absence of contamination. Quantitative analysis was made based on the cycle threshold (Ct) value and calculated using AriaMX Real Time software v.A1.2 (Agilent Technologies). Ct mean values from triplicate reactions were calculated for further analysis. The sequences of the primers used are shown in Table 8. Primers were designed with Primer3Plus software using FASTA sequences of each gene and synthesized by Invitrogen (Thermo Fisher).

### **Flow cytometry: Functional assays**

For functional assays, similar to what was explained in the previous chapters, PBMCs were thawed, counted, plated at  $1 \times 10^6$  cells/well in 48-well plates in NK cell culture medium and cultured overnight. Next, cells were stimulated with 50 ng/mL PMA and 2  $\mu$ M Ionomycin for 6h. APC-Vio770 anti-CD107a (REA792, Miltenyi Biotec) was added at the start of the stimulation time in addition to GolgiStop (monensin) and GolgiPlug



(brefeldin A) protein transport inhibitors (BD Biosciences) following manufacturer's recommendations. Next, PBMCs were washed with PBS and stained with LIVE/DEAD Fixable Aqua Dead Cell Stain Kit (Invitrogen) reagent to exclude dead cells, following manufacturer's recommendations. Afterwards, cells were washed with PBS containing 2.5% BSA (Sigma-Aldrich) and extracellular staining was performed. For that, cells were incubated for 30 minutes on ice in the dark with the following fluorochrome conjugated mAbs: BV510 anti-CD14 (M $\phi$ P9), BV510 anti-CD19 (SJ25C1), BV510 anti-CD123 (9F5), BV786 anti-CD56 (NCAM 16.2) and PerCP-Cy5.5 anti-CD3 (SK7) from BD Bioscience; PE-CF594 anti-CD9 (HI9a) from BioLegend and PE-Vio770 anti-NKp80 (4A4.D10) from Miltenyi Biotec. Cells were then washed again with PBS containing 2.5% BSA, and fixed and permeabilized using Cytotfix/Cytoperm Fixation/Permeabilization solution from BD Biosciences following manufacturer's recommendations. Next, cells were incubated for 30 minutes on ice in the dark with the following fluorochrome conjugated mAbs: BV421 anti-IL-8 (G265-8), BV605 anti-IFN $\gamma$  (B27), BV650 anti-IL-10 (JES3-9D7), FITC anti-MIP1 $\beta$  (D21-1351), R718 anti-granzyme B (GB11) from BD Bioscience; BV711 anti-perforin (dG9) and APC anti-TNF (Mab11) from BioLegend. Finally, cells were washed with 1x Perm/Wash Buffer (BD Bioscience) and resuspended in PBS. Samples were then acquired in a Fortessa X20 flow cytometer (BD Bioscience). Flow cytometry panel used for the functional assay is shown in Table 9.

### **Flow cytometry data analysis**

Flow cytometry data were analyzed using FlowJo v10. software. GraphPad Prism v.9 was used for graphical representation and statistical analysis. Non-parametric Wilcoxon matched-pairs signed rank test were used to determine significant differences. Data were represented as bar plots showing the median and interquartiles range.

## RESULTS

### **The transcriptome landscape of NK cells is drastically altered during their reconstitution after autoHSCT.**

As we observed in the data presented in Chapter II, NK cells undergo a profound phenotypical change during their reconstitution after autoHSCT. To gain further insight into other aspects of NK cell biology during subset reconstitution after autoHSCT, gene expression profiles of NK cells from 10 MM patients undergoing autoHSCT were compared at three different time points (T1, T2, T3), as described in the Methods section. Patients' characteristics are listed in Table 7.

Differential gene expression analysis revealed changes in the gene expression profiles of NK cells during their reconstitution, mainly at T2. Specifically, 194 genes were upregulated and 220 were downregulated in T2 compared to T1, and 197 genes were upregulated and 257 were downregulated in T2 compared to T3 (Figure 23A). In contrast, only few genes were altered in T3 compared to T1 (Figure 23B). Moreover, unsupervised hierarchical cluster analysis demonstrated a vast shift of gene expression pattern at T2 (Figure 23C). In general, genes were clearly separated in two main groups with different gene expression profile. The first group (G1) consisted of genes with high expression in T2 compared to T1 and T3, and in contrast, the fourth group (G4) consisted of genes with low expression in T2 that were highly expressed at T1 and T3. However, as revealed by genes in groups G2 and G3, that showed lower expression in T3 than in T1 and higher expression in T3 than in T1 respectively, NK cell gene profile was similar but not identical at T3 compared to T1 (Figure 23C), suggesting that some changes persist in NK cells gene profile one month (T3) after autoHSCT.

### **RNA-seq data validation by qPCR**

As for the analysis we considered genes with an unadjusted pValue < 0.05, we validated RNA-seq data by qPCR. For this, first we evaluated four genes as candidates housekeeping genes. *B2M* and *18S* were selected because they are commonly used as housekeeping genes. Moreover, *PPIA* and *HPRT1* were selected based on a study evaluating optimal reference genes in resting and activated NK cells [256] and because they showed a stable expression at the three different time points in our RNA-seq data. After the analysis of the expression of these genes by qPCR and after checking primer

efficiency, we selected *B2M* and *PPIA* as optimal candidates housekeeping genes. *18S* primers amplified a non-specific product in the negative control (data not shown) and *HPRT1* primers efficiency was not correct (Table 8). Next, we evaluated *B2M* and *PPIA* gene expression stability at the three different time points, and results showed not significant differences (Figure 24A). Therefore, *B2M* and *PPIA* were selected as optimal reference genes for our qPCR experiments.

Once the optimal housekeeping genes were found, we selected and validated four genes which expression was significantly altered at the three different time points. Two genes that were upregulated in T2 vs T1, *CD9* and *VIM* (*CD9* Log<sub>2</sub>FC: 2.45; *VIM* Log<sub>2</sub>FC: 1.29), and two genes that were downregulated in T2 vs T1, *CD160* and *FCRL6* (*CD160* Log<sub>2</sub>FC: -1.82; *FCRL6* Log<sub>2</sub>FC: -2.15) were chosen according to RNA-seq data. Primers efficiency was checked and results are shown in Table 8. Finally, the expression of these genes at the three different time points was compared. For this purpose, samples from three new MM patients undergoing autoHSCT and three samples on which RNA-seq had already been performed were used. We clearly observed an upregulation of *CD9* and *VIM* at T2, although the results in the case of *VIM* are not statistically significant. Moreover, there was a statistically significant downregulation of *CD160* at T2 (Figure 24B). In the case of *FCRL6*, we observed amplification of a non-specific product (data not shown) and therefore we did not continue with the analysis of this gene. Thus, the qPCRs data validated the results obtained with RNA-seq.

### **Cell division is the main biological process in NK cells early after autoHSCT**

The analysis of differentially expressed genes (DEGs) across the three different time points (T1, T2 and T3) is only a starting point to gain insight into the changes regarding NK cell biology occurring in the context of autoHSCT. Thus, as genes work in a connected manner in all biological processes, we performed functional enrichment analysis to obtain information about differentially expressed biological pathways.

Over representation analysis (ORA) performed against Reactome database revealed that the 10 most significant enriched pathways for upregulated genes at T2, compared to both T1 and T3, were pathways associated with cell cycle and DNA replication (Figure 25A). Similar results were obtained with Gene Ontology database (Figure 25B). However, cell cycle and DNA replication pathways were not enriched when ORA was performed with

upregulated genes in T3 compared to T1 (Annex), suggesting that while early after autoHSCT NK cells are clearly dividing, one month after autoHSCT (T3) NK cells recover pre-transplant (T1) division rate.

### **The synthesis of isoprenoids is significant during NK cell pool reconstitution**

Another widely used method for functional enrichment analysis is the method known as gene set enrichment analysis (GSEA), in which the data set is usually ranked according to the metrics of expression difference and then compared to a reference gene set to obtain enrichment significance.

Although cell division and DNA replication were the most significant enriched pathways at T2 compared to T1, GSEA against the Kyoto Encyclopedia of Genes and Genomes (KEGG) database also revealed an upregulation of metabolic pathways (NES: 2.76; adjusted p value:  $3 \times 10^{-10}$ ) (Annex). Among DEGs we found that *GAPDH* and *ENO1*, which encode two key enzymes of glycolysis; *SUCLA2* and *FH*, which encode enzymes that are part of the tricarboxylic acid cycle and *ACAA2*, which encode an enzyme involved in fatty acid  $\beta$ -oxidation, were upregulated at T2 compared to T1 (Figure 26A). Specifically, enrichment analysis performed against KEGG modules database showed an overrepresentation of the mevalonate pathway and pathways associated with nucleotide metabolism (Figure 26B). The mevalonate pathway, which is part of the terpenoid backbone biosynthetic pathway, is responsible for the synthesis of isopentenyl pyrophosphate, the essential building block of all isoprenoids including cholesterol. As shown in Figure 26C, genes encoding most of the key enzymes of the mevalonate pathway appeared upregulated at T2 compared to T1: *ACAT1*, *HMGCS1*, *HMGCR*, *PMVK* and *MVD*. These results suggest that the synthesis of isoprenoids may be key for NK cells early after autoHSCT.

### **NK cells acquire a decidual-like gene expression profile early after autoHSCT**

Once the functional enrichment analysis was completed, we focused on the analysis of individual DEGs to further characterize alterations in gene profile that occur during NK cell reconstitution following autoHSCT. We observed that a number of genes related to NK cell development and maturation (*LEF1*, *ZEB2*, *FCRL6*), cytotoxicity (*LGALS1*, *LGALS3*, *GZMB*, *TNFSF10*, *FCGR3A*), in addition to genes encoding activating receptors (*CD300C*, *CD38*, *CD160*) and chemokine receptors (*CCR1*, *CCR5*, *CCR7*) were differentially expressed at T2 compared to T1 (Figure 26A). Surprisingly, among the top

10 DEGs with lower p value and higher Log<sub>2</sub>FC value in T2 vs T1 comparison we found *CD9*, which encode a protein from the tetraspanin family. Although *CD9* is ubiquitously expressed by all the major subsets of leukocytes, it is considered as an exclusive marker of dNK cells [33]. As mentioned before, the upregulation of *CD9* at T2 was confirmed by qPCR (Figure 24B).

In contrast to pNK cell subsets (*CD56<sup>bright</sup>* and *CD56<sup>dim</sup>* NK cells), dNK cells have been described to, among others, exclusively express *CD9*, *CD151*, tetraspan-5 (*TSPAN5*), Glycodelin A (*PAEP*) and Core 2 $\beta$ -1,6-N-acetylglucosaminyl transferase (*GCNT1*) [33]. In addition, as other tissue resident NK cells, dNK cells also show expression of *CD103* (*ITGAE*) and *CD49a* (*ITGAI*) [32]. As shown in Figure 27A, NK cells showed a clear higher expression of *CD9* and *CD151* at T2 compared to both T1 and T3. Moreover, although not significant, the mean expression of *TSPAN5*, *GCNT1* and *PAEP* tended to be slightly higher at T2. Furthermore, they showed higher expression of galectin-1 (*LGALS1*) which has been described to be overexpressed in dNK in comparison to pNK [33]. Like *CD56<sup>dim</sup>* NK cells, dNK are known to express KIRs although the repertoire seems to be different [33]. The analysis of the detected KIRs revealed an interesting increment in the expression of *KIR2DL4* at T2 compared to T1 (Figure 27A). The ligand for this KIR is the non-classical HLA-G molecule whose expression is restricted to the fetal trophoblast cells that invade the maternal decidua during early pregnancy [257]. Similar results were obtained for *CD49a* (*ITGAI*) (Figure 27A). The chemokine receptors *CXCR3* and *CXCR4* seem to mediate the traffic of dNK towards maternal-fetal interface [258]. Results also demonstrated a tendency to an upregulation of *CXCR3* at T2 and a tendency to an upregulation of *CXCR4* at T3 (Figure 27A). Together, these data suggest that NK cells acquire a dNK-like gene expression profile early after autoHSCT (T2) that is not maintained overtime.

### **CD9 expressing NK cells exhibit altered effector functions**

Apart from exhibiting a distinct phenotype and unique transcriptional profile in comparison to pNK [33], dNK cells also present different functional characteristics. dNK cells have been described as poorly cytotoxic, although they express functional activating receptors and complete lytic machinery [32]. Moreover, they are able to produce several cytokines, such as IFN $\gamma$ , TNF, GM-CSF, transforming growth factor beta (TGF- $\beta$ ), and IL-10; chemokines, including, IL-8, MIP1 $\alpha$ , MIP1 $\beta$ , CCL5, CXCL10 and CXCL12; and angiogenic factors including angiopoietin-2, PLGF and VEGF, at least after stimulation

with IL-2 or IL-15 [32]. dNK cells have been showed to regulate key developmental processes during pregnancy, such as trophoblast invasion and vascular remodeling in the decidua [30]. Therefore, we were interested in studying the functionality of CD9-expressing NK cells expanded after autoHSCT and comparing them with CD9- NK cells. For that, we examined degranulation (CD107a), cytokine (IFN $\gamma$ , TNF and IL-10) and chemokine production (IL-8, MIP1 $\beta$ ) after stimulation with PMA and Ionomycin. Moreover, we also evaluated the cytotoxic potential of these cells by measuring granzyme B and perforin expression.

Flow cytometry data validated the results obtained with RNA-seq and, although not statistically significant, clearly showed an expansion of CD9+ NK cells early after autoHSCT (T2) (Figure 27B). Furthermore, it was observed that MM patients undergoing autoHSCT seem to exhibit a higher frequency of CD9-expressing NK cells compared to healthy donors (Figure 27B). Regarding effector functions in response to PMA and Ionomycin, our results showed a trend toward a lower frequency of CD107a+ cells, suggesting lower degranulation (Figure 27C), in addition to a tendency to a lower frequency of MIP1 $\beta$ + cells within CD9+ NK cells compared to CD9- NK cells (Figure 27D). No IL-8 expression was observed in NK cells, probably due to our experimental conditions (data not shown). Furthermore, no clear differences in cytokine production (IFN $\gamma$ , TNF, IL-10) were observed between CD9+ and CD9- NK cells at T2 (Figure 27E). Finally, analysis of granzyme B and perforin expression showed that CD9+ NK cells exhibited a trend toward a higher level of granzyme B and perforin compared to CD9- NK cells, as determined by MFI of these markers (Figure 27F). Together, these results suggest that CD9+ NK cells expanded early after autoHSCT may show altered effector functions (CD107a and MIP1 $\beta$ ) but enhanced cytotoxic potential (granzyme B and perforin).

#### **RNA-seq data do not reveal differences in terms of gene expression profile according the outcome of the patients**

Five out of ten patients used in the RNA-seq analysis showed progression of the disease after autoHSCT (Table 7). For this reason, we aimed to analyze differences in terms of gene expression profile at T2 between patients that present disease progression and the ones with no progression. Principal component analysis of these data revealed that, in general, samples were not grouped according to the outcome of the patients after

autoHSCT (Figure 28A). Interestingly, although not statistically significant, patients with disease progression showed a higher expression of *CD9* in the RNA-seq data (Figure 28B). These data suggest a possibility of using RNA-seq to further study the implication of NK cells in the outcome of patients undergoing autoHSCT.

## DISCUSSION

In this third chapter, we have examined global changes occurring in NK cells during their reconstitution after autoHSCT, by analyzing their transcriptome using RNA-seq technology. We have documented that the gene expression profile of NK cells changes immediately after leucocyte reconstitution, being cell cycle the main biological process at this point. Moreover, we have also described upregulation of metabolic pathways, such as the mevalonate pathway. Importantly, we have revealed that NK cells acquire a dNK-like phenotype early after autoHSCT and that these cells exhibit different effector functions when compared with conventional NK cells.

As described in Chapter II and as Jacobs and colleagues reported in their previous study [144], NK cells undergo a profound phenotypic change after autoHSCT. In line with these data, RNA-seq results demonstrate that the gene expression profile of NK cells is also drastically different early after leucocyte recovery (T2). In addition, in Chapter II we reported that some of the phenotypical changes that NK cells undergo last for more than 30 days after autoHSCT. In accordance with these results, we show that although the transcriptome landscape of NK cells at pre-transplant (T1) and 30 days after (T3) autoHSCT is similar, it is not the same, as demonstrated by the low number of DEGs identified between both samples (Figure 23B).

An early immune recovery after both alloHSCT and autoHSCT is key for patients' outcome [114–117,259]. Early lymphocyte recovery, and more importantly, early NK cell recovery were reported to predict superior survival after autoHSCT [115,122,123]. Moreover, NK cells have been described as the first lymphocyte population to show normal levels after autoHSCT, being NK cell count and functionality restored as early as day 14 post-transplant [126,129]. Therefore, that the major changes in the gene expression profile of NK cells occur before T3 (30 days after autoHSCT) is not unexpected. Our data demonstrate that immediately after transplantation NK cells are in the active phase of the cell cycle and that DNA replication and nucleotide metabolism are upregulated. However, the upregulation of these biological processes is not maintained 30 days after autoHSCT. These findings are in agreement with the dramatic increase in the frequency of Ki67-expressing cells immediately after autoHSCT (Figure 17C). Ki67 is a nuclear protein that is expressed during the cell cycle and absent in quiescence cells [215,260]. These results suggest that immediately after autoHSCT, the primary function of NK cells is to divide



and reach pre-transplant counts, processes that appear to be completed 1 month post-autoHSCT (T3).

As shown in Chapter II, NK cells exhibit an immature phenotype at leukocyte recovery and NK cell maturation occurs during their reconstitution after autoHSCT. Similar to what occurs with T cells [261], studies conducted in the last years indicate that NK cell differentiation status is closely associated to their metabolic signature [262,263]. Moreover, NK cell metabolism can also be modified by other processes, such as cell activation and some pathological conditions [245,263,264]. In this regard, our data demonstrate an upregulation of metabolic pathways, specifically of the mevalonate pathway, immediately after autoHSCT (Figure 26B, C). Mevalonate is the precursor of isoprenoids, such as cholesterol that is a key component of the eukaryotic cell membranes. This pathway is known to be essential for lymphocyte proliferation and cell cycle progression [265–267] which, in turn, is consistent with the above presented data. In addition, the mevalonate pathway is also important for NK cell cytotoxicity [266,268]. Fluvastatin, an inhibitor of the 3-hydroxy-3-methylglutaryl-coenzyme A (HMG-CoA) encoded by the *HMGCR* gene, is known to inhibit actin redistribution, RhoA activation (needed for actin assembly) and lipid raft formation [268]. In addition, fluvastatin inhibits the intracellular free calcium increase and Akt1/PKB activation mediated by activating receptors engagement, which are crucial for the release of cytotoxic granules [268]. Furthermore, fluvastatin was shown to inhibit perforin/granzyme containing granules release [268]. All these effects were reverted with the addition of mevalonate [268]. Thus, the synthesis of mevalonate is essential for the cytoskeleton assembly needed for cytotoxic granules polarization. Moreover, low cholesterol content of cell membranes caused by inhibition of the mevalonate pathway affects membrane mobility and the correct aggregation of signaling molecules in membrane rafts, which influence NK cell activation and cytotoxic granules release. On the other hand, FasL and TNF mediated killing appear to be independent of the mevalonate pathway [268].

Our data revealed, to our knowledge, a previously undescribed shift in NK cells phenotype towards a dNK-like phenotype immediately after autoHSCT (Figure 27B). pNK can acquire characteristics of dNK cells, such as de expression of CD9, by their culture with not only conditioned medium from decidual stromal cells, but also with TGF $\beta$  [269]. This cytokine has been reported to be expressed in the uterus. Conversion of pNK into a dNK-like phenotype is also achieved under hypoxia and TGF- $\beta$ 1 culture

conditions [270]. In addition, induction of the expression of CD9 is also observed when NK cells are activated with IL-2 and PHA [234]. Very recently, it has been reported that, in coculture experiments, the NK-92 cell line acquires CD9 from ovarian tumor cell lines through trogocytosis [271]. However, the acquisition of dNK-like phenotype after autoHSCT may not be explained by these mechanisms. In fact, the TGF- $\beta$ 1 serum levels were reported to be reduced during autologous bone marrow transplantation conditioning regimen and returned to normal levels between day 20-50 post-transplant, correlating with the recovery of normal white blood cell and platelet counts, major sources of TGF- $\beta$ 1 in the serum [272,273]. Nevertheless, the combination of TGF- $\beta$  with IL-15 and IL-18, cytokines also produced by decidual stroma cells, similarly induced the acquisition of dNK cell markers [274] and, as demonstrated in Chapter II, IL-15 plasma levels are highly incremented after autoHSCT. Thus, the unique cytokine milieu present immediately after autoHSCT may be responsible for this change in NK cell phenotype.

Besides a distinct phenotype, dNK cells also show different functional characteristics compared to pNK cells. dNK cells play crucial roles during pregnancy, such as regulating trophoblast invasion and promoting vascular growth in the decidua [30]. These functions are mediated by the secretion of different cytokines and chemokines. For example, dNK cells secrete IL-8 and interferon-inducible protein 10, which, upon binding to their receptors expressed on the trophoblast, regulate its invasion. Moreover, dNK cells secrete angiogenic growth factors, such as VEGF and PLGF, which promote vascular remodeling [32,275]. Although they display abundant cytolytic granules [33], dNK cells present low cytotoxic effect towards K562 cell line [276] and failed to polarize their microtubules organizing-centers and cytotoxic granules to the immunological synapse [34]. However, very recently it was demonstrated that dNK cells protect placenta from infections via selective transfer of granulysin [277,278]. In addition to dNK cells, TINK and tumor associated NK cells from NSCLC patients were also found to secrete proangiogenic factors, such as, VEGF, PLGF and IL-8 [279,280]. In this case, the proangiogenic activity of NK cells in tumors could have detrimental actions. Finally, the acquisition of CD9 from high-grade serous ovarian tumor cells via trogocytosis was shown to confer NK cells with immunosuppressive properties [271]. Although our data on the functional properties of CD9+ NK cells in the context of autoHSCT are limited due to the small number of samples available, they suggest that these cells exhibit effector functions and cytotoxic potential different from non-CD9-expressing NK cells. The altered

functionality of CD9+ NK cells, in addition to the clear expansion of this subset early after autoHSCT, may have clinical implications. Several publications have signaled that the increased frequency of CD9+ circulating NK cells associates with worse free survival in cancer patients [258,281]. Although our result regarding CD9 expression on NK cells and patients' outcome is not statistically significant, most likely due to the small number of samples and high intra-group variability, it is also in line with those results. Clearly, more studies are needed in this regard to properly assigned a specific role to CD9+ NK cells in the evolution MM patients undergoing autoHSCT.

In conclusion, to our knowledge, this is the first study to perform RNA-seq in NK cells from patients undergoing autoHSCT. We have demonstrated a change in the gene expression profile of NK cells at the beginning of autoHSCT, showing upregulation of biological processes such as cell cycle and metabolism. Importantly, we have also revealed that NK cells acquire a phenotype similar to that of dNK cells and that their effector functions and cytotoxic potential appear to be different, which may have implications for the outcome of patients undergoing autoHSCT. Despite the limitation in the number of samples analyzed, the results presented in this third chapter provide new insights on the biology of NK cells during their reconstitution after autoHSCT and suggest the potential use of RNA-seq technology to find new valuable biomarkers.

# DISCUSSION

The role of NK cells in tumor immunosurveillance was described in several studies carried out more than 20 years ago. Investigations in mouse models revealed an association between NK cell activity and tumors rejection [282,283]. On the other hand, in an 11-year follow-up study of human general population, it was found that low natural cytotoxic activity of PBMCs was associated with increased cancer risk [284]. Moreover, primary NK cell immunodeficiencies seems to be related to susceptibility to infections and cancer [285,286]. Finally, clinical trials in which NK cells from haploidentical donors are infused into patients with different malignancies have also provided encouraging results by inducing clinical responses [287].

In the context of HSCT the key role of NK cells have been also widely reported. The GvT effect mediated in the context of alloHSCT makes this therapeutic strategy to be potentially curative of otherwise incurable leukemias. However, one of its main limitations is the graft-versus-host disease (GvHD). Nevertheless, donor NK cells can also reduce GvHD, probably by eliminating alloreactive donor T cells and recipient antigen-presenting cells [58,213,288,289]. NK cells are well known to mediate anti-tumor responses [282,283] and thus contribute to the GvT effect and impact patients' outcome after alloHSCT. For example, in AML patients receiving alloreactive NK cells in the course of alloHSCT, a reduced incidence of relapse was observed in patients who lacked HLA ligands for donor inhibitory KIRs, which promoted GvT effect [58,290]. The survival benefit of KIR-HLA ligand mismatch was also observed in AML patients that receive CB transplants [291].

Although the GvT effect mediated by donor alloreactive immune effector cells in alloHSCT is fully accepted, for years, the possibility of a GvT effect after autoHSCT was not considered. Nonetheless, studies carried out in the last 15-20 years argue in favor of the existence of a GvT also in autoHSCT setting [113]. These studies also evidenced the association between an early lymphocyte recovery after autoHSCT and a prolonged survival of patients [114–117]. Moreover, they also indicated that among lymphocytes, a rapid recovery of NK cells is especially important [122,123].

Based on these data and taking into account the broad diversity of NK cells [13,21,22], we hypothesize that not only post-transplant NK cell counts, but also an adequate grade of maturation, expression of specific receptors and the distribution of different NK cell subsets will have a significant impact on the outcome of patients undergoing an

autoHSCT. The results obtained in this doctoral thesis regarding the study of NK cells' biology during their reconstitution after autoHSCT also provide a better comprehension of NK cells and the possible benefit that they may have in this therapeutic strategy.

Since the focus of this doctoral thesis was the study of NK cells, a proper identification of this population was of utmost importance. In contrast to T and B lymphocytes, in which a well-known specific lineage marker exists, CD3 and CD19 respectively, NK cells are usually identified by the absence of other lineage markers. Moreover, NK cells subsets are typically distinguish based on the differential expression of CD56 and CD16 surface markers. However, as shown in Chapter I, the expression of CD16 is altered after sample cryopreservation and cell activation. The variation on the expression of CD16 hinders CD56<sup>neg</sup> NK cell subset adequate identification, and can explain the inconsistent results obtained regarding CD56<sup>neg</sup> NK cell phenotype and functionality among different studies [47,49,174,175]. For that reason, the study of other NK cell surface markers, rather than CD16, that leads to a better identification of NK cells is fundamental. Results obtained in Chapter I support the use of NKp80 as an NK cell identification marker. NKp80, an activating receptor expressed by virtually all NK cells, is an NK cell-specific marker among human ILCs and its expression is not downregulated, at least after sample cryopreservation and stimulation with the K562 cell line or IL-12+IL-18, making it a worthy alternative to CD16. In contrast to other studies, in which surface markers distinct to NKp80 have been investigated, such as the combination of CD7 and CD16 [175,182], the NKp80-based identification strategy proposed in Chapter I has the advantage of not using CD16 marker, avoiding the problems related to its unstable expression. The NKp80-based gating strategy also eludes the need of using an additional mAb and an extra flow cytometry detector, which can be very relevant for many laboratories that do not have very sophisticated equipments.

In contrast to alloHSCT, autoHSCT does not involve the development of GvHD or the use of immunosuppressive drugs, thus giving a more reliable view of the biology of NK cell reconstitution after stem cell engraftment. As observed in Chapter II, the phenotype of NK cells changes profoundly immediately after autoHSCT. Furthermore, the frequency of the distinct NK cell subsets is also modulated during post-transplant period, being the immature CD56<sup>bright</sup> NK cells much more abundant immediately after autoHSCT. In line with this, NK cells exhibit a more immature phenotype (NKG2A+CD57- NK cells are predominant after autoHSCT), which is in accordance

whit the proposed linear model of NK cell development, in where NK cell lose the expression of NKG2A while acquire CD57. Moreover, all the studied NK cell subsets had a higher proliferative capacity (Ki67+) and CD56<sup>bright</sup> NK cells have a higher cytotoxic potential (Granzyme B+), which both correlate with high IL-15 plasma levels observed immediately after autoHSCT. Cytokines are known to play a pivotal role in regulating different aspects of immune responses, such as lymphoid development, homeostasis, differentiation and memory [72]. IL-15, in addition to IL-2, IL-12 and IL-18, among others, is involved in NK cell maturation, activation and survival [292]. It is well known that stimulation of NK cells with IL-12, IL-15 and IL-18 induced changes in the expression of activating and inhibitory receptors, and chemokine and cytokine receptors [187,293]. Taking into account that the cytokine milieu also changes after HSCT [294,295], it is tempting to think that some of the alterations observed in the phenotype of NK cells, are probably due to the singular cytokine environment.

The characterization and identification of biomarkers is key to the healthcare system. Biomarkers can be used not only as an early warning signal for certain health risks or to control the progression of a specific disease, but can also help in the development of more individualized treatments. In autoHSCT, ALC-15 has been identified as a prognostic indicator for OS and PFS in breast cancer, MM, NHL, HL and AML patients receiving an autoHSCT (Table 2) [114–117]. Furthermore, NK cell count has been identified as a prognostic indicator for OS and PFS in NHL and MM (Table 2) [122,123], and KIR and HLA genotypes have also been associated with the outcome of cancer patients undergoing autoHSCT (Table 2) [134–136,138,140]. Although the frequency of CD57+ mature NK cells has also been linked to the clinical outcome of different cancer patients [224,225], to our knowledge, this is the first time that the frequency of NKG2A-CD57+ NK cells is associated with the outcome of MM undergoing autoHSCT. Therefore, the data presented in Chapter II provide a step forward in the study of NK cell reconstitution after autoHSCT and the identification of a new biomarker for MM patients treated with this therapeutic strategy.

Since their development, NGS technologies are revolutionizing biology and medicine for their ability to acquire an unprecedented amount of data in a short time. The emergence of these technologies has also transformed RNA research with the development of RNA-seq, which allows the study of the whole transcriptome in a very high-throughput and quantitative manner. Thus, RNA-seq is usually used, among others, to compare gene

expression between different experimental conditions [231,232]. As explained in Chapter III, we have used RNA-seq to study the changes occurring during NK cell reconstitution after autoHSCT by analyzing the transcriptome of these cells at three different time points. The data from these experiments, in which a significant change of gene expression profile was observed immediately after autoHSCT, were in accordance with data obtained with flow cytometry experiments in Chapter II. Very importantly, RNA-seq experiments revealed, to our knowledge, a previously undescribed shift in the NK cells gene expression profile after autoHSCT towards a dNK-like phenotype that expressed, among others, the CD9 marker [33]. Moreover, these CD9+ NK cells seem to have different effector functions compared to CD9- NK cells.

Although RNA-seq and scRNA-seq have been widely used for the study of NK cell biology in different experimental settings [29,234,249,250,235–237,240–242,247,248], this is the first time that this technology is applied to the study of NK cells in the autoHSCT context. Despite the low number of patient samples analyzed by RNA-seq, which is the main limitation of the study, and the high variability between samples, the data obtained leave open the possibility of using this technology with the aim of finding a biomarker for patients undergoing autoHSCT. Indeed, the results suggest an association between CD9 expression on NK cells and patients' outcome. Undoubtedly, more experiments in this direction are needed to decipher the implication of CD9+ NK cells in autoHSCT. Moreover, performing scRNA-seq experiments in NK cells at the three studied time points would certainly provide exciting data regarding the distribution of NK cell subsets and the variations in their gene expression profile.

In summary, NK cells reconstitution after autoHSCT have an important implication in patients' outcome. The results obtained in this doctoral thesis will contribute to the better understanding of NK cell biology and NK cell subsets reconstitution after autoHSCT. The observed results regarding the use of NKp80 as an alternative to CD16, provide a new strategy for the identification of NK cell subsets. Importantly, the fact that the frequency of NKG2A-CD57+ NK cells after autoHSCT is associated with MM patients' outcome, suggest that the maturation stage of NK cells may be a potential biomarker of disease progression after autoHSCT. Finally, the results obtained from RNA-seq analyses reveal the potential of using this technology to further decipher the involvement of NK cells in the prognosis of patients undergoing autoHSCT.



## CONCLUSIONS

1. NKp80 is a more precise marker than CD16 in order to identify CD56<sup>neg</sup> NK cells in cryopreserved samples.
2. The effector functions of CD56<sup>neg</sup> NK cells are not as diminished as previously described.
3. Early after autoHSCT, there is an extensive redistribution of NK cell subsets.
4. After autoHSCT, NK cells undergo a profound phenotypic change characterized, among others, by their immature phenotype and proliferative capacity.
5. IL-15 plasma levels are highly incremented early after autoHSCT and correlate with the number, proliferation capacity and cytotoxic potential of NK cells.
6. There is an association between NK cell maturation stage and the outcome of MM patients undergoing autoHSCT.
7. The gene expression profile of NK cells dramatically changes early after autoHSCT.
8. After autoHSCT, NK cells acquire a dNK-like phenotype with different effector functions compared to conventional NK cells.

## REFERENCES

1. Mjösberg, J.; Spits, H. Human innate lymphoid cells. *J. Allergy Clin. Immunol.* **2016**, *138*, 1265–1276, doi:10.1016/j.jaci.2016.09.009.
2. Vivier, E.; Artis, D.; Colonna, M.; Diefenbach, A.; Di Santo, J.P.; Eberl, G.; Koyasu, S.; Locksley, R.M.; McKenzie, A.N.J.; Mebius, R.E.; et al. Innate Lymphoid Cells: 10 Years On. *Cell* **2018**, *174*, 1054–1066, doi:10.1016/j.cell.2018.07.017.
3. Guillerey, C. Roles of cytotoxic and helper innate lymphoid cells in cancer. *Mamm. Genome* **2018**, *29*, 777–789, doi:10.1007/s00335-018-9781-4.
4. Krabbendam, L.; Bernink, J.H.; Spits, H. Innate lymphoid cells: from helper to killer. *Curr. Opin. Immunol.* **2021**, *68*, 28–33, doi:10.1016/j.coi.2020.08.007.
5. Cortez, V.S.; Colonna, M. Diversity and function of group 1 innate lymphoid cells. *Immunol. Lett.* **2016**, *179*, 19–24, doi:10.1016/j.imlet.2016.07.005.
6. Spits, H.; Bernink, J.H.; Lanier, L. NK cells and type 1 innate lymphoid cells: partners in host defense. *Nat. Immunol.* **2016**, *17*, 758–764, doi:10.1038/ni.3482.
7. Björklund, Å.K.; Forkel, M.; Picelli, S.; Konya, V.; Theorell, J.; Friberg, D.; Sandberg, R.; Mjösberg, J. The heterogeneity of human CD127+ innate lymphoid cells revealed by single-cell RNA sequencing. *Nat. Immunol.* **2016**, *17*, 451–460, doi:10.1038/ni.3368.
8. Simoni, Y.; Newell, E.W. Dissecting human ILC heterogeneity: more than just three subsets. *Immunology* **2018**, *153*, 297–303, doi:10.1111/imm.12862.
9. Gao, Y.; Souza-Fonseca-Guimaraes, F.; Bald, T.; Ng, S.S.; Young, A.; Ngiow, S.F.; Rautela, J.; Straube, J.; Waddell, N.; Blake, S.J.; et al. Tumor immunoevasion by the conversion of effector NK cells into type 1 innate lymphoid cells. *Nat. Immunol.* **2017**, *18*, 1004–1015, doi:10.1038/ni.3800.
10. Seillet, C.; Brossay, L.; Vivier, E. Natural killers or ILC1s? That is the question. *Curr. Opin. Immunol.* **2021**, *68*, 48–53, doi:10.1016/j.coi.2020.08.009.
11. Cooper, M.A.; Fehniger, T.A.; Caligiuri, M.A. The biology of human natural killer-cell subsets. *Trends Immunol.* **2001**, *22*, 633–40, doi:10.1016/s1471-4906(01)02060-9.
12. Schwane, V.; Huynh-Tran, V.H.; Vollmers, S.; Yakup, V.M.; Sauter, J.; Schmidt, A.H.; Peine, S.; Altfeld, M.; Richert, L.; Körner, C. Distinct Signatures in the Receptor Repertoire Discriminate CD56bright and CD56dim Natural Killer Cells. *Front. Immunol.* **2020**, *11*, 1–13, doi:10.3389/fimmu.2020.568927.
13. Freud, A.G.; Mundy-Bosse, B.L.; Yu, J.; Caligiuri, M.A. The Broad Spectrum of Human Natural Killer Cell Diversity. *Immunity* **2017**, *47*, 820–833, doi:10.1016/j.immuni.2017.10.008.
14. Michel, T.; Poli, A.; Cuapio, A.; Briquemont, B.; Iserentant, G.; Ollert, M.; Zimmer, J. Human CD56 bright NK Cells: An Update. *J. Immunol.* **2016**, *196*, 2923–2931, doi:10.4049/jimmunol.1502570.

15. Wagner, J.A.; Rosario, M.; Romee, R.; Berrien-Elliott, M.M.; Schneider, S.E.; Leong, J.W.; Sullivan, R.P.; Jewell, B.A.; Becker-Hapak, M.; Schappe, T.; et al. CD56bright NK cells exhibit potent antitumor responses following IL-15 priming. *J. Clin. Invest.* **2017**, *127*, 4042–4058, doi:10.1172/JCI90387.
16. Poznanski, S.M.; Nham, T.; Chew, M. V.; Lee, A.J.; Hammill, J.A.; Fan, I.Y.; Butcher, M.; Bramson, J.L.; Lee, D.A.; Hirte, H.W.; et al. Expanded CD56 superbright CD16 + NK Cells from Ovarian Cancer Patients Are Cytotoxic against Autologous Tumor in a Patient-Derived Xenograft Murine Model. *Cancer Immunol. Res.* **2018**, *6*, 1174–1185, doi:10.1158/2326-6066.CIR-18-0144.
17. Fauriat, C.; Long, E.O.; Ljunggren, H.-G.; Bryceson, Y.T. Regulation of human NK-cell cytokine and chemokine production by target cell recognition. *Blood* **2010**, *115*, 2167–2176, doi:10.1182/blood-2009-08-238469.
18. De Maria, A.; Bozzano, F.; Cantoni, C.; Moretta, L. Revisiting human natural killer cell subset function revealed cytolytic CD56dimCD16+ NK cells as rapid producers of abundant IFN- on activation. *Proc. Natl. Acad. Sci.* **2011**, *108*, 728–732, doi:10.1073/pnas.1012356108.
19. Roberto, A.; Di Vito, C.; Zaghi, E.; Mazza, E.M.C.; Capucetti, A.; Calvi, M.; Tentorio, P.; Zanon, V.; Sarina, B.; Mariotti, J.; et al. The early expansion of anergic NKG2A pos /CD56 dim /CD16 neg natural killer represents a therapeutic target in haploidentical hematopoietic stem cell transplantation. *Haematologica* **2018**, *103*, 1390–1402, doi:10.3324/haematol.2017.186619.
20. Castriconi, R.; Carrega, P.; Dondero, A.; Bellora, F.; Casu, B.; Regis, S.; Ferlazzo, G.; Bottino, C. Molecular Mechanisms Directing Migration and Retention of Natural Killer Cells in Human Tissues. *Front. Immunol.* **2018**, *9*, 1–14, doi:10.3389/fimmu.2018.02324.
21. Horowitz, A.; Strauss-Albee, D.M.; Leipold, M.; Kubo, J.; Nemat-Gorgani, N.; Dogan, O.C.; Dekker, C.L.; Mackey, S.; Maecker, H.; Swan, G.E.; et al. Genetic and environmental determinants of human NK cell diversity revealed by mass cytometry. *Sci. Transl. Med.* **2013**, *5*, 208ra145, doi:10.1126/scitranslmed.3006702.
22. Smith, S.L.; Kennedy, P.R.; Stacey, K.B.; Worboys, J.D.; Yarwood, A.; Seo, S.; Solloa, E.H.; Mistretta, B.; Chatterjee, S.S.; Gunaratne, P.; et al. Diversity of peripheral blood human NK cells identified by single-cell RNA sequencing. *Blood Adv.* **2020**, *4*, 1388–1406, doi:10.1182/bloodadvances.2019000699.
23. Björkström, N.K.; Ljunggren, H.-G.; Michaëlsson, J. Emerging insights into natural killer cells in human peripheral tissues. *Nat. Rev. Immunol.* **2016**, *16*, 310–320, doi:10.1038/nri.2016.34.
24. Evans, J.H.; Horowitz, A.; Mehrabi, M.; Wise, E.L.; Pease, J.E.; Riley, E.M.; Davis, D.M. A distinct subset of human NK cells expressing HLA-DR expand in response to IL-2 and can aid immune responses to BCG. *Eur. J. Immunol.* **2011**, *41*, 1924–1933, doi:10.1002/eji.201041180.
25. Erokhina, S.A.; Streltsova, M.A.; Kanevskiy, L.M.; Telford, W.G.; Sapozhnikov, A.M.; Kovalenko, E.I. HLA-DR + NK cells are mostly characterized by less

- mature phenotype and high functional activity. *Immunol. Cell Biol.* **2018**, *96*, 212–228, doi:10.1111/imcb.1032.
26. Grzywacz, B.; Kataria, N.; Sikora, M.; Oostendorp, R.A.; Dzierzak, E.A.; Blazar, B.R.; Miller, J.S.; Verneris, M.R. Coordinated acquisition of inhibitory and activating receptors and functional properties by developing human natural killer cells. *Blood* **2006**, *108*, 3824–3833, doi:10.1182/blood-2006-04-020198.
  27. Ostrowski, S.R.; Ullum, H.; Pedersen, B.K.; Gerstoft, J.; Katzenstein, T.L. 2B4 expression on natural killer cells increases in HIV-1 infected patients followed prospectively during highly active antiretroviral therapy. *Clin. Exp. Immunol.* **2005**, *141*, 526–533, doi:10.1111/j.1365-2249.2005.02869.x.
  28. Peng, H.; Tian, Z. Diversity of tissue-resident NK cells. *Semin. Immunol.* **2017**, *31*, 3–10, doi:10.1016/j.smim.2017.07.006.
  29. Crinier, A.; Milpied, P.; Escalière, B.; Piperoglou, C.; Galluso, J.; Balsamo, A.; Spinelli, L.; Cervera-Marzal, I.; Ebbo, M.; Girard-Madoux, M.; et al. High-Dimensional Single-Cell Analysis Identifies Organ-Specific Signatures and Conserved NK Cell Subsets in Humans and Mice. *Immunity* **2018**, *49*, 971–986.e5, doi:10.1016/j.immuni.2018.09.009.
  30. Hanna, J.; Goldman-Wohl, D.; Hamani, Y.; Avraham, I.; Greenfield, C.; Natanson-Yaron, S.; Prus, D.; Cohen-Daniel, L.; Arnon, T.I.; Manaster, I.; et al. Decidual NK cells regulate key developmental processes at the human fetal-maternal interface. *Nat. Med.* **2006**, *12*, 1065–1074, doi:10.1038/nm1452.
  31. Guerrero, B.; Hassouneh, F.; Delgado, E.; Casado, J.G.; Tarazona, R. Natural killer cells in recurrent miscarriage: An overview. *J. Reprod. Immunol.* **2020**, *142*, 103209, doi:10.1016/j.jri.2020.103209.
  32. Jabrane-Ferrat, N. Features of Human Decidual NK Cells in Healthy Pregnancy and During Viral Infection. *Front. Immunol.* **2019**, *10*, 1–10, doi:10.3389/fimmu.2019.01397.
  33. Koopman, L.A.; Kopcow, H.D.; Rybalov, B.; Boyson, J.E.; Orange, J.S.; Schatz, F.; Masch, R.; Lockwood, C.J.; Schachter, A.D.; Park, P.J.; et al. Human Decidual Natural Killer Cells Are a Unique NK Cell Subset with Immunomodulatory Potential. *J. Exp. Med.* **2003**, *198*, 1201–1212, doi:10.1084/jem.20030305.
  34. Kopcow, H.D.; Allan, D.S.J.; Chen, X.; Rybalov, B.; Andzelm, M.M.; Ge, B.; Strominger, J.L. Human decidual NK cells form immature activating synapses and are not cytotoxic. *Proc. Natl. Acad. Sci.* **2005**, *102*, 15563–15568, doi:10.1073/pnas.0507835102.
  35. Muntasell, A.; Vilches, C.; Angulo, A.; López-Botet, M. Adaptive reconfiguration of the human NK-cell compartment in response to cytomegalovirus: A different perspective of the host-pathogen interaction. *Eur. J. Immunol.* **2013**, *43*, 1133–1141, doi:10.1002/eji.201243117.
  36. Gumá, M.; Angulo, A.; Vilches, C.; Gómez-Lozano, N.; Malats, N.; López-Botet, M. Imprint of human cytomegalovirus infection on the NK cell receptor repertoire. *Blood* **2004**, *104*, 3664–3671, doi:10.1182/blood-2004-05-2058.

37. Gumá, M.; Budt, M.; Sáez, A.; Brckalo, T.; Hengel, H.; Angulo, A.; López-Botet, M. Expansion of CD94/NKG2C<sup>+</sup> NK cells in response to human cytomegalovirus-infected fibroblasts. *Blood* **2006**, *107*, 3624–3631, doi:10.1182/blood-2005-09-3682.
38. Foley, B.; Cooley, S.; Verneris, M.R.; Pitt, M.; Curtsinger, J.; Luo, X.; Lopez-Vergès, S.; Lanier, L.L.; Weisdorf, D.; Miller, J.S. Cytomegalovirus reactivation after allogeneic transplantation promotes a lasting increase in educated NKG2C<sup>+</sup> natural killer cells with potent function. *Blood* **2012**, *119*, 2665–2674, doi:10.1182/blood-2011-10-386995.
39. O’Sullivan, T.E.; Sun, J.C.; Lanier, L.L. Natural Killer Cell Memory. *Immunity* **2015**, *43*, 634–645, doi:10.1016/j.immuni.2015.09.013.
40. Campos, C.; Pera, A.; Sanchez-Correa, B.; Alonso, C.; Lopez-Fernandez, I.; Morgado, S.; Tarazona, R.; Solana, R. Effect of age and CMV on NK cell subpopulations. *Exp. Gerontol.* **2014**, *54*, 130–137, doi:10.1016/j.exger.2014.01.008.
41. Schlums, H.; Cichocki, F.; Tesi, B.; Theorell, J.; Beziat, V.; Holmes, T.D.; Han, H.; Chiang, S.C.C.; Foley, B.; Mattsson, K.; et al. Cytomegalovirus Infection Drives Adaptive Epigenetic Diversification of NK Cells with Altered Signaling and Effector Function. *Immunity* **2015**, *42*, 443–456, doi:10.1016/j.immuni.2015.02.008.
42. Zhang, T.; Scott, J.M.; Hwang, I.; Kim, S. Cutting Edge: Antibody-Dependent Memory-like NK Cells Distinguished by FcR $\gamma$  Deficiency. *J. Immunol.* **2013**, *190*, 1402–1406, doi:10.4049/jimmunol.1203034.
43. Muntasell, A.; Pupuleku, A.; Cisneros, E.; Vera, A.; Moraru, M.; Vilches, C.; López-Botet, M. Relationship of NKG2C Copy Number with the Distribution of Distinct Cytomegalovirus-Induced Adaptive NK Cell Subsets. *J. Immunol.* **2016**, *196*, 3818–3827, doi:10.4049/jimmunol.1502438.
44. Kim, K.H.; Yu, H.T.; Hwang, I.; Park, S.; Park, S.-H.; Kim, S.; Shin, E.-C. Phenotypic and Functional Analysis of Human NK Cell Subpopulations According to the Expression of Fc $\epsilon$ RI $\gamma$  and NKG2C. *Front. Immunol.* **2019**, *10*, 1–13, doi:10.3389/fimmu.2019.02865.
45. Lugli, E.; Marcenaro, E.; Mavilio, D. NK Cell Subset Redistribution during the Course of Viral Infections. *Front. Immunol.* **2014**, *5*, 1–7, doi:10.3389/fimmu.2014.00390.
46. Hu, P.F.; Hultin, L.E.; Hultin, P.; Hausner, M.A.; Hirji, K.; Jewett, A.; Bonavida, B.; Detels, R.; Giorgi, J. V Natural killer cell immunodeficiency in HIV disease is manifest by profoundly decreased numbers of CD16<sup>+</sup>CD56<sup>+</sup> cells and expansion of a population of CD16<sup>dim</sup>CD56<sup>-</sup> cells with low lytic activity. *J. Acquir. Immune Defic. Syndr. Hum. Retrovirol.* **1995**, *10*, 331–40.
47. Björkström, N.K.; Ljunggren, H.-G.; Sandberg, J.K. CD56 negative NK cells: origin, function, and role in chronic viral disease. *Trends Immunol.* **2010**, *31*, 401–406, doi:10.1016/j.it.2010.08.003.
48. Voigt, J.; Malone, D.F.G.; Dias, J.; Leeansyah, E.; Björkström, N.K.; Ljunggren, H.-G.; Gröbe, L.; Klawonn, F.; Heyner, M.; Sandberg, J.K.; et al. Proteome

- analysis of human CD56 neg NK cells reveals a homogeneous phenotype surprisingly similar to CD56 dim NK cells. *Eur. J. Immunol.* **2018**, *48*, 1456–1469, doi:10.1002/eji.201747450.
49. Mavilio, D.; Lombardo, G.; Benjamin, J.; Kim, D.; Follman, D.; Marcenaro, E.; O’Shea, M.A.; Kinter, A.; Kovacs, C.; Moretta, A.; et al. Characterization of CD56-/CD16+ natural killer (NK) cells: A highly dysfunctional NK subset expanded in HIV-infected viremic individuals. *Proc. Natl. Acad. Sci.* **2005**, *102*, 2886–2891, doi:10.1073/pnas.0409872102.
  50. Solana, R.; Campos, C.; Pera, A.; Tarazona, R. Shaping of NK cell subsets by aging. *Curr. Opin. Immunol.* **2014**, *29*, 56–61, doi:10.1016/j.coi.2014.04.002.
  51. Mahapatra, S.; Mace, E.M.; Minard, C.G.; Forbes, L.R.; Vargas-Hernandez, A.; Duryea, T.K.; Makedonas, G.; Banerjee, P.P.; Shearer, W.T.; Orange, J.S. High-resolution phenotyping identifies NK cell subsets that distinguish healthy children from adults. *PLoS One* **2017**, *12*, e0181134, doi:10.1371/journal.pone.0181134.
  52. Pegram, H.J.; Andrews, D.M.; Smyth, M.J.; Darcy, P.K.; Kershaw, M.H. Activating and inhibitory receptors of natural killer cells. *Immunol. Cell Biol.* **2011**, *89*, 216–224, doi:10.1038/icb.2010.78.
  53. Pende, D.; Falco, M.; Vitale, M.; Cantoni, C.; Vitale, C.; Munari, E.; Bertaina, A.; Moretta, F.; Del Zotto, G.; Pietra, G.; et al. Killer Ig-Like Receptors (KIRs): Their Role in NK Cell Modulation and Developments Leading to Their Clinical Exploitation. *Front. Immunol.* **2019**, *10*, doi:10.3389/fimmu.2019.01179.
  54. Borrego, F.; Masilamani, M.; Kabat, J.; Sanni, T.B.; Coligan, J.E. The cell biology of the human natural killer cell CD94/NKG2A inhibitory receptor. *Mol. Immunol.* **2005**, *42*, 485–488, doi:10.1016/j.molimm.2004.07.031.
  55. Braud, V.M.; Allan, D.S.J.; O’Callaghan, C.A.; Söderström, K.; D’Andrea, A.; Ogg, G.S.; Lazetic, S.; Young, N.T.; Bell, J.I.; Phillips, J.H.; et al. HLA-E binds to natural killer cell receptors CD94/NKG2A, B and C. *Nature* **1998**, *391*, 795–799, doi:10.1038/35869.
  56. Ljunggren, H.-G.; Kärre, K. In search of the ‘missing self’: MHC molecules and NK cell recognition. *Immunol. Today* **1990**, *11*, 237–244, doi:10.1016/0167-5699(90)90097-S.
  57. Malmberg, K.J.; Schaffer, M.; Ringdén, O.; Remberger, M.; Ljunggren, H.G. KIR-ligand mismatch in allogeneic hematopoietic stem cell transplantation. *Mol. Immunol.* **2005**, *42*, 531–534, doi:10.1016/j.molimm.2004.07.037.
  58. Ruggeri, L.; Capanni, M.; Urbani, E.; Perruccio, K.; Shlomchik, W.D.; Tosti, A.; Posati, S.; Rogaia, D.; Frassoni, F.; Aversa, F.; et al. Effectiveness of Donor Natural Killer Cell Alloreactivity in Mismatched Hematopoietic Transplants. *Science (80-. )*. **2002**, *295*, 2097–2100, doi:10.1126/science.1068440.
  59. Ruggeri, L.; Capanni, M.; Casucci, M.; Volpi, I.; Tosti, A.; Perruccio, K.; Urbani, E.; Negrin, R.S.; Martelli, M.F.; Velardi, A. Role of natural killer cell alloreactivity in HLA-mismatched hematopoietic stem cell transplantation. *Blood* **1999**, *94*, 333–9.

60. He, Y.; Tian, Z. NK cell education via nonclassical MHC and non-MHC ligands. *Cell. Mol. Immunol.* **2017**, *14*, 321–330, doi:10.1038/cmi.2016.26.
61. Jonsson, A.H.; Yokoyama, W.M. Natural killer cell tolerance licensing and other mechanisms. *Adv. Immunol.* **2009**, *101*, 27–79, doi:10.1016/S0065-2776(08)01002-X.
62. Vitallé, J.; Terrén, I.; Orrantia, A.; Pérez-Garay, R.; Vidal, F.; Iribarren, J.A.; Rodríguez, C.; Lirola, A.M.L.; Bernal, E.; Zenarruzabeitia, O.; et al. CD300a inhibits CD16-mediated NK cell effector functions in HIV-1-infected patients. *Cell. Mol. Immunol.* **2019**, *16*, 940–942, doi:10.1038/s41423-019-0275-4.
63. Sanchez-Correa, B.; Valhondo, I.; Hassouneh, F.; Lopez-Sejas, N.; Pera, A.; Bergua, J.M.; Arcos, M.J.; Bañas, H.; Casas-Avilés, I.; Durán, E.; et al. DNAM-1 and the TIGIT/PVRIG/TACTILE Axis: Novel Immune Checkpoints for Natural Killer Cell-Based Cancer Immunotherapy. *Cancers (Basel)*. **2019**, *11*, 877, doi:10.3390/cancers11060877.
64. Morvan, M.G.; Lanier, L.L. NK cells and cancer: you can teach innate cells new tricks. *Nat. Rev. Cancer* **2016**, *16*, 7–19, doi:10.1038/nrc.2015.5.
65. Bottino, C.; Biassoni, R.; Millo, R.; Moretta, L.; Moretta, A. The human natural cytotoxicity receptors (NCR) that induce HLA class I-independent NK cell triggering. *Hum. Immunol.* **2000**, *61*, 1–6, doi:10.1016/S0198-8859(99)00162-7.
66. Barrow, A.D.; Martin, C.J.; Colonna, M. The natural cytotoxicity receptors in health and disease. *Front. Immunol.* **2019**, *10*, 1–20, doi:10.3389/fimmu.2019.00909.
67. Dhar, P.; Wu, J.D. NKG2D and its ligands in cancer. *Curr. Opin. Immunol.* **2018**, *51*, 55–61, doi:10.1016/j.coi.2018.02.004.
68. Biassoni, R.; Bottino, C.; Cantoni, C.; Moretta, A. Human Natural Killer Receptors and Their Ligands. *Curr. Protoc. Immunol.* **2001**, *46*, 333–370, doi:10.1002/0471142735.im1410s46.
69. Vivier, E.; Ugolini, S.; Blaise, D.; Chabannon, C.; Brossay, L. Targeting natural killer cells and natural killer T cells in cancer. *Nat. Rev. Immunol.* **2012**, *12*, 239–252, doi:10.1038/nri3174.
70. Huntington, N.D.; Legrand, N.; Alves, N.L.; Jaron, B.; Weijer, K.; Plet, A.; Corcuff, E.; Mortier, E.; Jacques, Y.; Spits, H.; et al. IL-15 trans-presentation promotes human NK cell development and differentiation in vivo. *J. Exp. Med.* **2009**, *206*, 25–34, doi:10.1084/jem.20082013.
71. Becknell, B.; Caligiuri, M.A. Interleukin-2, Interleukin-15, and Their Roles in Human Natural Killer Cells. In *Advances in Immunology*; 2005; Vol. 86, pp. 209–239.
72. Zwirner, N.W.; Domaica, C.I. Cytokine regulation of natural killer cell effector functions. *BioFactors* **2010**, *36*, 274–288, doi:10.1002/biof.107.
73. Prager, I.; Watzl, C. Mechanisms of natural killer cell-mediated cellular cytotoxicity. *J. Leukoc. Biol.* **2019**, *105*, 1319–1329, doi:10.1002/JLB.MR0718-269R.

74. Lopez, J.A.; Susanto, O.; Jenkins, M.R.; Lukoyanova, N.; Sutton, V.R.; Law, R.H.P.; Johnston, A.; Bird, C.H.; Bird, P.I.; Whisstock, J.C.; et al. Perforin forms transient pores on the target cell plasma membrane to facilitate rapid access of granzymes during killer cell attack. *Blood* **2013**, *121*, 2659–2668, doi:10.1182/blood-2012-07-446146.
75. Chowdhury, D.; Lieberman, J. Death by a Thousand Cuts: Granzyme Pathways of Programmed Cell Death. *Annu. Rev. Immunol.* **2008**, *26*, 389–420, doi:10.1146/annurev.immunol.26.021607.090404.
76. von Karstedt, S.; Montinaro, A.; Walczak, H. Exploring the TRAILs less travelled: TRAIL in cancer biology and therapy. *Nat. Rev. Cancer* **2017**, *17*, 352–366, doi:10.1038/nrc.2017.28.
77. Peter, M.E.; Krammer, P.H. The CD95(APO-1/Fas) DISC and beyond. *Cell Death Differ.* **2003**, *10*, 26–35, doi:10.1038/sj.cdd.4401186.
78. Jorgovanovic, D.; Song, M.; Wang, L.; Zhang, Y. Roles of IFN- $\gamma$  in tumor progression and regression: a review. *Biomark. Res.* **2020**, *8*, 49, doi:10.1186/s40364-020-00228-x.
79. Vivier, E.; Tomasello, E.; Baratin, M.; Walzer, T.; Ugolini, S. Functions of natural killer cells. *Nat. Immunol.* **2008**, *9*, 503–510, doi:10.1038/ni1582.
80. Eissens, D.N.; Spanholtz, J.; van der Meer, A.; van Cranenbroek, B.; Dolstra, H.; Kwekkeboom, J.; Preijers, F.W.M.B.; Joosten, I. Defining Early Human NK Cell Developmental Stages in Primary and Secondary Lymphoid Tissues. *PLoS One* **2012**, *7*, e30930, doi:10.1371/journal.pone.0030930.
81. Di Vito, C.; Mikulak, J.; Mavilio, D. On the Way to Become a Natural Killer Cell. *Front. Immunol.* **2019**, *10*, 1–15, doi:10.3389/fimmu.2019.01812.
82. Cichocki, F.; Sitnicka, E.; Bryceson, Y.T. NK cell development and function – Plasticity and redundancy unleashed. *Semin. Immunol.* **2014**, *26*, 114–126, doi:10.1016/j.smim.2014.02.003.
83. Adolfsson, J.; Månsson, R.; Buza-Vidas, N.; Hultquist, A.; Liuba, K.; Jensen, C.T.; Bryder, D.; Yang, L.; Borge, O.-J.; Thoren, L.A.M.; et al. Identification of Flt3+ Lympho-Myeloid Stem Cells Lacking Erythro-Megakaryocytic Potential. *Cell* **2005**, *121*, 295–306, doi:10.1016/j.cell.2005.02.013.
84. Cichocki, F.; Grzywacz, B.; Miller, J.S. Human NK Cell Development: One Road or Many? *Front. Immunol.* **2019**, *10*, 2078, doi:10.3389/fimmu.2019.02078.
85. Miller, J.S.; Alley, K.A.; McGlave, P. Differentiation of natural killer (NK) cells from human primitive marrow progenitors in a stroma-based long-term culture system: identification of a CD34+7+ NK progenitor. *Blood* **1994**, *83*, 2594–2601.
86. Miller, J.S.; McCullar, V.; Punzel, M.; Lemischka, I.R.; Moore, K.A. Single adult human CD34(+)/Lin-/CD38(-) progenitors give rise to natural killer cells, B-lineage cells, dendritic cells, and myeloid cells. *Blood* **1999**, *93*, 96–106.
87. Hao, Q.-L.; Zhu, J.; Price, M.A.; Payne, K.J.; Barsky, L.W.; Crooks, G.M. Identification of a novel, human multilymphoid progenitor in cord blood. *Blood* **2001**, *97*, 3683–3690, doi:10.1182/blood.V97.12.3683.



88. Galy, A.; Travis, M.; Cen, D.; Chen, B. Human T, B, natural killer, and dendritic cells arise from a common bone marrow progenitor cell subset. *Immunity* **1995**, *3*, 459–473, doi:10.1016/1074-7613(95)90175-2.
89. Chen, L.; Youssef, Y.; Robinson, C.; Ernst, G.F.; Carson, M.Y.; Young, K.A.; Scoville, S.D.; Zhang, X.; Harris, R.; Sekhri, P.; et al. CD56 Expression Marks Human Group 2 Innate Lymphoid Cell Divergence from a Shared NK Cell and Group 3 Innate Lymphoid Cell Developmental Pathway. *Immunity* **2018**, *49*, 464–476.e4, doi:10.1016/j.immuni.2018.08.010.
90. Renoux, V.M.; Zriwil, A.; Peitzsch, C.; Michaëlsson, J.; Friberg, D.; Soneji, S.; Sitnicka, E. Identification of a Human Natural Killer Cell Lineage-Restricted Progenitor in Fetal and Adult Tissues. *Immunity* **2015**, *43*, 394–407, doi:10.1016/j.immuni.2015.07.011.
91. Freud, A.G.; Caligiuri, M.A. Human natural killer cell development. *Immunol. Rev.* **2006**, *214*, 56–72, doi:10.1111/j.1600-065X.2006.00451.x.
92. Freud, A.G.; Yokohama, A.; Becknell, B.; Lee, M.T.; Mao, H.C.; Ferketich, A.K.; Caligiuri, M.A. Evidence for discrete stages of human natural killer cell differentiation in vivo. *J. Exp. Med.* **2006**, *203*, 1033–1043, doi:10.1084/jem.20052507.
93. Freud, A.G.; Yu, J.; Caligiuri, M.A. Human natural killer cell development in secondary lymphoid tissues. *Semin. Immunol.* **2014**, *26*, 132–137, doi:10.1016/j.smim.2014.02.008.
94. Yu, J.; Freud, A.G.; Caligiuri, M.A. Location and cellular stages of natural killer cell development. *Trends Immunol.* **2013**, *34*, 573–582, doi:10.1016/j.it.2013.07.005.
95. Freud, A.G.; Keller, K.A.; Scoville, S.D.; Mundy-Bosse, B.L.; Cheng, S.; Youssef, Y.; Hughes, T.; Zhang, X.; Mo, X.; Porcu, P.; et al. NKp80 Defines a Critical Step during Human Natural Killer Cell Development. *Cell Rep.* **2016**, *16*, 379–391, doi:10.1016/j.celrep.2016.05.095.
96. Scoville, S.D.; Mundy-Bosse, B.L.; Zhang, M.H.; Chen, L.; Zhang, X.; Keller, K.A.; Hughes, T.; Chen, L.; Cheng, S.; Bergin, S.M.; et al. A Progenitor Cell Expressing Transcription Factor ROR $\gamma$ t Generates All Human Innate Lymphoid Cell Subsets. *Immunity* **2016**, *44*, 1140–1150, doi:10.1016/j.immuni.2016.04.007.
97. Scoville, S.D.; Freud, A.G.; Caligiuri, M.A. Modeling Human Natural Killer Cell Development in the Era of Innate Lymphoid Cells. *Front. Immunol.* **2017**, *8*, 4–11, doi:10.3389/fimmu.2017.00360.
98. Abel, A.M.; Yang, C.; Thakar, M.S.; Malarkannan, S. Natural Killer Cells: Development, Maturation, and Clinical Utilization. *Front. Immunol.* **2018**, *9*, 1–23, doi:10.3389/fimmu.2018.01869.
99. Mace, E.M.; Hsu, A.P.; Monaco-Shawver, L.; Makedonas, G.; Rosen, J.B.; Dropulic, L.; Cohen, J.I.; Frenkel, E.P.; Bagwell, J.C.; Sullivan, J.L.; et al. Mutations in GATA2 cause human NK cell deficiency with specific loss of the CD56bright subset. *Blood* **2013**, *121*, 2669–2677, doi:10.1182/blood-2012-09-453969.

100. Romagnani, C.; Juelke, K.; Falco, M.; Morandi, B.; D'Agostino, A.; Costa, R.; Ratto, G.; Forte, G.; Carrega, P.; Lui, G.; et al. CD56 bright CD16 – Killer Ig-Like Receptor – NK Cells Display Longer Telomeres and Acquire Features of CD56 dim NK Cells upon Activation. *J. Immunol.* **2007**, *178*, 4947–4955, doi:10.4049/jimmunol.178.8.4947.
101. Dulphy, N.; Haas, P.; Busson, M.; Belhadj, S.; Peffault de Latour, R.; Robin, M.; Carmagnat, M.; Loiseau, P.; Tamouza, R.; Scieux, C.; et al. An Unusual CD56 bright CD16 low NK Cell Subset Dominates the Early Posttransplant Period following HLA-Matched Hematopoietic Stem Cell Transplantation. *J. Immunol.* **2008**, *181*, 2227–2237, doi:10.4049/jimmunol.181.3.2227.
102. Collins, P.L.; Cella, M.; Porter, S.I.; Li, S.; Gurewitz, G.L.; Hong, H.S.; Johnson, R.P.; Oltz, E.M.; Colonna, M. Gene Regulatory Programs Conferring Phenotypic Identities to Human NK Cells. *Cell* **2019**, *176*, 348-360.e12, doi:10.1016/j.cell.2018.11.045.
103. Lopez-Vergès, S.; Milush, J.M.; Pandey, S.; York, V.A.; Arakawa-Hoyt, J.; Pircher, H.; Norris, P.J.; Nixon, D.F.; Lanier, L.L. CD57 defines a functionally distinct population of mature NK cells in the human CD56dimCD16+ NK-cell subset. *Blood* **2010**, *116*, 3865–3874, doi:10.1182/blood-2010-04-282301.
104. Björkström, N.K.; Riese, P.; Heuts, F.; Andersson, S.; Fauriat, C.; Ivarsson, M.A.; Björklund, A.T.; Flodström-Tullberg, M.; Michaëlsson, J.; Rottenberg, M.E.; et al. Expression patterns of NKG2A, KIR, and CD57 define a process of CD56dim NK-cell differentiation uncoupled from NK-cell education. *Blood* **2010**, *116*, 3853–3864, doi:10.1182/blood-2010-04-281675.
105. Béziat, V.; Descours, B.; Parizot, C.; Debré, P.; Vieillard, V. NK Cell Terminal Differentiation: Correlated Stepwise Decrease of NKG2A and Acquisition of KIRs. *PLoS One* **2010**, *5*, e11966, doi:10.1371/journal.pone.0011966.
106. Béziat, V.; Duffy, D.; Quoc, S.N.; Le Garff-Tavernier, M.; Decocq, J.; Combadière, B.; Debré, P.; Vieillard, V. CD56 bright CD16 + NK Cells: A Functional Intermediate Stage of NK Cell Differentiation. *J. Immunol.* **2011**, *186*, 6753–6761, doi:10.4049/jimmunol.1100330.
107. Bozzano, F.; Della Chiesa, M.; Pelosi, A.; Antonini, F.; Ascierto, M.L.; Del Zotto, G.; Moretta, F.; Muccio, L.; Luganini, A.; Gribaudo, G.; et al. HCMV-controlling NKG2C+ NK cells originate from novel circulating inflammatory precursors. *J. Allergy Clin. Immunol.* **2021**, doi:10.1016/j.jaci.2020.12.648.
108. Bazinet, A.; Popradi, G. A general practitioner's guide to hematopoietic stem-cell transplantation. *Curr. Oncol.* **2019**, *26*, 187–191, doi:10.3747/co.26.5033.
109. Copelan, E.A. Hematopoietic Stem-Cell Transplantation. *N. Engl. J. Med.* **2006**, *354*, 1813–1826, doi:10.1056/NEJMra052638.
110. Niederwieser, D.; Baldomero, H.; Szer, J.; Gratwohl, M.; Aljurf, M.; Atsuta, Y.; Bouzas, L.F.; Confer, D.; Greinix, H.; Horowitz, M.; et al. Hematopoietic stem cell transplantation activity worldwide in 2012 and a SWOT analysis of the Worldwide Network for Blood and Marrow Transplantation Group including the global survey. *Bone Marrow Transplant.* **2016**, *51*, 778–785, doi:10.1038/bmt.2016.18.

111. Passweg, J.R.; Baldomero, H.; Chabannon, C.; Basak, G.W.; Corbacioglu, S.; Duarte, R.; Dolstra, H.; Lankester, A.C.; Mohty, M.; Montoto, S.; et al. The EBMT activity survey on hematopoietic-cell transplantation and cellular therapy 2018: CAR-T's come into focus. *Bone Marrow Transplant.* **2020**, *55*, 1604–1613, doi:10.1038/s41409-020-0826-4.
112. Dickinson, A.M.; Norden, J.; Li, S.; Hromadnikova, I.; Schmid, C.; Schmetzer, H.; Jochem-Kolb, H. Graft-versus-Leukemia Effect Following Hematopoietic Stem Cell Transplantation for Leukemia. *Front. Immunol.* **2017**, *8*, doi:10.3389/fimmu.2017.00496.
113. Porrata, L.F. Autologous Graft-versus-Tumor Effect: Reality or Fiction? *Adv. Hematol.* **2016**, *2016*, 1–8, doi:10.1155/2016/5385972.
114. Porrata, L.; Ingle, J.; Litzow, M.; Geyer, S.; Markovic, S. Prolonged survival associated with early lymphocyte recovery after autologous hematopoietic stem cell transplantation for patients with metastatic breast cancer. *Bone Marrow Transplant.* **2001**, *28*, 865–871, doi:10.1038/sj.bmt.1703236.
115. Porrata, L.F.; Gertz, M.A.; Inwards, D.J.; Litzow, M.R.; Lacy, M.Q.; Tefferi, A.; Gastineau, D.A.; Dispenzieri, A.; Ansell, S.M.; Micallef, I.N.M.; et al. Early lymphocyte recovery predicts superior survival after autologous hematopoietic stem cell transplantation in multiple myeloma or non-Hodgkin lymphoma. *Blood* **2001**, *98*, 579–585, doi:10.1182/blood.V98.3.579.
116. Porrata, L.F.; Inwards, D.J.; Micallef, I.N.; Ansell, S.M.; Geyer, S.M.; Markovic, S.N. Early lymphocyte recovery post-autologous haematopoietic stem cell transplantation is associated with better survival in Hodgkin's disease. *Br. J. Haematol.* **2002**, *117*, 629–633, doi:10.1046/j.1365-2141.2002.03478.x.
117. Porrata, L.; Litzow, M.; Tefferi, A.; Letendre, L.; Kumar, S.; Geyer, S.; Markovic, S. Early lymphocyte recovery is a predictive factor for prolonged survival after autologous hematopoietic stem cell transplantation for acute myelogenous leukemia. *Leukemia* **2002**, *16*, 1311–1318, doi:10.1038/sj.leu.2402503.
118. Porrata, L.F.; Gastineau, D.A.; Padley, D.; Bundy, K.; Markovic, S.N. Re-infused Autologous Graft Natural Killer Cells Correlates with Absolute Lymphocyte Count Recovery after Autologous Stem Cell Transplantation. *Leuk. Lymphoma* **2003**, *44*, 997–1000, doi:10.1080/1042819031000077089.
119. Rutella, S.; Rumi, C.; Laurenti, L.; Pierelli, L.; Sora', F.; Sica, S.; Leone, G. Immune reconstitution after transplantation of autologous peripheral CD34 + cells: analysis of predictive factors and comparison with unselected progenitor transplants. *Br. J. Haematol.* **2000**, *108*, 105–115, doi:10.1046/j.1365-2141.2000.01824.x.
120. Hiwase, D.K.; Hiwase, S.; Bailey, M.; Bollard, G.; Schwarzer, A.P. Higher Infused Lymphocyte Dose Predicts Higher Lymphocyte Recovery, Which in Turn, Predicts Superior Overall Survival following Autologous Hematopoietic Stem Cell Transplantation for Multiple Myeloma. *Biol. Blood Marrow Transplant.* **2008**, *14*, 116–124, doi:10.1016/j.bbmt.2007.08.051.
121. Porrata, L.F.; Litzow, M.R.; Inwards, D.J.; Gastineau, D.A.; Moore, S.B.; Pineda,

- A.A.; Bundy, K.L.; Padley, D.J.; Persky, D.; Ansell, S.M.; et al. Infused peripheral blood autograft absolute lymphocyte count correlates with day 15 absolute lymphocyte count and clinical outcome after autologous peripheral hematopoietic stem cell transplantation in non-Hodgkin's lymphoma. *Bone Marrow Transplant.* **2004**, *33*, 291–298, doi:10.1038/sj.bmt.1704355.
122. Porrata, L.F.; Inwards, D.J.; Ansell, S.M.; Micallef, I.N.; Johnston, P.B.; Gastineau, D.A.; Litzow, M.R.; Winters, J.L.; Markovic, S.N. Early Lymphocyte Recovery Predicts Superior Survival after Autologous Stem Cell Transplantation in Non-Hodgkin Lymphoma: A Prospective Study. *Biol. Blood Marrow Transplant.* **2008**, *14*, 807–816, doi:10.1016/j.bbmt.2008.04.013.
123. Rueff, J.; Medinger, M.; Heim, D.; Passweg, J.; Stern, M. Lymphocyte Subset Recovery and Outcome after Autologous Hematopoietic Stem Cell Transplantation for Plasma Cell Myeloma. *Biol. Blood Marrow Transplant.* **2014**, *20*, 896–899, doi:10.1016/j.bbmt.2014.03.007.
124. Porrata, L.F.; Inwards, D.J.; Micallef, I.N.; Johnston, P.B.; Ansell, S.M.; Hogan, W.J.; Markovic, S.N. Interleukin-15 Affects Patient Survival through Natural Killer Cell Recovery after Autologous Hematopoietic Stem Cell Transplantation for Non-Hodgkin Lymphomas. *Clin. Dev. Immunol.* **2010**, *2010*, 1–13, doi:10.1155/2010/914945.
125. Porrata, L.F.; Markovic, S.N. Timely reconstitution of immune competence affects clinical outcome following autologous stem cell transplantation. *Clin. Exp. Med.* **2004**, *4*, 78–85, doi:10.1007/s10238-004-0041-4.
126. Porrata, L.F.; Litzow, M.R.; Markovic, S.N. Immune Reconstitution After Autologous Hematopoietic Stem Cell Transplantation. *Mayo Clin. Proc.* **2001**, *76*, 407–412, doi:10.4065/76.4.407.
127. Ali, M.; Oyama, Y.; Monreal, J.; Winter, J.; Tallman, M.; Gordon, L.; Williams, S.; Singhal, S.; Mehta, J. Reassessing the definition of myeloid engraftment after autotransplantation: it is not necessary to see  $0.5 \times 10^9/l$  neutrophils on 3 consecutive days to define myeloid recovery. *Bone Marrow Transplant.* **2002**, *30*, 749–752, doi:10.1038/sj.bmt.1703741.
128. Heck, C.; Steiner, S.; Kaebisch, E.M.; Frentsch, M.; Wittenbecher, F.; Scheibenbogen, C.; Hanitsch, L.G.; Nogai, A.; le Coutre, P.; Bullinger, L.; et al. CD4+ T Cell Dependent B Cell Recovery and Function After Autologous Hematopoietic Stem Cell Transplantation. *Front. Immunol.* **2021**, *12*, 1–12, doi:10.3389/fimmu.2021.736137.
129. Storek, J.; Geddes, M.; Khan, F.; Huard, B.; Helg, C.; Chalandon, Y.; Passweg, J.; Roosnek, E. Reconstitution of the immune system after hematopoietic stem cell transplantation in humans. *Semin. Immunopathol.* **2008**, *30*, 425–437, doi:10.1007/s00281-008-0132-5.
130. Foley, B.; Felices, M.; Cichocki, F.; Cooley, S.; Verneris, M.R.; Miller, J.S. The biology of NK cells and their receptors affects clinical outcomes after hematopoietic cell transplantation (HCT). *Immunol. Rev.* **2014**, *258*, 45–63, doi:10.1111/imr.12157.
131. Ruggeri, L.; Aversa, F.; Martelli, M.F.; Velardi, A. Allogeneic hematopoietic

- transplantation and natural killer cell recognition of missing self. *Immunol. Rev.* **2006**, *214*, 202–218, doi:10.1111/j.1600-065X.2006.00455.x.
132. Yu, J.; Venstrom, J.M.; Liu, X.-R.; Pring, J.; Hasan, R.S.; O'Reilly, R.J.; Hsu, K.C. Breaking tolerance to self, circulating natural killer cells expressing inhibitory KIR for non-self HLA exhibit effector function after T cell-depleted allogeneic hematopoietic cell transplantation. *Blood* **2009**, *113*, 3875–3884, doi:10.1182/blood-2008-09-177055.
  133. Sun, J.C.; Lanier, L.L. Tolerance of NK cells encountering their viral ligand during development. *J. Exp. Med.* **2008**, *205*, 1819–1828, doi:10.1084/jem.20072448.
  134. Skerrett, D.; Rosina, O.; Bodian, C.; Isola, L.; Gudzowaty, O.; Scigliano, E.; Fruchtmann, S. Human Leukocyte Antigens (HLA)-Cw as Prognostic Indicators in Autologous Transplantation for Lymphoma. *Cancer Invest.* **2001**, *19*, 487–494, doi:10.1081/CNV-100103847.
  135. Leung, W.; Handgretinger, R.; Iyengar, R.; Turner, V.; Holladay, M.S.; Hale, G.A. Inhibitory KIR–HLA receptor–ligand mismatch in autologous haematopoietic stem cell transplantation for solid tumour and lymphoma. *Br. J. Cancer* **2007**, *97*, 539–542, doi:10.1038/sj.bjc.6603913.
  136. Venstrom, J.M.; Zheng, J.; Noor, N.; Danis, K.E.; Yeh, A.W.; Cheung, I.Y.; Dupont, B.; O'Reilly, R.J.; Cheung, N.-K. V.; Hsu, K.C. KIR and HLA Genotypes Are Associated with Disease Progression and Survival following Autologous Hematopoietic Stem Cell Transplantation for High-Risk Neuroblastoma. *Clin. Cancer Res.* **2009**, *15*, 7330–7334, doi:10.1158/1078-0432.CCR-09-1720.
  137. Stern, M.; Paulussen, M.; Rischewski, J.; Tichelli, A.; Gratwohl, A. Missing ligand model in autologous stem cell transplantation. *Br. J. Cancer* **2008**, *98*, 852–853, doi:10.1038/sj.bjc.6604153.
  138. Marra, J.; Greene, J.; Hwang, J.; Du, J.; Damon, L.; Martin, T.; Venstrom, J.M. KIR and HLA Genotypes Predictive of Low-Affinity Interactions Are Associated with Lower Relapse in Autologous Hematopoietic Cell Transplantation for Acute Myeloid Leukemia. *J. Immunol.* **2015**, *194*, 4222–4230, doi:10.4049/jimmunol.1402124.
  139. Cella, M.; Longo, A.; Ferrara, G.B.; Strominger, J.L.; Colonna, M. NK3-specific natural killer cells are selectively inhibited by Bw4-positive HLA alleles with isoleucine 80. *J. Exp. Med.* **1994**, *180*, 1235–1242, doi:10.1084/jem.180.4.1235.
  140. Gabriel, I.H.; Sergeant, R.; Szydlo, R.; Apperley, J.F.; DeLavallade, H.; Alsuliman, A.; Khoder, A.; Marin, D.; Kanfer, E.; Cooper, N.; et al. Interaction between KIR3DS1 and HLA-Bw4 predicts for progression-free survival after autologous stem cell transplantation in patients with multiple myeloma. *Blood* **2010**, *116*, 2033–2039, doi:10.1182/blood-2010-03-273706.
  141. López-Vázquez, A.; Rodrigo, L.; Martínez-Borra, J.; Pérez, R.; Rodríguez, M.; Fdez-Morera, J.L.; Fuentes, D.; Rodríguez-Rodero, S.; González, S.; López-Larrea, C. Protective Effect of the HLA-Bw4I80 Epitope and the Killer Cell Immunoglobulin-Like Receptor 3DS1 Gene against the Development of

- Hepatocellular Carcinoma in Patients with Hepatitis C Virus Infection. *J. Infect. Dis.* **2005**, *192*, 162–165, doi:10.1086/430351.
142. Arteche-López, A.; Kreutzman, A.; Alegre, A.; Sanz Martín, P.; Aguado, B.; González-Pardo, M.; Espiño, M.; Villar, L.M.; García Belmonte, D.; de la Cámara, R.; et al. Multiple myeloma patients in long-term complete response after autologous stem cell transplantation express a particular immune signature with potential prognostic implication. *Bone Marrow Transplant.* **2017**, *52*, 832–838, doi:10.1038/bmt.2017.29.
  143. Bhutani, M.; Foureau, D.; Zhang, Q.; Robinson, M.; Wynn, A.S.; Steuerwald, N.M.; Druhan, L.J.; Guo, F.; Rigby, K.; Turner, M.; et al. Peripheral Immunotype Correlates with Minimal Residual Disease Status and Is Modulated by Immunomodulatory Drugs in Multiple Myeloma. *Biol. Blood Marrow Transplant.* **2019**, *25*, 459–465, doi:10.1016/j.bbmt.2018.11.015.
  144. Jacobs, B.; Tognarelli, S.; Poller, K.; Bader, P.; Mackensen, A.; Ullrich, E. NK Cell Subgroups, Phenotype, and Functions After Autologous Stem Cell Transplantation. *Front. Immunol.* **2015**, *6*, 583, doi:10.3389/fimmu.2015.00583.
  145. Vulpis, E.; Stabile, H.; Soriani, A.; Fionda, C.; Petrucci, M.; Mariggio', E.; Ricciardi, M.; Cippitelli, M.; Gismondi, A.; Santoni, A.; et al. Key Role of the CD56<sup>low</sup>CD16<sup>low</sup> Natural Killer Cell Subset in the Recognition and Killing of Multiple Myeloma Cells. *Cancers (Basel).* **2018**, *10*, 473, doi:10.3390/cancers10120473.
  146. Merino, A.M.; Mehta, R.S.; Luo, X.; Kim, H.; De For, T.; Janakiram, M.; Cooley, S.; Wangen, R.; Cichocki, F.; Weisdorf, D.J.; et al. Early Adaptive Natural Killer Cell Expansion Is Associated with Decreased Relapse After Autologous Transplantation for Multiple Myeloma. *Transplant. Cell. Ther.* **2021**, *27*, 310.e1-310.e6, doi:10.1016/j.jtct.2020.10.023.
  147. Cichocki, F.; Taras, E.; Chiuppesi, F.; Wagner, J.E.; Blazar, B.R.; Brunstein, C.; Luo, X.; Diamond, D.J.; Cooley, S.; Weisdorf, D.J.; et al. Adaptive NK cell reconstitution is associated with better clinical outcomes. *JCI Insight* **2019**, *4*, doi:10.1172/jci.insight.125553.
  148. Cichocki, F.; Cooley, S.; Davis, Z.; DeFor, T.E.; Schlums, H.; Zhang, B.; Brunstein, C.G.; Blazar, B.R.; Wagner, J.; Diamond, D.J.; et al. CD56<sup>dim</sup>CD57<sup>+</sup>NKG2C<sup>+</sup> NK cell expansion is associated with reduced leukemia relapse after reduced intensity HCT. *Leukemia* **2016**, *30*, 456–463, doi:10.1038/leu.2015.260.
  149. Della Chiesa, M.; Falco, M.; Podestà, M.; Locatelli, F.; Moretta, L.; Frassoni, F.; Moretta, A. Phenotypic and functional heterogeneity of human NK cells developing after umbilical cord blood transplantation: a role for human cytomegalovirus? *Blood* **2012**, *119*, 399–410, doi:10.1182/blood-2011-08-372003.
  150. Lu, X.; Kondo, Y.; Takamatsu, H.; Ohata, K.; Yamazaki, H.; Takami, A.; Akatsuka, Y.; Nakao, S. CD16 + CD56 – NK cells in the peripheral blood of cord blood transplant recipients: a unique subset of NK cells possibly associated with graft-versus-leukemia effect. *Eur. J. Haematol.* **2008**, *81*, 18–25, doi:10.1111/j.1600-0609.2008.01073.x.

151. De Angelis, C.; Mancusi, A.; Ruggeri, L.; Capanni, M.; Urbani, E.; Velardi, A.; Stern, M. Expansion of CD56-Negative, CD16-Positive, KIR-Expressing Natural Killer Cells after T Cell-Depleted Haploidentical Hematopoietic Stem Cell Transplantation. *Acta Haematol.* **2011**, *126*, 13–20, doi:10.1159/000323661.
152. Mjösberg, J.; Spits, H. Human innate lymphoid cells. *J. Allergy Clin. Immunol.* **2016**, *138*, 1265–1276, doi:10.1016/j.jaci.2016.09.009.
153. Spits, H.; Artis, D.; Colonna, M.; Dieffenbach, A.; Di Santo, J.P.; Eberl, G.; Koyasu, S.; Locksley, R.M.; McKenzie, A.N.J.; Mebius, R.E.; et al. Innate lymphoid cells — a proposal for uniform nomenclature. *Nat. Rev. Immunol.* **2013**, *13*, 145–149, doi:10.1038/nri3365.
154. Trabanelli, S.; Gomez-Cadena, A.; Salomé, B.; Michaud, K.; Mavilio, D.; Landis, B.N.; Jandus, P.; Jandus, C. Human innate lymphoid cells (ILCs): Toward a uniform immune-phenotyping. *Cytom. Part B Clin. Cytom.* **2018**, *94*, 392–399, doi:10.1002/cyto.b.21614.
155. Artis, D.; Spits, H. The biology of innate lymphoid cells. *Nature* **2015**, *517*, 293–301, doi:10.1038/nature14189.
156. Bal, S.M.; Golebski, K.; Spits, H. Plasticity of innate lymphoid cell subsets. *Nat. Rev. Immunol.* **2020**, 1–14, doi:10.1038/s41577-020-0282-9.
157. Colonna, M. Innate Lymphoid Cells: Diversity, Plasticity, and Unique Functions in Immunity. *Immunity* **2018**, *48*, 1104–1117, doi:10.1016/j.immuni.2018.05.013.
158. Montaldo, E.; Zotto, G. Del; Chiesa, M. Della; Mingari, M.C.; Moretta, A.; Maria, A. De; Moretta, L. Human NK cell receptors/markers: A tool to analyze NK cell development, subsets and function. *Cytom. Part A* **2013**, *83A*, 702–713, doi:10.1002/cyto.a.22302.
159. Vallentin, B.; Barlogis, V.; Piperoglou, C.; Cypowj, S.; Zucchini, N.; Chene, M.; Navarro, F.; Farnarier, C.; Vivier, E.; Vely, F. Innate Lymphoid Cells in Cancer. *Cancer Immunol. Res.* **2015**, *3*, 1109–1114, doi:10.1158/2326-6066.CIR-15-0222.
160. Borrego, F.; Lopez-Beltran, A.; Peña, J.; Solana, R. Downregulation of Fcγ Receptor IIIAα (CD16-II) on Natural Killer Cells Induced by Anti-CD16 mAb Is Independent of Protein Tyrosine Kinases and Protein Kinase C. *Cell. Immunol.* **1994**, *158*, 208–217, doi:10.1006/cimm.1994.1268.
161. Grzywacz, B.; Kataria, N.; Verneris, M.R. CD56dimCD16+ NK cells downregulate CD16 following target cell induced activation of matrix metalloproteinases. *Leukemia* **2007**, *21*, 356–359, doi:10.1038/sj.leu.2404499.
162. Romee, R.; Foley, B.; Lenvik, T.; Wang, Y.; Zhang, B.; Ankarlo, D.; Luo, X.; Cooley, S.; Verneris, M.; Walcheck, B.; et al. NK cell CD16 surface expression and function is regulated by a disintegrin and metalloprotease-17 (ADAM17). *Blood* **2013**, *121*, 3599–3608, doi:10.1182/blood-2012-04-425397.
163. Peruzzi, G.; Femnou, L.; Gil-Krzewska, A.; Borrego, F.; Weck, J.; Krzewski, K.; Coligan, J.E. Membrane-Type 6 Matrix Metalloproteinase Regulates the Activation-Induced Downmodulation of CD16 in Human Primary NK Cells. *J. Immunol.* **2013**, *191*, 1883–1894, doi:10.4049/jimmunol.1300313.

164. Zhou, Q.; Gil-Krzewska, A.; Peruzzi, G.; Borrego, F. Matrix metalloproteinases inhibition promotes the polyfunctionality of human natural killer cells in therapeutic antibody-based anti-tumour immunotherapy. *Clin. Exp. Immunol.* **2013**, *173*, 131–139, doi:10.1111/cei.12095.
165. Lugthart, G.; van Ostaijen-ten Dam, M.M.; van Tol, M.J.D.; Lankester, A.C.; Schilham, M.W. CD56(dim)CD16<sup>-</sup> NK cell phenotype can be induced by cryopreservation. *Blood* **2015**, *125*, 1842–3, doi:10.1182/blood-2014-11-610311.
166. Tarazona, R.; Casado, J.G.; Delarosa, O.; Torre-Cisneros, J.; Villanueva, J.L.; Sanchez, B.; Galiani, M.D.; Gonzalez, R.; Solana, R.; Pena, J. Selective depletion of CD56dim NK cell subsets and maintenance of CD56bright NK cells in treatment-naive HIV-1-seropositive individuals. *J. Clin. Immunol.* **2002**, *22*, 176–183, doi:10.1023/A:1015476114409.
167. Müller-Durovic, B.; Grählert, J.; Devine, O.P.; Akbar, A.N.; Hess, C. CD56-negative NK cells with impaired effector function expand in CMV and EBV co-infected healthy donors with age. *Aging (Albany. NY)*. **2019**, *11*, 724–740, doi:10.18632/aging.101774.
168. Alter, G.; Teigen, N.; Davis, B.T.; Addo, M.M.; Suscovich, T.J.; Waring, M.T.; Streeck, H.; Johnston, M.N.; Staller, K.D.; Zaman, M.T.; et al. Sequential deregulation of NK cell subset distribution and function starting in acute HIV-1 infection. *Blood* **2005**, *106*, 3366–3369, doi:10.1182/blood-2005-03-1100.
169. Barker, E.; Martinson, J.; Brooks, C.; Landay, A.; Deeks, S. Dysfunctional natural killer cells, in vivo, are governed by HIV viremia regardless of whether the infected individual is on antiretroviral therapy. *AIDS* **2007**, *21*, 2363–2365, doi:10.1097/QAD.0b013e3282f1d658.
170. Brunetta, E.; Fogli, M.; Varchetta, S.; Bozzo, L.; Hudspeth, K.L.; Marcenaro, E.; Moretta, A.; Mavilio, D. The decreased expression of Siglec-7 represents an early marker of dysfunctional natural killer-cell subsets associated with high levels of HIV-1 viremia. *Blood* **2009**, *114*, 3822–3830, doi:10.1182/blood-2009-06-226332.
171. Bradley, T.; Peppas, D.; Pedroza-Pacheco, I.; Li, D.; Cain, D.W.; Henao, R.; Venkat, V.; Hora, B.; Chen, Y.; Vandergrift, N.A.; et al. RAB11FIP5 Expression and Altered Natural Killer Cell Function Are Associated with Induction of HIV Broadly Neutralizing Antibody Responses. *Cell* **2018**, *175*, 387-399.e17, doi:10.1016/j.cell.2018.08.064.
172. Gonzalez, V.D.; Falconer, K.; Björkström, N.K.; Blom, K.G.; Weiland, O.; Ljunggren, H.-G.; Alaeus, A.; Sandberg, J.K. Expansion of Functionally Skewed CD56-Negative NK Cells in Chronic Hepatitis C Virus Infection: Correlation with Outcome of Pegylated IFN- $\alpha$  and Ribavirin Treatment. *J. Immunol.* **2009**, *183*, 6612–6618, doi:10.4049/jimmunol.0901437.
173. Gonzalez, V.D.; Falconer, K.; Michaëlsson, J.; Moll, M.; Reichard, O.; Alaeus, A.; Sandberg, J.K. Expansion of CD56<sup>-</sup> NK cells in chronic HCV/HIV-1 co-infection: Reversion by antiviral treatment with pegylated IFN $\alpha$  and ribavirin. *Clin. Immunol.* **2008**, *128*, 46–56, doi:10.1016/j.clim.2008.03.521.
174. Eller, M.A.; Eller, L.A.; Ouma, B.J.; Thelian, D.; Gonzalez, V.D.; Guwatudde,



- D.; McCutchan, F.E.; Marovich, M.A.; Michael, N.L.; de Souza, M.S.; et al. Elevated Natural Killer Cell Activity Despite Altered Functional and Phenotypic Profile in Ugandans With HIV-1 Clade A or Clade D Infection. *JAIDS J. Acquir. Immune Defic. Syndr.* **2009**, *51*, 380–389, doi:10.1097/QAI.0b013e3181aa256e.
175. Milush, J.M.; López-Vergès, S.; York, V.A.; Deeks, S.G.; Martin, J.N.; Hecht, F.M.; Lanier, L.L.; Nixon, D.F. CD56negCD16+NK cells are activated mature NK cells with impaired effector function during HIV-1 infection. *Retrovirology* **2013**, *10*, 158, doi:10.1186/1742-4690-10-158.
176. Vitale, M.; Falco, M.; Castriconi, R.; Parolini, S.; Zambello, R.; Semenzato, G.; Biassoni, R.; Bottino, C.; Moretta, L.; Moretta, A. Identification of NKp80, a novel triggering molecule expressed by human NK cells. *Eur. J. Immunol.* **2001**, *31*, 233–242, doi:10.1002/1521-4141(200101)31:1<233::AID-IMMU233>3.0.CO;2-4.
177. Collin, M.; McGovern, N.; Haniffa, M. Human dendritic cell subsets. *Immunology* **2013**, *140*, 22–30, doi:10.1111/imm.12117.
178. Han, X.; Jorgensen, J.L.; Brahmandam, A.; Schlette, E.; Huh, Y.O.; Shi, Y.; Awagu, S.; Chen, W. Immunophenotypic study of basophils by multiparameter flow cytometry. *Arch. Pathol. Lab. Med.* **2008**, *132*, 813–9, doi:10.1043/1543-2165(2008)132[813:ISOBBM]2.0.CO;2.
179. McKenna, K.; Beignon, A.-S.; Bhardwaj, N. Plasmacytoid Dendritic Cells: Linking Innate and Adaptive Immunity. *J. Virol.* **2005**, *79*, 17–27, doi:10.1128/JVI.79.1.17-27.2005.
180. Vitallé, J.; Terrén, I.; Orrantia, A.; Segurolo, A.; Seras, Y.; Gamboa, P.M.; Borrego, F.; Zenarruzabeitia, O. Increased expression levels of CD300c on basophils from allergic individuals. *World Allergy Organ. J.* **2019**, *12*, 100060, doi:10.1016/j.waojou.2019.100060.
181. Zenarruzabeitia, O.; Vitallé, J.; Terrén, I.; Orrantia, A.; Astigarraga, I.; Dopazo, L.; Gonzalez, C.; Santos-Díez, L.; Tutau, C.; Gamboa, P.M.; et al. CD300c costimulates IgE-mediated basophil activation, and its expression is increased in patients with cow's milk allergy. *J. Allergy Clin. Immunol.* **2019**, *143*, 700-711.e5, doi:10.1016/J.JACI.2018.05.022.
182. Milush, J.M.; Long, B.R.; Snyder-Cappione, J.E.; Cappione, A.J.; York, V.A.; Ndhlovu, L.C.; Lanier, L.L.; Michaëlsson, J.; Nixon, D.F. Functionally distinct subsets of human NK cells and monocyte/DC-like cells identified by coexpression of CD56, CD7, and CD4. *Blood* **2009**, *114*, 4823–4831, doi:10.1182/blood-2009-04-216374.
183. Zenarruzabeitia, O.; Vitallé, J.; García-Obregón, S.; Astigarraga, I.; Eguizabal, C.; Santos, S.; Simhadri, V.R.; Borrego, F. The expression and function of human CD300 receptors on blood circulating mononuclear cells are distinct in neonates and adults. *Sci. Rep.* **2016**, *6*, 32693, doi:10.1038/srep32693.
184. Dimitrova, M.; Zenarruzabeitia, O.; Borrego, F.; Simhadri, V.R. CD300c is uniquely expressed on CD56bright Natural Killer Cells and differs from CD300a upon ligand recognition. *Sci. Rep.* **2016**, *6*, 23942, doi:10.1038/srep23942.
185. Endt, J.; Eissmann, P.; Hoffmann, S.C.; Meinke, S.; Giese, T.; Watzl, C.

- Modulation of 2B4 (CD244) activity and regulated SAP expression in human NK cells. *Eur. J. Immunol.* **2007**, *37*, 193–198, doi:10.1002/eji.200636341.
186. Alter, G.; Malenfant, J.M.; Altfeld, M. CD107a as a functional marker for the identification of natural killer cell activity. *J. Immunol. Methods* **2004**, *294*, 15–22, doi:10.1016/j.jim.2004.08.008.
  187. Terrén, I.; Mikelez, I.; Odriozola, I.; Gredilla, A.; González, J.; Orrantia, A.; Vitallé, J.; Zenarruzabeitia, O.; Borrego, F. Implication of Interleukin-12/15/18 and Ruxolitinib in the Phenotype, Proliferation, and Polyfunctionality of Human Cytokine-Preactivated Natural Killer Cells. *Front. Immunol.* **2018**, *9*, doi:10.3389/fimmu.2018.00737.
  188. Ortaldo, J.R.; Winkler-Pickett, R.T.; Yagita, H.; Young, H.A. Comparative studies of CD3<sup>−</sup> and CD3<sup>+</sup> CD56<sup>+</sup> cells: Examination of morphology, functions, T cell receptor rearrangement, and pore-forming protein expression. *Cell. Immunol.* **1991**, *136*, 486–495, doi:10.1016/0008-8749(91)90369-M.
  189. Knox, J.J.; Cosma, G.L.; Betts, M.R.; McLane, L.M. Characterization of T-Bet and Eomes in Peripheral Human Immune Cells. *Front. Immunol.* **2014**, *5*, 217, doi:10.3389/fimmu.2014.00217.
  190. Narayanan, S.; Silva, R.; Peruzzi, G.; Alvarez, Y.; Simhadri, V.R.; Debell, K.; Coligan, J.E.; Borrego, F. Human Th1 Cells That Express CD300a Are Polyfunctional and After Stimulation Up-Regulate the T-Box Transcription Factor Eomesodermin. *PLoS One* **2010**, *5*, e10636, doi:10.1371/journal.pone.0010636.
  191. Forconi, C.S.; Cosgrove, C.P.; Saikumar-Lakshmi, P.; Nixon, C.E.; Foley, J.; Ong'echa, J.M.; Otieno, J.A.; Alter, G.; Münz, C.; Moormann, A.M. Poorly cytotoxic terminally differentiated CD56<sup>neg</sup>CD16<sup>pos</sup> NK cells accumulate in Kenyan children with Burkitt lymphomas. *Blood Adv.* **2018**, *2*, 1101–1114, doi:10.1182/bloodadvances.2017015404.
  192. Frias, M.; Rivero-Juarez, A.; Gordon, A.; Camacho, A.; Cantisan, S.; Cuenca-Lopez, F.; Torre-Cisneros, J.; Peña, J.; Rivero, A. Persistence of Pathological Distribution of NK Cells in HIV-Infected Patients with Prolonged Use of HAART and a Sustained Immune Response. *PLoS One* **2015**, *10*, e0121019, doi:10.1371/journal.pone.0121019.
  193. Jiang, Y.; He, L.; Chen, H.; Bice, T.; Zhang, Z.; Liu, J.; Ding, H.; Han, X.; Shang, H. Alteration of inhibitory and activating NK cell receptor expression on NK cells in HIV-infected Chinese. *Cell. Immunol.* **2011**, *271*, 219–226, doi:10.1016/j.cellimm.2011.06.026.
  194. Zarife, M.A.S.; Reis, E.A.G.; Carmo, T.M.A.; Lopes, G.B.; Brandão, E.C.M.; Silva, H.R.; Santana, N.; Martins-Filho, O.A.; Reis, M.G. Increased frequency of CD56<sup>Bright</sup> NK-cells, CD3<sup>−</sup>CD16<sup>+</sup>CD56<sup>−</sup> NK-cells and activated CD4<sup>+</sup>T-cells or B-cells in parallel with CD4<sup>+</sup>CDC25<sup>High</sup> T-cells control potentially viremia in blood donors with HCV. *J. Med. Virol.* **2009**, *81*, 49–59, doi:10.1002/jmv.21340.
  195. Ong, S.-M.; Teng, K.; Newell, E.; Chen, H.; Chen, J.; Loy, T.; Yeo, T.-W.; Fink, K.; Wong, S.-C. A Novel, Five-Marker Alternative to CD16–CD14 Gating to

- Identify the Three Human Monocyte Subsets. *Front. Immunol.* **2019**, *10*, 1761, doi:10.3389/fimmu.2019.01761.
196. Ziegler-Heitbrock, L.; Ancuta, P.; Crowe, S.; Dalod, M.; Grau, V.; Hart, D.N.; Leenen, P.J.M.; Liu, Y.-J.; MacPherson, G.; Randolph, G.J.; et al. Nomenclature of monocytes and dendritic cells in blood. *Blood* **2010**, *116*, e74–e80, doi:10.1182/blood-2010-02-258558.
  197. Jacobson, A.; Bell, F.; Lejarcegui, N.; Mitchell, C.; Frenkel, L.; Horton, H. Healthy Neonates Possess a CD56-Negative NK Cell Population with Reduced Anti-Viral Activity. *PLoS One* **2013**, *8*, e67700, doi:10.1371/journal.pone.0067700.
  198. Jia, M.; Li, D.; He, X.; Zhao, Y.; Peng, H.; Ma, P.; Hong, K.; Liang, H.; Shao, Y. Impaired natural killer cell-induced antibody-dependent cell-mediated cytotoxicity is associated with human immunodeficiency virus-1 disease progression. *Clin. Exp. Immunol.* **2013**, *171*, 107–116, doi:10.1111/j.1365-2249.2012.04672.x.
  199. Nabatanzi, R.; Bayigga, L.; Cose, S.; Rowland-Jones, S.; Canderan, G.; Joloba, M.; Nakanjako, D. Aberrant natural killer (NK) cell activation and dysfunction among ART-treated HIV-infected adults in an African cohort. *Clin. Immunol.* **2019**, *201*, 55–60, doi:10.1016/j.clim.2019.02.010.
  200. Rao, D.; Venkataswamy, M.M.; Vasanthapuram, R.; Satishchandra, P.; Desai, A. Alterations in natural killer and dendritic cell subsets in individuals with HIV-associated neurotuberculosis. *J. Med. Virol.* **2018**, *90*, 899–906, doi:10.1002/jmv.25042.
  201. Zulu, M.Z.; Naidoo, K.K.; Mncube, Z.; Jaggernath, M.; Goulder, P.J.R.; Ndung'u, T.; Altfeld, M.; Thobakgale, C.F. Reduced Expression of Siglec-7, NKG2A, and CD57 on Terminally Differentiated CD56 – CD16 + Natural Killer Cell Subset Is Associated with Natural Killer Cell Dysfunction in Chronic HIV-1 Clade C Infection. *AIDS Res. Hum. Retroviruses* **2017**, *33*, 1205–1213, doi:10.1089/aid.2017.0095.
  202. Lim, A.I.; Menegatti, S.; Bustamante, J.; Le Bourhis, L.; Allez, M.; Rogge, L.; Casanova, J.-L.; Yssel, H.; Di Santo, J.P. IL-12 drives functional plasticity of human group 2 innate lymphoid cells. *J. Exp. Med.* **2016**, *213*, 569–583, doi:10.1084/jem.20151750.
  203. Pohlmeier, C.W.; Gonzalez, V.D.; Irrinki, A.; Ramirez, R.N.; Li, L.; Mulato, A.; Murry, J.P.; Arvey, A.; Hoh, R.; Deeks, S.G.; et al. Identification of NK Cell Subpopulations That Differentiate HIV-Infected Subject Cohorts with Diverse Levels of Virus Control. *J. Virol.* **2019**, *93*, doi:10.1128/JVI.01790-18.
  204. Kuttruff, S.; Koch, S.; Kelp, A.; Pawelec, G.; Rammensee, H.-G.; Steinle, A. Nkp80 defines and stimulates a reactive subset of CD8 T cells. *Blood* **2009**, *113*, 358–369, doi:10.1182/blood-2008-03-145615.
  205. Harrison, D.; Phillips, J.H.; Lanier, L.L. Involvement of a metalloprotease in spontaneous and phorbol ester-induced release of natural killer cell-associated Fc gamma RIII (CD16-II). *J. Immunol.* **1991**, *147*, 3459–65.
  206. Klimosch, S.N.; Bartel, Y.; Wiemann, S.; Steinle, A. Genetically coupled

- receptor–ligand pair NKp80-AICL enables autonomous control of human NK cell responses. *Blood* **2013**, *122*, 2380–2389, doi:10.1182/blood-2013-01-479790.
207. Welte, S.; Kuttruff, S.; Waldhauer, I.; Steinle, A. Mutual activation of natural killer cells and monocytes mediated by NKp80-AICL interaction. *Nat. Immunol.* **2006**, *7*, 1334–1342, doi:10.1038/ni1402.
  208. Devarakonda, S.; Efebera, Y.; Sharma, N. Role of Stem Cell Transplantation in Multiple Myeloma. *Cancers (Basel)*. **2021**, *13*, 863, doi:10.3390/cancers13040863.
  209. Rajkumar, S.V. Multiple myeloma: 2016 update on diagnosis, risk-stratification, and management. *Am. J. Hematol.* **2016**, *91*, 719–734, doi:10.1002/ajh.24402.
  210. Ricciuti, G.; Falcone, A.; Cascavilla, N.; Martinelli, G.; Cerchione, C. Autologous stem cell transplantation in multiple myeloma. *Panminerva Med.* **2020**, *62*, 220–224, doi:10.23736/S0031-0808.20.04114-2.
  211. Ntanasis-Stathopoulos, I.; Gavriatopoulou, M.; Kastritis, E.; Terpos, E.; Dimopoulos, M.A. Multiple myeloma: Role of autologous transplantation. *Cancer Treat. Rev.* **2020**, *82*, 101929, doi:10.1016/j.ctrv.2019.101929.
  212. Shaffer, B.C.; Hsu, K.C. How important is NK alloreactivity and KIR in allogeneic transplantation? *Best Pract. Res. Clin. Haematol.* **2016**, *29*, 351–358, doi:10.1016/j.beha.2016.10.010.
  213. Ullah, M.A.; Hill, G.R.; Tey, S.-K. Functional Reconstitution of Natural Killer Cells in Allogeneic Hematopoietic Stem Cell Transplantation. *Front. Immunol.* **2016**, *7*, 1–8, doi:10.3389/fimmu.2016.00144.
  214. Borrego, F.; Peña, J.; Solana, R. Regulation of CD69 expression on human natural killer cells: differential involvement of protein kinase C and protein tyrosine kinases. *Eur. J. Immunol.* **1993**, *23*, 1039–1043, doi:10.1002/eji.1830230509.
  215. Miller, I.; Min, M.; Yang, C.; Tian, C.; Gookin, S.; Carter, D.; Spence, S.L. Ki67 is a Graded Rather than a Binary Marker of Proliferation versus Quiescence Graphical Abstract HHS Public Access. *Cell Rep* **2018**, *24*, 1105–1112, doi:10.1016/j.celrep.2018.06.110.Ki67.
  216. Carson, W.E.; Giri, J.G.; Lindemann, M.J.; Linett, M.L.; Ahdieh, M.; Paxton, R.; Anderson, D.; Eisenmann, J.; Grabstein, K.; Caligiuri, M. a Interleukin (IL) 15 is a novel cytokine that activates human natural killer cells via components of the IL-2 receptor. *J. Exp. Med.* **1994**, *180*, 1395–1403, doi:10.1084/jem.180.4.1395.
  217. Pical-Izard, C.; Crocchiolo, R.; Granjeaud, S.; Kochbati, E.; Just-Landi, S.; Chabannon, C.; Frassati, C.; Picard, C.; Blaise, D.; Olive, D.; et al. Reconstitution of Natural Killer Cells in HLA-Matched HSCT after Reduced-Intensity Conditioning: Impact on Clinical Outcome. *Biol. Blood Marrow Transplant.* **2015**, *21*, 429–439, doi:10.1016/j.bbmt.2014.11.681.
  218. Hwang, I.; Zhang, T.; Scott, J.M.; Kim, A.R.; Lee, T.; Kakarla, T.; Kim, A.; Sunwoo, J.B.; Kim, S. Identification of human NK cells that are deficient for signaling adaptor FcR and specialized for antibody-dependent immune functions.

- Int. Immunol.* **2012**, *24*, 793–802, doi:10.1093/intimm/dxs080.
219. Hammer, Q.; Rückert, T.; Borst, E.M.; Dunst, J.; Haubner, A.; Durek, P.; Heinrich, F.; Gasparoni, G.; Babic, M.; Tomic, A.; et al. Peptide-specific recognition of human cytomegalovirus strains controls adaptive natural killer cells. *Nat. Immunol.* **2018**, *19*, 453–463, doi:10.1038/s41590-018-0082-6.
  220. Jaffe, E.F.; Lejtenyi, M.C.; Noya, F.J.D.; Mazer, B.D. Secondary hypogammaglobulinemia. *Immunol. Allergy Clin. North Am.* **2001**, *21*, 141–163, doi:10.1016/S0889-8561(05)70197-1.
  221. Jain, T.; John, J.; Kotecha, A.; Deol, A.; Saliminia, T.; Revankar, S.; Chandrasekar, P. Cytomegalovirus infection in autologous stem cell transplant recipients in the era of rituximab. *Ann. Hematol.* **2016**, *95*, 1323–1327, doi:10.1007/s00277-016-2700-4.
  222. Marchesi, F.; Pimpinelli, F.; Gumenyuk, S.; Renzi, D.; Palombi, F.; Pisani, F.; Romano, A.; Spadea, A.; Papa, E.; Canfora, M.; et al. Cytomegalovirus reactivation after autologous stem cell transplantation in myeloma and lymphoma patients: A single-center study. *World J. Transplant.* **2015**, *5*, 129–36, doi:10.5500/wjt.v5.i3.129.
  223. Boyiadzis, M.; Memon, S.; Carson, J.; Allen, K.; Szczepanski, M.J.; Vance, B.A.; Dean, R.; Bishop, M.R.; Gress, R.E.; Hakim, F.T. Up-regulation of NK Cell Activating Receptors Following Allogeneic Hematopoietic Stem Cell Transplantation under a Lymphodepleting Reduced Intensity Regimen is Associated with Elevated IL-15 Levels. *Biol. Blood Marrow Transplant.* **2008**, *14*, 290–300, doi:10.1016/j.bbmt.2007.12.490.
  224. Nielsen, C.M.; White, M.J.; Goodier, M.R.; Riley, E.M. Functional Significance of CD57 Expression on Human NK Cells and Relevance to Disease. *Front. Immunol.* **2013**, *4*, 422, doi:10.3389/fimmu.2013.00422.
  225. Muntasell, A.; Servitja, S.; Cabo, M.; Bermejo, B.; Pérez-Buira, S.; Rojo, F.; Costa-García, M.; Arpí, O.; Moraru, M.; Serrano, L.; et al. High Numbers of Circulating CD57 + NK Cells Associate with Resistance to HER2-Specific Therapeutic Antibodies in HER2 + Primary Breast Cancer. *Cancer Immunol. Res.* **2019**, *7*, 1280–1292, doi:10.1158/2326-6066.CIR-18-0896.
  226. Van den Hove, L.; Van Gool, S.; Vandenberghe, P.; Boogaerts, M.; Ceuppens, J. CD57+/CD28– T cells in untreated hemato-oncological patients are expanded and display a Th1-type cytokine secretion profile, ex vivo cytolytic activity and enhanced tendency to apoptosis. *Leukemia* **1998**, *12*, 1573–1582, doi:10.1038/sj.leu.2401146.
  227. Characiejus, D.; Pasukoniene, V.; Jacobs, J.J.L.; Eidukevicius, R.; Jankevicius, F.; Dobrovolskiene, N.; Mauricas, M.; Van Moorselaar, R.J.A.; Den Otter, W. Prognostic significance of peripheral blood CD8highCD57+ lymphocytes in bladder carcinoma patients after intravesical IL-2. *Anticancer Res.* **2011**, *31*, 699–703.
  228. Waldmann, T.A. The biology of interleukin-2 and interleukin-15: implications for cancer therapy and vaccine design. *Nat. Rev. Immunol.* **2006**, *6*, 595–601, doi:10.1038/nri1901.

229. Conlon, K.C.; Lugli, E.; Welles, H.C.; Rosenberg, S.A.; Fojo, A.T.; Morris, J.C.; Fleisher, T.A.; Dubois, S.P.; Perera, L.P.; Stewart, D.M.; et al. Redistribution, Hyperproliferation, Activation of Natural Killer Cells and CD8 T Cells, and Cytokine Production During First-in-Human Clinical Trial of Recombinant Human Interleukin-15 in Patients With Cancer. *J. Clin. Oncol.* **2015**, *33*, 74–82, doi:10.1200/JCO.2014.57.3329.
230. Hudspeth, K.; Wang, S.; Wang, J.; Rahman, S.; Smith, M.A.; Casey, K.A.; Manna, Z.; Sanjuan, M.; Kolbeck, R.; Hasni, S.; et al. Natural killer cell expression of Ki67 is associated with elevated serum IL-15, disease activity and nephritis in systemic lupus erythematosus. *Clin. Exp. Immunol.* **2019**, *196*, 226–236, doi:10.1111/cei.13263.
231. Han, Y.; Gao, S.; Muegge, K.; Zhang, W.; Zhou, B. Advanced Applications of RNA Sequencing and Challenges. *Bioinform. Biol. Insights* **2015**, *9s1*, BBI.S28991, doi:10.4137/BBI.S28991.
232. Ozsolak, F.; Milos, P.M. RNA sequencing: advances, challenges and opportunities. *Nat. Rev. Genet.* **2011**, *12*, 87–98, doi:10.1038/nrg2934.
233. Papalexis, E.; Satija, R. Single-cell RNA sequencing to explore immune cell heterogeneity. *Nat. Rev. Immunol.* **2018**, *18*, 35–45, doi:10.1038/nri.2017.76.
234. Hanna, J.; Bechtel, P.; Zhai, Y.; Youssef, F.; McLachlan, K.; Mandelboim, O. Novel Insights on Human NK Cells' Immunological Modalities Revealed by Gene Expression Profiling. *J. Immunol.* **2004**, *173*, 6547–6563, doi:10.4049/jimmunol.173.11.6547.
235. Wendt, K.; Wilk, E.; Buyny, S.; Buer, J.; Schmidt, R.E.; Jacobs, R. Gene and protein characteristics reflect functional diversity of CD56 dim and CD56 bright NK cells. *J. Leukoc. Biol.* **2006**, *80*, 1529–1541, doi:10.1189/jlb.0306191.
236. Smith, S.L.; Kennedy, P.R.; Stacey, K.B.; Worboys, J.D.; Yarwood, A.; Seo, S.; Solloa, E.H.; Mistretta, B.; Chatterjee, S.S.; Gunaratne, P.; et al. Diversity of peripheral blood human NK cells identified by single-cell RNA sequencing. *Blood Adv.* **2020**, *4*, 1388–1406, doi:10.1182/bloodadvances.2019000699.
237. Yang, C.; Siebert, J.R.; Burns, R.; Gerbec, Z.J.; Bonacci, B.; Rymaszewski, A.; Rau, M.; Riese, M.J.; Rao, S.; Carlson, K.-S.; et al. Heterogeneity of human bone marrow and blood natural killer cells defined by single-cell transcriptome. *Nat. Commun.* **2019**, *10*, 3931, doi:10.1038/s41467-019-11947-7.
238. Xiong, S.; Sharkey, A.M.; Kennedy, P.R.; Gardner, L.; Farrell, L.E.; Chazara, O.; Bauer, J.; Hiby, S.E.; Colucci, F.; Moffett, A. Maternal uterine NK cell-activating receptor KIR2DS1 enhances placentation. *J. Clin. Invest.* **2013**, *123*, 4264–4272, doi:10.1172/JCI68991.
239. Kopcow, H.D.; Eriksson, M.; Mselle, T.F.; Damrauer, S.M.; Wira, C.R.; Sentman, C.L.; Strominger, J.L. Human Decidual NK Cells from Gravid Uteri and NK Cells from Cycling Endometrium are Distinct NK Cell Subsets. *Placenta* **2010**, *31*, 334–338, doi:10.1016/j.placenta.2010.01.003.
240. Vento-Tormo, R.; Efremova, M.; Botting, R.A.; Turco, M.Y.; Vento-Tormo, M.; Meyer, K.B.; Park, J.-E.; Stephenson, E.; Polański, K.; Goncalves, A.; et al. Single-cell reconstruction of the early maternal–fetal interface in humans. *Nature*

- 2018**, 563, 347–353, doi:10.1038/s41586-018-0698-6.
241. Jameson, G.; Robinson, M.W. Insights Into Human Intrahepatic NK Cell Function From Single Cell RNA Sequencing Datasets. *Front. Immunol.* **2021**, *12*, 1–12, doi:10.3389/fimmu.2021.649311.
  242. Dybkaer, K.; Iqbal, J.; Zhou, G.; Geng, H.; Xiao, L.; Schmitz, A.; D'Amore, F.; Chan, W.C. Genome wide transcriptional analysis of resting and IL2 activated human natural killer cells: gene expression signatures indicative of novel molecular signaling pathways. *BMC Genomics* **2007**, *8*, 230, doi:10.1186/1471-2164-8-230.
  243. Rajagopalan, S.; Long, E.O. Cellular senescence induced by CD158d reprograms natural killer cells to promote vascular remodeling. *Proc. Natl. Acad. Sci.* **2012**, *109*, 20596–20601, doi:10.1073/pnas.1208248109.
  244. Melaiu, O.; Lucarini, V.; Cifaldi, L.; Fruci, D. Influence of the Tumor Microenvironment on NK Cell Function in Solid Tumors. *Front. Immunol.* **2020**, *10*, doi:10.3389/fimmu.2019.03038.
  245. Terrén, I.; Orrantia, A.; Vitallé, J.; Zenarruzabeitia, O.; Borrego, F. NK cell metabolism and tumor microenvironment. *Front. Immunol.* **2019**, *10*, 1–9, doi:10.3389/fimmu.2019.02278.
  246. Wang, F.; Tian, Z.; Wei, H. Genomic expression profiling of NK cells in health and disease. *Eur. J. Immunol.* **2015**, *45*, 661–678, doi:10.1002/eji.201444998.
  247. Gillard-Bocquet, M.; Caer, C.; Cagnard, N.; Crozet, L.; Perez, M.; Fridman, W.H.; Sautès-Fridman, C.; Cremer, I. Lung Tumor Microenvironment Induces Specific Gene Expression Signature in Intratumoral NK Cells. *Front. Immunol.* **2013**, *4*, 1–6, doi:10.3389/fimmu.2013.00019.
  248. de Andrade, L.F.; Lu, Y.; Luoma, A.; Ito, Y.; Pan, D.; Pyrdol, J.W.; Yoon, C.H.; Yuan, G.-C.; Wucherpfennig, K.W. Discovery of specialized NK cell populations infiltrating human melanoma metastases. *JCI insight* **2019**, *4*, doi:10.1172/jci.insight.133103.
  249. Venton, G.; Labiad, Y.; Colle, J.; Fino, A.; Afridi, S.; Torres, M.; Monteuil, S.; Lorient, B.; Fernandez-Nunez, N.; Farnault, L.; et al. Natural killer cells in acute myeloid leukemia patients: from phenotype to transcriptomic analysis. *Immunol. Res.* **2016**, *64*, 1225–1236, doi:10.1007/s12026-016-8848-0.
  250. Böttcher, A.; Ostwald, J.; Koczan, D.; Knecht, R.; Kramp, B.; Dommerich, S. Gene expression profiling of circulating natural killer cells in head and neck squamous cell carcinoma. *Cancer Genomics Proteomics* **2013**, *10*, 197–207.
  251. Xu, Y.; Xu, Q.; Ni, S.; Liu, F.; Cai, G.; Wu, F.; Ye, X.; Meng, X.; Mougin, B.; Cai, S.; et al. Decrease in natural killer cell associated gene expression as a major characteristic of the immune status in the bloodstream of colorectal cancer patients. *Cancer Biol. Ther.* **2011**, *11*, 188–195, doi:10.4161/cbt.11.2.13670.
  252. Li, B.; Dewey, C.N. RSEM: accurate transcript quantification from RNA-Seq data with or without a reference genome. *BMC Bioinformatics* **2011**, *12*, 323, doi:10.1186/1471-2105-12-323.
  253. Luo, W.; Brouwer, C. Pathview: an R/Bioconductor package for pathway-based

- data integration and visualization. *Bioinformatics* **2013**, *29*, 1830–1831, doi:10.1093/bioinformatics/btt285.
254. Yu, G.; He, Q.-Y. ReactomePA: an R/Bioconductor package for reactome pathway analysis and visualization. *Mol. Biosyst.* **2016**, *12*, 477–479, doi:10.1039/C5MB00663E.
255. Yu, G.; Wang, L.-G.; Han, Y.; He, Q.-Y. clusterProfiler: an R Package for Comparing Biological Themes Among Gene Clusters. *Omi. A J. Integr. Biol.* **2012**, *16*, 284–287, doi:10.1089/omi.2011.0118.
256. Kaszubowska, L.; Wierzbicki, P.M.; Karsznia, S.; Damska, M.; Ślebioda, T.J.; Foerster, J.; Kmieć, Z. Optimal reference genes for qPCR in resting and activated human NK cells—Flow cytometric data correspond to qPCR gene expression analysis. *J. Immunol. Methods* **2015**, *422*, 125–129, doi:10.1016/j.jim.2015.04.013.
257. Rajagopalan, S.; Long, E.O. KIR2DL4 (CD158d): An activation receptor for HLA-G. *Front. Immunol.* **2012**, *3*, 1–6, doi:10.3389/fimmu.2012.00258.
258. Albin, A.; Noonan, D.M. Decidual-Like NK Cell Polarization: From Cancer Killing to Cancer Nurturing. *Cancer Discov.* **2021**, *11*, 28–33, doi:10.1158/2159-8290.CD-20-0796.
259. Pavletic, Z.; Joshi, S.; Pirruccello, S.; Tarantolo, S.; Kollath, J.; Reed, E.; Bierman, P.; Vose, J.; Warkentin, P.; Gross, T.; et al. Lymphocyte reconstitution after allogeneic blood stem cell transplantation for hematologic malignancies. *Bone Marrow Transplant.* **1998**, *21*, 33–41, doi:10.1038/sj.bmt.1701037.
260. Scholzen, T.; Gerdes, J. The Ki-67 protein: From the known and the unknown. *J. Cell. Physiol.* **2000**, *182*, 311–322, doi:10.1002/(SICI)1097-4652(200003)182:3<311::AID-JCP1>3.0.CO;2-9.
261. Bantug, G.R.; Galluzzi, L.; Kroemer, G.; Hess, C. The spectrum of T cell metabolism in health and disease. *Nat. Rev. Immunol.* **2018**, *18*, 19–34, doi:10.1038/nri.2017.99.
262. Marçais, A.; Cherfils-Vicini, J.; Viant, C.; Degouve, S.; Viel, S.; Fenis, A.; Rabilloud, J.; Mayol, K.; Tavares, A.; Bienvenu, J.; et al. The metabolic checkpoint kinase mTOR is essential for IL-15 signaling during the development and activation of NK cells. *Nat. Immunol.* **2014**, *15*, 749–757, doi:10.1038/ni.2936.
263. Terrén, I.; Orrantia, A.; Vitallé, J.; Astarloa-Pando, G.; Zenarruzabeitia, O.; Borrego, F. Modulating NK cell metabolism for cancer immunotherapy. *Semin. Hematol.* **2020**, *57*, 213–224, doi:10.1053/j.seminhematol.2020.10.003.
264. O'Brien, K.L.; Finlay, D.K. Immunometabolism and natural killer cell responses. *Nat. Rev. Immunol.* **2019**, *19*, 282–290, doi:10.1038/s41577-019-0139-2.
265. Cuthbert, J.A.; Lipsky, P.E. Inhibition by 6-fluoromevalonate demonstrates that mevalonate or one of the mevalonate phosphates is necessary for lymphocyte proliferation. *J. Biol. Chem.* **1990**, *265*, 18568–18575, doi:10.1016/S0021-9258(17)44789-2.
266. Crosbie, J.; Magnussen, M.; Dornbier, R.; Iannone, A.; Steele, T.A. Statins

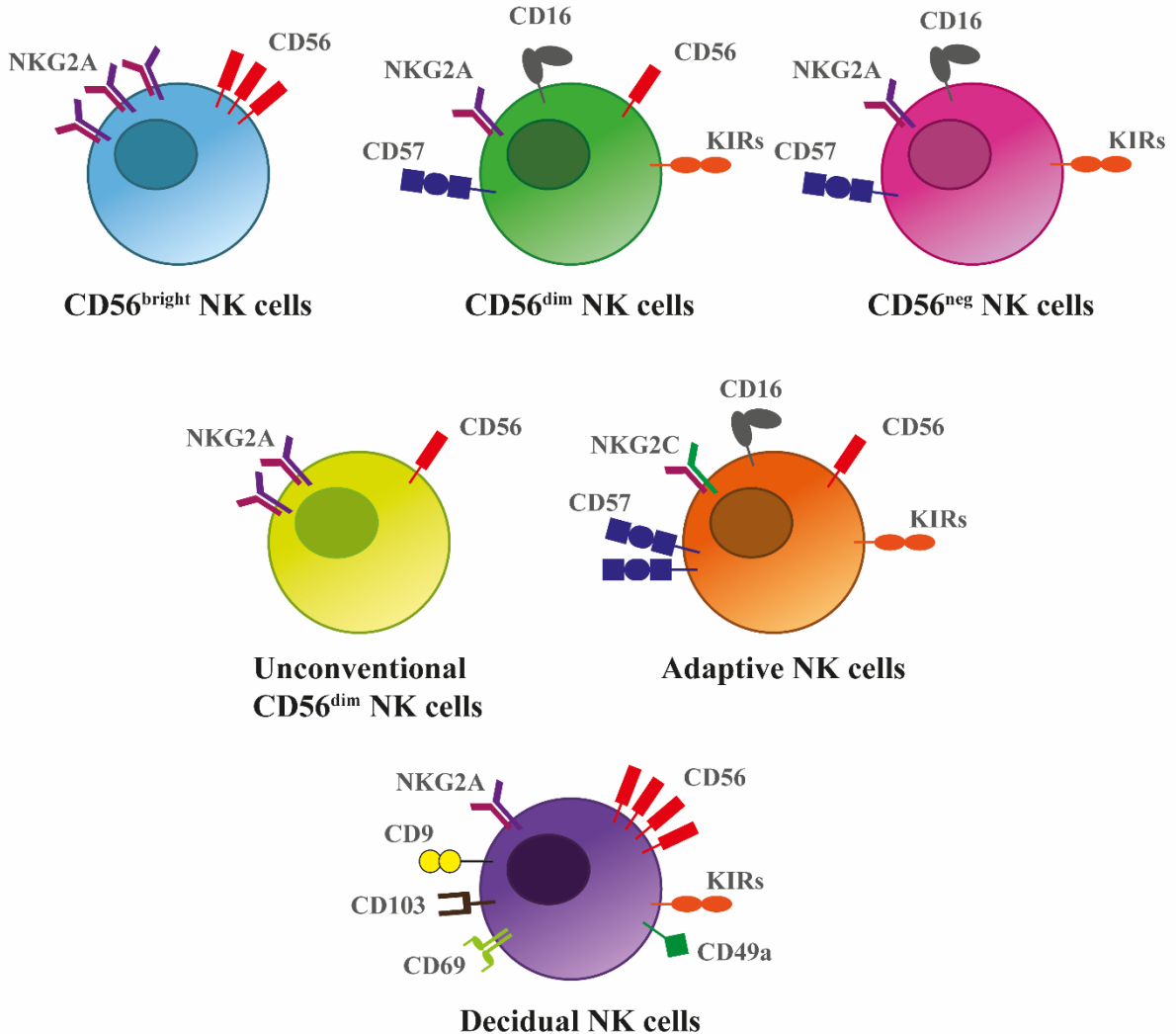


- inhibit proliferation and cytotoxicity of a human leukemic natural killer cell line. *Biomark. Res.* **2013**, *1*, 33, doi:10.1186/2050-7771-1-33.
267. Chakrabarti, R.; Engleman, E.G. Interrelationships between mevalonate metabolism and the mitogenic signaling pathway in T lymphocyte proliferation. *J. Biol. Chem.* **1991**, *266*, 12216–12222, doi:10.1016/S0021-9258(18)98884-8.
  268. Poggi, A.; Boero, S.; Musso, A.; Zocchi, M.R. Selective Role of Mevalonate Pathway in Regulating Perforin but Not FasL and TNFalpha Release in Human Natural Killer Cells. *PLoS One* **2013**, *8*, e62932, doi:10.1371/journal.pone.0062932.
  269. Keskin, D.B.; Allan, D.S.J.; Rybalov, B.; Andzelm, M.M.; Stern, J.N.H.; Kopcow, H.D.; Koopman, L.A.; Strominger, J.L. TGFbeta promotes conversion of CD16+ peripheral blood NK cells into CD16- NK cells with similarities to decidual NK cells. *Proc. Natl. Acad. Sci. U. S. A.* **2007**, *104*, 3378–83, doi:10.1073/pnas.0611098104.
  270. Cerdeira, A.S.; Rajakumar, A.; Royle, C.M.; Lo, A.; Husain, Z.; Thadhani, R.I.; Sukhatme, V.P.; Karumanchi, S.A.; Kopcow, H.D. Conversion of Peripheral Blood NK Cells to a Decidual NK-like Phenotype by a Cocktail of Defined Factors. *J. Immunol.* **2013**, *190*, 3939–3948, doi:10.4049/jimmunol.1202582.
  271. Gonzalez, V.D.; Huang, Y.-W.; Delgado-Gonzalez, A.; Chen, S.-Y.; Donoso, K.; Sachs, K.; Gentles, A.J.; Allard, G.M.; Kolahi, K.S.; Howitt, B.E.; et al. High-grade serous ovarian tumor cells modulate NK cell function to create an immune-tolerant microenvironment. *Cell Rep.* **2021**, *36*, 109632, doi:10.1016/j.celrep.2021.109632.
  272. Liem, L.M.; Fibbe, W.E.; van Houwelingen, H.C.; Goulmy, E. Serum transforming growth factor-beta1 levels in bone marrow transplant recipients correlate with blood cell counts and chronic graft-versus-host disease. *Transplantation* **1999**, *67*, 59–65, doi:10.1097/00007890-199901150-00009.
  273. Coomes, S.M.; Moore, B.B. Pleiotropic Effects of Transforming Growth Factor- $\beta$  in Hematopoietic Stem-Cell Transplantation. *Transplantation* **2010**, *90*, 1139–1144, doi:10.1097/TP.0b013e3181efd018.
  274. Siewiera, J.; Gouilly, J.; Hocine, H.-R.; Cartron, G.; Levy, C.; Al-Daccak, R.; Jabrane-Ferrat, N. Natural cytotoxicity receptor splice variants orchestrate the distinct functions of human natural killer cell subtypes. *Nat. Commun.* **2015**, *6*, 10183, doi:10.1038/ncomms10183.
  275. Zhang, X.; Li, Y.; Huang, C.; Liu, S.; Chen, X.; Yu, S.; Diao, L.; Zeng, Y. The role of decidual natural killer cell-derived soluble factors in early pregnancy. *Am. J. Reprod. Immunol.* **2021**, *86*, doi:10.1111/aji.13477.
  276. King, A.; Jokhi, P.P.; Burrows, T.D.; Gardner, L.; Sharkey, A.M.; Lore, Y.W. Functions of Human Decidual NK Cells. *Am. J. Reprod. Immunol.* **1996**, *35*, 258–260, doi:10.1111/j.1600-0897.1996.tb00041.x.
  277. Crespo, Â.C.; Mulik, S.; Dotiwala, F.; Ansara, J.A.; Sen Santara, S.; Ingersoll, K.; Ovies, C.; Junqueira, C.; Tilburgs, T.; Strominger, J.L.; et al. Decidual NK Cells Transfer Granulysin to Selectively Kill Bacteria in Trophoblasts. *Cell* **2020**, *182*, 1125–1139.e18, doi:10.1016/j.cell.2020.07.019.

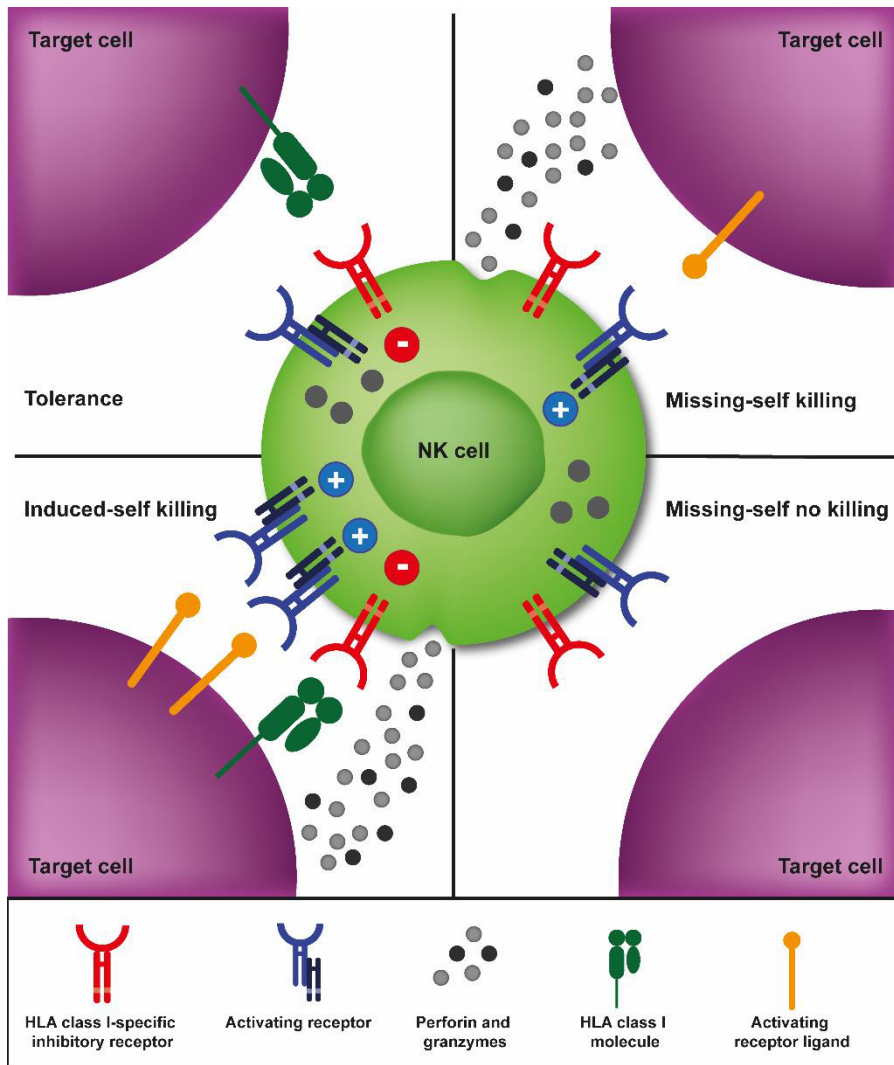
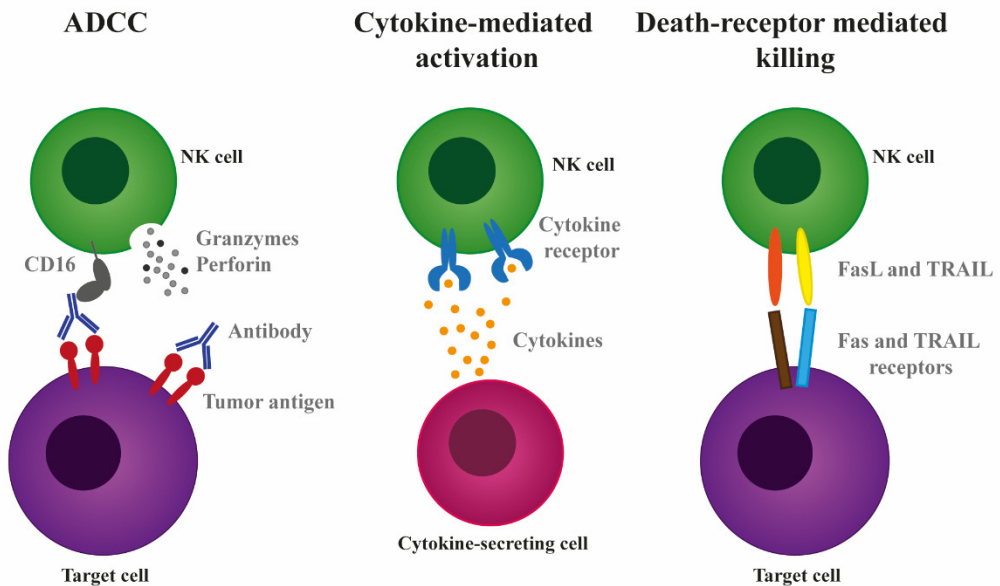
278. Liu, Y.; Gao, S.; Zhao, Y.; Wang, H.; Pan, Q.; Shao, Q. Decidual Natural Killer Cells: A Good Nanny at the Maternal-Fetal Interface During Early Pregnancy. *Front. Immunol.* **2021**, *12*, 1–11, doi:10.3389/fimmu.2021.663660.
279. Bruno, A.; Focaccetti, C.; Pagani, A.; Imperatori, A.S.; Spagnoletti, M.; Rotolo, N.; Cantelmo, A.R.; Franzi, F.; Capella, C.; Ferlazzo, G.; et al. The Proangiogenic Phenotype of Natural Killer Cells in Patients with Non-Small Cell Lung Cancer. *Neoplasia* **2013**, *15*, 133–IN7, doi:10.1593/neo.121758.
280. Bruno, A.; Ferlazzo, G.; Albin, A.; Noonan, D.M. A Think Tank of TINK/TANKs: Tumor-Infiltrating/Tumor-Associated Natural Killer Cells in Tumor Progression and Angiogenesis. *JNCI J. Natl. Cancer Inst.* **2014**, *106*, 1–13, doi:10.1093/jnci/dju200.
281. Kim, K.-J.; Kwon, H.J.; Kim, M.C.; Bae, Y.K. CD9 Expression in Colorectal Carcinomas and Its Prognostic Significance. *J. Pathol. Transl. Med.* **2016**, *50*, 459–468, doi:10.4132/jptm.2016.10.02.
282. Cerwenka, A.; Baron, J.L.; Lanier, L.L. Ectopic expression of retinoic acid early inducible-1 gene (RAE-1) permits natural killer cell-mediated rejection of a MHC class I-bearing tumor in vivo. *Proc. Natl. Acad. Sci.* **2001**, *98*, 11521–11526, doi:10.1073/pnas.201238598.
283. Kim, S.; Iizuka, K.; Aguila, H.L.; Weissman, I.L.; Yokoyama, W.M. In vivo natural killer cell activities revealed by natural killer cell-deficient mice. *Proc. Natl. Acad. Sci.* **2000**, *97*, 2731–2736, doi:10.1073/pnas.050588297.
284. Imai, K.; Matsuyama, S.; Miyake, S.; Suga, K.; Nakachi, K. Natural cytotoxic activity of peripheral-blood lymphocytes and cancer incidence: an 11-year follow-up study of a general population. *Lancet* **2000**, *356*, 1795–1799, doi:10.1016/S0140-6736(00)03231-1.
285. Moon, W.Y.; Powis, S.J. Does Natural Killer Cell Deficiency (NKD) Increase the Risk of Cancer? NKD May Increase the Risk of Some Virus Induced Cancer. *Front. Immunol.* **2019**, *10*, 1703, doi:10.3389/fimmu.2019.01703.
286. Lorenzi, L.; Tabellini, G.; Vermi, W.; Moratto, D.; Porta, F.; Notarangelo, L.D.; Patrizi, O.; Sozzani, S.; de Saint Basile, G.; Latour, S.; et al. Occurrence of Nodular Lymphocyte-Predominant Hodgkin Lymphoma in Hermansky-Pudlak Type 2 Syndrome Is Associated to Natural Killer and Natural Killer T Cell Defects. *PLoS One* **2013**, *8*, e80131, doi:10.1371/journal.pone.0080131.
287. Shimasaki, N.; Jain, A.; Campana, D. NK cells for cancer immunotherapy. *Nat. Rev. Drug Discov.* **2020**, *19*, 200–218, doi:10.1038/s41573-019-0052-1.
288. Asai, O.; Longo, D.L.; Tian, Z.G.; Hornung, R.L.; Taub, D.D.; Ruscetti, F.W.; Murphy, W.J. Suppression of graft-versus-host disease and amplification of graft-versus-tumor effects by activated natural killer cells after allogeneic bone marrow transplantation. *J. Clin. Invest.* **1998**, *101*, 1835–1842, doi:10.1172/JCI1268.
289. Olson, J.A.; Leveson-Gower, D.B.; Gill, S.; Baker, J.; Beilhack, A.; Negrin, R.S. NK cells mediate reduction of GVHD by inhibiting activated, alloreactive T cells while retaining GVT effects. *Blood* **2010**, *115*, 4293–4301, doi:10.1182/blood-2009-05-222190.

290. Hsu, K.C.; Keever-Taylor, C.A.; Wilton, A.; Pinto, C.; Heller, G.; Arkun, K.; O'Reilly, R.J.; Horowitz, M.M.; Dupont, B. Improved outcome in HLA-identical sibling hematopoietic stem-cell transplantation for acute myelogenous leukemia predicted by KIR and HLA genotypes. *Blood* **2005**, *105*, 4878–4884, doi:10.1182/blood-2004-12-4825.
291. Willemze, R.; Rodrigues, C.A.; Labopin, M.; Sanz, G.; Michel, G.; Socié, G.; Rio, B.; Sirvent, A.; Renaud, M.; Madero, L.; et al. KIR-ligand incompatibility in the graft-versus-host direction improves outcomes after umbilical cord blood transplantation for acute leukemia. *Leukemia* **2009**, *23*, 492–500, doi:10.1038/leu.2008.365.
292. Wu, Y.; Tian, Z.; Wei, H. Developmental and Functional Control of Natural Killer Cells by Cytokines. *Front. Immunol.* **2017**, *8*, doi:10.3389/fimmu.2017.00930.
293. Vendrame, E.; Fukuyama, J.; Strauss-Albee, D.M.; Holmes, S.; Blish, C.A. Mass Cytometry Analytical Approaches Reveal Cytokine-Induced Changes in Natural Killer Cells. *Cytom. Part B Clin. Cytom.* **2017**, *92*, 57–67, doi:10.1002/cyto.b.21500.
294. Kielsen, K.; Oostenbrink, L.V.E.; von Asmuth, E.G.J.; Jansen-Hoogendijk, A.M.; van Ostaijen-ten Dam, M.M.; Ifversen, M.; Heilmann, C.; Schilham, M.W.; van Halteren, A.G.S.; Bredius, R.G.M.; et al. IL-7 and IL-15 Levels Reflect the Degree of T Cell Depletion during Lymphopenia and Are Associated with an Expansion of Effector Memory T Cells after Pediatric Hematopoietic Stem Cell Transplantation. *J. Immunol.* **2021**, *206*, 2828–2838, doi:10.4049/jimmunol.2001077.
295. Melenhorst, J.J.; Tian, X.; Xu, D.; Sandler, N.G.; Scheinberg, P.; Biancotto, A.; Scheinberg, P.; McCoy, J.P.; Hensel, N.F.; McIver, Z.; et al. Cytopenia and leukocyte recovery shape cytokine fluctuations after myeloablative allogeneic hematopoietic stem cell transplantation. *Haematologica* **2012**, *97*, 867–873, doi:10.3324/haematol.2011.053363.

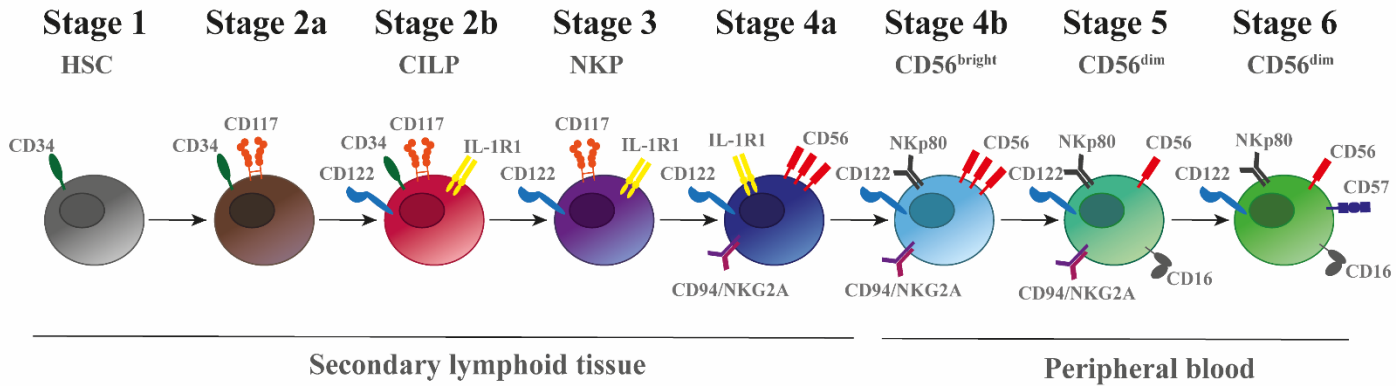
# FIGURES AND TABLES



**Figure 1. NK cell subset diversity.** Representation of some phenotypic characteristics of different NK cell subsets. Traditionally, according to the differential expression of CD56 and CD16, human NK cells are divided in two major subsets: CD56<sup>bright</sup> and CD56<sup>dim</sup>. However, studies published in the last years have revealed a vast NK cell subset diversity. An expansion of CD56<sup>neg</sup> NK cell subset have been described after HIV-1 infection. Unconventional CD56<sup>dim</sup> NK cells that lack expression of CD16 have been identified in patients undergoing haploidentical HSCT. Increased number of adaptive NK cells have been observed following CMV infection or reactivation. Moreover, NK cells from different human tissues have distinct phenotypic profiles, such as, decidual NK cells.

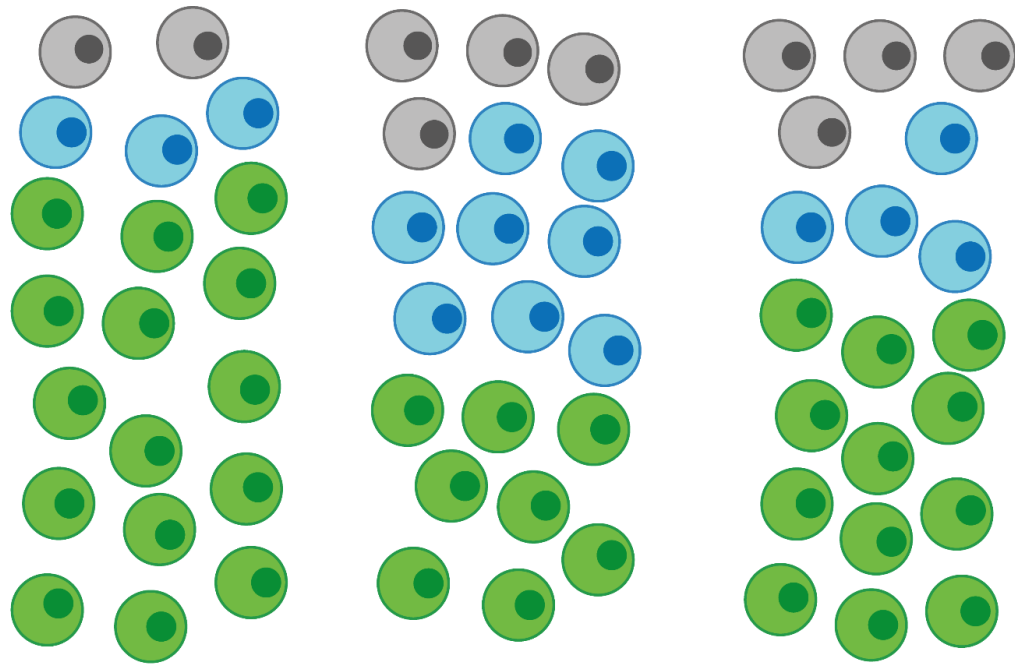
**A****B**




**Figure 2. NK cell activation and function.** (A) NK cell activation is determined by an intricate balance between activating and inhibitory signals transmitted by surface receptors. Target cells expressing HLA class I molecules that engage HLA class I-specific inhibitory receptors expressed by NK cells will not be killed (tolerance) due to inhibitory signals transmitted by the inhibitory receptors. Target cells that display an upregulation of activating receptor ligands will be killed (induced-self killing) as activating signals will overcome the inhibitory signals. Target cells that downregulate HLA class I molecules will be eliminated depending on the presence of signals transmitted by the activating receptors (missing-self). After activation, NK cells will mediate different effector mechanisms to eliminate target cells, such as the release of cytolytic granules containing perforin and granzymes. (B) NK cells can also be activated through CD16, which recognize the Fc portion of IgG antibodies bound to target cell antigens and mediate ADCC (left); through cytokines secreted by other cells that bind to cytokine receptors expressed by NK cells (center) or through engagement of Fas and TRAIL death receptors expressed by target cells with their corresponding ligands expressed by NK cells, which activate the enzymatic caspases cascade that triggers target cell apoptosis (right).



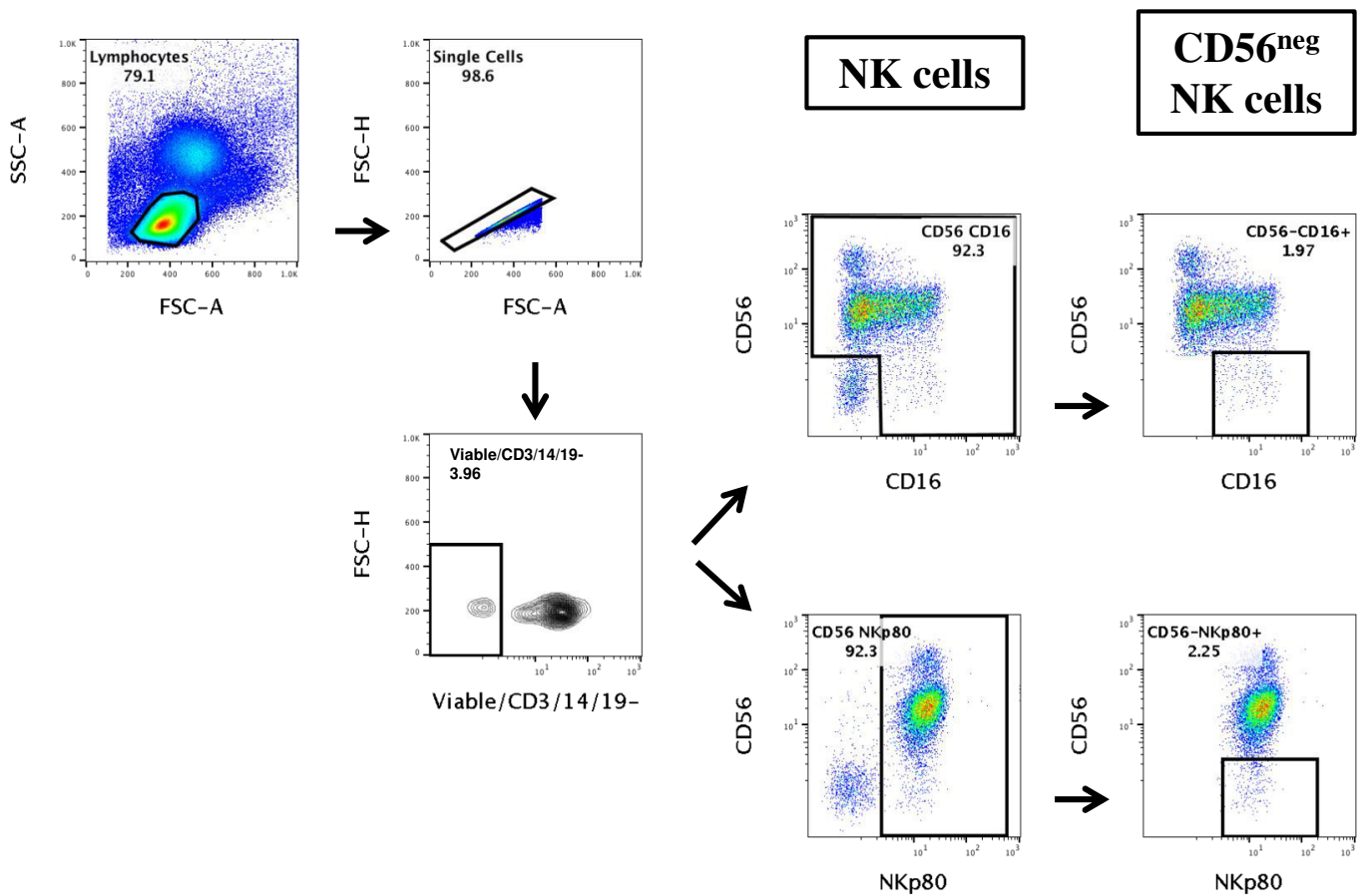
**Figure 3. Linear model of NK cell differentiation.** Schematic representation of the different stages of NK cell differentiation in secondary lymphoid tissues and peripheral blood. Some of the receptors expressed by each stage are shown. HSC: hematopoietic stem cells; CILP: common ILC progenitors; NKP: NK cell progenitors.



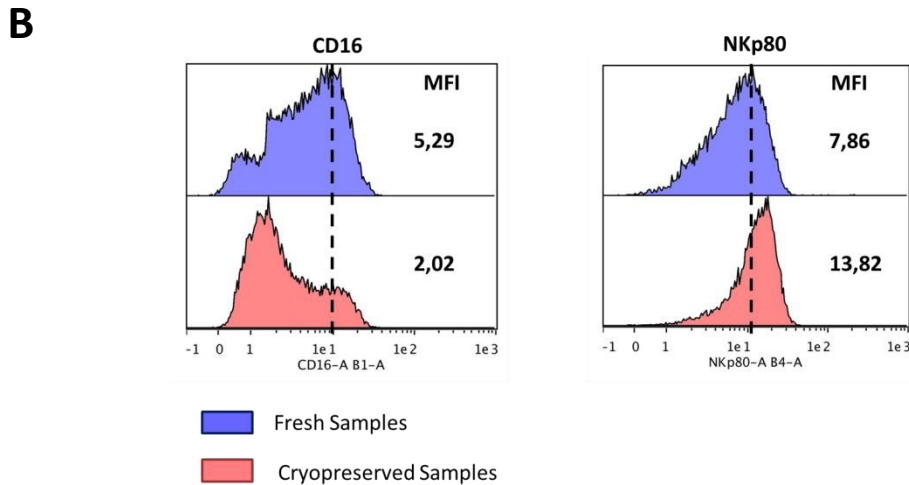
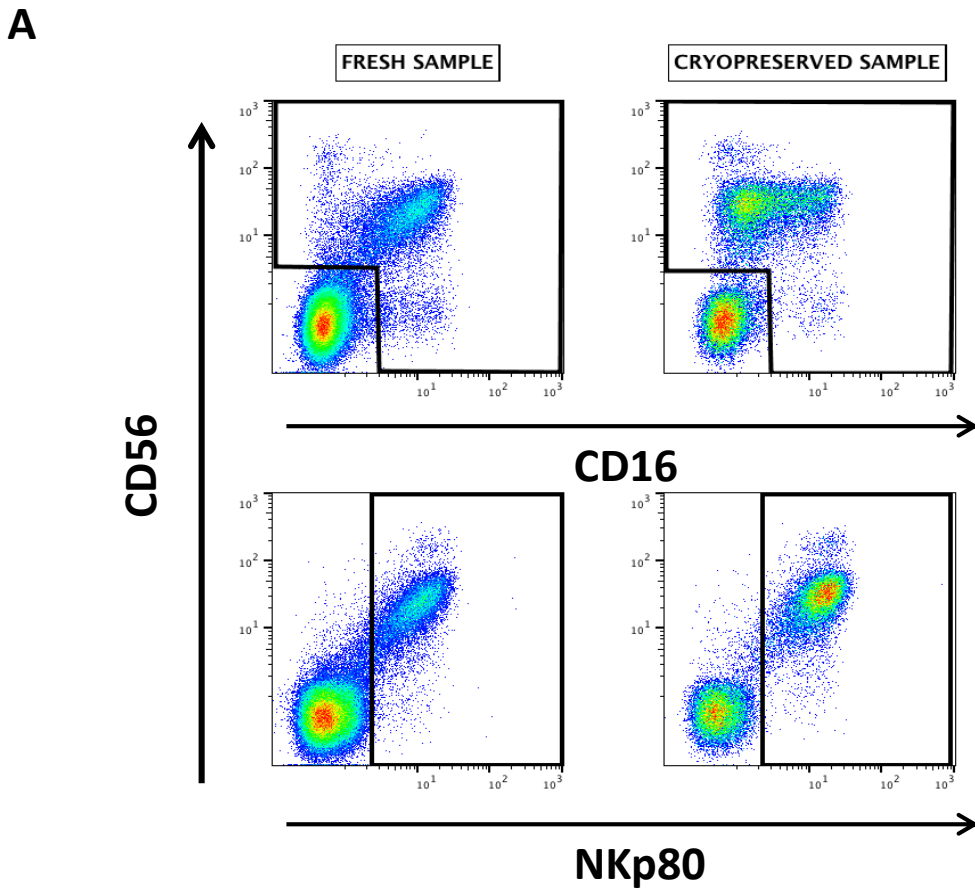


		Pre-autoHSCT	After LR	2wk after LR
 CD56 <sup>bright</sup> CD16 <sup>-</sup>	<b>NKG2A</b>	++++	++++	+++++
	<b>CD57</b>	-	++	+
	<b>KIR</b>	-	+	+
 CD56 <sup>bright</sup> CD16 <sup>+</sup>	<b>NKG2A</b>	++++	++++	+++++
	<b>CD57</b>	+	+++	++
	<b>KIR</b>	+	+++	++
 CD56 <sup>dim</sup> CD16 <sup>++</sup>	<b>NKG2A</b>	+++	+++	++++
	<b>CD57</b>	+++	++++	+++
	<b>KIR</b>	+++	+++	+++

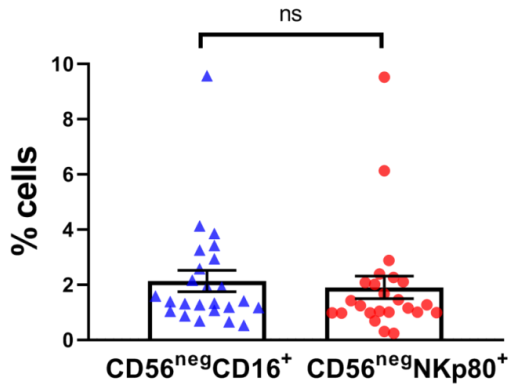
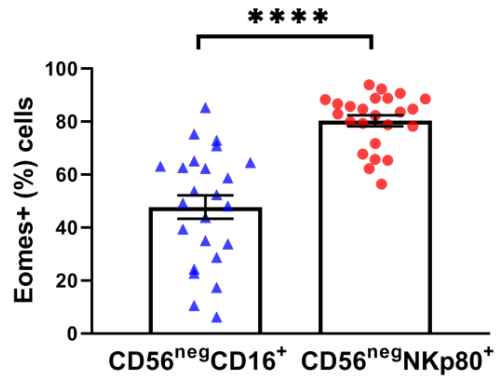
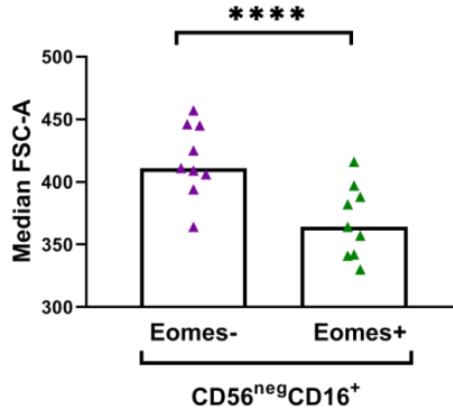
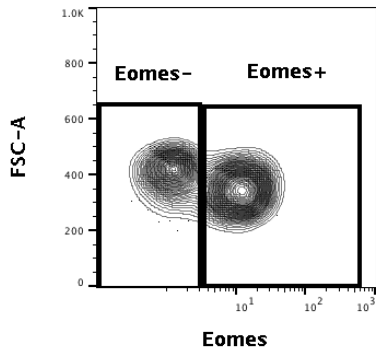
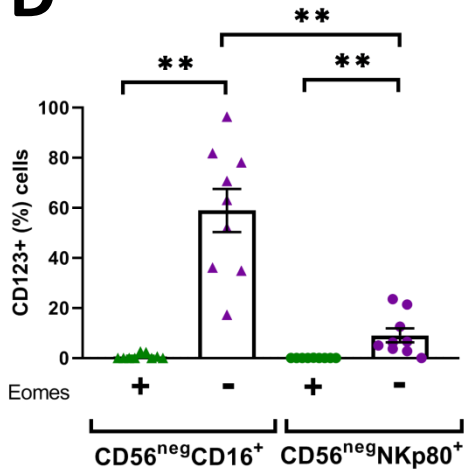
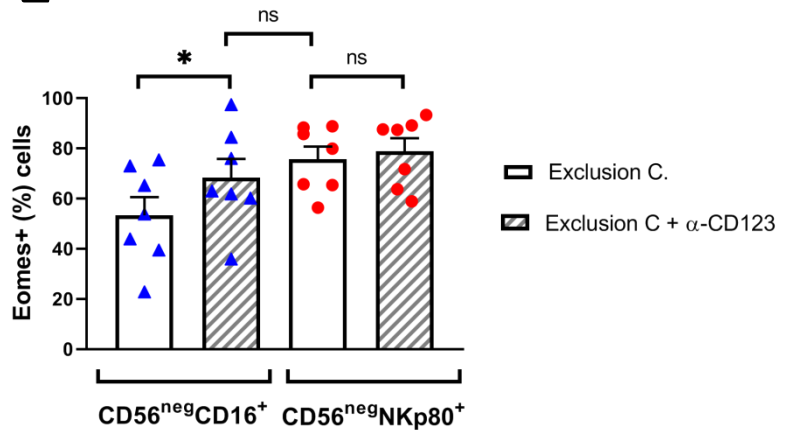
**Figure 4. NK cell subset and receptor repertoire redistribution during NK cell reconstitution after autoHSCT.** The distribution of the three NK cell subsets (CD56<sup>bright</sup>CD16<sup>-</sup>, CD56<sup>bright</sup>CD16<sup>+</sup> and CD56<sup>dim</sup>CD16<sup>++</sup>) changes significantly at leucocyte recovery and some changes are still evident 2 weeks after leucocyte recovery. Moreover, the frequency of NK cells expressing the surface receptors NKG2A, CD57 and KIR in the different NK cell subsets is also altered. The frequency of NKG2A+, CD57+ and KIR+ NK cells within each subset is represented with the + symbol. After LR: after leucocyte recovery; 2wk after LR: 2 weeks after leucocyte recovery.



**Figure 5. Identification of CD56<sup>neg</sup> NK cells.** Pseudocolor and contour plot graphs representing the gating strategy used for the identification of CD56<sup>neg</sup> NK cells. Data from a representative cryopreserved sample from a healthy donor is shown. Lymphocytes were electronically gated based on their forward and side scatter parameters and then single cells were selected. To identify NK cells, the population negative for the exclusion channel (viability, CD3, CD14 and CD19) was selected. Then CD56<sup>neg</sup> NK cells were identified using different gating strategies. The different NK cell subsets are identified based on the expression of CD56 and CD16 (top) or CD56 and NKp80 (bottom).



**Figure 6. CD16 but not NKp80 is downregulated after cell cryopreservation.** (A) Representative pseudocolor plot graphs comparing the expression of CD16 (top) and NKp80 (bottom) in fresh and cryopreserved samples. Data from a representative healthy donor is shown. (B) Histograms showing the median fluorescence intensity (MFI) of CD16 and NKp80 on NK cells in fresh (blue) and cryopreserved (red) samples. Data from a representative healthy donor is shown.

**A****B****C****D****E**

**Figure 7. NKp80 better identifies CD56<sup>neg</sup> NK cells than CD16 in healthy individuals.** (A) Bar graph showing the percentage of CD56<sup>neg</sup>CD16<sup>+</sup> and CD56<sup>neg</sup>NKp80<sup>+</sup> cells in healthy donors. (B) Bar graph showing the percentage of Eomes<sup>+</sup> cells within CD56<sup>neg</sup>CD16<sup>+</sup> and CD56<sup>neg</sup>NKp80<sup>+</sup> populations. (C) Left part, representative contour plot showing the Eomes expression vs the size (FSC-A) of CD56<sup>neg</sup>CD16<sup>+</sup> cells. Data from a representative healthy donor is shown. Right part, bar graph showing the median of FSC-A parameter within CD56<sup>neg</sup>CD16<sup>+</sup>Eomes<sup>-</sup> and CD56<sup>neg</sup>CD16<sup>+</sup>Eomes<sup>+</sup> cell populations. (D) Bar graph showing the percentage of CD123<sup>+</sup> cells within CD56<sup>neg</sup>CD16<sup>+</sup>Eomes<sup>+</sup>, CD56<sup>neg</sup>CD16<sup>+</sup>Eomes<sup>-</sup>, CD56<sup>neg</sup>NKp80<sup>+</sup>Eomes<sup>+</sup> and CD56<sup>neg</sup>NKp80<sup>+</sup>Eomes<sup>-</sup> populations. (E) Bar graph showing the percentage of Eomes<sup>+</sup> cells within CD56<sup>neg</sup>CD16<sup>+</sup> and CD56<sup>neg</sup>NKp80<sup>+</sup> populations with or without the addition of anti-CD123 mAb to the exclusion channel (Exclusion C.). The mean with the standard error of the mean (SEM) is represented, except for (C) in which the median is represented. Each dot represents a donor. \*p<0.05, \*\*p<0.01, \*\*\*\*p<0.0001, ns: not significant.

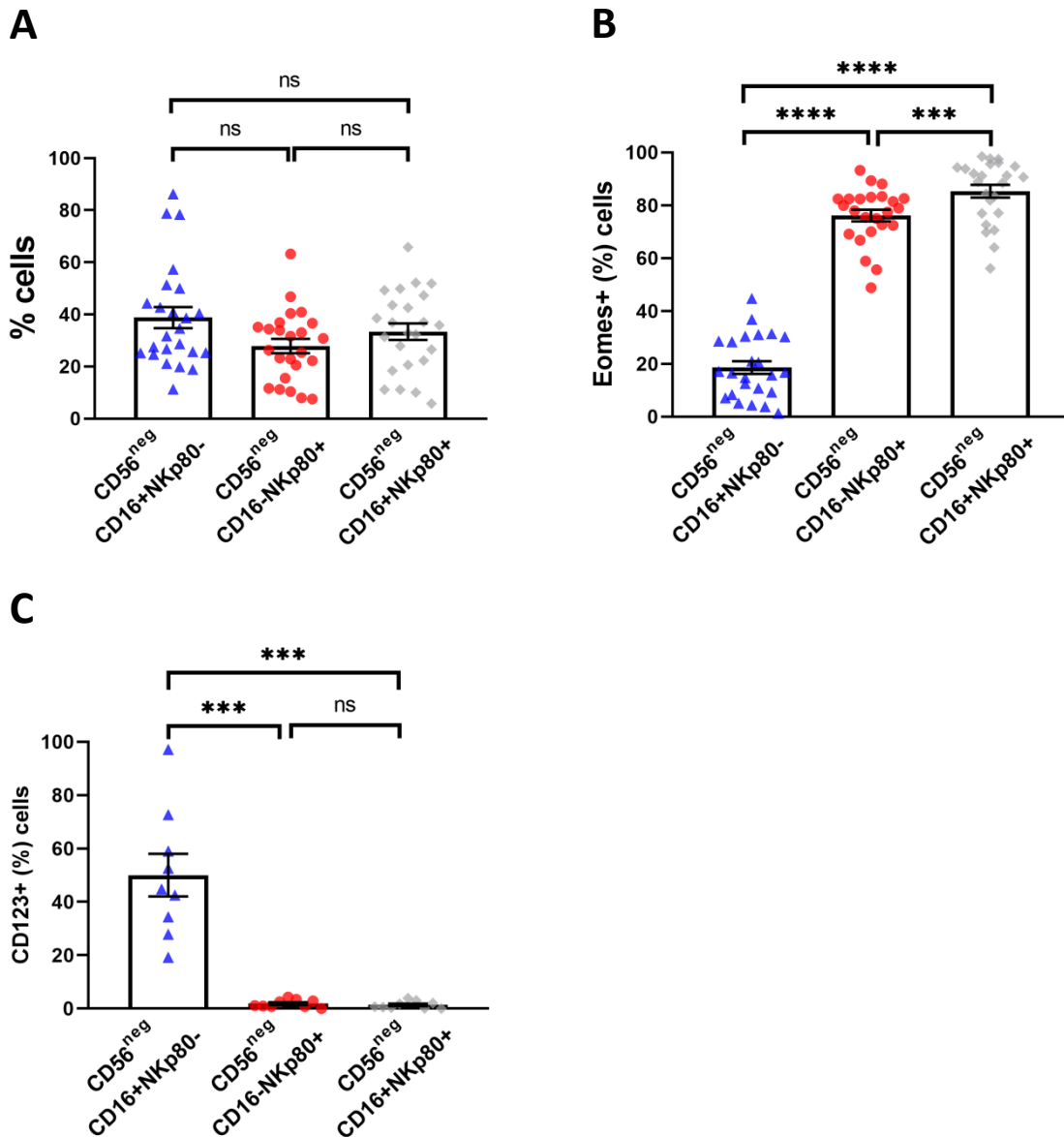


**Figure 8. CD56<sup>neg</sup>CD16+NKp80- subset mostly include non-NK cells.** (A) Bar graph showing the percentage of CD16+NKp80-, CD16-NKp80+ and CD16+NKp80+ subsets within the CD56<sup>neg</sup> NK cells. (B) Bar graph showing the percentage of Eomes+ cells within the CD56<sup>neg</sup>CD16+NKp80-, CD56<sup>neg</sup>CD16-NKp80+ and CD56<sup>neg</sup>CD16+NKp80+ populations. (C) Bar graphs showing the percentage of CD123+ cells within the CD56<sup>neg</sup>CD16+NKp80-, CD56<sup>neg</sup>CD16-NKp80+ and CD56<sup>neg</sup>CD16+NKp80+ populations. The mean with the standard error of the mean (SEM) is represented. Each dot represents a donor. \*\*\*p<0.001, \*\*\*\*p<0.0001, ns: not significant.

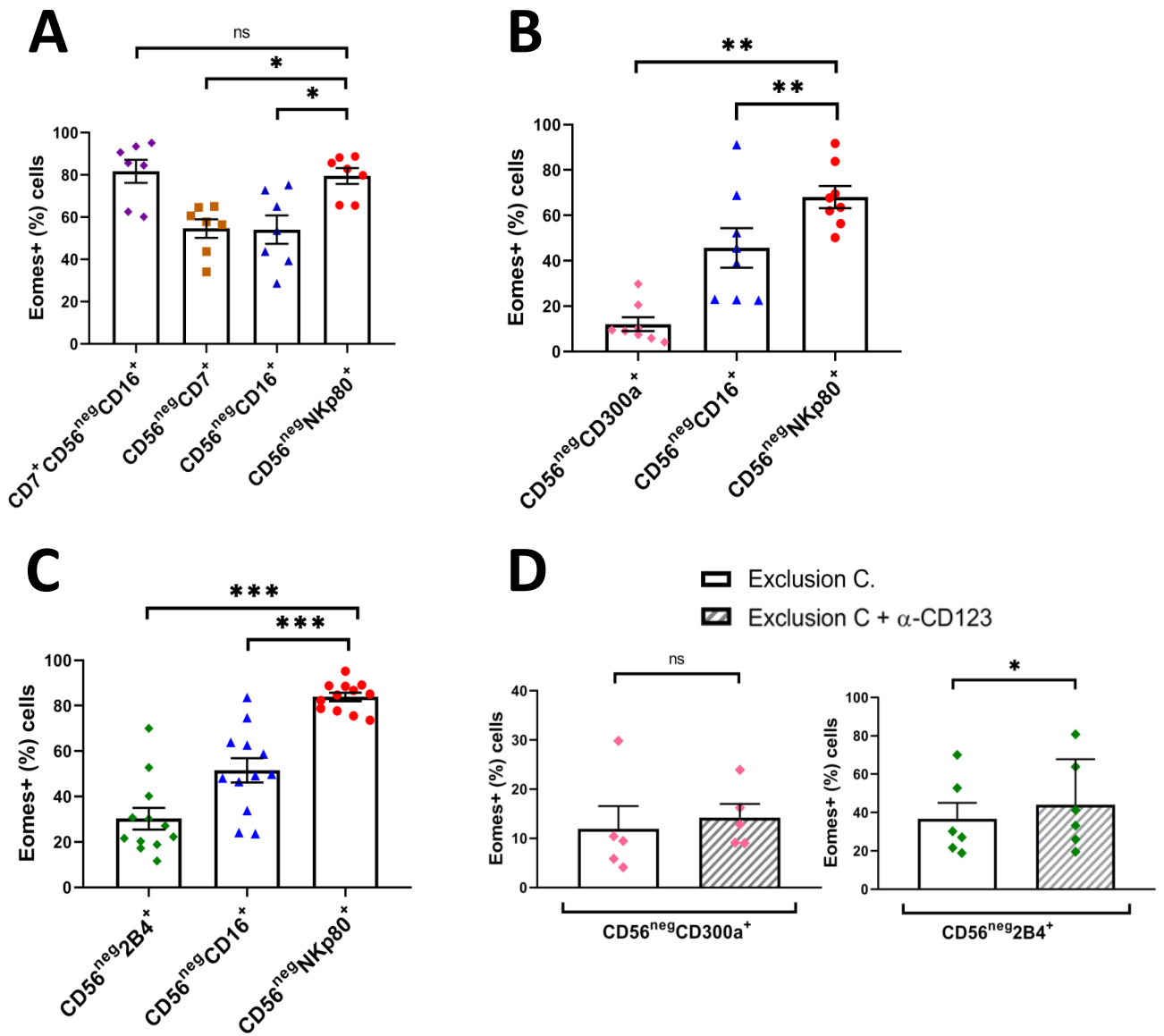


**Figure 9. NKp80 better identifies CD56<sup>neg</sup> NK cells than CD7, CD300a and 2B4 (CD244) in healthy individuals.** (A) Bars graph showing the percentage of Eomes<sup>+</sup> cells within CD7<sup>+</sup>CD56<sup>neg</sup>CD16<sup>+</sup>, CD56<sup>neg</sup>CD7<sup>+</sup>, CD56<sup>neg</sup>CD16<sup>+</sup> and CD56<sup>neg</sup>NKp80<sup>+</sup> populations. (B) Bar graph showing the percentage of Eomes<sup>+</sup> cells within CD56<sup>neg</sup>CD300a<sup>+</sup>, CD56<sup>neg</sup>CD16<sup>+</sup> and CD56<sup>neg</sup>NKp80<sup>+</sup> populations. (C) Bar graph showing the percentage of Eomes<sup>+</sup> cells within CD56<sup>neg</sup>2B4<sup>+</sup>, CD56<sup>neg</sup>CD16<sup>+</sup> and CD56<sup>neg</sup>NKp80<sup>+</sup> populations. (D) Bar graphs showing the percentage of Eomes<sup>+</sup> cells within CD56<sup>neg</sup>CD300a<sup>+</sup> and CD56<sup>neg</sup>2B4<sup>+</sup> populations with or without the addition of anti-CD123 mAb to the exclusion channel (Exclusion C.). The mean with the standard error of the mean (SEM) is represented. Each dot represents a donor. \*p<0.05, \*\*p<0.01, \*\*\*p<0.001, ns: not significant.

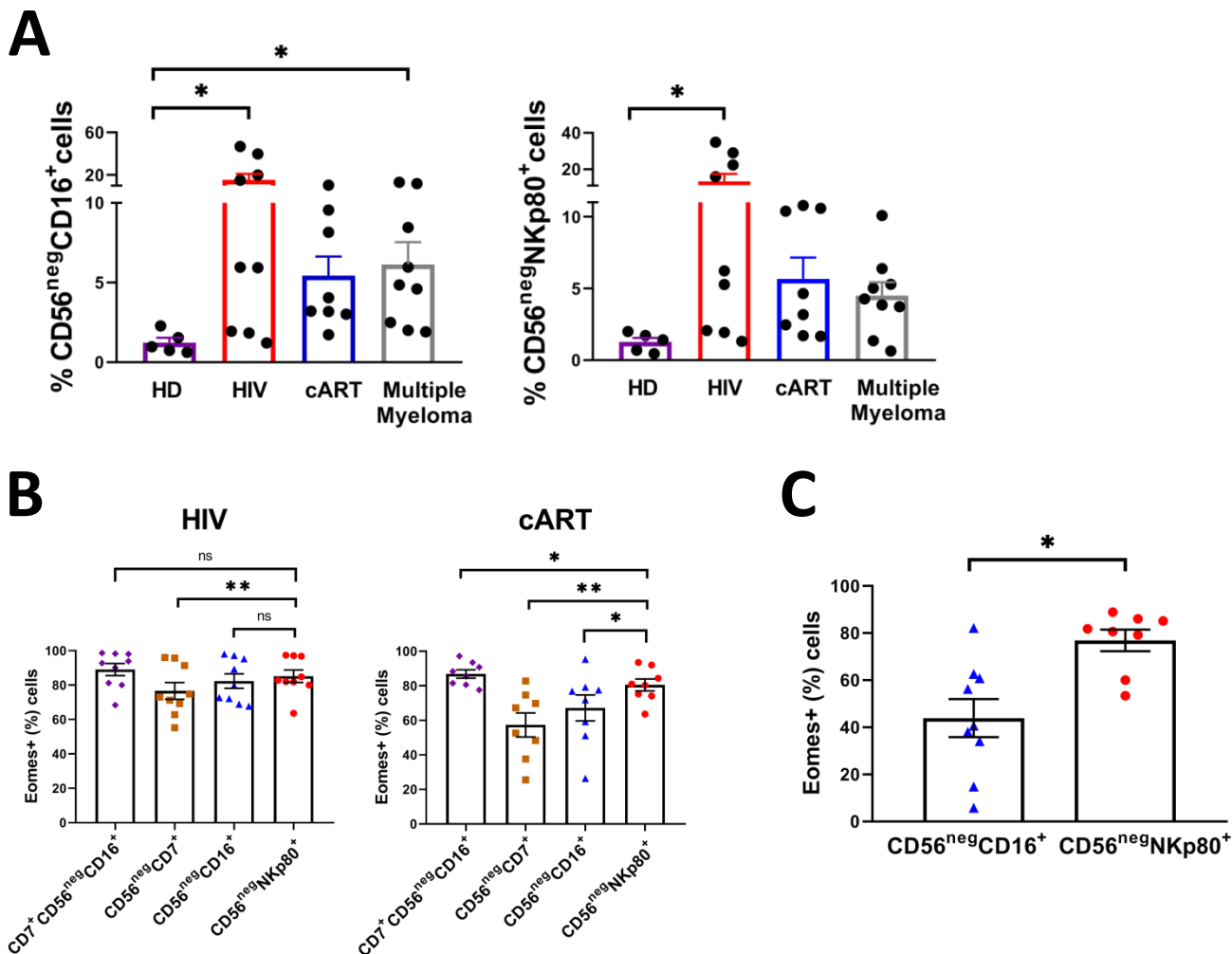


**Figure 10. Nkp80 better identifies CD56<sup>neg</sup> NK cells than CD16 in disease conditions.** (A) Bar graphs showing the percentage of CD56<sup>neg</sup>CD16<sup>+</sup> (left part) and CD56<sup>neg</sup>Nkp80<sup>+</sup> (right part) subsets within total NK cells from healthy donors (HD), untreated HIV-1 infected people (HIV), HIV-1 infected patients under cART (cART) and multiple myeloma patients. (B) Bar graphs showing the percentage of Eomes<sup>+</sup> cells within CD7<sup>+</sup>CD56<sup>neg</sup>CD16<sup>+</sup>, CD56<sup>neg</sup>CD7<sup>+</sup>, CD56<sup>neg</sup>CD16<sup>+</sup> and CD56<sup>neg</sup>Nkp80<sup>+</sup> populations in untreated HIV-1 infected subjects (HIV) and HIV-1 infected patients under cART (cART). (C) Bar graph showing the percentage of Eomes<sup>+</sup> cells within CD56<sup>neg</sup>CD16<sup>+</sup> and CD56<sup>neg</sup>Nkp80<sup>+</sup> populations in MM patients. The mean with the standard error of the mean (SEM) is represented. Each dot represents a donor. \*p<0.05, \*\*p<0.01, ns: not significant



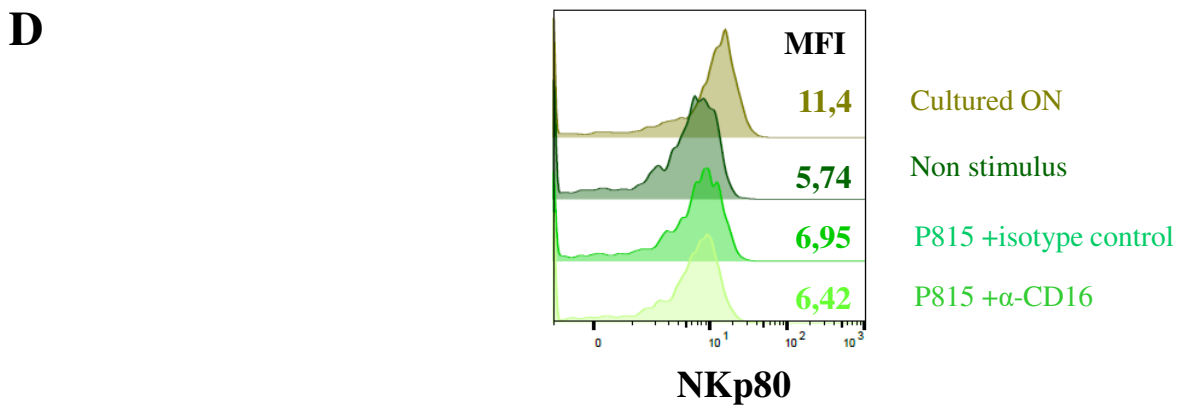
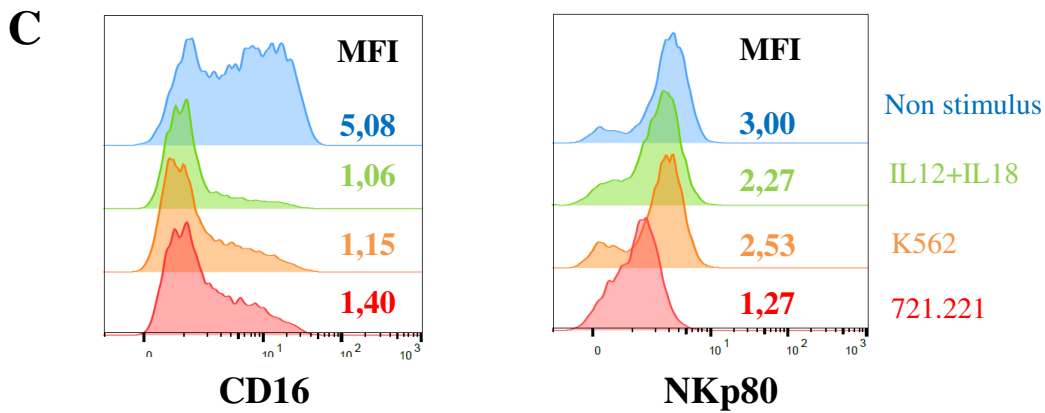
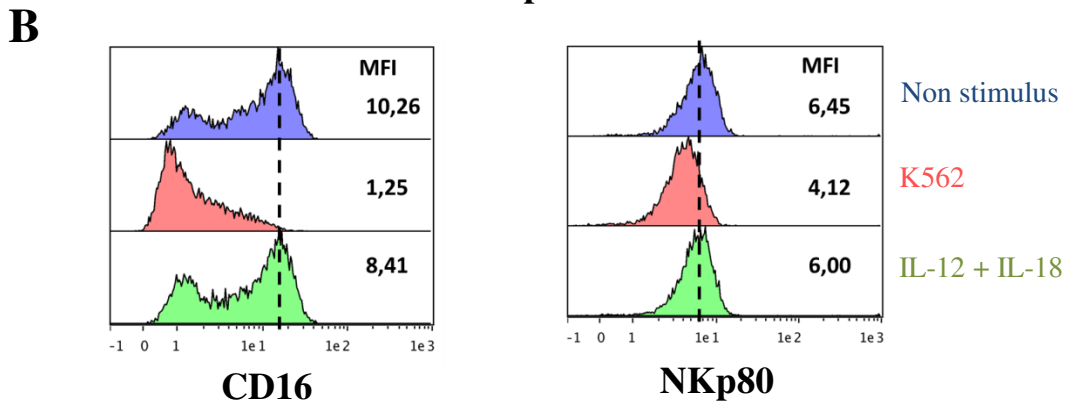
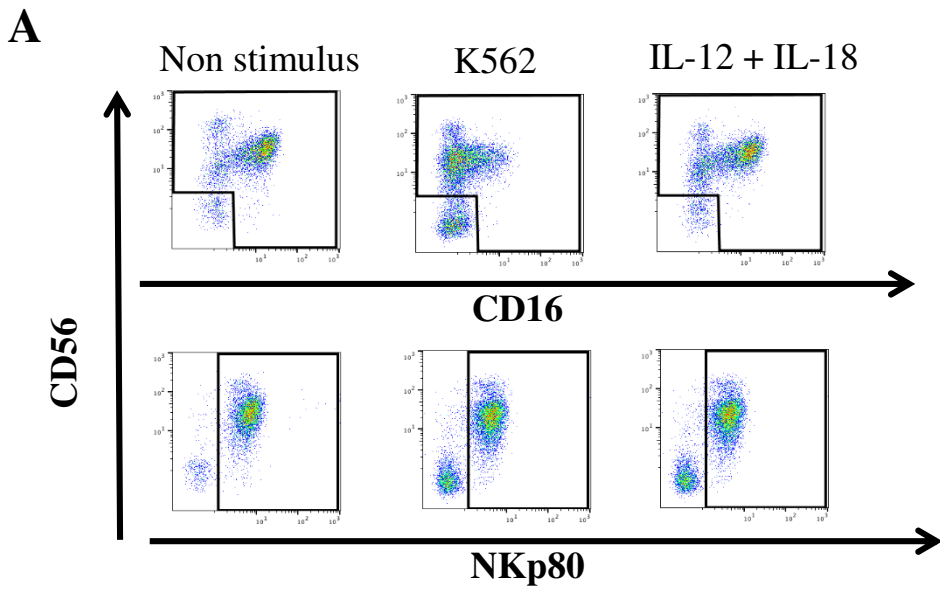
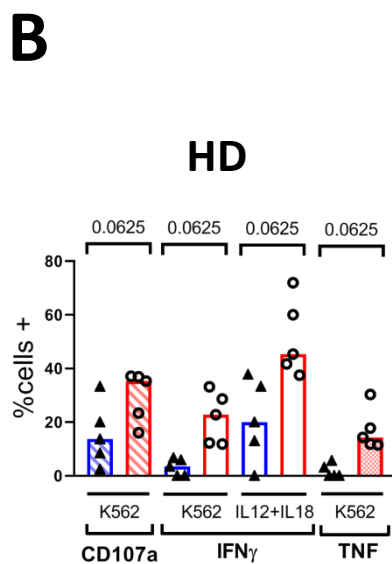
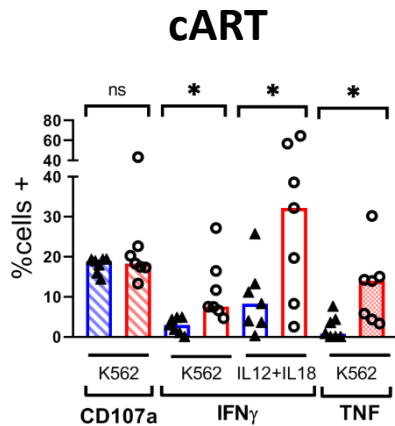
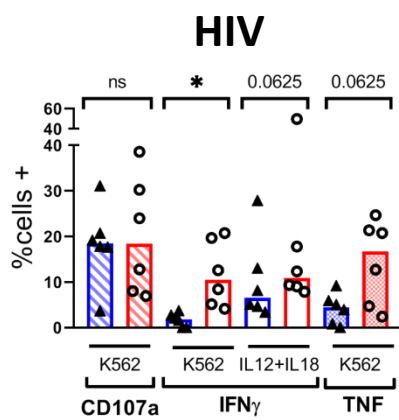


**Figure 11. CD16, but no NKp80, is downregulated after K562 cell line and IL-12+IL18 cytokine stimulation.** (A) Representative pseudocolor plot graphs comparing the expression of CD16 and NKp80 in non-stimulated condition, and after K562 cell line and IL-12+IL-18 cytokine stimulation. Data from a representative healthy donor is shown. (B) Histograms showing the median fluorescence intensity (MFI) of CD16 and NKp80 on NK cells in non-stimulus condition and after K562 cell line and IL-12+IL-18 cytokine stimulation. Data from a representative healthy donor is shown. (C) Histograms showing the MFI of CD16 and NKp80 on NK cells in non-stimulus condition and after IL-12+IL-18 cytokines, K562 and 721.221 cell lines stimulation. Data from a healthy donor is shown. (D) Histogram showing the MFI of NKp80 on NK cells cultured overnight (ON), non-stimulus condition and after stimulation with the P815 cell line and isotype control or anti-CD16 mAb after 6 hours of stimulation. Data from a healthy donor is shown.

**A**  CD56<sup>neg</sup>CD16<sup>+</sup>  
 CD56<sup>neg</sup>NKp80<sup>+</sup>

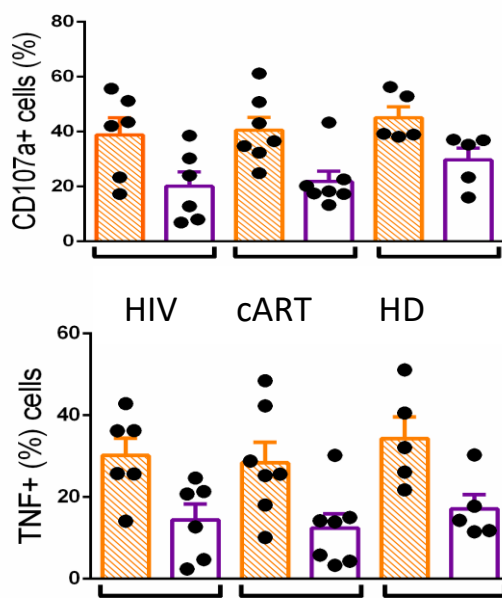
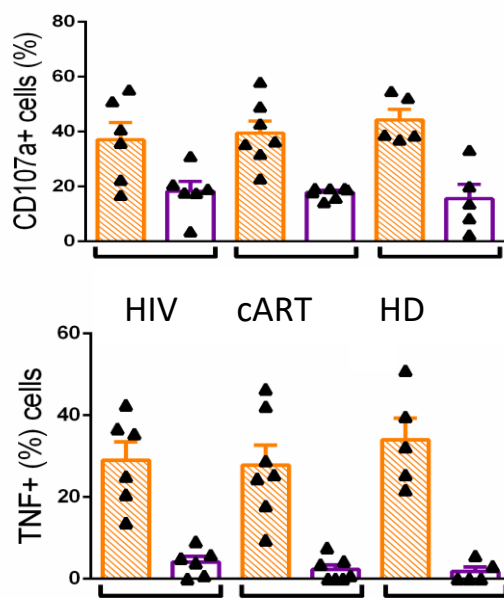


**C**  CD56<sup>dim</sup>  
 CD56<sup>neg</sup>

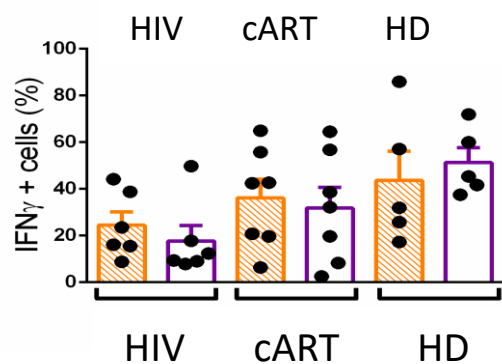
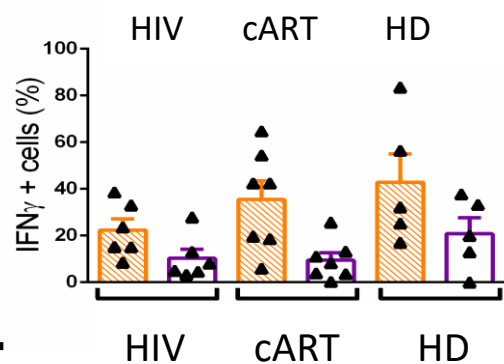
**CD16 based gating**

**NKp80 based gating**

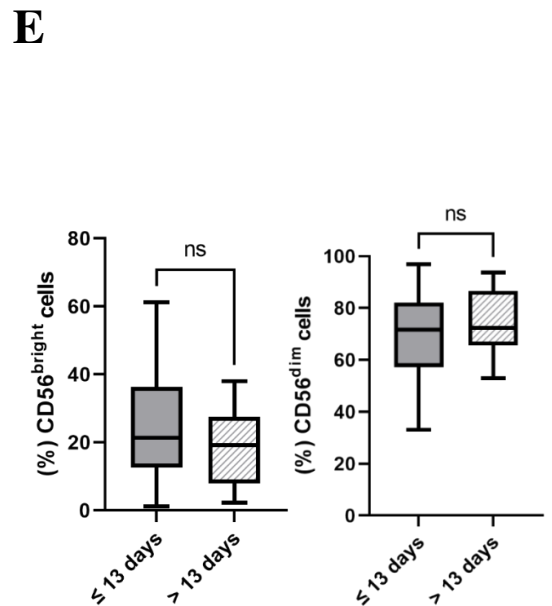
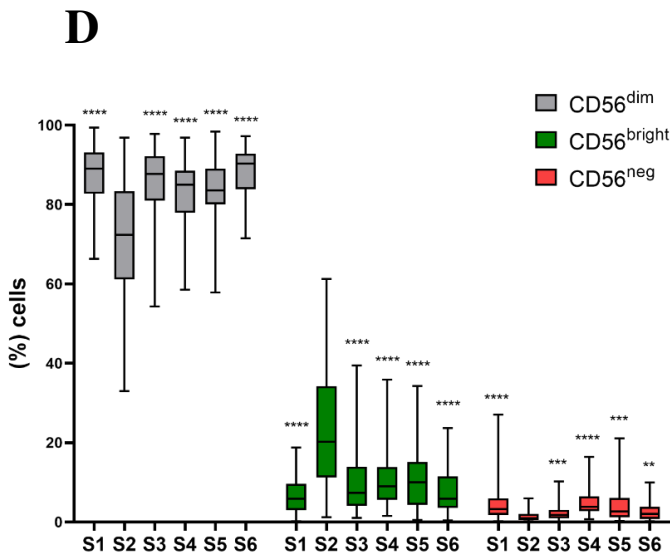
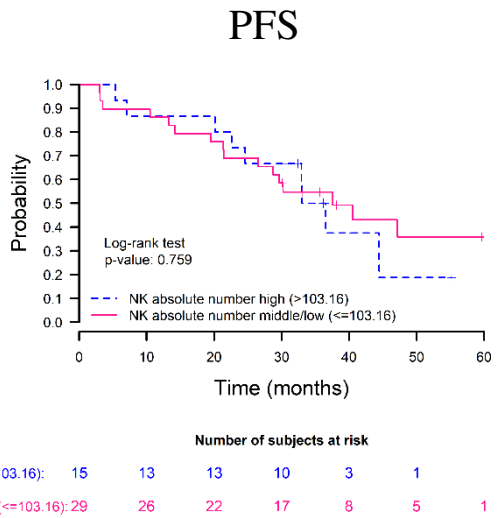
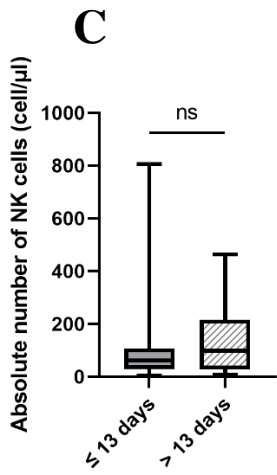
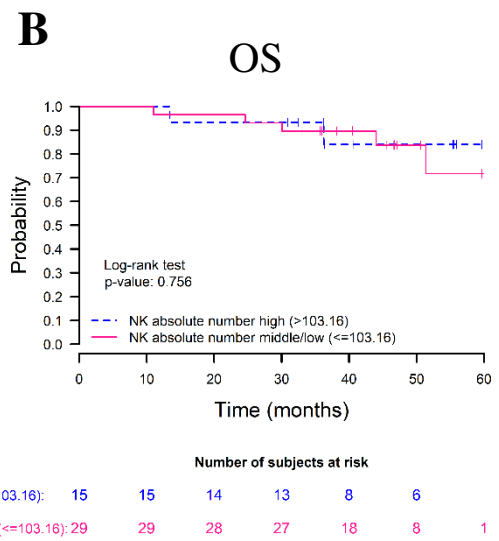
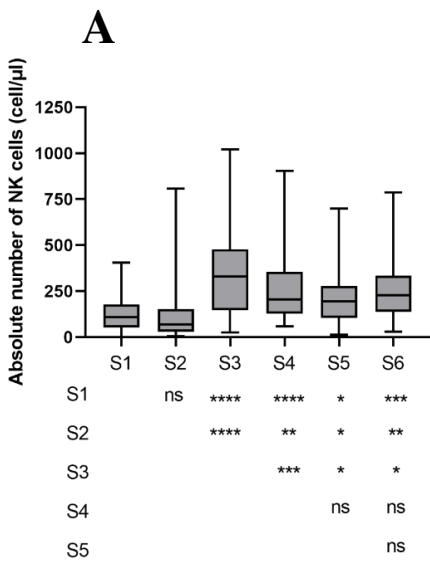
**K562 cell line**



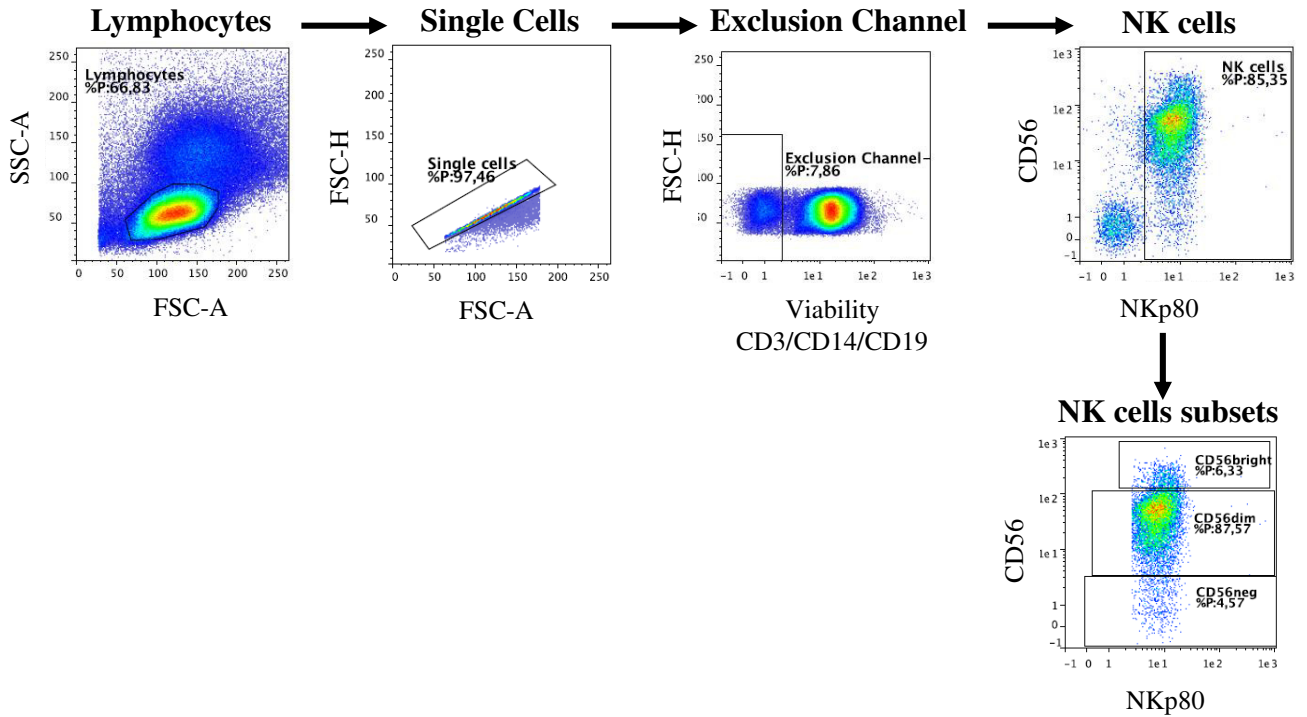
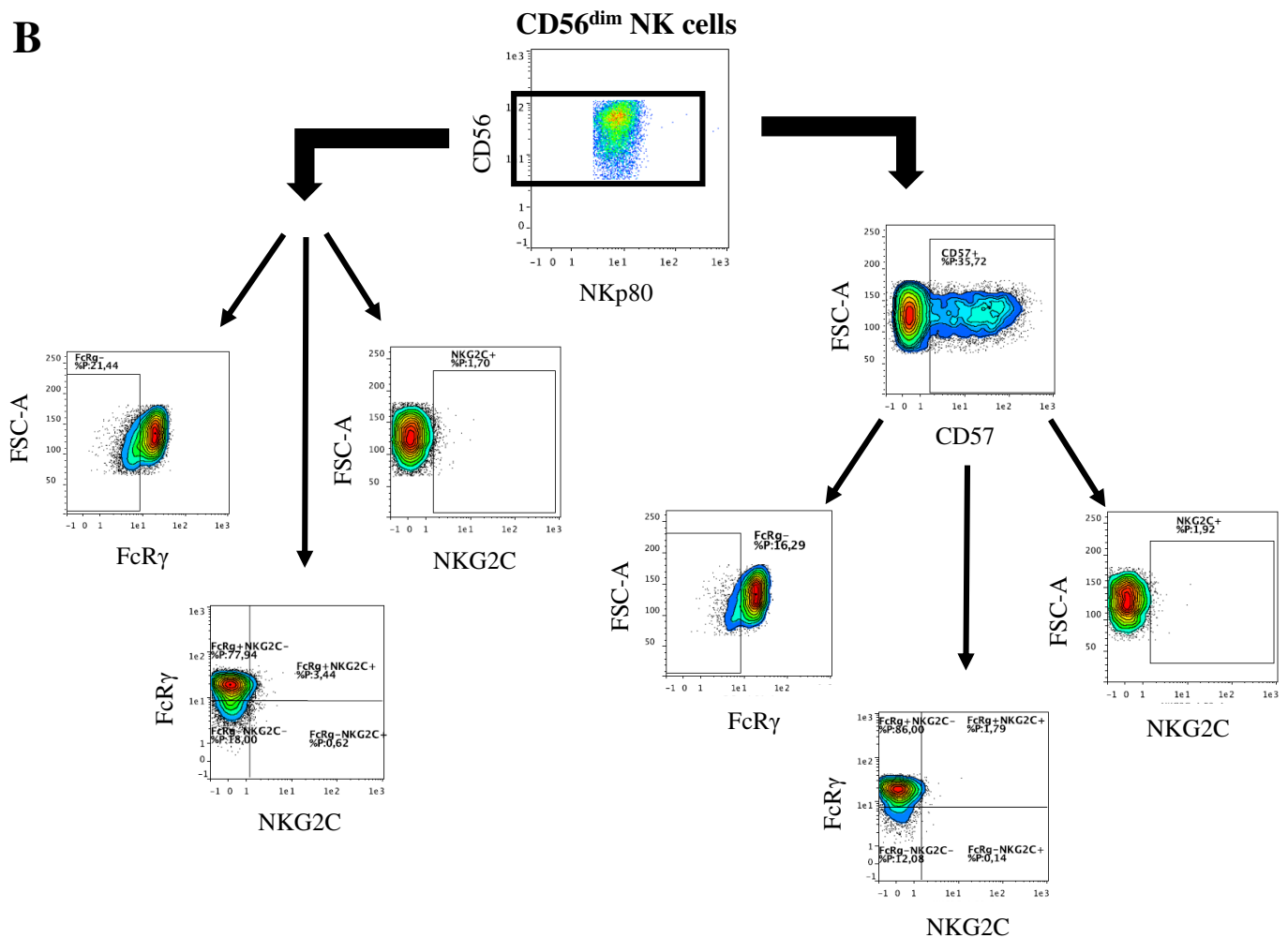
**IL-12 + IL-18**



**Figure 12. Effector functions of CD56neg NK cells in response to the K562 cell line and IL-12+IL-18 stimulation.** (A) Bar graphs showing the percentage of positive cells for CD107a, IFN $\gamma$  and TNF from HIV-1 infected subjects (HIV) and HIV-1 infected patients under cART (cART) after stimulation with the K562 cell line and IL-12+IL-18 cytokines within CD56negCD16+ and CD56negNKp80+ NK cells. (B) Bar graph showing the percentage of positive cells for CD107a, IFN $\gamma$  and TNF from healthy donors (HD) after stimulation with the K562 cell line and IL-12+IL-18 cells within CD56negCD16+ and CD56negNKp80+ NK cells. (C) Bar graphs showing the percentage of CD56dim and CD56neg NK cells positive for CD107a and TNF after K562 cell line stimulation and IFN $\gamma$  after IL-12+IL-18 cytokine stimulation from HIV-1 infected subjects (HIV), HIV-1 infected patients under cART (cART) and healthy donors (HD). In A and B the median is represented. In C the mean with the standard error of the mean (SEM) is represented Each dot represents a donor. \*p<0.05, ns: not significant.

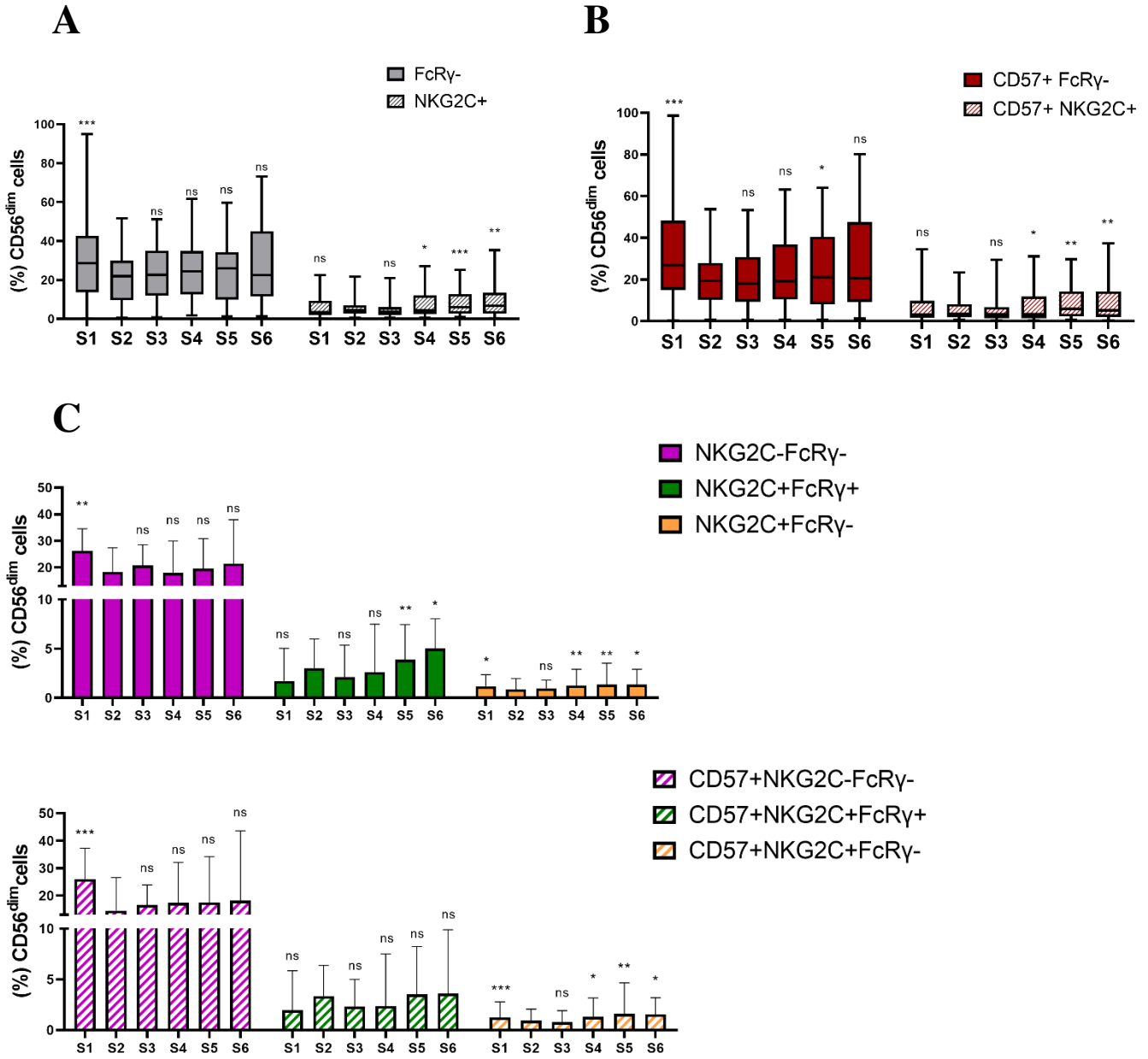


**Figure 13. NK cell subsets distribution is altered during NK cell reconstitution after autoHSCT.** (A) Boxplot graph showing the absolute number of NK cells at the six studied time points (S1-S6) (S1 n=52; S2 n=45; S3 n=43; S4 n=41; S5 n=33; S6 n=35). (B) Survival rates of OS and PFS in patients with MM treated with autoHSCT. Patients are grouped based on the frequency of NK cells absolute number at S2. Patients were grouped based on 66<sup>th</sup> percentile: high group (>66<sup>th</sup> percentile) and middle/low group ( $\leq$ 66<sup>th</sup> percentile). (C) Boxplot graph showing the absolute number of NK cells in sample S2 from patients with a time period of  $\leq$ 13 days or >13 days between autoHSCT and S2 (D) Boxplot graph showing the percentage of CD56<sup>dim</sup>, CD56<sup>bright</sup> and CD56<sup>neg</sup> NK cells. (S1 n=54; S2 n=45; S3 n=45; S4 n=43; S5 n=37; S6 n=37). (E) Boxplot graph showing the percentage of CD56<sup>bright</sup> and CD56<sup>dim</sup> in sample S2 from patients with a time period of  $\leq$ 13 days or >13 days between autoHSCT and S2. Boxplots show the median and 25–75th percentiles, and the whiskers denote lowest and highest values. Significance of data was determined by comparing each sample with sample S2, except in (A). \*p<0.05, \*\*p<0.01, \*\*\*p<0.001, \*\*\*\*p<0.0001 and ns: no significant.

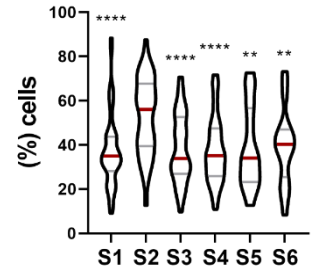
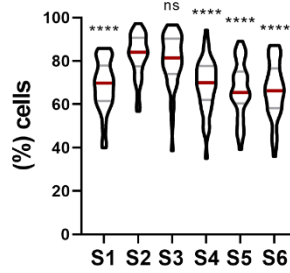
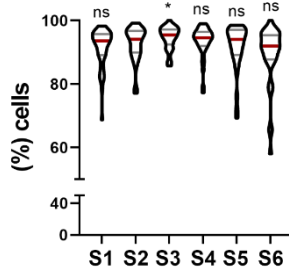
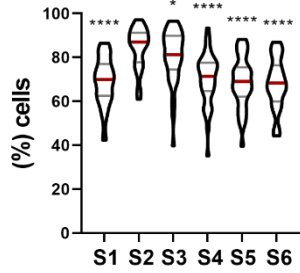
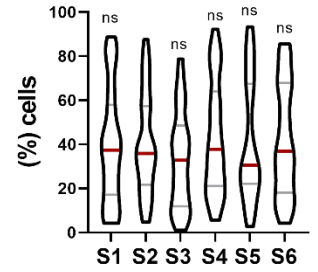
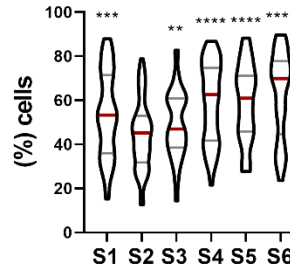
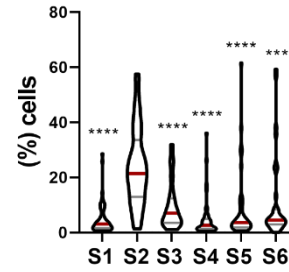
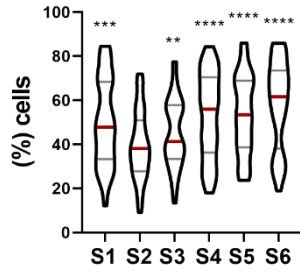
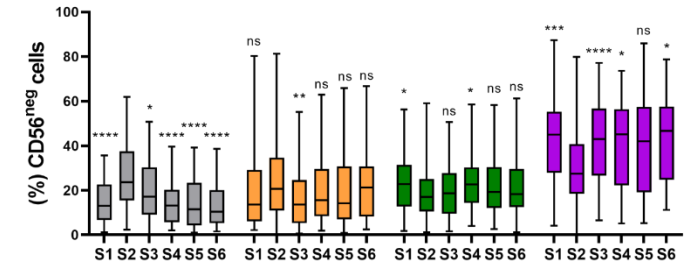
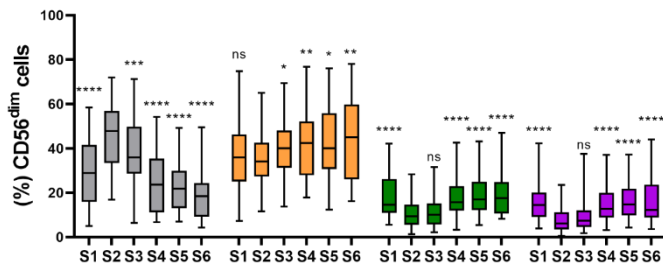
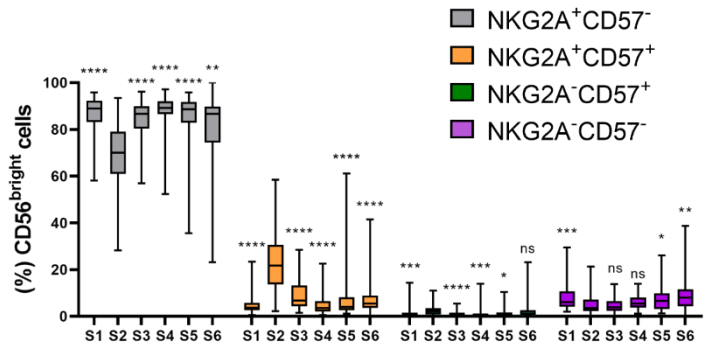
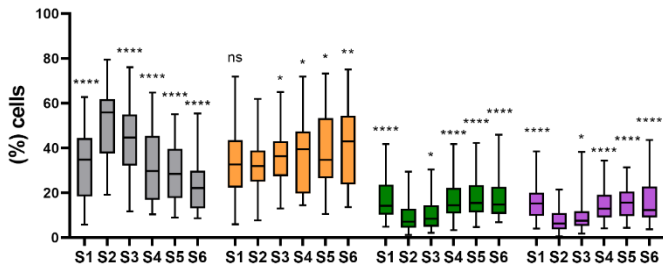
**A****B**

**Figure 14. Gating strategy for the identification of NK cells.** (A) Pseudocolor plot graphs representing the gating strategy utilized for the identification of NK cells and NK cell subsets. Data from a representative patient is shown. Lymphocytes were electronically gated based on their forward and side scatter parameters and then single cells were selected. To identify NK cells, the population negative for the exclusion channel (viability, CD3, CD14 and CD19) was selected. After that CD56<sup>bright</sup>, CD56<sup>dim</sup> and CD56<sup>neg</sup> NK cell subsets were identified based on the CD56 and NKp80 markers. Finally, the expression of different markers were analyzed within total NK cells or NK cell subsets. (B) Pseudocolor and contour plot graphs representing the gating strategy utilized for the identification of adaptive NK cells. Data from a representative patient is shown. The frequency of the different adaptive NK cells was analyzed within CD56<sup>dim</sup> NK cell subset. The individual expression of FcR $\gamma$  and NKG2C in addition to the co-expression of both markers was analyzed within CD56<sup>dim</sup> NK cells (left) and within CD56<sup>dim</sup>CD57<sup>+</sup> NK cells (right).



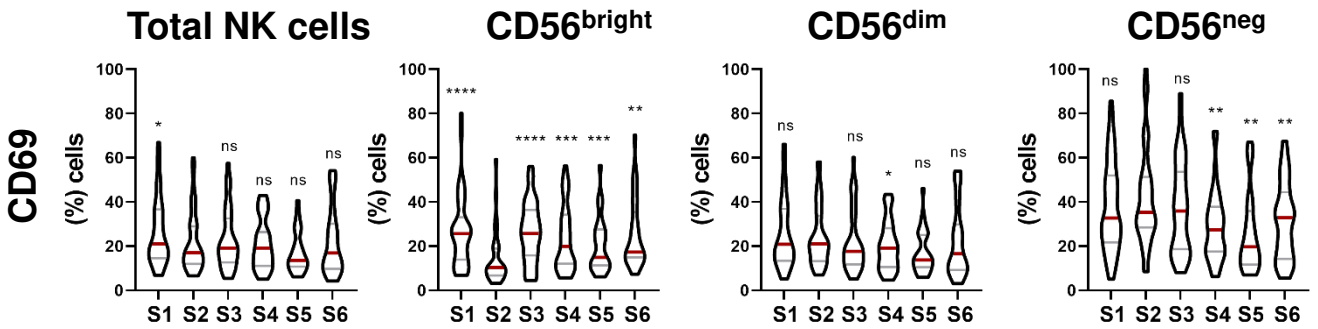


**Figure 15. The reconstitution pattern among adaptive NK cell subsets is different.** (A) Boxplot graph showing the percentage of CD56<sup>dim</sup>FcR $\gamma$ - and CD56<sup>dim</sup>NKG2C+ adaptive NK cells (S1 n=54; S2 n=45; S3 n=44; S4 n=43; S5 n=37; S6 n=37). (B) Boxplot graph showing the percentage of CD57+FcR $\gamma$ - and CD57+NKG2C+ adaptive NK cells within CD56<sup>dim</sup> NK cells (S1 n=54; S2 n=45; S3 n=44; S4 n=43; S5 n=37; S6 n=37). (C) Boxplot graphs showing the percentage NKG2C-FcR $\gamma$ -, NKG2C+FcR $\gamma$ + and NKG2C+FcR $\gamma$ - adaptive CD56<sup>dim</sup> NK cells (upper panel) and CD57+NKG2C-FcR $\gamma$ -, CD57+NKG2C+FcR $\gamma$ + and CD57+NKG2C+FcR $\gamma$ - adaptive NK cells within CD56<sup>dim</sup> NK cells (bottom panel) (S1 n=54; S2 n=45; S3 n=44; S4 n=43; S5 n=37; S6 n=37). Boxplots show the median and 25–75th percentiles, and the whiskers denote lowest and highest values. Bar graphs show the median with interquartile range. Significance of data was determined by comparing each sample with sample S2. \*p<0.05, \*\*p<0.01, \*\*\*p<0.001, and ns: no significant.

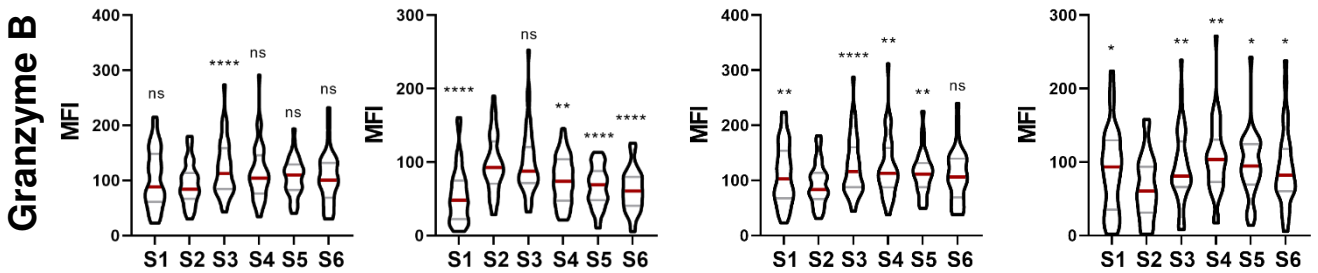
**A****Total NK cells****CD56<sup>bright</sup>****CD56<sup>dim</sup>****CD56<sup>neg</sup>****NKG2A****B****Total NK cells****CD56<sup>bright</sup>****CD56<sup>dim</sup>****CD56<sup>neg</sup>****CD57****C**

**Figure 16. NK cells exhibit a predominantly immature phenotype shortly after autoHSCT.** (A) Violin plots showing the percentage of NKG2A+ cells within total NK cells and CD56<sup>bright</sup>, CD56<sup>dim</sup> and CD56<sup>neg</sup> subsets at the six studied time points (S1-S6). (B) Violin plots showing the percentage of CD57+ cells within total NK cells and CD56<sup>bright</sup>, CD56<sup>dim</sup> and CD56<sup>neg</sup> subsets. (C) Boxplot graphs showing the percentage of NKG2A+CD57-, NKG2A+CD57+, NKG2A-CD57+ and NKG2A-CD57- within total NK cells (upper line, left) and within CD56<sup>bright</sup> (upper line, right), CD56<sup>dim</sup> (bottom line, left) and CD56<sup>neg</sup> (bottom line, right) subsets. Violin plots show the median and the quartiles. Boxplots show the median and 25–75th percentiles, and the whiskers denote lowest and highest values (S1 n=54; S2 n=45; S3 n=45; S4 n=43; S5 n=37; S6 n=37). Significance of data was determined by comparing each sample with sample S2. \*p<0.05, \*\*p<0.01, \*\*\*p<0.001, \*\*\*\*p<0.0001 and ns: no significant.

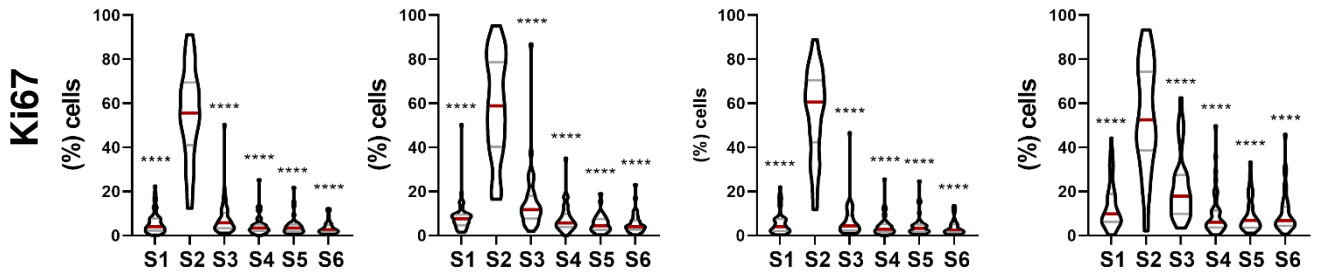
**A**



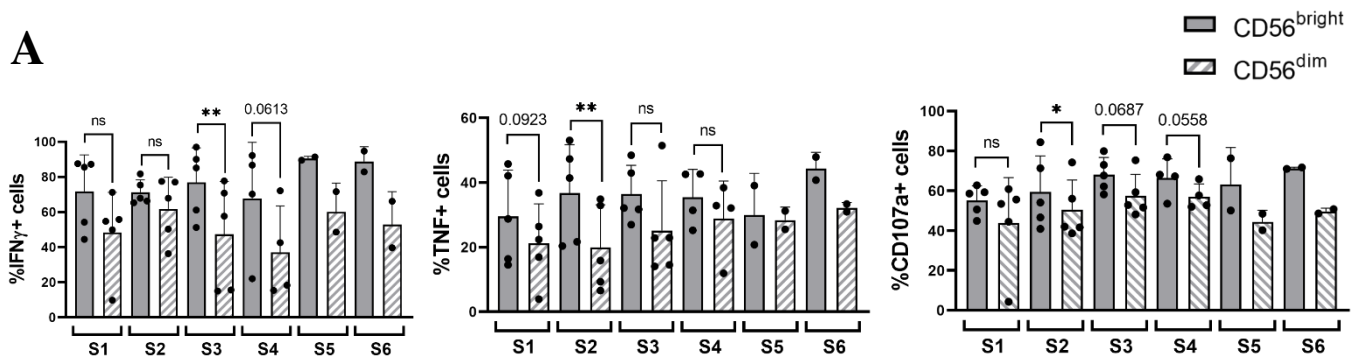
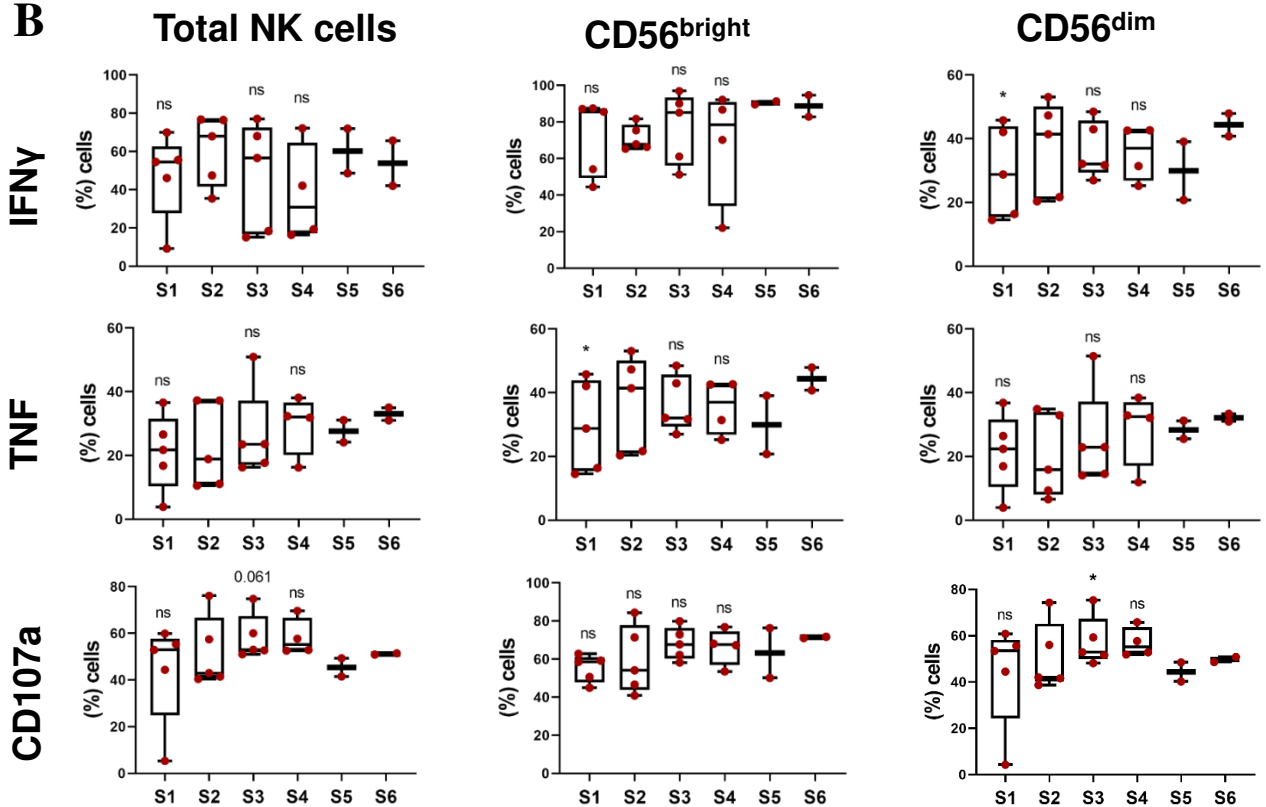
**B**



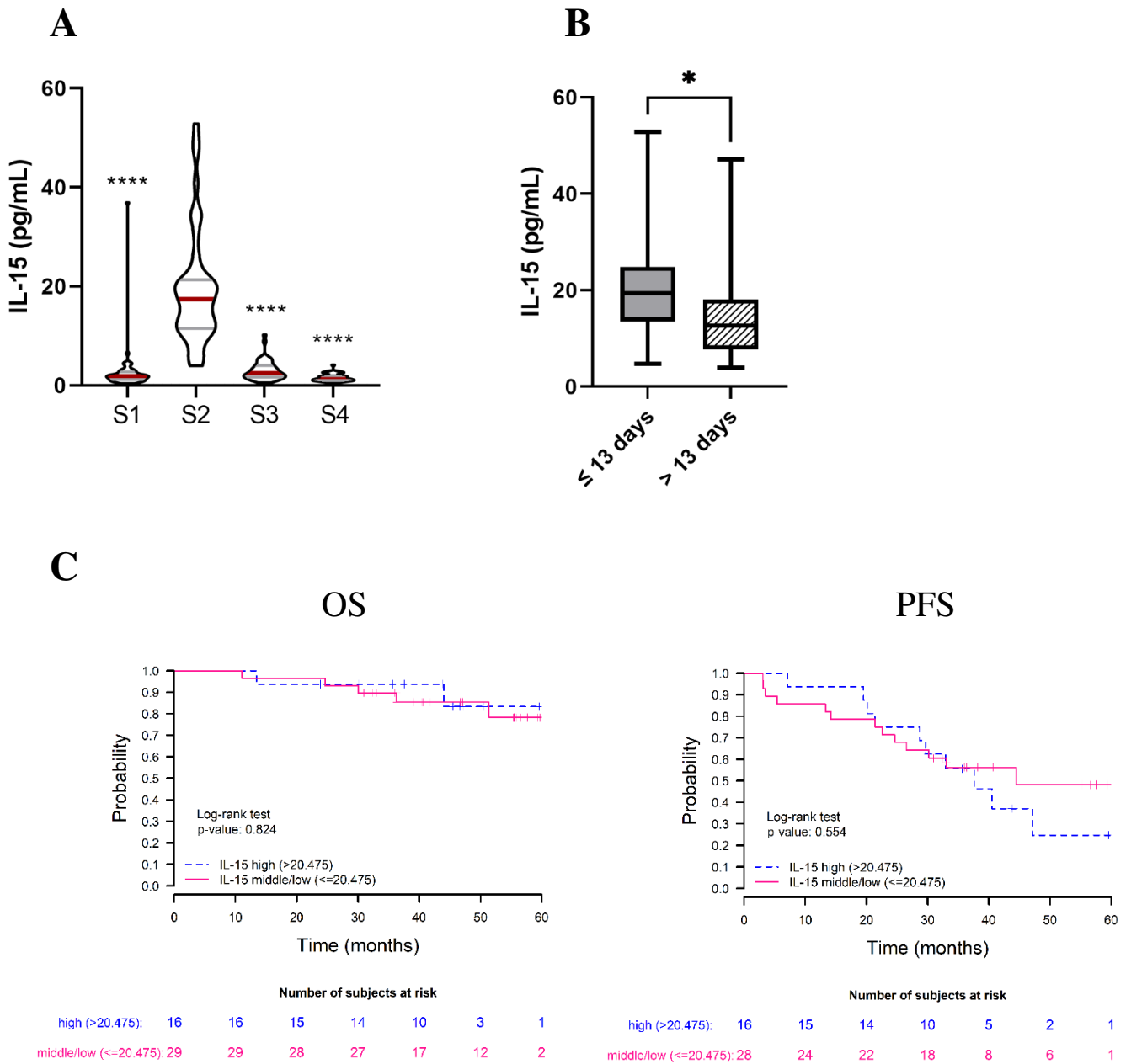
**C**



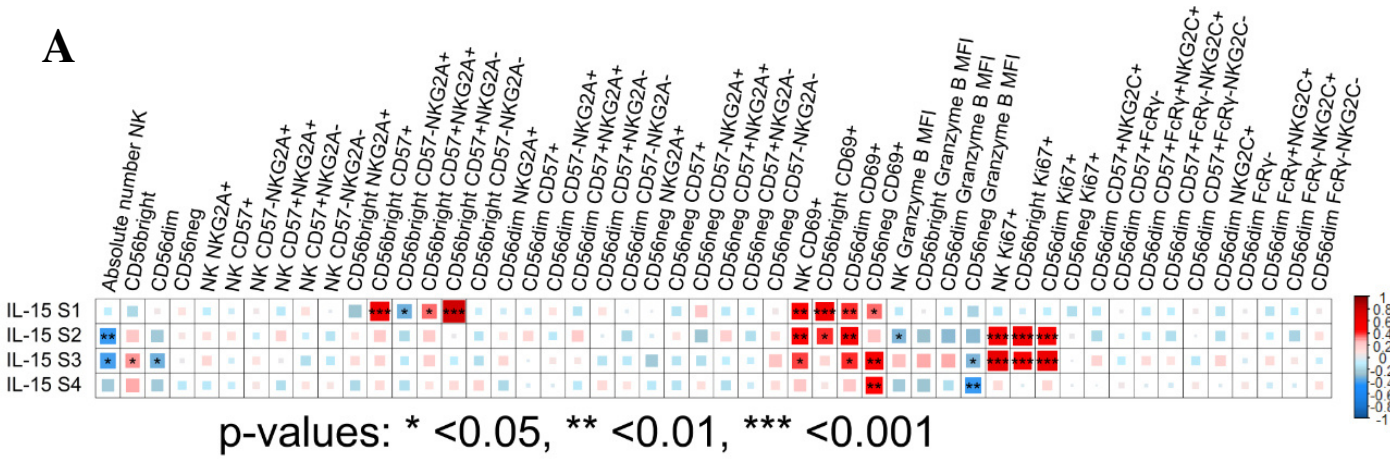
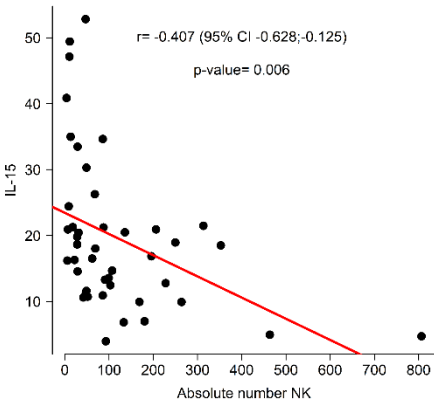
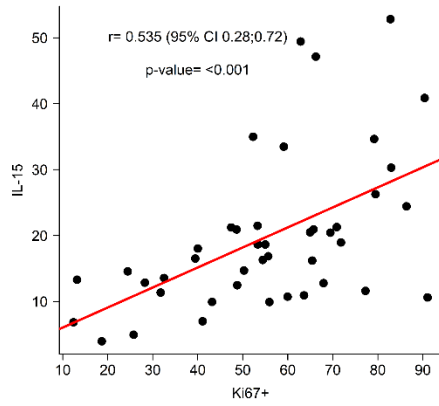
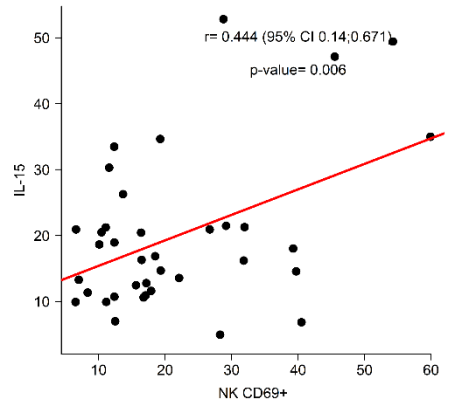
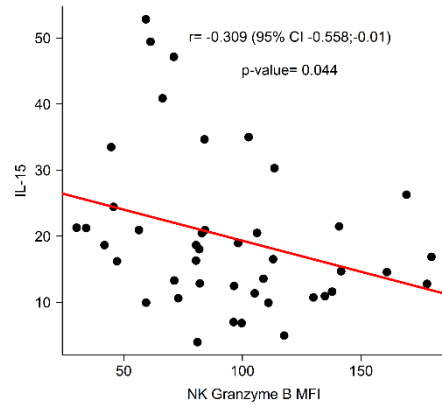
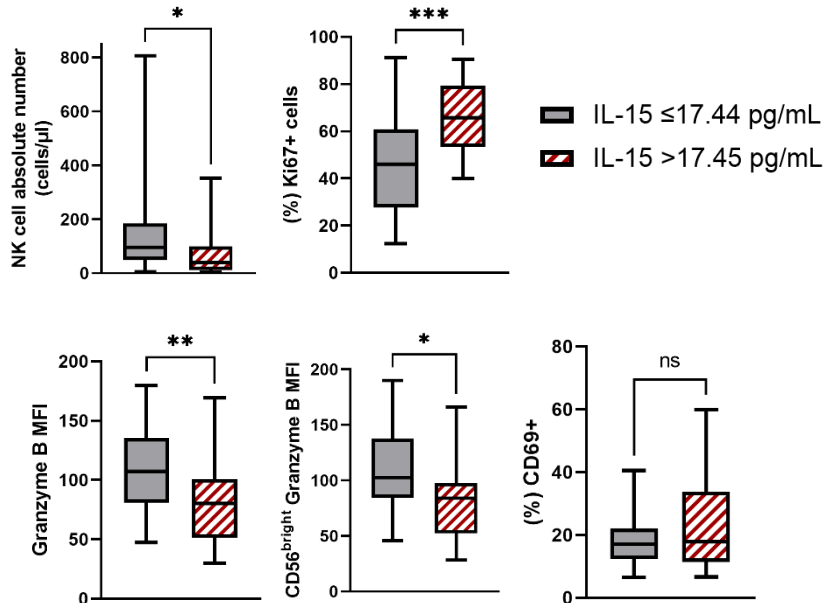
**Figure 17. NK cell activation, cytotoxic potential and proliferation capacity are modulated during NK cell reconstitution after autoHSCT.** (A) Violin plots showing the percentage of CD69<sup>+</sup> cells within total NK cells and CD56<sup>bright</sup>, CD56<sup>dim</sup> and CD56<sup>neg</sup> subsets at the six studied time points (S1-S6) (S1 n=46; S2 n=37; S3 n=37; S4 n=35; S5 n=29; S6 n=29). (B) Violin plots showing the MFI of granzyme B within total NK cells and CD56<sup>bright</sup>, CD56<sup>dim</sup> and CD56<sup>neg</sup> subsets (S1 n=54; S2 n=43; S3 n=44; S4 n=43; S5 n=35; S6 n=36). (C) Violin plots showing the percentage of Ki67<sup>+</sup> cells within total NK cells and CD56<sup>bright</sup>, CD56<sup>dim</sup> and CD56<sup>neg</sup> subsets (S1 n=54; S2 n=43; S3 n=44; S4 n=43; S5 n=35; S6 n=36). Violin plots show the median and the quartiles. Significance of data was determined by comparing each sample with sample S2. \*p<0.05, \*\*p<0.01, \*\*\*p<0.001, \*\*\*\*p<0.0001 and ns: no significant.

**A****B**

**Figure 18. NK cells are functional shortly after autoHSCT.** (A) Bar graphs showing the percentages of IFN $\gamma$ +, TNF+ and CD107a+ cells within CD56<sup>bright</sup> and CD56<sup>dim</sup> NK cell subsets at the six studied time points (S1-S6). (B) Boxplot graphs showing the percentage of IFN $\gamma$ +, TNF+ and CD107a+ cells within total NK cells and CD56<sup>bright</sup> and CD56<sup>dim</sup> NK cell subsets at the six studied time points (S1-S6). The production of IFN $\gamma$  by NK cells was measured after stimulation with IL-12+IL-18 for 25-26 hours. The production of TNF and degranulation (CD107a) of NK cells were measured after stimulation with 721.221 cell line for 5 hours. The percentage of NK cells positive for IFN $\gamma$ , TNF and CD107a was calculated after subtracting the non-stimulus condition. Bar graphs show the mean with standard deviation (SD). Boxplots show the median and 25–75th percentiles, and the whiskers denote lowest and highest values. Each dot represent a donor. \*p<0.05, \*\*p<0.01 and ns: no significant.

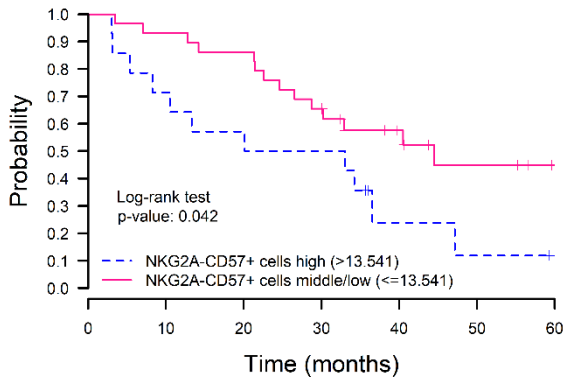


**Figure 19. IL-15 plasma levels are elevated at leukocyte recovery (S2).** (A) Violin plots showing the IL-15 plasma levels (pg/mL) at the four studied time points (S1-S4). (B) Boxplot graph showing the IL-15 plasma levels (pg/mL) from patients with a time period of  $\leq 13$  days or  $> 13$  days between autoHSCT and S2. (C) Survival rates of OS and PFS in patients with MM treated with autoHSCT. Patients are grouped based on the IL-15 plasma levels at S2. Patients were grouped based on 66<sup>th</sup> percentile: high group ( $>66^{\text{th}}$  percentile) and middle/low group ( $\leq 66^{\text{th}}$  percentile). Violin plots show the median and the quartiles. Boxplots show the median and 25–75th percentiles, and the whiskers denote lowest and highest values. Significance of data in (A) was determined by comparing each sample with sample S2 \* $p < 0.05$ , \*\* $p < 0.01$ , \*\*\* $p < 0.001$ , \*\*\*\* $p < 0.0001$  and ns: no significant.

**A****B****C****D****E****F**

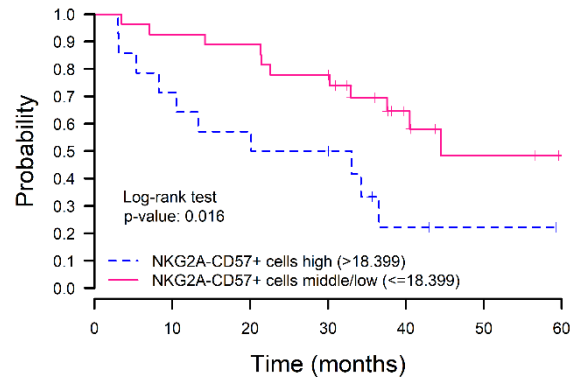
**Figure 20. IL-15 plasma levels at leukocyte recovery associate with the number, proliferation capacity and the cytotoxic potential of NK cells after autoHSCT. (A)** Correlogram showing Spearman correlation of the indicated flow cytometry data at S2 and IL-15 plasma levels. Correlation plots showing association between IL-15 plasma levels at S2 and the absolute number of NK cells (**B**), the percentage of Ki67+ (**C**) and CD69+ (**D**) NK cells and the MFI of granzyme B in NK cells at S2 (**E**). (**F**) Boxplot graphs showing the NK cell absolute number (cells/ $\mu$ l), percentage of Ki67+ within total NK cells, MFI of granzyme B within total NK cells and within CD56<sup>bright</sup> NK cells and the percentage of CD69+ cells within total NK cells of S2 in patients with IL-15 plasma levels of  $\leq 17.44$  pg/mL or  $> 17.45$  pg/mL (median IL-15 levels at S2: 17.45 pg/mL). Boxplots show the median and 25–75th percentiles, and the whiskers denote lowest and highest values. Significance of data in (A) was determined by comparing each sample with sample S2 \* $p < 0.05$ , \*\* $p < 0.01$ , \*\*\* $p < 0.001$  and ns: no significant.



**A****PFS**

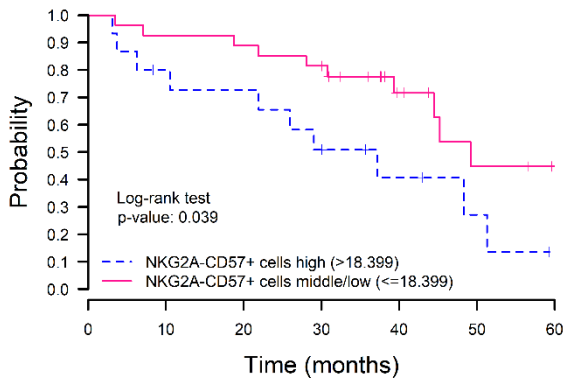
Number of subjects at risk

high (>13.541):	14	10	8	7	2	1	
middle/low (<=13.541):	29	27	25	19	11	6	2

**B****PFS**

Number of subjects at risk

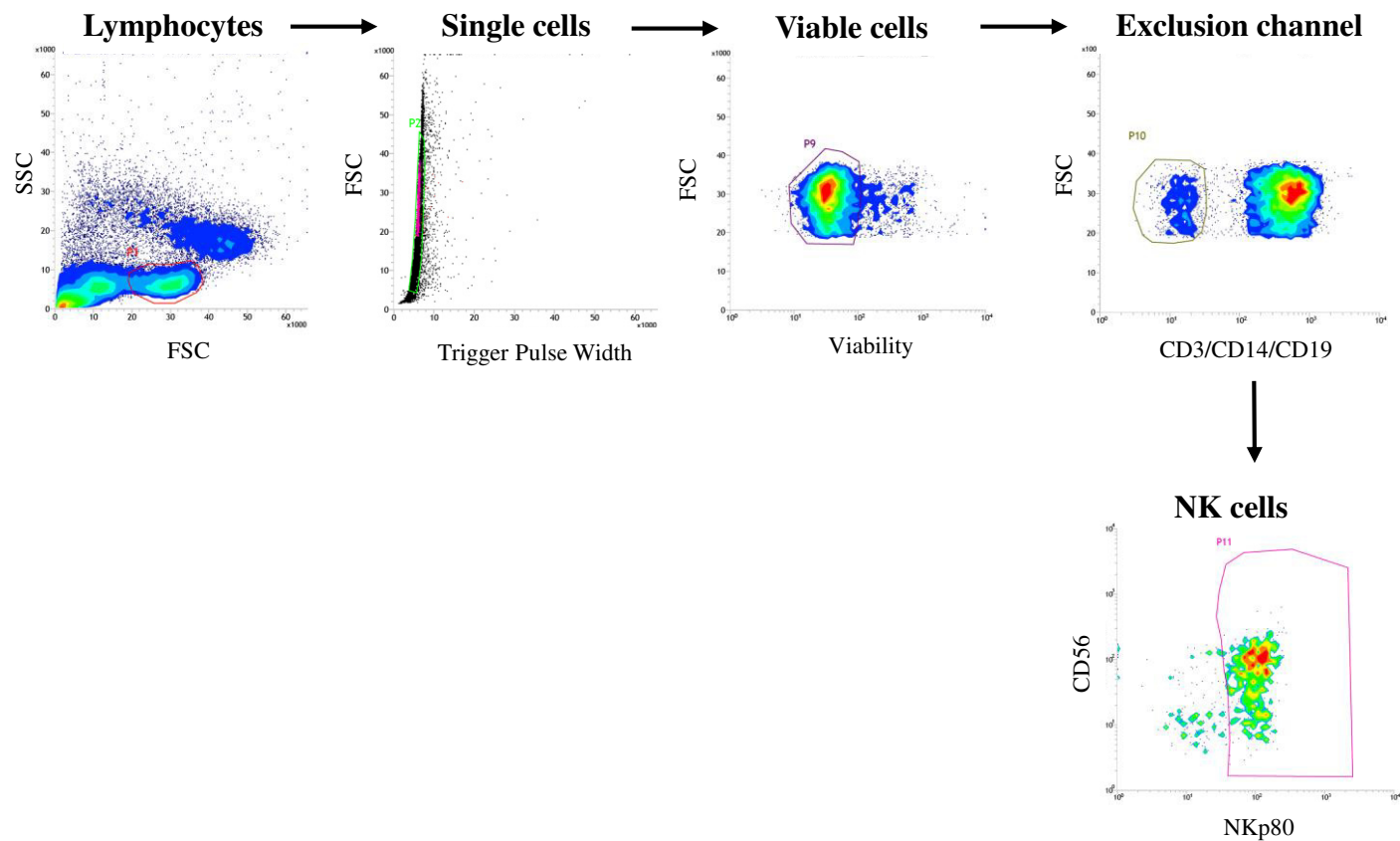
high (>18.399):	14	10	8	7	2	1	
middle/low (<=18.399):	27	25	24	21	10	5	2

**C****TTNT**

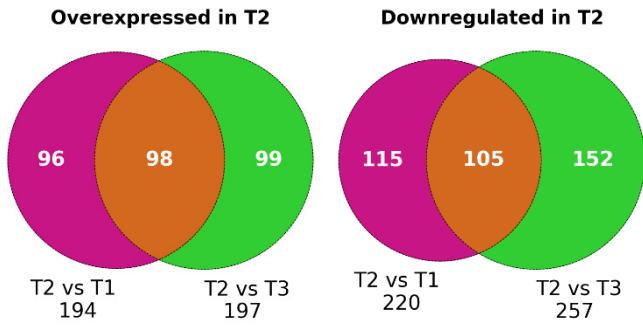
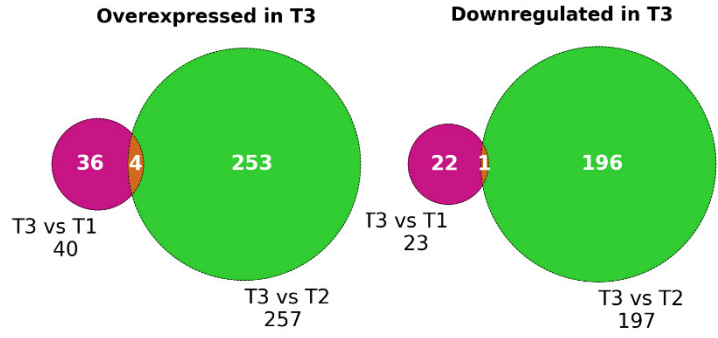
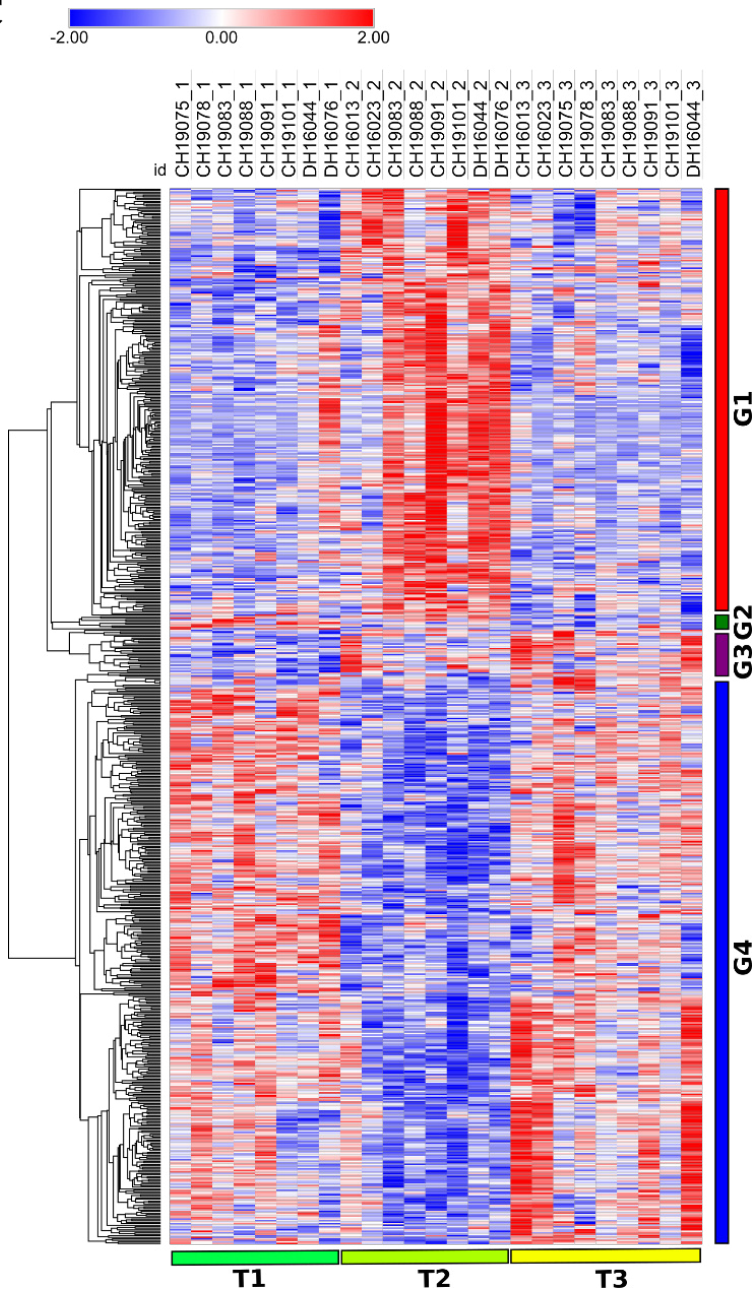
Number of subjects at risk

high (>18.399):	15	11	10	7	4	2	
middle/low (<=18.399):	27	25	24	22	11	5	2

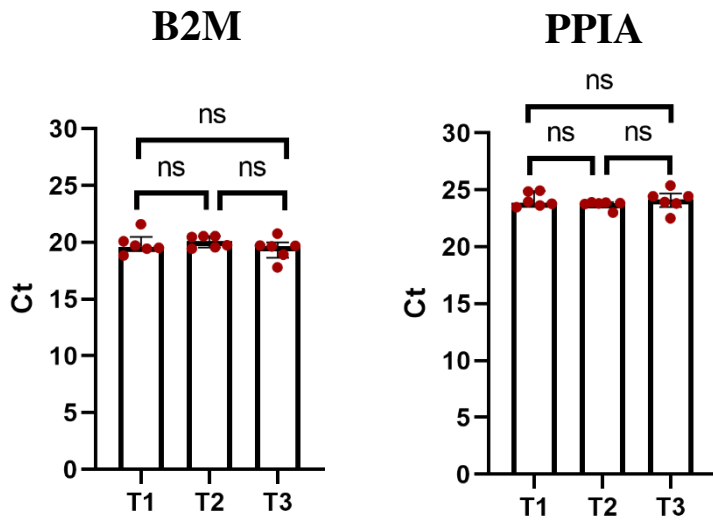
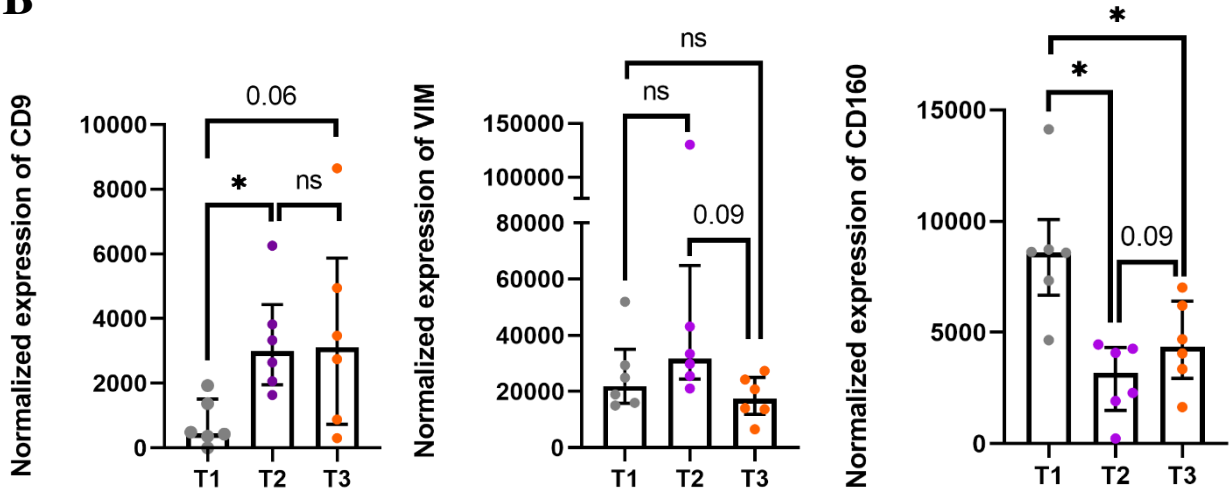
**Figure 21. High frequencies of terminally differentiated NKG2A-CD57+ NK cells associate with poor prognosis after autoHSCT in MM patients.** Survival rates of PFS (A, B) and TTNT (C) in patients with MM treated with autoHSCT. Patients are grouped based on the frequency of NKG2A-CD57+ NK cells on day 30 (S3) (A) and day 100 (S4) (B, C) after autoHSCT. Patients were grouped based on 66<sup>th</sup> percentile: high group (>66<sup>th</sup> percentile) and middle/low group ( $\leq$ 66<sup>th</sup> percentile).



**Figure 22. Gating strategy used for NK cell isolation.** Pseudocolor plot graphs representing the gating strategy utilized for the isolation of NK cells. Data from a representative patient is shown. Lymphocytes were electronically gated based on their forward and side scatter parameters and then single cells were selected. Next, dead cells were excluded. To identify NK cells, the population negative for the exclusion channel (CD3, CD14 and CD19) was selected. After that, NK cells were identified based on the expression of CD56 and NKp80 markers.

**A****B****C**

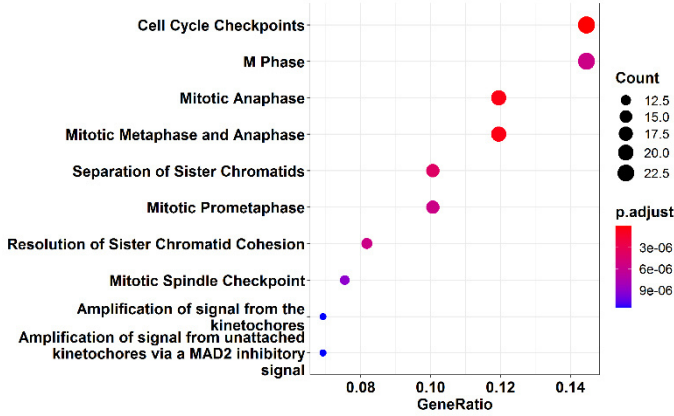
**Figure 23. The gene expression profile of NK cells significantly changes immediately after autoHSCT.** (A) Venn diagrams showing the number of differentially expressed genes (DEGs) in T2 compared to T1 and T3. (B) Venn diagrams showing the number of DEGs in T3 compared to T1 and T2. (C) Heatmap showing the relative expression of DEGs in the three time points (T1, T2 and T3). Genes were hierarchically grouped according to their homology. Patients' samples (in columns) were grouped based on the time points (T1, T2 and T3). Four gene groups were identified according to the gene expression pattern profile among time points (G1, G2, G3 and G4). G1 is composed of genes with high expression in T2 compared to T1 and T3; G2 is composed of genes with lower expression in T3 than in T1; G3 is composed of genes with higher expression in T3 than in T1; and G4 is composed of genes with lower expression in T2 compared to T1 and T3.

**A****B**

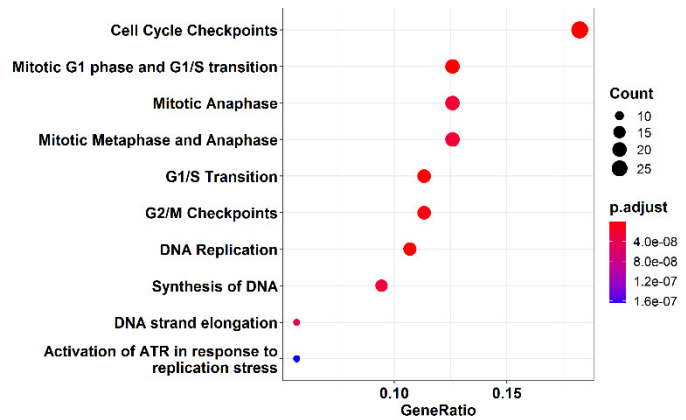
**Figure 24. Validation of RNA-seq data by qPCR.** (A) Bar graphs showing the Ct values of *B2M* and *PPIA* housekeeping genes at the three different time points (T1, T2 and T3). Median and the interquartile range are shown. (B) Graphs showing the normalized expression of *CD9*, *VIM* and *CD160* genes. Median and interquartile range are shown. *PPIA* gene was selected as reference gene for data representation. The expression of each gene of interest was normalized to the expression of *PPIA* gene. In the graphical representation the normalized expression of each gene is shown considering that there were 100.000 particles of *PPIA* gene.

**A**

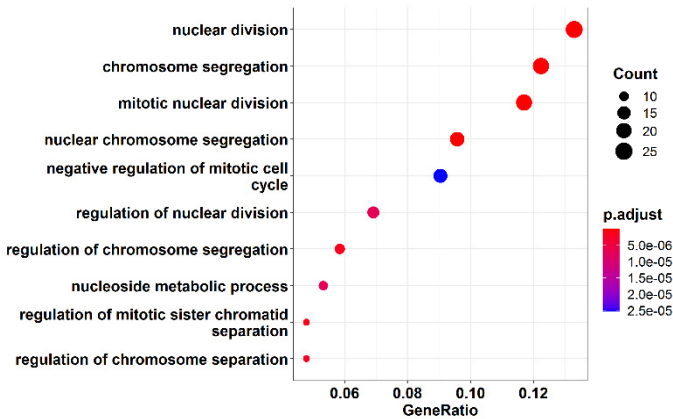
Upregulated T2 over T1



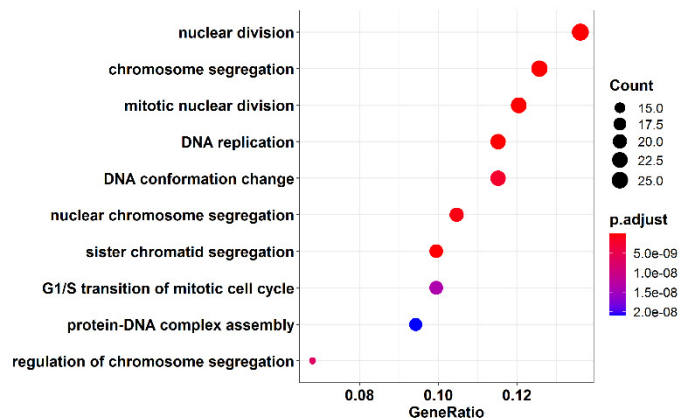
Upregulated T2 over T3

**B**

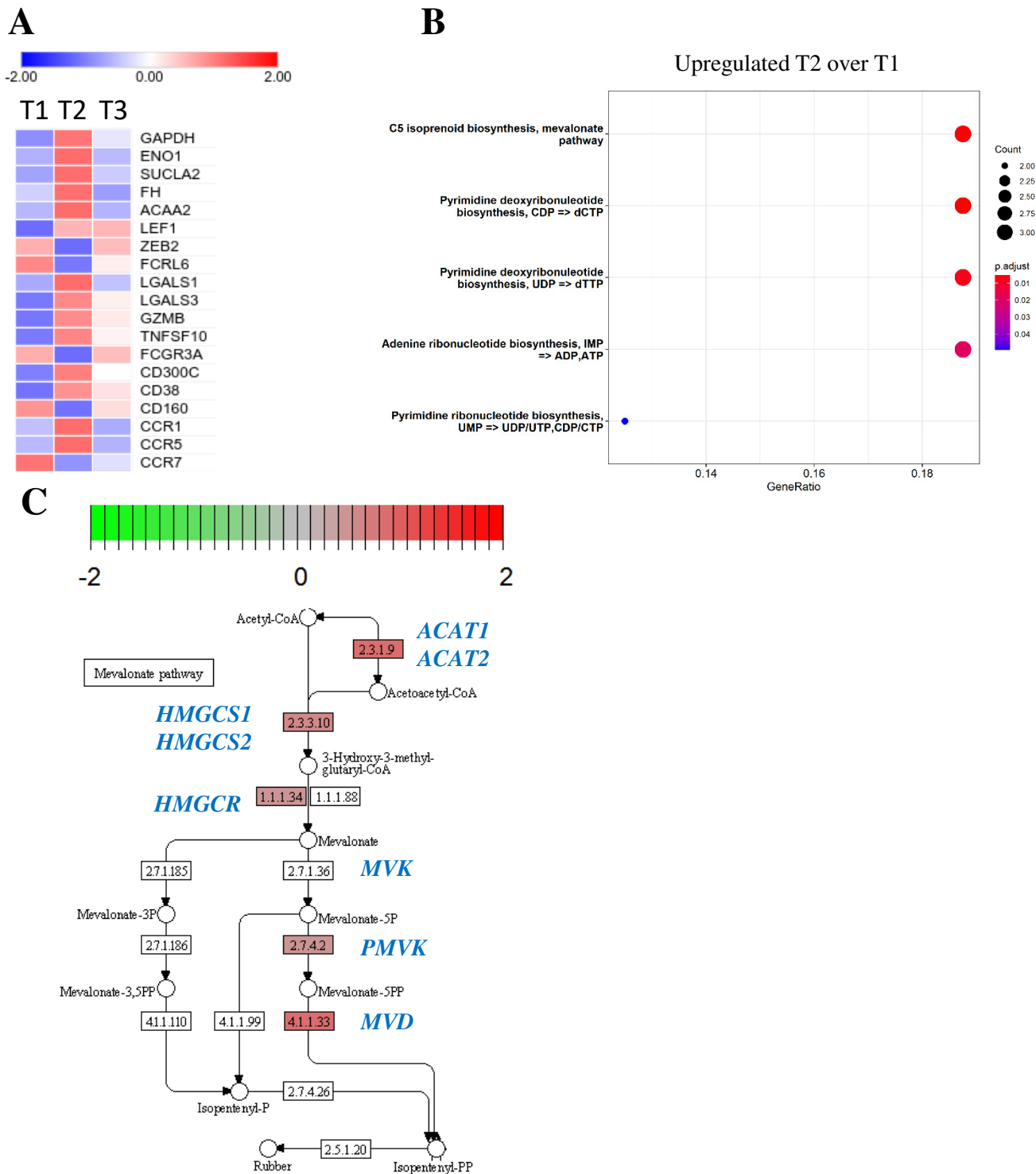
Upregulated T2 over T1



Upregulated T2 over T3



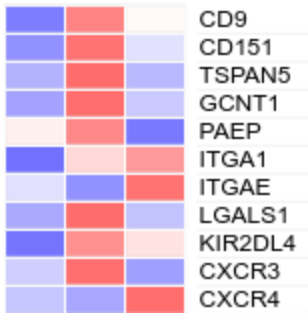
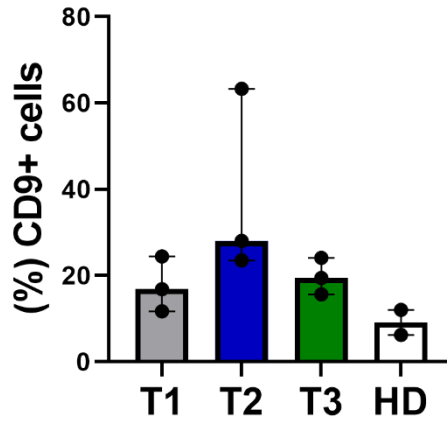
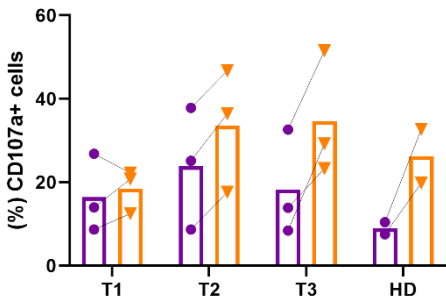
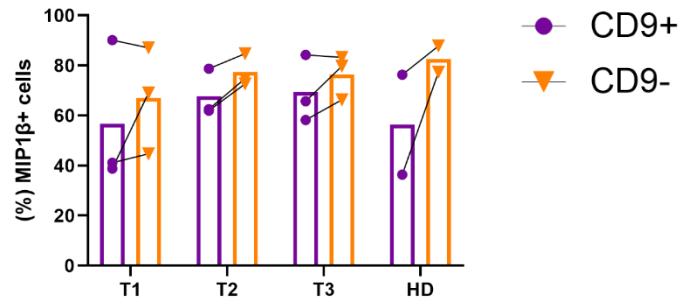
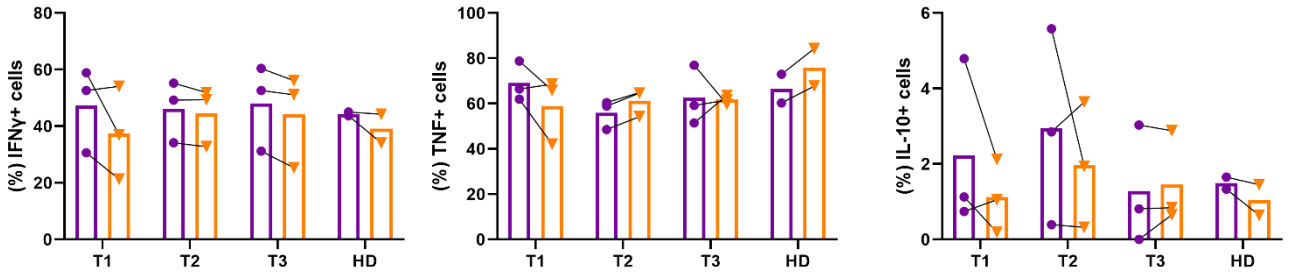
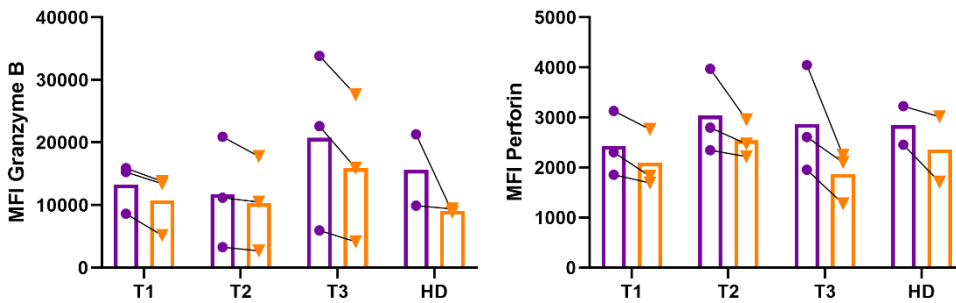
**Figure 25. Cell cycle is the main upregulated biological process at T2.** (A) Enrichment dot plot graphs showing the 10 most significant upregulated biological processes at T2 compared to T1 and T3. Reactome database was used for this analysis. (B) Enrichment dot plot graphs showing the 10 most significant upregulated biological processes at T2 compared to T1 and T3. Gene ontology database was used for this analysis. Biological processes are ranked based on the gene ratio. The size of the dot represents the number of genes upregulated within each category and the color of the dot represents the significance of the enrichment.



**Figure 26. Metabolic pathways are upregulated at T2.** (A) Heatmap showing the mean relative expression of genes related to metabolism (*GAPDH*, *ENO1*, *SUCLA2*, *FH*, *ACAA2*), to NK cell development and maturation (*LEF1*, *ZEB2*, *FCRL6*), cytotoxicity (*LGALS1*, *LGALS3*, *GZMB*, *TNFSF10*, *FCGR3A*) and genes encoding activating receptors (*CD300C*, *CD38*, *CD160*) and chemokine receptors (*CCR1*, *CCR5*, *CCR7*) at the three time points (T1, T2 and T3) (B) Enrichment dot plot graphs showing upregulated biological process at T2 over T1. KEGG modules database was used for this analysis. Modules are ranked based on the gene ratio. The size of the dot represent the number of genes upregulated within each category and the color of the dot represent the significance of the enrichment. (C) A portion of the KEGG pathway map of the terpenoid backbone biosynthesis (hsa00900), showing the mevalonate pathway at T2 over T1. The color inside the boxes refers to the Log<sub>2</sub>FC. The numbers inside the boxes refers to KEGG identification numbers, which represents the gene or gene family found at that position in the pathway.

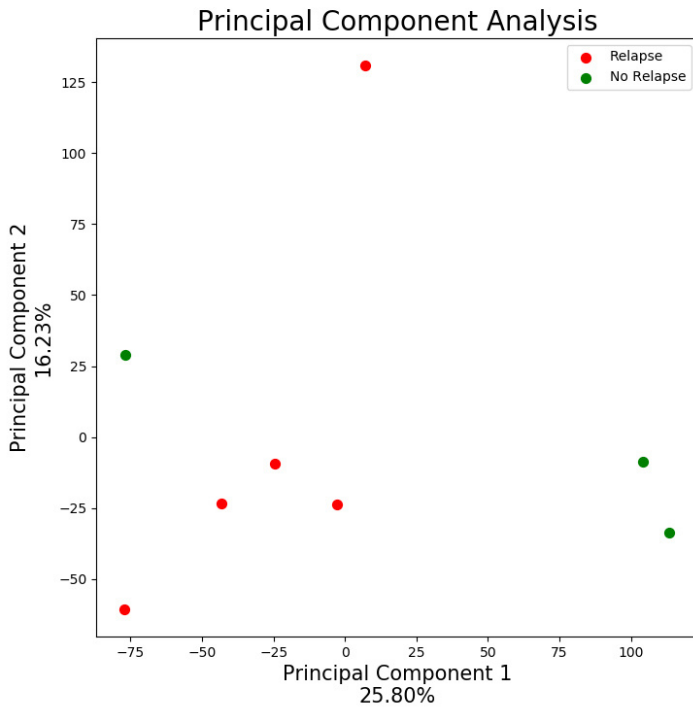
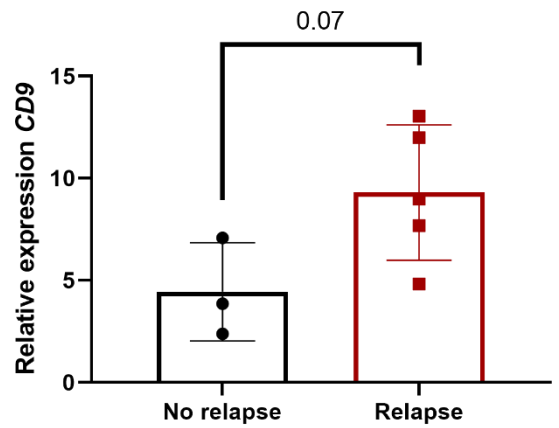
**A**

T1 T2 T3

**B****C****D****E****F**



**Figure 27. NK cells acquire a dNK-like phenotype immediately after autoHSCT. (A)** Heatmap showing the mean relative expression of genes related to dNK cell phenotype at the three time points (T1, T2 and T3). **(B)** Bar graph showing the frequency of CD9+ NK cells at T1, T2, T3 and on healthy donors (HD). **(C)** Bar graph showing the frequency of CD107a+ cells within CD9+ or CD9- NK cells at T1, T2, T3 and on HD. **(D)** Bar graph showing the frequency of cells positive for MIP1 $\beta$  within CD9+ or CD9- NK cells at T1, T2, T3 and on HD. **(E)** Bar graph showing the frequency of cells positive for IFN $\gamma$ , TNF and IL-10 cytokines within CD9+ or CD9- NK cells at T1, T2, T3 and on HD. **(F)** Bar graph showing the MFI of granzyme B and perforin within CD9+ or CD9- NK cells at T1, T2, T3 and on HD. Each dot represents a patient. Data are compared pairwise. In (B) median and interquartile range are represent. In (C-F) the median is represented. Percentage of NK cells positive for CD107a, MIP1 $\beta$ , IFN $\gamma$ , TNF and IL-10 was calculated after subtracting the non-stimulus condition to the PMA+Ionomycin stimulation condition. Granzyme B and perforin MFI are calculated in the non-stimulus condition. Data from B-F were not statistically significant.

**A****B**

**Figure 28. Patient's outcome is not associated with changes in gene expression profile. (A)** Representation of the principal component analysis results obtained when comparing gene expression profile of patients that had relapse vs no relapse **(B)** Graph bar showing the normalized relative expression of *CD9* at T2 in patients that showed no progression (no relapse) of the disease and patients that showed progression (relapse) of the disease. Each dot represents a patient. Mean with SD is represented.

**Table 1.** Inhibitory and activating KIRs and their HLA class I ligands.

<b>Inhibitory KIRs</b>	<b>Ligands</b>
KIR2DL1	HLA-C C2 <sup>‡</sup>
KIR2DL2	HLA-C C1 <sup>‡</sup> HLA-B*46:01 HLA-B*73:01
KIR2DL3	HLA-C C1 <sup>‡</sup> HLA-B*46:01 HLA-B*73:01
KIR2DL4	HLA-G
KIR2DL5	Unknown
KIR3DL1	HLA-B Bw4 HLA-A*23 HLA-A*24 HLA-A*32
KIR3DL2	HLA-A*03 HLA-A*11 HLA-F
KIR3DL3	Unknown
<b>Activating KIRs</b>	<b>Ligands</b>
KIR2DS1	HLA-C C2 <sup>‡</sup>
KIR2DS2	HLA-C C1 <sup>‡</sup> HLA-A*11:01
KIR2DS3	Unknown
KIR2DS4	HLA-C*02:02 HLA-C*04:01 HLA-C*05:01 HLA-C*01:02 HLA-C*14:02 HLA-C*16:01 HLA-A*11:01 HLA-F
KIR2DS5	HLA-C C2 <sup>‡</sup>
KIR3DS1	HLA-F HLA-B*51

<sup>‡</sup> HLA-C C1 alleles: HLA-C\*01/\*03/\*07/\*08/\*12/\*14/\*16. and HLA-C C2 alleles: HLA C\*02/\*04/\*05/\*06/\*15/\*17\*/18

**Table 2.** Factors affecting autoHSCT outcome.

<b>Factors</b>	<b>Prognostic indicator for</b>	<b>Pathology</b>	<b>Reference</b>
<b>Absolute lymphocyte count at day 15 (ALC-15)</b>	OS, PFS	Breast cancer, MM, NHL, HL, AML.	113-116
<b>Autograft absolute lymphocyte count (A-ALC)</b>	OS, PFS	NHL	120
<b>NK cell count at day 15 (NK-15)</b>	OS, PFS	NHL	121
<b>NK cell count at 1 month</b>	PFS	MM	122
<b>IL-15 levels at day 15</b>	OS, PFS	NHL	123
<b>HLA-Cw8 genotype</b>	OS	Lymphoma	133
<b>KIR-HLA receptor-ligand mismatch</b>	Disease progression	Lymphoma, solid tumour, neuroblastoma	134,135
<b>KIR and HLA genotypes predictive of low-affinity interactions</b>	Relapse	AML	137
<b>KIR3DS1 genotype</b>	PFS	MM in complete response or partial remission at autoHSCT	139
<b>Adaptive NK cell count at day 28</b>	Relapse	MM, NHL, HL	145

AML: acute myeloid leukemia; HL: Hodgkin lymphoma; IL-15: interleukin 15; MM: multiple myeloma; NHL: non-Hodgkin lymphoma; OS: overall survival; PFS: progression free survival.

**Table 3. Clinical data of untreated HIV-1 infected subjects, under cART HIV-1 infected patients and multiple myeloma patients.**

	Untreated HIV-1 subjects		HIV-1 patients on cART		Multiple myeloma patients	
	Median	Range (min-max)	Median	Range (min-max)	Median	Range (min-max)
<b>Sex</b>	Female: n=0 Male: n=9	-	Female: n=1 Male: n=7	-	Female: n=6 Male: n=3	-
<b>Age (years)</b>	39	(32-59)	49	(34-56)	63	(53-74)
<b>cART (months)</b>	-	-	13	(10-27)	-	-

**Table 4. Flow cytometry panels****Phenotype panel 1**

Laser	Filter	Fluorochrome	Marker	Manufacturer	Clone
405	450/50	BV421	CD56	BD Bioscience	NCAM 16.2
	525/50	BV510	CD3/CD14/CD19	BD Bioscience	UCHT1/ M $\phi$ P9/ SJ25C1
	525/50	Aqua Dead	Viability	Invitrogen	
488	525/50	FITC	CD16	BioLegend	B73.1
	585/40	PE	CD123	BD Bioscience	9F5
	655-730				
	750LP	PEVio770	NKp80	Miltenyi Biotec	4A4.D10
635	655-730	eFluor660	Eomes	Invitrogen	WD1928
	750LP				

**Phenotype panel 2**

Laser	Filter	Fluorochrome	Marker	Manufacturer	Clone
405	450/50	BV421	CD56	BD Bioscience	NCAM 16.2
	525/50	BV510	CD3/CD14/CD19/CD1 23	BD Bioscience	UCHT1/ M $\phi$ P9/ SJ25C1/9F5
	525/50	Aqua Dead	Viability	Invitrogen	
488	525/50	FITC	CD16	BioLegend	B73.1
	585/40	PE	CD7	BD Bioscience	M-T701
	655-730				
	750LP	PEVio770	NKp80	Miltenyi Biotec	4A4.D10
635	655-730	eFluor660	Eomes	Invitrogen	WD1928
	750LP				

**Table 4. Flow cytometry panels (continuation)****Phenotype panel 3**

Laser	Filter	Fluorochrome	Marker	Manufacturer	Clone
405	450/50	BV421	CD56	BD Bioscience	NCAM 16.2
	525/50	BV510	CD3/CD14/CD19/CD123	BD Bioscience	UCHT1/ MφP9/ SJ25C1/9F5
	525/50	Aqua Dead	Viability	Invitrogen	
488	525/50	FITC	CD16	BioLegend	B73.1
	585/40	PE	CD300a	Beckman Coulter	/E59.126
	655-730				
	750LP	PEVio770	NKp80	Miltenyi Biotec	4A4.D10
635	655-730	eFluor660	Eomes	Invitrogen	WD1928
	750LP				

**Phenotype panel 4**

Laser	Filter	Fluorochrome	Marker	Manufacturer	Clone
405	450/50	BV421	CD56	BD Bioscience	NCAM 16.2
	525/50	BV510	CD3/CD14/CD19/CD123	BD Bioscience	UCHT1/ MφP9/ SJ25C1/9F5
	525/50	Aqua Dead	Viability	Invitrogen	
488	525/50	FITC	CD16	BioLegend	B73.1
	585/40	PE	2B4	Beckman Coulter	C1.7
	655-730				
	750LP	PEVio770	NKp80	Miltenyi Biotec	4A4.D10
635	655-730	eFluor660	Eomes	Invitrogen	WD1928
	750LP				

**Table 4. Flow cytometry panels (continuation)****Functional panel**

Laser	Filter	Fluorochrome	Marker	Manufacturer	Clone
<b>405</b>	450/50	BV421	CD56	BD Bioscience	NCAM 16.2
	525/50	BV510	CD3/CD14/CD19	BD Bioscience	UCHT1/ MφP9/ SJ25C1
	525/50	Aqua Dead	Viability	Invitrogen	
<b>488</b>	525/50	FITC	CD16	BioLegend	B73.1
	585/40	PE	CD107a	Miltenyi Biotec	REA792
	655-730	PerCP-Cy5.5	IFN $\gamma$	BD Biosciences	B27
	750LP	PEVio770	NKp80	BD Bioscience	4A4.D10
<b>635</b>	655-730	APC	TNF	BioLegend	MAb11
	750LP				



**Table 5. Patients' characteristics**

		<b>n (%)</b>
<b>Gender</b>	Male	30 (55.6%)
	Female	24 (44.4%)
<b>Myeloma classification: ISS</b>	ISS 1	23 (42.6%)
	ISS 2	16 (29.6%)
	ISS 3	14 (25.9%)
<b>Myeloma classification: Durie-Salmon Staging System</b>	I-A	6 (11.1%)
	II-A	19 (35.2%)
	II-B	2 (3.7%)
	III-A	22 (40.7%)
	III-B	5 (9.3%)
<b>Conditioning regimens</b>	Melphalan 140	2 (3.7%)
	Melphalan 200	47 (87.1%)
	BUMEL	5 (9.3%)
<b>CMV serostatus</b>	CMV+	48 (88.9%)
	CMV-	5 (9.3%)
<b>Pre-autoHSCT response</b>	CR	13 (24.1%)
	VGPR	22 (40.7%)
	PR	17 (31.5%)
	SD	2 (3.7%)
<b>Post-autoHSCT response (+100 days)</b>	CR	25 (46.3%)
	VGPR	19 (35.2%)
	PR	9 (16.7%)
	SR	1 (1.9%)
<b>Maintenance regimen or consolidation regimen</b>	Yes	29 (53.7%)
	No	25 (46.3%)
<b>Type of maintenance or consolidation treatment</b>	IFN	1 (1.9%)
	KRD/R	3 (5.6%)
	R	15 (27.8%)
	R/V	2 (3.7%)
	RD	2 (3.7%)
	RD/alloHSCT	1 (1.9%)
	VCD	1 (1.9%)
	VRD/R	2 (3.7%)
	VRD/RD	1 (1.9%)
Other	1 (1.9%)	
<b>Disease progression</b>	Yes	29 (53.7%)
	No	25 (46.3%)
<b>Alive</b>	Yes	45 (83.3%)
	No	9 (16.7%)
		<b>median</b>
		<b>(interquartile range)</b>
<b>Age</b>		62 (33-73)
<b>Months to disease progression</b>		21 (2-46)
<b>Months to death</b>		29 (8-57)
<b>Months to next treatment line</b>		25.5 (3-50)

ISS indicates International Staging System; CMV, cytomegalovirus; BUMEL, busulfan-melphalan; CR, complete remission; VGPR, very good partial response; PR, partial response; SD,

stable disease; SR, stable response. IFN, interferon; KRd/R, Carfilzomib-Lenalidomide-Dexamethasone/Lenalidomide; R, Lenalidomide; R/V, Lenalidomide/Velcade; Rd, Lenalidomide-Dexamethasone; VCD, Velcade-cyclophosphamide-dexamethasone; VRd/R, Velcade-Lenalidomide-Dexamethasone/ Lenalidomide; VRd/Rd, Velcade-Lenalidomide-Dexamethasone/Lenalidomide-Dexamethasone.

**Table 6. Flow cytometry panels****Phenotype panel 1**

Laser	Filter	Fluorochrome	Marker	Manufacturer	Clone
405	450/50	BV421	CD56	BD Bioscience	NCAM 16.2
	525/50	BV510	CD3/CD14/CD19	BD Bioscience	UCHT1/ MφP9/ SJ25C1
	525/50	Aqua Dead	Viability	Invitrogen	
488	525/50	FITC	FcεRγ	Merck	
	585/40	PE	NKG2C	R&D systems	134591
	655-730				
	750LP	PEVio770	NKp80	Miltenyi Biotec	4A4.D10
635	655-730	APC	NKG2A	Beckman Coulter	Z199
	750LP	APCVio770	CD57	Miltenyi Biotec	REA769

**Phenotype panel 2**

Laser	Filter	Fluorochrome	Marker	Manufacturer	Clone
<b>405</b>	450/50	BV421	CD56	BD Bioscience	NCAM 16.2
	525/50	BV510	CD3/CD14/CD19	BD Bioscience	UCHT1/ MφP9/ SJ25C1
	525/50	Aqua Dead	Viability	Invitrogen	
<b>488</b>	525/50	FITC	Ki67	Invitrogen	20Raj1
	585/40	PE	Granzyme B	BD Bioscience	GB11
	655-730				
	750LP	PEVio770	NKp80	BD Bioscience	4A4.D10
<b>635</b>	655-730				
	750LP	APCVio770	CD69	Miltenyi Biotec	REA824

**Functional panel**

Laser	Filter	Fluorochrome	Marker	Manufacturer	Clone
<b>405</b>	450/50	BV421	CD56	BD Bioscience	NCAM 16.2
	525/50	BV510	CD3/CD14/CD19	BD Bioscience	UCHT1/ MφP9/ SJ25C1
	525/50	Aqua Dead	Viability	Invitrogen	
<b>488</b>	525/50				
	585/40	PE	CD107a	Miltenyi Biotec	REA792
	655-730	PerCP-Cy5.5	IFNγ	BD Biosciences	B27
	750LP	PEVio770	NKp80	BD Bioscience	4A4.D10
<b>635</b>	655-730	APC	TNF	BioLegend	MAb11
	750LP				

**Table 7. Patient's clinical characteristics**

		<b>n (%)</b>
<b>Gender</b>	Male	9 (56.3%)
	Female	7 (43.8%)
<b>Myeloma classification: ISS</b>	ISS1	3 (18.8%)
	ISS2	8 (50.0%)
	ISS3	5 (31.3%)
<b>Myeloma classification: Durie-Salmon Staging System</b>	I-A	2 (12.5%)
	II-A	4 (25.0%)
	III-A	8 (50.0%)
	III-B	1 (6.3%)
<b>Mobilization regimen</b>	G-CSF	16 (100%)
<b>Conditioning regimen</b>	Melphalan 200	14 (87.5%)
	Melphalan 140 + BUMEL	2 (12.5%)
<b>CMV serostatus</b>	Yes	15 (93.8%)
	No	1 (6.3%)
<b>Maintenance or consolidation regimen</b>	Yes	11 (68.8%)
	No	5 (31.3%)
<b>Tandem autoHSCT</b>	Yes	8 (50.0%)
	No	8 (50.0%)
<b>Disease progression</b>	Yes	8 (50.0%)
	No	8 (50.0%)
		<b>Median (interquartile range)</b>
<b>Age</b>		59 (46-72)
<b>Infused CD34+ cells (x10<sup>6</sup> cells/kg)</b>		2.82 (2.20-5.59)

ISS indicates International Staging System; BUMEL, busulfan-melphalan; CMV, cytomegalovirus; G-CSF: granulocyte colony-stimulating factor.

**Table 8. qPCR primer characteristics**

<b>Gene symbol</b>	<b>Gene name</b>	<b>Sequence</b>	<b>PCR efficiency</b>	<b>Amplicon Length</b>
<i>B2M</i>	Beta-2-Microglobulin	F 5' CACCCCACTGAAAAAGATG 3' R 5' CCTCCATGATGCTGCTTACA 3'	96.42 %	106 bp
<i>PPIA</i>	Peptidylprolyl Isomerase A	F 5' CACCGTGTTCCTTCGACATTG 3' R 5' CTGTGAAAGCAGGAACCCTTA 3'	105.70 %	153 bp
<i>18S</i>	18S	F 5' GTGGAGCGATTTGTCTGGTT 3' R 5' AACGCCACTTGTCCTCTAA 3'	--	115 bp
<i>HPRT1</i>	Hypoxanthine phosphoribosyltransferase 1	F 5' TGCTCGAGATGTGATGAAGG 3' R 5' TCCCCTGTTGACTGGTCATT 3'	226.5 %	192 bp
<i>CD9</i>	CD9	F 5' GGGGATATTCCCACAAGGAT 3' R 5' GCAGTTCAACGCATAGTGGA 3'	104.38 %	131 bp
<i>VIM</i>	Vimentin	F 5' GAAATTGCAGGAGGAGATGC 3' R 5' GACGCATTGTCAACATCCTG 3'	105.24 %	81 bp
<i>CD160</i>	CD160	F 5' CCCCCAGTCTGAGAACAAGA 3' R 5' CGGGAGTTCACGGATGTAGT 3'	91.42 %	106 bp
<i>FCRL6</i>	Fc Receptor Like 6	F 5' TATTGCTGCTGCACTTCTGG 3' R 5' CAGACCTGGCTTCACTCCTC 3'	97.96%	194 bp

**Table 9. Flow cytometry panel**

Laser	Filter	Fluorochrome	Marker	Manufacturer	Clone
405	450/50	BV421	IL-8	BD Bioscience	G265-8
	525/50	BV510	CD14/CD19/CD123	BD Bioscience	MφP9/ SJ25C1/9F5
	525/50	Aqua Dead	Viability	Invitrogen	
	610/20	BV605	IFN $\gamma$	BD Bioscience	B27
	670/30	BV650	IL-10	BD Bioscience	JES3-9D7
	710/50	BV711	Perforin	BioLegend	dG9
	780/60	BV786	CD56	BD Bioscience	NCAM 16.2
488	530/30	FITC	MIP1 $\beta$	BD Bioscience	D21-1351
	575/25	PE	VEGF	R&D system	23410
	610/20	PE-CF594	CD9	BioLegend	HI9a
	710/50	PerCP-Cy5.5	CD3	BD Bioscience	SK7
	780/60	PEVio770	NKp80	Miltenyi Biotec	4A4.D10
	637	670/30	APC	TNF	BioLegend
637	730/45	R718	Granzyme B	BD Bioscience	GB11
	780/60	APC-Cy7	CD107a	Miltenyi Biotec	REA792

# **ANNEX**

Data from RNA-seq analysis

## Summary of Content

Differentially expressed genes T2 over T1 .....	1 -
Differentially expressed genes T3 over T1 .....	9 -
Differentially expressed genes T2 over T3 .....	10 -
Upregulated genes T2 over T1. Gene Ontology database: Biological Processes.....	19 -
Downregulated genes T2 over T1. Gene Ontology database: Biological Processes..	23 -
Upregulated genes T2 over T1. Reactome database.....	23 -
Downregulated genes T2 over T1. Reactome database.....	26 -
GSEA performed with DEG T2 over T1. KEGG database.....	26 -
Upregulated genes T2 over T1. KEGG modules database.....	26 -
Downregulated genes T2 over T1. KEGG modules database.....	26 -
Upregulated genes T3 over T1. Gene Ontology database: Biological Processes.....	27 -
Downregulated genes T3 over T1. Gene Ontology database: Biological Processes..	27 -
Upregulated genes T3 over T1. Reactome database.....	28 -
Downregulated genes T3 over T1. Reactome database.....	28 -
GSEA performed with DEG T3 over T1. KEGG database.....	28 -
Upregulated genes T3 over T1. KEGG modules database.....	29 -
Downregulated genes T3 over T1. KEGG modules database.....	29 -
Upregulated genes T2 over T3. Gene Ontology database: Biological Processes.....	29 -
Downregulated genes T2 over T3. Gene Ontology database: Biological Processes..	32 -
Upregulated genes T2 over T3. Reactome database.....	32 -
Downregulated genes T2 over T3. Reactome database.....	36 -
GSEA performed with DEG T2 over T3. KEGG database.....	36 -
Upregulated genes T2 over T3. KEGG modules database.....	37 -
Downregulated genes T2 over T3. KEGG modules database.....	37 -



## Differentially expressed genes T2 over T1

Gene name	Log2(Time_1)	Log2(Time_2)	Log2(FC)	pValue	p.adjust.
HBB	1,1800	4,2920	3,1120	0,0183	0,2922
CD9	0,6542	3,1032	2,4490	0,0001	0,0450
DPP4	0,8437	2,6854	1,8417	0,0003	0,0576
NUSAP1	1,0736	2,8363	1,7626	0,0122	0,2491
KIR2DL4	3,0590	4,8173	1,7583	0,0022	0,1313
TPX2	0,9370	2,6313	1,6943	0,0006	0,0788
TOP2A	0,9903	2,5959	1,6056	0,0201	0,2994
LGALS1	5,2311	6,8276	1,5965	0,0013	0,1013
YWHAE	3,4929	5,0484	1,5555	0,0019	0,1201
SLC4A10	1,1957	2,7254	1,5296	0,0002	0,0459
BIRC5	0,8691	2,3777	1,5085	0,0066	0,2022
LGALS3	1,0446	2,4378	1,3932	0,0024	0,1372
VIM	3,1186	4,4051	1,2865	0,0001	0,0444
APOBEC3B	0,5244	1,8040	1,2797	0,0238	0,3189
PTTG1	1,4205	2,6363	1,2159	0,0022	0,1312
PRDX3	3,6303	4,8436	1,2133	0,0045	0,1718
ANXA2	5,6198	6,8268	1,2070	0,0006	0,0788
ZWINT	0,8524	2,0562	1,2038	0,0225	0,3119
MCM6	2,0509	3,2443	1,1934	0,0239	0,3190
IFI30	1,3165	2,5020	1,1855	0,0018	0,1170
CST3	0,5692	1,7269	1,1577	0,0000	0,0260
CCNB2	0,4221	1,5674	1,1453	0,0148	0,2723
CENPF	1,1108	2,2556	1,1448	0,0166	0,2836
MKI67	0,6824	1,8171	1,1347	0,0212	0,3073
TK1	0,4369	1,5613	1,1244	0,0067	0,2024
FAR2	0,5454	1,6576	1,1122	0,0000	0,0233
CCNB1	0,7046	1,8005	1,0959	0,0316	0,3504
CCR5	0,2694	1,3624	1,0930	0,0001	0,0375
CDKN2A	0,4388	1,5226	1,0838	0,0000	0,0189
IL1RL1	0,2453	1,3151	1,0698	0,0002	0,0490
FABP5	0,5929	1,6373	1,0444	0,0000	0,0040
TNFRSF18	0,4906	1,5336	1,0429	0,0198	0,2980
RRM1	2,1485	3,1551	1,0066	0,0166	0,2836
MLC1	1,5328	2,5369	1,0040	0,0185	0,2938
RBBP8	1,0492	2,0459	0,9968	0,0004	0,0671
MCM4	1,3321	2,3258	0,9937	0,0303	0,3444
ADA	2,3045	3,2979	0,9934	0,0018	0,1185
APOBEC3H	1,4196	2,4019	0,9823	0,0007	0,0788
HELLS	0,9199	1,8832	0,9632	0,0062	0,1963
CDKN3	0,3679	1,3276	0,9597	0,0279	0,3355
GZMB	8,6728	9,6309	0,9581	0,0049	0,1797
HMGB3	0,5518	1,4948	0,9430	0,0013	0,1016
MVD	0,7942	1,7198	0,9256	0,0463	0,3937
KNL1	0,5026	1,4248	0,9221	0,0279	0,3355
KIF11	0,3205	1,2422	0,9217	0,0174	0,2866
IFITM3	3,8219	4,7413	0,9194	0,0264	0,3305
NMI	3,3852	4,3010	0,9158	0,0040	0,1648
SMC4	2,3352	3,2490	0,9138	0,0039	0,1610
DLGAP5	0,2884	1,1964	0,9079	0,0232	0,3165
CDCP1	0,3680	1,2736	0,9056	0,0071	0,2062

CCL23	0,1615	1,0638	0,9023	0,0055	0,1870
CDC20	0,1080	0,9974	0,8894	0,0071	0,2062
LMNB1	1,7969	2,6784	0,8815	0,0028	0,1419
NME1	2,0200	2,8909	0,8709	0,0068	0,2024
STAP1	2,1326	3,0020	0,8694	0,0031	0,1464
ERI1	1,3534	2,2191	0,8658	0,0051	0,1810
COTL1	2,2999	3,1623	0,8624	0,0439	0,3844
CCDC28B	2,1086	2,9696	0,8610	0,0020	0,1233
ANXA5	3,1731	4,0301	0,8570	0,0076	0,2105
ACAT1	1,9182	2,7696	0,8514	0,0002	0,0490
AC006064.4	1,1517	1,9990	0,8473	0,0237	0,3189
HMBS	0,7884	1,6315	0,8431	0,0000	0,0071
CD300C	1,0215	1,8640	0,8424	0,0077	0,2117
FKBP1A	4,5118	5,3447	0,8329	0,0000	0,0178
MCUB	2,1660	2,9966	0,8306	0,0158	0,2773
EZH2	0,8773	1,7067	0,8293	0,0045	0,1713
HMMR	0,3659	1,1896	0,8237	0,0317	0,3504
S100A9	0,4841	1,2965	0,8124	0,0398	0,3743
RAD51	0,3625	1,1559	0,7933	0,0328	0,3544
NIPSNAP3A	2,1464	2,9396	0,7932	0,0362	0,3660
MAL	0,1329	0,9249	0,7920	0,0032	0,1484
LAP3	3,1316	3,9216	0,7900	0,0008	0,0841
CBR1	1,9310	2,7179	0,7869	0,0008	0,0829
UTP11	2,3614	3,1456	0,7842	0,0099	0,2291
PSMA4	4,9207	5,7041	0,7834	0,0152	0,2751
ASPM	0,5535	1,3338	0,7802	0,0225	0,3119
UBASH3B	1,1725	1,9455	0,7730	0,0004	0,0662
ANTXR2	0,8827	1,6556	0,7729	0,0011	0,0961
KIF15	0,4219	1,1920	0,7701	0,0251	0,3243
PDLIM1	1,5082	2,2759	0,7677	0,0004	0,0630
PDE6G	2,0211	2,7886	0,7675	0,0037	0,1564
CASP3	2,5667	3,3295	0,7627	0,0215	0,3093
FANCI	1,7536	2,5112	0,7576	0,0142	0,2653
PLSCR1	3,2752	4,0266	0,7514	0,0084	0,2188
ERAL1	1,8002	2,5512	0,7510	0,0003	0,0578
CENPM	0,4594	1,2093	0,7499	0,0446	0,3865
CENPE	0,6781	1,4244	0,7463	0,0138	0,2642
CD38	4,0943	4,8369	0,7426	0,0093	0,2253
CDCA7	0,3424	1,0843	0,7419	0,0030	0,1458
KIF14	0,1554	0,8941	0,7387	0,0137	0,2639
PRKCQ-AS1	1,1436	1,8784	0,7347	0,0005	0,0722
GLUL	3,5051	4,2385	0,7334	0,0003	0,0613
PCTP	1,6158	2,3478	0,7321	0,0006	0,0770
TSPO	2,3853	3,1137	0,7284	0,0066	0,2022
PSMA5	3,8532	4,5814	0,7282	0,0118	0,2458
LPCAT3	1,6083	2,3353	0,7270	0,0034	0,1501
UCHL3	1,7427	2,4673	0,7246	0,0141	0,2653
GALE	0,8148	1,5381	0,7233	0,0008	0,0838
CSRPI	1,5198	2,2398	0,7199	0,0238	0,3189
RACGAP1	1,3557	2,0727	0,7170	0,0093	0,2253
CD151	0,6880	1,4040	0,7159	0,0094	0,2260
IDH1	1,0947	1,8106	0,7159	0,0025	0,1379

MPST	0,8250	1,5394	0,7144	0,0156	0,2760
TIAM1	1,2180	1,9244	0,7064	0,0204	0,3019
MRPL15	1,8976	2,6030	0,7054	0,0018	0,1170
SERPINE2	0,6563	1,3615	0,7052	0,0064	0,2014
PARVG	2,7485	3,4515	0,7030	0,0005	0,0708
TNFSF10	2,8888	3,5875	0,6987	0,0174	0,2866
CD320	2,9759	3,6742	0,6983	0,0072	0,2072
ASL	1,7268	2,4250	0,6982	0,0005	0,0709
NCBP1	1,5715	2,2659	0,6944	0,0084	0,2183
CORO1C	1,8471	2,5396	0,6925	0,0138	0,2642
NDC80	0,7335	1,4252	0,6917	0,0204	0,3019
KIF18A	0,4006	1,0903	0,6897	0,0249	0,3237
CCR1	1,5068	2,1962	0,6894	0,0475	0,3961
HMGB2	3,7847	4,4726	0,6879	0,0100	0,2301
GSTP1	4,9368	5,6246	0,6879	0,0006	0,0770
S100A10	3,7380	4,4245	0,6865	0,0001	0,0444
SLC25A5	5,4477	6,1311	0,6834	0,0391	0,3740
LDHB	4,9344	5,6169	0,6825	0,0065	0,2017
MRPS22	1,6386	2,3185	0,6799	0,0012	0,0976
GAPDH	5,9985	6,6774	0,6789	0,0002	0,0450
CARHSP1	1,7948	2,4732	0,6784	0,0001	0,0340
MTHFD1	1,6935	2,3715	0,6779	0,0090	0,2245
TFDP1	1,1203	1,7972	0,6770	0,0123	0,2502
ADCY7	1,2853	1,9600	0,6747	0,0437	0,3839
CSTF2	1,2444	1,9188	0,6744	0,0252	0,3244
TROAP	0,2520	0,9194	0,6675	0,0034	0,1501
APOBEC3D	0,6526	1,3160	0,6634	0,0458	0,3915
EIF3M	3,7099	4,3716	0,6617	0,0029	0,1441
IKBKE	1,1487	1,8062	0,6575	0,0029	0,1438
CALM3	3,0192	3,6762	0,6570	0,0290	0,3409
LEF1	1,3703	2,0272	0,6569	0,0127	0,2550
MRPL16	2,5408	3,1969	0,6561	0,0081	0,2145
BLMH	1,6944	2,3492	0,6548	0,0015	0,1110
HBD	0,0163	0,6705	0,6541	0,0071	0,2062
NME2	2,5646	3,2170	0,6524	0,0093	0,2253
MT1X	1,0201	1,6721	0,6520	0,0003	0,0588
AIMP2	1,4596	2,1087	0,6491	0,0056	0,1876
PAICS	1,3797	2,0284	0,6487	0,0323	0,3528
MCM7	1,1939	1,8419	0,6479	0,0359	0,3653
PRR11	0,5299	1,1768	0,6470	0,0061	0,1961
ATIC	1,9464	2,5932	0,6468	0,0011	0,0962
PSMB8	4,9383	5,5845	0,6463	0,0013	0,1000
CDK6	1,8219	2,4664	0,6445	0,0104	0,2326
CCT6A	3,7759	4,4194	0,6434	0,0064	0,2014
MAPKAPK3	1,4140	2,0571	0,6431	0,0274	0,3339
TPM4	4,1471	4,7886	0,6415	0,0237	0,3189
SLC1A5	0,3781	1,0186	0,6406	0,0012	0,0995
CAPZA1	6,3186	6,9591	0,6405	0,0122	0,2491
WDR18	0,4966	1,1312	0,6347	0,0421	0,3799
PSMG1	0,8829	1,5164	0,6335	0,0034	0,1518
PRDX4	2,0631	2,6957	0,6326	0,0301	0,3444
HMGCS1	2,1484	2,7791	0,6308	0,0498	0,4012

AGK	3,9691	4,5976	0,6284	0,0107	0,2353
ADSL	1,9752	2,6019	0,6267	0,0106	0,2348
SMCO4	0,3952	1,0215	0,6263	0,0018	0,1170
SQLE	1,5966	2,2166	0,6201	0,0409	0,3776
RAE1	2,3544	2,9724	0,6180	0,0052	0,1810
STX3	0,3603	0,9768	0,6165	0,0019	0,1201
ARHGEF6	3,2317	3,8480	0,6163	0,0014	0,1067
MEIS1	0,3812	0,9907	0,6094	0,0001	0,0444
PTTG1IP	2,1756	2,7840	0,6084	0,0025	0,1379
NANS	1,8268	2,4350	0,6082	0,0245	0,3213
BUB1	0,2152	0,8234	0,6082	0,0047	0,1740
E2F2	0,1651	0,7728	0,6077	0,0193	0,2955
GOLIM4	2,0255	2,6331	0,6075	0,0145	0,2685
HSPD1	3,1738	3,7812	0,6074	0,0233	0,3165
MPDU1	0,8439	1,4503	0,6064	0,0084	0,2188
RPS27L	3,3596	3,9654	0,6058	0,0186	0,2938
UBE2C	0,1775	0,7821	0,6046	0,0178	0,2884
DCLRE1A	1,0574	1,6609	0,6035	0,0496	0,4008
RUNX2	1,0629	1,6645	0,6017	0,0070	0,2051
RIOK3	3,2192	3,8199	0,6007	0,0001	0,0399
SCD	0,5274	1,1279	0,6005	0,0172	0,2865
IAHI	2,3904	2,9906	0,6003	0,0010	0,0917
ASF1B	0,3044	0,9045	0,6001	0,0279	0,3355
MTAP	1,0203	1,6165	0,5962	0,0005	0,0697
DNPEP	1,5766	2,1700	0,5934	0,0001	0,0444
CASP7	2,3420	2,9354	0,5934	0,0070	0,2051
SRP54	2,5949	3,1864	0,5915	0,0139	0,2642
ILK	3,3578	3,9492	0,5913	0,0073	0,2074
NCAPG	0,2617	0,8495	0,5877	0,0110	0,2385
NUP37	1,6247	2,2110	0,5862	0,0091	0,2247
CMAS	1,6059	2,1917	0,5858	0,0007	0,0788
TMEM171	0,4593	1,0442	0,5848	0,0162	0,2798
RFXANK	1,5905	2,1752	0,5847	0,0000	0,0040
WWP2	1,4495	2,0341	0,5846	0,0270	0,3329
SNRPE	2,8750	3,4589	0,5839	0,0279	0,3355
DERA	2,7827	3,3660	0,5833	0,0180	0,2904
AURKAIP1	1,9039	2,4870	0,5831	0,0019	0,1201
PIMREG	0,2147	0,7962	0,5815	0,0090	0,2245
UBE2T	0,3372	0,9183	0,5811	0,0322	0,3524
MUL1	1,3432	1,9243	0,5811	0,0301	0,3444
MPHOSPH8	3,7759	3,1956	-0,5803	0,0109	0,2379
ZNF431	1,5214	0,9409	-0,5805	0,0015	0,1110
MED21	2,1831	1,6013	-0,5818	0,0363	0,3668
LRRC37A2	1,4610	0,8784	-0,5826	0,0025	0,1379
ARID4B	4,0784	3,4936	-0,5848	0,0040	0,1648
CEP120	1,6159	1,0309	-0,5850	0,0047	0,1761
BRWD1	2,9258	2,3399	-0,5858	0,0061	0,1963
GALNT11	2,0018	1,4151	-0,5867	0,0386	0,3734
NFATC2	3,7061	3,1185	-0,5876	0,0071	0,2062
FUT11	2,8621	2,2735	-0,5886	0,0030	0,1464
TAOK1	2,8544	2,2645	-0,5899	0,0067	0,2024
JADE1	2,5615	1,9710	-0,5904	0,0041	0,1671

ZNF281	2,2154	1,6247	-0,5907	0,0038	0,1589
ZNF506	1,4706	0,8754	-0,5953	0,0015	0,1108
WNK1	2,9676	2,3711	-0,5965	0,0026	0,1379
OSTM1	3,0908	2,4933	-0,5975	0,0219	0,3109
PTPN4	4,7610	4,1626	-0,5984	0,0004	0,0662
MARF1	2,1126	1,5114	-0,6013	0,0018	0,1193
PNRC1	2,4972	1,8955	-0,6017	0,0013	0,1013
PCYOX1	2,6439	2,0416	-0,6024	0,0005	0,0708
KIF21A	1,6644	1,0605	-0,6039	0,0133	0,2612
SPOCK2	1,7787	1,1733	-0,6054	0,0400	0,3746
BMPR2	2,4301	1,8246	-0,6055	0,0010	0,0917
ATXN1	1,9583	1,3517	-0,6066	0,0056	0,1882
Z93241.1	1,3581	0,7507	-0,6074	0,0406	0,3774
PIP4P2	1,1919	0,5834	-0,6085	0,0006	0,0732
BTN3A1	3,2705	2,6617	-0,6088	0,0081	0,2143
AL358781.1	0,8022	0,1929	-0,6092	0,0059	0,1937
PAXIP1-AS2	1,5725	0,9621	-0,6104	0,0048	0,1767
EZR	4,8213	4,2109	-0,6105	0,0014	0,1044
HLA-E	8,5402	7,9287	-0,6114	0,0183	0,2923
IFIT5	1,7245	1,1128	-0,6117	0,0097	0,2276
SLC16A6	1,0072	0,3946	-0,6126	0,0033	0,1494
GDF11	0,8662	0,2533	-0,6129	0,0005	0,0708
RFFL	1,9351	1,3209	-0,6142	0,0002	0,0454
CRLF3	3,6690	3,0548	-0,6142	0,0019	0,1201
NPAT	3,5228	2,9064	-0,6164	0,0010	0,0917
GAB3	2,8478	2,2310	-0,6169	0,0009	0,0864
CLK4	2,0855	1,4657	-0,6198	0,0003	0,0565
CCDC186	3,1076	2,4845	-0,6230	0,0064	0,2014
TGFBR3	4,4231	3,8000	-0,6231	0,0004	0,0630
ELMSAN1	2,1672	1,5425	-0,6247	0,0114	0,2436
FAM172A	2,8175	2,1921	-0,6254	0,0000	0,0241
UBL3	2,3127	1,6870	-0,6256	0,0003	0,0557
NFX1	1,9607	1,3346	-0,6261	0,0051	0,1810
ZBTB4	1,1101	0,4837	-0,6264	0,0002	0,0529
KLF12	2,5803	1,9526	-0,6277	0,0007	0,0788
ATL3	4,1565	3,5286	-0,6279	0,0419	0,3791
JADE2	1,3152	0,6868	-0,6284	0,0033	0,1496
AHCTF1	1,7937	1,1638	-0,6299	0,0008	0,0829
ANKRD49	2,6026	1,9720	-0,6306	0,0011	0,0962
BBX	4,6145	3,9822	-0,6323	0,0004	0,0671
MBNL2	2,4586	1,8258	-0,6327	0,0091	0,2249
C18orf32	3,6320	2,9989	-0,6332	0,0099	0,2291
REL	2,7850	2,1501	-0,6350	0,0083	0,2170
GABARAPL1	2,1384	1,5023	-0,6362	0,0086	0,2195
GFOD1	2,2089	1,5690	-0,6399	0,0028	0,1419
NRIP1	1,8495	1,2088	-0,6407	0,0013	0,1000
CCDC191	0,8179	0,1760	-0,6419	0,0291	0,3409
TTC3	3,7750	3,1323	-0,6427	0,0188	0,2943
ILF3-AS1	2,3992	1,7511	-0,6481	0,0051	0,1807
KLHL9	2,3554	1,7072	-0,6482	0,0013	0,1004
KLHL8	1,9634	1,3138	-0,6496	0,0038	0,1584
RAD1	1,8920	1,2397	-0,6523	0,0041	0,1671

NFAT5	1,7174	1,0648	-0,6526	0,0002	0,0529
MBP	4,4217	3,7677	-0,6539	0,0036	0,1539
SMG1	3,3331	2,6785	-0,6547	0,0005	0,0708
ATP2B4	3,9288	3,2725	-0,6564	0,0017	0,1170
CHD2	3,9960	3,3389	-0,6570	0,0019	0,1201
SCRN1	1,6752	1,0171	-0,6580	0,0086	0,2195
HLA-DPB1	5,2305	4,5716	-0,6588	0,0154	0,2757
ZNF184	1,6016	0,9420	-0,6596	0,0122	0,2492
ZNF566	1,3964	0,7355	-0,6610	0,0019	0,1229
RSRP1	2,6510	1,9887	-0,6624	0,0103	0,2317
ZNF677	1,2942	0,6306	-0,6636	0,0007	0,0817
SORL1	5,1102	4,4450	-0,6652	0,0495	0,4001
AOAH	5,1731	4,5078	-0,6653	0,0115	0,2444
SBDS	3,4389	2,7728	-0,6661	0,0183	0,2922
PSTPIP2	2,5651	1,8989	-0,6662	0,0071	0,2066
RFX3	1,1226	0,4553	-0,6672	0,0046	0,1740
RORA	3,1019	2,4342	-0,6677	0,0030	0,1458
ZNF441	1,1603	0,4919	-0,6684	0,0070	0,2051
TGFBR2	1,7046	1,0350	-0,6696	0,0079	0,2137
ST6GAL1	2,5825	1,9105	-0,6720	0,0005	0,0708
RANBP6	2,1954	1,5233	-0,6721	0,0117	0,2456
MYO9A	1,8317	1,1573	-0,6744	0,0065	0,2014
SYNE2	5,3222	4,6466	-0,6755	0,0024	0,1372
AC012615.1	1,4530	0,7774	-0,6756	0,0253	0,3244
ENPP4	3,0856	2,4077	-0,6779	0,0284	0,3385
BMI1	1,9175	1,2367	-0,6808	0,0025	0,1379
MEX3C	2,1119	1,4304	-0,6815	0,0020	0,1233
RNF19A	2,5526	1,8709	-0,6817	0,0148	0,2719
PDCD4	4,9798	4,2981	-0,6818	0,0043	0,1693
TRBC1	5,9372	5,2553	-0,6819	0,0046	0,1740
TXNIP	7,5327	6,8494	-0,6834	0,0268	0,3325
L3MBTL4	1,0977	0,4140	-0,6837	0,0073	0,2074
FCGR3A	7,8015	7,1175	-0,6840	0,0008	0,0829
EIF4A2	5,2302	4,5454	-0,6848	0,0001	0,0314
ZNF292	3,8740	3,1857	-0,6883	0,0004	0,0682
ARID4A	2,9779	2,2867	-0,6911	0,0010	0,0917
ATM	3,8673	3,1758	-0,6915	0,0000	0,0102
KLHL28	2,9322	2,2404	-0,6918	0,0005	0,0699
LRIF1	2,4593	1,7650	-0,6943	0,0163	0,2810
TRAF6	2,6741	1,9782	-0,6959	0,0373	0,3698
MARCH6	4,0306	3,3345	-0,6961	0,0004	0,0667
PNRC2	4,5522	3,8522	-0,7001	0,0002	0,0459
USPL1	2,6951	1,9928	-0,7022	0,0037	0,1570
PHC3	2,9410	2,2315	-0,7096	0,0007	0,0788
DDX5	6,9279	6,2175	-0,7104	0,0000	0,0244
BRAF	1,4669	0,7564	-0,7104	0,0008	0,0841
BTN3A2	5,5059	4,7924	-0,7135	0,0008	0,0838
EBLN3P	2,9060	2,1914	-0,7146	0,0007	0,0788
ANKRD12	4,2177	3,5026	-0,7151	0,0025	0,1379
LINC01871	2,0161	1,2998	-0,7164	0,0199	0,2984
TSPAN3	2,6675	1,9510	-0,7165	0,0429	0,3828
ARHGAP5	2,2023	1,4848	-0,7175	0,0019	0,1201

NAP1L2	0,8892	0,1712	-0,7180	0,0008	0,0838
ZNF652	2,3043	1,5788	-0,7256	0,0001	0,0429
SEC62	4,1110	3,3847	-0,7263	0,0000	0,0102
KMT2A	2,9239	2,1965	-0,7273	0,0004	0,0671
NR3C1	4,1589	3,4276	-0,7313	0,0089	0,2236
CLIP4	1,8048	1,0733	-0,7315	0,0165	0,2833
HEXIM1	2,4429	1,7114	-0,7315	0,0099	0,2291
PPM1K	2,5548	1,8228	-0,7320	0,0008	0,0829
COQ10B	3,5715	2,8388	-0,7327	0,0232	0,3165
GVINP1	2,5593	1,8207	-0,7386	0,0004	0,0671
GSTM3	0,9956	0,2569	-0,7387	0,0009	0,0858
RABGEF1	1,2990	0,5596	-0,7394	0,0436	0,3839
PPP1R15B	2,3069	1,5658	-0,7412	0,0027	0,1399
ZNF571	1,0172	0,2722	-0,7450	0,0018	0,1170
CD40	0,9609	0,2121	-0,7488	0,0041	0,1675
FOXP1	4,9809	4,2316	-0,7494	0,0024	0,1372
G2E3	1,7879	1,0353	-0,7526	0,0008	0,0829
TNRC6B	4,5150	3,7595	-0,7556	0,0005	0,0708
KMT2E	4,7533	3,9897	-0,7635	0,0004	0,0641
DTHD1	2,2764	1,5122	-0,7642	0,0097	0,2276
CNOT4	2,3920	1,6268	-0,7652	0,0008	0,0829
ZNF766	3,0963	2,3306	-0,7657	0,0004	0,0671
TVP23B	2,9152	2,1487	-0,7665	0,0017	0,1170
ZEB2	4,4197	3,6529	-0,7668	0,0005	0,0708
TTN	1,4540	0,6863	-0,7676	0,0160	0,2783
AGO1	2,4145	1,6449	-0,7696	0,0002	0,0459
FAM169A	1,0799	0,3088	-0,7711	0,0001	0,0444
ZNF430	2,5797	1,8072	-0,7725	0,0023	0,1348
TULP4	2,9922	2,2185	-0,7737	0,0002	0,0459
ZNF595	1,7182	0,9442	-0,7740	0,0010	0,0917
ARID5B	3,8369	3,0573	-0,7796	0,0175	0,2873
CTSO	3,2475	2,4638	-0,7836	0,0003	0,0613
AC058791.1	1,8619	1,0781	-0,7838	0,0164	0,2816
HIPK3	3,1594	2,3726	-0,7869	0,0152	0,2751
HIPK2	3,1246	2,3364	-0,7882	0,0001	0,0444
CLK1	3,3611	2,5727	-0,7884	0,0129	0,2565
MAPK1	3,5727	2,7828	-0,7899	0,0048	0,1768
SNHG14	1,5305	0,7395	-0,7910	0,0000	0,0186
RBM12B	1,2035	0,4062	-0,7973	0,0000	0,0151
NME8	1,0664	0,2685	-0,7979	0,0018	0,1170
AC109326.1	3,2286	2,4304	-0,7981	0,0499	0,4017
ARHGAP12	1,7340	0,9353	-0,7987	0,0006	0,0783
AC007406.5	1,9791	1,1797	-0,7994	0,0074	0,2089
MYLIP	2,0764	1,2768	-0,7996	0,0106	0,2348
DNAJB9	2,9793	2,1776	-0,8017	0,0175	0,2871
TGFBR1	3,8367	3,0287	-0,8080	0,0081	0,2145
FBXO32	1,7365	0,9190	-0,8175	0,0007	0,0808
ATP8A1	2,5031	1,6811	-0,8220	0,0038	0,1591
CCPG1	3,4285	2,6063	-0,8222	0,0004	0,0671
SLC15A4	2,3220	1,4953	-0,8267	0,0043	0,1683
ZNF91	3,6875	2,8467	-0,8408	0,0031	0,1469
DSTYK	1,9813	1,1240	-0,8573	0,0001	0,0444

CMKLR1	1,4341	0,5750	-0,8590	0,0021	0,1284
CCDC65	1,6581	0,7949	-0,8632	0,0085	0,2191
BAZ2B	3,1968	2,3331	-0,8638	0,0026	0,1385
RNF38	2,1751	1,3108	-0,8644	0,0007	0,0788
PLEKHA1	3,2055	2,3317	-0,8738	0,0001	0,0408
ASH1L	3,1325	2,2575	-0,8751	0,0001	0,0444
DNAJB1	3,7821	2,9059	-0,8762	0,0136	0,2637
MGAT4A	3,9895	3,1105	-0,8790	0,0445	0,3859
JAKMIP2	2,7867	1,9054	-0,8814	0,0032	0,1487
FAM126B	3,1401	2,2587	-0,8814	0,0004	0,0630
ADRB2	2,3940	1,5035	-0,8905	0,0026	0,1394
HERC1	2,9921	2,0927	-0,8994	0,0002	0,0529
ZNF600	2,5553	1,6502	-0,9051	0,0025	0,1379
FGL2	3,3392	2,4271	-0,9121	0,0191	0,2951
FGFBP2	6,2255	5,3040	-0,9215	0,0002	0,0504
MAN1A1	2,6085	1,6776	-0,9309	0,0012	0,0982
EPM2AIP1	1,9508	1,0197	-0,9311	0,0006	0,0738
CXCR2	2,6165	1,6727	-0,9438	0,0082	0,2169
F2R	3,2048	2,2545	-0,9504	0,0273	0,3337
SMIM14	3,6423	2,6827	-0,9596	0,0010	0,0917
KIAA1551	4,6520	3,6891	-0,9629	0,0000	0,0239
TMCC3	1,7263	0,7614	-0,9649	0,0096	0,2273
SERPINI1	1,9007	0,9320	-0,9687	0,0001	0,0372
ZBTB44	3,7441	2,7690	-0,9751	0,0005	0,0708
PDGFD	3,7667	2,7650	-1,0017	0,0001	0,0446
ALOX5AP	5,4154	4,4027	-1,0127	0,0292	0,3415
GLIPR1	4,5829	3,5579	-1,0250	0,0002	0,0459
BCL11B	3,1147	2,0833	-1,0314	0,0065	0,2014
TOB1	4,1956	3,1464	-1,0492	0,0000	0,0151
BNC2	1,6101	0,5581	-1,0520	0,0009	0,0889
PCMTD1	3,3959	2,3334	-1,0625	0,0000	0,0173
CD3D	2,3429	1,2386	-1,1043	0,0474	0,3961
ADAM28	1,6896	0,5851	-1,1046	0,0001	0,0366
PCSK5	1,5582	0,4464	-1,1117	0,0171	0,2863
TRAC	2,6898	1,5574	-1,1324	0,0023	0,1347
PRSS23	4,3642	3,2055	-1,1587	0,0228	0,3137
LY9	1,7660	0,5949	-1,1711	0,0002	0,0504
ARRDC3	4,3537	3,1293	-1,2244	0,0001	0,0366
ZFP36L1	4,1541	2,9119	-1,2423	0,0021	0,1289
LYST	4,2119	2,9616	-1,2503	0,0002	0,0450
FEZ1	1,7380	0,4741	-1,2640	0,0101	0,2307
CLEC2D	3,7581	2,3960	-1,3621	0,0004	0,0671
ENPP5	2,9517	1,5306	-1,4211	0,0002	0,0529
ZBTB20	2,7659	1,3374	-1,4285	0,0000	0,0020
IL7R	2,6487	1,1919	-1,4568	0,0272	0,3337
MALAT1	10,1690	8,5624	-1,6066	0,0001	0,0399
CD160	4,9393	3,1158	-1,8234	0,0000	0,0105
CD3G	3,3677	1,4602	-1,9074	0,0038	0,1595
RGS2	3,8063	1,8531	-1,9532	0,0013	0,1004
FCRL3	3,5529	1,5664	-1,9865	0,0001	0,0370
CCR7	2,2874	0,2633	-2,0241	0,0089	0,2236
FCRL6	4,4360	2,2893	-2,1466	0,0000	0,0040



### Differentially expressed genes T3 over T1

Gene name	Log2(Time_1)	Log2(Time_3)	Log2(FC)	pValue	p.adjust
KIR3DL1	3,7285	5,1615	1,4330	0,0033	0,9249
CD9	0,6542	1,9660	1,3119	0,0005	0,8254
KIR2DS4	3,0637	4,3341	1,2704	0,0352	0,9249
KIR2DL4	3,0590	4,2438	1,1848	0,0014	0,9084
KIR3DX1	0,9517	2,0456	1,0939	0,0072	0,9249
BHLHE40	1,5946	2,6121	1,0174	0,0286	0,9249
MXD1	1,2129	2,1545	0,9416	0,0171	0,9249
GOLIM4	2,0255	2,9583	0,9328	0,0098	0,9249
LMNB1	1,7969	2,7285	0,9315	0,0281	0,9249
DUSP10	2,1524	2,9846	0,8322	0,0362	0,9249
LGALS3	1,0446	1,8658	0,8212	0,0155	0,9249
MRPL10	2,5797	3,3522	0,7725	0,0102	0,9249
LRRC8C	1,2643	2,0269	0,7627	0,0115	0,9249
SLC4A10	1,1957	1,9530	0,7573	0,0033	0,9249
KCTD9	1,1851	1,9020	0,7169	0,0060	0,9249
NPIPB12	0,0433	0,7583	0,7150	0,0007	0,8254
CST3	0,5692	1,2819	0,7127	0,0160	0,9249
FOSL2	1,9166	2,6281	0,7115	0,0496	0,9249
ZNF14	0,9044	1,6056	0,7011	0,0405	0,9249
USP38	1,5629	2,2605	0,6976	0,0049	0,9249
MTHFD2	2,4533	3,1443	0,6910	0,0319	0,9249
HIST2H2AA4	1,4501	2,1333	0,6832	0,0183	0,9249
CDKN2A	0,4388	1,1109	0,6721	0,0001	0,7207
STAT1	4,4445	5,1123	0,6678	0,0413	0,9249
PDE6G	2,0211	2,6885	0,6674	0,0017	0,9249
LEF1	1,3703	2,0264	0,6561	0,0115	0,9249
CD55	3,0671	3,7219	0,6548	0,0120	0,9249
NAMPT	2,0096	2,6616	0,6520	0,0070	0,9249
CYTIP	4,1673	4,8139	0,6466	0,0165	0,9249
MEIS1	0,3812	1,0251	0,6439	0,0091	0,9249
SYAP1	3,6529	4,2960	0,6430	0,0195	0,9249
SELL	7,2696	7,9062	0,6366	0,0045	0,9249
KIR2DL3	4,3814	5,0065	0,6251	0,0233	0,9249
JAK3	3,3306	3,9327	0,6021	0,0180	0,9249
GZMB	8,6728	9,2739	0,6010	0,0126	0,9249
IL1RL1	0,2453	0,8450	0,5997	0,0081	0,9249
MLC1	1,5328	2,1238	0,5909	0,0214	0,9249
MGAM	0,3997	0,9813	0,5816	0,0005	0,8254
PLEKHA2	2,2867	2,8679	0,5812	0,0405	0,9249
ISOC1	2,1608	2,7408	0,5800	0,0121	0,9249
JAKMIP2	2,7867	2,1979	-0,5888	0,0315	0,9249
IMPACT	1,4712	0,8655	-0,6057	0,0098	0,9249
CD40	0,9609	0,3510	-0,6100	0,0143	0,9249
FAM169A	1,0799	0,4660	-0,6139	0,0006	0,8254
LRIF1	2,4593	1,8359	-0,6234	0,0256	0,9249
MYO6	1,4064	0,7641	-0,6424	0,0424	0,9249
RBM12B	1,2035	0,5511	-0,6524	0,0001	0,7207
NAP1L2	0,8892	0,2342	-0,6550	0,0008	0,8493
IKZF3	3,8905	3,2153	-0,6753	0,0004	0,8254
RAB3GAP1	1,0902	0,4080	-0,6822	0,0019	0,9249

PECAM1	3,6774	2,9925	-0,6849	0,0146	0,9249
CRTAM	2,4215	1,7342	-0,6873	0,0208	0,9249
LIMA1	1,8817	1,1904	-0,6913	0,0033	0,9249
LY9	1,7660	1,0676	-0,6985	0,0035	0,9249
ZFP36L1	4,1541	3,4386	-0,7155	0,0171	0,9249
FCRL6	4,4360	3,5831	-0,8529	0,0007	0,8254
FCRL3	3,5529	2,6712	-0,8817	0,0098	0,9249
PCSK5	1,5582	0,6095	-0,9487	0,0213	0,9249
TGFBR1	3,8367	2,8866	-0,9501	0,0007	0,8254
CLEC2D	3,7581	2,7386	-1,0195	0,0018	0,9249
FEZ1	1,7380	0,6264	-1,1117	0,0128	0,9249
SWAP70	2,3514	1,0804	-1,2711	0,0426	0,9249
CCR7	2,2874	0,8855	-1,4019	0,0194	0,9249

### Differentially expressed genes T2 over T3

Gene name	Log2(Time_3)	Log2(Time_2)	Log2(FC)	pValue	p.adjust
STMN1	2,8362	5,0272	2,1910	0,0048	0,2153
BIRC5	0,5250	2,3777	1,8526	0,0012	0,1398
TPX2	0,8050	2,6313	1,8263	0,0002	0,0858
TOP2A	0,8341	2,5959	1,7618	0,0101	0,2685
NUSAP1	1,1212	2,8363	1,7151	0,0074	0,2497
DPP4	1,0984	2,6854	1,5870	0,0004	0,0986
CENPF	0,7176	2,2556	1,5380	0,0003	0,0937
APOBEC3B	0,2892	1,8040	1,5148	0,0067	0,2428
ZWINT	0,5709	2,0562	1,4853	0,0068	0,2443
CCNB1	0,3478	1,8005	1,4527	0,0060	0,2316
MKI67	0,3881	1,8171	1,4289	0,0012	0,1399
LGALS1	5,4005	6,8276	1,4271	0,0008	0,1333
PTTG1	1,3036	2,6363	1,3327	0,0005	0,1033
CCNB2	0,2441	1,5674	1,3232	0,0050	0,2171
DTL	0,2630	1,5691	1,3060	0,0049	0,2171
PCLAF	0,6617	1,9424	1,2807	0,0318	0,3835
RRM2	1,2077	2,4739	1,2662	0,0115	0,2789
VIM	3,1495	4,4051	1,2557	0,0001	0,0814
TYMS	0,3685	1,6006	1,2320	0,0165	0,3123
DHCR24	0,5792	1,7803	1,2011	0,0442	0,4189
YWHAE	3,8485	5,0484	1,1999	0,0045	0,2099
CDK1	0,2184	1,4150	1,1966	0,0138	0,2903
MCM4	1,1389	2,3258	1,1869	0,0109	0,2741
GGH	0,4521	1,6240	1,1719	0,0062	0,2350
SPTSSB	2,5742	3,7337	1,1595	0,0130	0,2860
PRDX3	3,6982	4,8436	1,1454	0,0048	0,2143
CAPG	2,5100	3,6524	1,1424	0,0443	0,4189
CD9	1,9660	3,1032	1,1372	0,0039	0,2004
PCNA	2,5716	3,7068	1,1352	0,0142	0,2920
CCR5	0,2351	1,3624	1,1272	0,0000	0,0457
GIN52	0,3843	1,5040	1,1197	0,0122	0,2789
PTPN6	2,7835	3,8979	1,1144	0,0192	0,3254
TK1	0,4473	1,5613	1,1140	0,0051	0,2171
CDC6	0,2000	1,3108	1,1108	0,0219	0,3398
MCM6	2,1403	3,2443	1,1040	0,0187	0,3227

FAR2	0,5986	1,6576	1,0591	0,0000	0,0342
MCM10	0,1244	1,1823	1,0579	0,0021	0,1610
HELLS	0,8485	1,8832	1,0346	0,0022	0,1614
HMGB3	0,4676	1,4948	1,0272	0,0006	0,1163
ASPM	0,3434	1,3338	0,9904	0,0017	0,1449
MCM7	0,8520	1,8419	0,9899	0,0046	0,2133
HMMR	0,2194	1,1896	0,9702	0,0059	0,2311
ANXA2	5,8641	6,8268	0,9626	0,0016	0,1430
CCDC28B	2,0090	2,9696	0,9606	0,0014	0,1399
CENPK	1,8120	2,7465	0,9345	0,0393	0,4024
DLGAP5	0,2736	1,1964	0,9228	0,0120	0,2789
RRM1	2,2363	3,1551	0,9188	0,0107	0,2726
KIF15	0,2740	1,1920	0,9180	0,0067	0,2428
PGM2	2,1809	3,0974	0,9165	0,0038	0,1989
RBBP8	1,1320	2,0459	0,9139	0,0001	0,0592
TPM4	3,8844	4,7886	0,9042	0,0017	0,1440
CDKN3	0,4339	1,3276	0,8937	0,0232	0,3458
OAS1	2,5014	3,3901	0,8887	0,0418	0,4104
KNL1	0,5373	1,4248	0,8875	0,0138	0,2900
CENPM	0,3229	1,2093	0,8865	0,0147	0,2968
SQLE	1,3351	2,2166	0,8815	0,0035	0,1937
CDC20	0,1185	0,9974	0,8789	0,0047	0,2143
STAP1	2,1480	3,0020	0,8540	0,0023	0,1634
PAICS	1,1754	2,0284	0,8530	0,0084	0,2579
HMBS	0,7797	1,6315	0,8518	0,0001	0,0592
KIF11	0,3951	1,2422	0,8471	0,0134	0,2869
FANCI	1,6686	2,5112	0,8426	0,0060	0,2311
NMI	3,4614	4,3010	0,8396	0,0086	0,2592
CLSPN	0,6482	1,4774	0,8292	0,0363	0,3965
DHFR	0,8285	1,6521	0,8236	0,0271	0,3600
TUBA1B	4,1320	4,9549	0,8228	0,0088	0,2620
MAD2L1	1,4906	2,3019	0,8113	0,0369	0,3972
PRR11	0,3671	1,1768	0,8097	0,0003	0,0937
AC087632.1	0,1750	0,9809	0,8059	0,0109	0,2741
NCBP1	1,4659	2,2659	0,8000	0,0033	0,1900
ILK	3,1493	3,9492	0,7999	0,0015	0,1420
RACGAP1	1,2768	2,0727	0,7959	0,0041	0,2050
TNFRSF9	0,9219	1,7047	0,7828	0,0148	0,2981
CDCA7	0,3054	1,0843	0,7790	0,0014	0,1405
TROAP	0,1412	0,9194	0,7782	0,0004	0,1014
SLC4A10	1,9530	2,7254	0,7723	0,0041	0,2050
RAD51	0,3875	1,1559	0,7683	0,0289	0,3703
ACTL6A	1,5492	2,3078	0,7585	0,0095	0,2648
CCR1	1,4408	2,1962	0,7554	0,0127	0,2832
ACTB	8,7963	9,5493	0,7530	0,0458	0,4213
PIMREG	0,0432	0,7962	0,7530	0,0009	0,1339
PRKCQ-AS1	1,1260	1,8784	0,7524	0,0003	0,0951
MRPL15	1,8535	2,6030	0,7496	0,0001	0,0703
PARVG	2,7060	3,4515	0,7455	0,0003	0,0937
KIF14	0,1491	0,8941	0,7450	0,0093	0,2648
CCT5	4,1292	4,8709	0,7416	0,0125	0,2809
GART	2,1304	2,8673	0,7370	0,0005	0,1100

PDLIM1	1,5431	2,2759	0,7328	0,0001	0,0803
SRSF1	3,0080	3,7381	0,7301	0,0044	0,2084
NSMAF	0,9725	1,7026	0,7301	0,0002	0,0874
ARHGAP45	1,0046	1,7310	0,7264	0,0331	0,3870
LXN	0,8753	1,6005	0,7251	0,0089	0,2628
ADCY7	1,2377	1,9600	0,7222	0,0249	0,3496
APOBEC3H	1,6801	2,4019	0,7217	0,0031	0,1868
FARSA	2,1180	2,8380	0,7201	0,0079	0,2533
CCL23	0,3470	1,0638	0,7168	0,0114	0,2786
NME1	2,1745	2,8909	0,7164	0,0140	0,2908
FH	1,4216	2,1357	0,7141	0,0073	0,2485
FAM111B	0,2301	0,9439	0,7138	0,0262	0,3561
ACAT1	2,0561	2,7696	0,7135	0,0015	0,1412
MELK	0,0372	0,7497	0,7125	0,0115	0,2789
MRPS9	1,8984	2,6103	0,7119	0,0029	0,1814
CPSF6	2,4070	3,1135	0,7066	0,0002	0,0887
DDX39A	3,1131	3,8192	0,7061	0,0025	0,1702
PSMA5	3,8768	4,5814	0,7047	0,0109	0,2741
RNF145	1,6422	2,3464	0,7042	0,0077	0,2506
NIPSNAP3A	2,2361	2,9396	0,7035	0,0307	0,3805
CBX5	1,6651	2,3620	0,6969	0,0026	0,1749
UBE2C	0,0864	0,7821	0,6957	0,0052	0,2171
ZW10	1,0488	1,7299	0,6811	0,0117	0,2789
ACTG1	6,7388	7,4162	0,6774	0,0009	0,1339
AC084033.3	0,9093	1,5866	0,6772	0,0038	0,1989
TNFAIP8L2	1,4626	2,1388	0,6762	0,0105	0,2707
EZH2	1,0309	1,7067	0,6758	0,0070	0,2460
SKA3	0,1965	0,8671	0,6706	0,0246	0,3496
ETFDH	1,4231	2,0917	0,6686	0,0035	0,1939
RFC5	1,2104	1,8783	0,6678	0,0308	0,3814
DECR1	3,5063	4,1716	0,6653	0,0215	0,3397
ASF1B	0,2397	0,9045	0,6647	0,0108	0,2741
MCCC2	1,5038	2,1676	0,6638	0,0006	0,1161
TADA3	1,9956	2,6586	0,6630	0,0246	0,3496
CKAP2L	0,1631	0,8253	0,6622	0,0144	0,2924
SMC4	2,5891	3,2490	0,6600	0,0094	0,2648
SNRPA1	2,1022	2,7602	0,6580	0,0028	0,1804
SLC29A1	0,1313	0,7888	0,6575	0,0003	0,0951
RAB10	3,0155	3,6698	0,6542	0,0173	0,3153
DAXX	2,6726	3,3252	0,6526	0,0320	0,3836
COPB2	3,2270	3,8773	0,6504	0,0180	0,3205
FABP5	0,9875	1,6373	0,6498	0,0002	0,0814
TXNDC17	1,5106	2,1600	0,6494	0,0005	0,1123
GNB4	0,5119	1,1604	0,6485	0,0235	0,3471
MRPS34	1,7802	2,4279	0,6477	0,0005	0,1123
APOBEC3G	5,4117	6,0585	0,6469	0,0109	0,2741
RUVBL1	1,8786	2,5244	0,6458	0,0053	0,2188
AIMP2	1,4636	2,1087	0,6450	0,0045	0,2103
MTHFD1	1,7269	2,3715	0,6446	0,0130	0,2860
PDHX	1,5695	2,2108	0,6413	0,0047	0,2143
PSMA4	5,0638	5,7041	0,6403	0,0208	0,3352
PRDX4	2,0564	2,6957	0,6392	0,0134	0,2874

HMGN2	6,2841	6,9233	0,6392	0,0388	0,4023
ESD	1,8936	2,5318	0,6382	0,0032	0,1870
LPCAT3	1,6981	2,3353	0,6372	0,0051	0,2171
PSMC6	2,5169	3,1536	0,6367	0,0173	0,3153
CBR1	2,0814	2,7179	0,6365	0,0047	0,2143
UHRF1	0,1454	0,7806	0,6352	0,0015	0,1420
SPTLC2	2,7061	3,3411	0,6350	0,0034	0,1900
CENPE	0,7908	1,4244	0,6336	0,0096	0,2651
GOT2	1,9482	2,5810	0,6328	0,0050	0,2171
SHMT2	1,7545	2,3840	0,6295	0,0023	0,1634
CDCA7L	0,8206	1,4472	0,6266	0,0428	0,4143
RFT1	1,0690	1,6942	0,6252	0,0030	0,1832
ASL	1,8002	2,4250	0,6248	0,0015	0,1412
CORO1C	1,9150	2,5396	0,6246	0,0388	0,4023
ERAL1	1,9266	2,5512	0,6246	0,0019	0,1493
E2F2	0,1512	0,7728	0,6216	0,0097	0,2653
NCAPG	0,2289	0,8495	0,6205	0,0051	0,2171
S100A11	3,9614	4,5819	0,6204	0,0495	0,4310
LRPPRC	2,2680	2,8883	0,6203	0,0428	0,4143
SRP54	2,5667	3,1864	0,6197	0,0184	0,3214
FARSB	2,4531	3,0718	0,6187	0,0051	0,2171
SHCBP1	0,2709	0,8886	0,6176	0,0477	0,4243
UACA	0,4899	1,1067	0,6168	0,0379	0,3994
NDUFB3	2,5249	3,1399	0,6150	0,0339	0,3892
MGST2	1,1193	1,7331	0,6138	0,0001	0,0574
PSMB8	4,9725	5,5845	0,6120	0,0010	0,1339
HMGB2	3,8610	4,4726	0,6116	0,0041	0,2050
LRRC58	2,0330	2,6440	0,6111	0,0113	0,2786
CMAS	1,5813	2,1917	0,6104	0,0006	0,1176
MCM3	2,4755	3,0854	0,6099	0,0186	0,3227
CDK2AP2	3,5527	4,1619	0,6093	0,0001	0,0803
EIF2B2	2,1065	2,7138	0,6073	0,0117	0,2789
SLC25A5	5,5254	6,1311	0,6056	0,0369	0,3972
CASP7	2,3302	2,9354	0,6052	0,0030	0,1832
INPP5B	0,9112	1,5142	0,6030	0,0061	0,2316
CCT6A	3,8172	4,4194	0,6022	0,0058	0,2304
NOC3L	1,2051	1,8055	0,6003	0,0073	0,2497
DDX39B	1,8365	2,4360	0,5996	0,0114	0,2786
MRPL32	2,2740	2,8731	0,5991	0,0439	0,4184
STOML2	2,4907	3,0897	0,5990	0,0014	0,1399
CSTF2	1,3205	1,9188	0,5983	0,0293	0,3728
FBXO22	1,5892	2,1870	0,5978	0,0376	0,3982
MAPKAPK3	1,4607	2,0571	0,5964	0,0249	0,3496
TALDO1	2,4954	3,0914	0,5960	0,0004	0,0995
NDUFS2	3,5010	4,0970	0,5959	0,0001	0,0612
CDC45	0,1073	0,7012	0,5939	0,0014	0,1399
GALK1	0,3516	0,9443	0,5926	0,0001	0,0612
ARHGEF6	3,2590	3,8480	0,5890	0,0009	0,1339
UBE2T	0,3300	0,9183	0,5883	0,0178	0,3179
UBASH3B	1,3592	1,9455	0,5863	0,0010	0,1339
MRPL3	2,5370	3,1226	0,5855	0,0016	0,1430
FEN1	1,6535	2,2374	0,5839	0,0263	0,3561

CRTAM	1,7342	2,3176	0,5834	0,0232	0,3463
SCD	0,5446	1,1279	0,5832	0,0160	0,3066
PRMT3	0,6273	1,2095	0,5822	0,0159	0,3041
MTCH2	2,5002	3,0808	0,5806	0,0097	0,2653
RASSF2	1,5009	2,0815	0,5806	0,0010	0,1339
CAPZA1	6,3786	6,9591	0,5805	0,0324	0,3849
ZNF24	3,4107	2,8297	-0,5810	0,0018	0,1469
ZNF766	2,9121	2,3306	-0,5815	0,0271	0,3602
FNIP1	1,8751	1,2918	-0,5834	0,0092	0,2641
SLC16A6	0,9806	0,3946	-0,5859	0,0110	0,2741
CNEP1R1	2,2078	1,6214	-0,5864	0,0223	0,3430
PTAR1	2,1588	1,5719	-0,5870	0,0217	0,3397
SNIP1	0,9666	0,3785	-0,5881	0,0133	0,2863
CHIC2	2,1921	1,6038	-0,5883	0,0075	0,2497
HSPA13	3,0511	2,4618	-0,5894	0,0202	0,3313
CHIC1	0,9618	0,3723	-0,5895	0,0012	0,1399
TTC3	3,7219	3,1323	-0,5895	0,0038	0,1992
PCMTD2	3,4533	2,8635	-0,5898	0,0219	0,3398
THUMPD1	4,5730	3,9811	-0,5919	0,0041	0,2050
TMEM167B	3,4320	2,8387	-0,5933	0,0010	0,1339
MAPK1	3,3763	2,7828	-0,5935	0,0004	0,1014
WDR20	1,8181	1,2243	-0,5938	0,0199	0,3295
CRCP	2,3909	1,7958	-0,5951	0,0119	0,2789
TAOK1	2,8597	2,2645	-0,5952	0,0104	0,2707
RBM48	2,6123	2,0168	-0,5955	0,0166	0,3125
RRN3P2	1,5778	0,9822	-0,5956	0,0098	0,2664
HIPK2	2,9327	2,3364	-0,5963	0,0013	0,1399
ARID4B	4,0901	3,4936	-0,5965	0,0038	0,1989
DSTYK	1,7210	1,1240	-0,5970	0,0102	0,2685
TET2	3,2204	2,6191	-0,6013	0,0089	0,2628
ELMSAN1	2,1441	1,5425	-0,6016	0,0121	0,2789
GCC2	3,9287	3,3258	-0,6029	0,0053	0,2179
ZNF484	1,0486	0,4456	-0,6030	0,0259	0,3546
GALNT11	2,0189	1,4151	-0,6038	0,0009	0,1339
BPGM	4,3319	3,7253	-0,6066	0,0031	0,1860
CCDC174	2,3971	1,7892	-0,6079	0,0080	0,2533
ANKRD36B	2,1207	1,5125	-0,6083	0,0118	0,2789
MBNL2	2,4353	1,8258	-0,6094	0,0080	0,2533
ZNF675	1,6398	1,0303	-0,6095	0,0088	0,2620
IKZF2	1,7141	1,1038	-0,6103	0,0200	0,3301
ATXN1	1,9625	1,3517	-0,6108	0,0038	0,1989
NHLRC3	1,5878	0,9751	-0,6127	0,0016	0,1430
CHD6	2,2829	1,6698	-0,6131	0,0000	0,0342
UTRN	5,2268	4,6137	-0,6131	0,0023	0,1646
CMKLR1	1,1891	0,5750	-0,6140	0,0284	0,3672
RASSF1	3,0352	2,4207	-0,6145	0,0468	0,4232
IFIT5	1,7301	1,1128	-0,6173	0,0033	0,1900
FTL	7,4291	6,8116	-0,6176	0,0097	0,2655
ODF2L	2,4013	1,7838	-0,6176	0,0000	0,0342
CENPC	3,1996	2,5818	-0,6178	0,0194	0,3259
YTHDC1	2,6208	2,0016	-0,6192	0,0007	0,1266
RUFY2	1,3893	0,7688	-0,6205	0,0043	0,2054

MAP3K2	2,6294	2,0088	-0,6207	0,0008	0,1333
GAN	1,4229	0,8019	-0,6210	0,0042	0,2054
DCTN4	1,7090	1,0880	-0,6210	0,0168	0,3129
ELF2	2,4980	1,8768	-0,6212	0,0050	0,2171
RNF19A	2,4925	1,8709	-0,6216	0,0241	0,3490
LINC01871	1,9219	1,2998	-0,6221	0,0111	0,2755
UBL3	2,3091	1,6870	-0,6221	0,0012	0,1399
CCR7	0,8855	0,2633	-0,6222	0,0171	0,3148
LCORL	2,0777	1,4542	-0,6234	0,0010	0,1339
MEX3C	2,0544	1,4304	-0,6240	0,0427	0,4143
HLA-E	8,5529	7,9287	-0,6242	0,0095	0,2648
AP001157.1	1,4380	0,8132	-0,6248	0,0127	0,2832
ZNF548	1,4446	0,8189	-0,6257	0,0291	0,3714
TMEM170A	2,0055	1,3787	-0,6268	0,0091	0,2630
ITM2B	4,9128	4,2858	-0,6270	0,0011	0,1363
KCTD9	1,9020	1,2749	-0,6271	0,0102	0,2686
RUNX3	4,5782	3,9502	-0,6279	0,0012	0,1399
GGNBP2	3,2401	2,6105	-0,6296	0,0016	0,1430
COX19	2,7668	2,1357	-0,6311	0,0349	0,3929
PTPN4	4,7938	4,1626	-0,6312	0,0016	0,1431
SERPINI1	1,5633	0,9320	-0,6313	0,0138	0,2903
TVP23B	2,7806	2,1487	-0,6319	0,0132	0,2863
LITAF	6,1548	5,5229	-0,6319	0,0328	0,3868
COIL	2,3116	1,6790	-0,6326	0,0037	0,1989
ZNF184	1,5753	0,9420	-0,6333	0,0105	0,2709
CXCR2	2,3069	1,6727	-0,6342	0,0258	0,3541
KPNA4	3,6631	3,0288	-0,6343	0,0151	0,3002
FAM126B	2,8943	2,2587	-0,6355	0,0007	0,1244
FCGR3A	7,7550	7,1175	-0,6375	0,0016	0,1430
ZBTB6	0,9468	0,3063	-0,6405	0,0015	0,1420
BBX	4,6248	3,9822	-0,6426	0,0089	0,2628
HLA-DPB1	5,2145	4,5716	-0,6429	0,0243	0,3490
ZNF254	1,1983	0,5546	-0,6436	0,0074	0,2497
MOAP1	2,8751	2,2314	-0,6438	0,0153	0,3011
WDR47	1,4211	0,7764	-0,6447	0,0206	0,3343
ADAM28	1,2300	0,5851	-0,6450	0,0049	0,2171
TIMM23B	1,9084	1,2626	-0,6458	0,0186	0,3227
LATS1	1,9557	1,3091	-0,6466	0,0237	0,3477
AC116366.1	1,7426	1,0959	-0,6467	0,0087	0,2614
GVINP1	2,4675	1,8207	-0,6468	0,0014	0,1399
EAF1	3,0852	2,4376	-0,6477	0,0008	0,1333
KMT2A	2,8465	2,1965	-0,6499	0,0001	0,0710
HIPK1	2,5239	1,8730	-0,6509	0,0038	0,1989
SMG1	3,3307	2,6785	-0,6522	0,0002	0,0887
APOL6	4,5932	3,9409	-0,6523	0,0057	0,2296
FBXO32	1,5713	0,9190	-0,6523	0,0003	0,0937
ZNF292	3,8383	3,1857	-0,6525	0,0005	0,1033
S1PR1	3,5278	2,8749	-0,6529	0,0271	0,3602
IRF1	4,5636	3,9080	-0,6556	0,0423	0,4130
VCPKMT	1,8798	1,2221	-0,6577	0,0058	0,2305
BCLAF1	5,8631	5,2039	-0,6592	0,0376	0,3982
PHC3	2,8926	2,2315	-0,6611	0,0183	0,3214

ADRB2	2,1653	1,5035	-0,6618	0,0029	0,1822
OSTM1	3,1555	2,4933	-0,6621	0,0141	0,2918
YTHDF3	3,2803	2,6176	-0,6627	0,0219	0,3398
DNAJB6	5,4694	4,8045	-0,6648	0,0055	0,2245
CSGALNACT2	2,6181	1,9507	-0,6674	0,0012	0,1399
SIRT1	1,1461	0,4782	-0,6680	0,0076	0,2506
BAZ2B	3,0025	2,3331	-0,6694	0,0071	0,2471
C2orf69	1,6504	0,9797	-0,6707	0,0117	0,2789
BTN3A1	3,3378	2,6617	-0,6760	0,0006	0,1161
BICRAL	1,4584	0,7821	-0,6763	0,0000	0,0522
RASGEF1B	1,1028	0,4225	-0,6803	0,0438	0,4179
EIF1	6,1618	5,4806	-0,6812	0,0356	0,3945
ITPRIP	2,0699	1,3885	-0,6815	0,0332	0,3870
CCSER2	3,4312	2,7496	-0,6816	0,0008	0,1316
PLEKHA1	3,0156	2,3317	-0,6839	0,0032	0,1899
ZNF845	1,7752	1,0900	-0,6852	0,0115	0,2789
ARAP2	3,5807	2,8937	-0,6870	0,0026	0,1735
PGRMC2	1,5068	0,8184	-0,6884	0,0368	0,3972
RORA	3,1245	2,4342	-0,6902	0,0002	0,0814
SERTAD1	1,7073	1,0168	-0,6905	0,0475	0,4241
CCL5	8,9514	8,2604	-0,6910	0,0040	0,2037
TAF13	1,6090	0,9175	-0,6915	0,0351	0,3931
TULP4	2,9105	2,2185	-0,6919	0,0084	0,2580
ZBTB33	1,7848	1,0919	-0,6929	0,0008	0,1333
CLIP4	1,7694	1,0733	-0,6961	0,0034	0,1910
GLIPR1	4,2549	3,5579	-0,6970	0,0106	0,2726
TNRC6B	4,4566	3,7595	-0,6972	0,0003	0,0951
ANKRA2	2,4551	1,7567	-0,6984	0,0000	0,0342
TSPYL1	4,1579	3,4566	-0,7013	0,0227	0,3441
CEP120	1,7351	1,0309	-0,7042	0,0018	0,1490
ANKRD36C	2,7446	2,0396	-0,7050	0,0123	0,2789
GABARAPL1	2,2075	1,5023	-0,7053	0,0256	0,3529
MED13	3,1075	2,4021	-0,7054	0,0030	0,1832
SDE2	2,5287	1,8229	-0,7058	0,0427	0,4143
MT-ND1	5,6715	4,9654	-0,7061	0,0241	0,3490
PNRC1	2,6025	1,8955	-0,7070	0,0001	0,0592
KBTD8	0,9296	0,2219	-0,7077	0,0179	0,3195
SUSD6	2,2802	1,5714	-0,7088	0,0188	0,3227
AOAH	5,2168	4,5078	-0,7090	0,0061	0,2326
HIPK3	3,0837	2,3726	-0,7111	0,0140	0,2910
AC010733.2	2,5116	1,8002	-0,7114	0,0363	0,3965
MAN1A1	2,3899	1,6776	-0,7123	0,0005	0,1100
BTN3A2	5,5054	4,7924	-0,7129	0,0069	0,2456
AL357060.2	1,6602	0,9461	-0,7141	0,0082	0,2567
ALG13	2,6494	1,9337	-0,7157	0,0154	0,3012
ISCA1	3,3891	2,6695	-0,7195	0,0102	0,2685
PIGA	1,2155	0,4954	-0,7201	0,0229	0,3445
PDGFD	3,4874	2,7650	-0,7224	0,0452	0,4191
ZNF571	0,9951	0,2722	-0,7229	0,0036	0,1971
EPC1	3,4310	2,7067	-0,7244	0,0091	0,2630
ZEB2	4,3784	3,6529	-0,7255	0,0000	0,0342
FBXO8	1,7209	0,9941	-0,7268	0,0063	0,2379



BPTF	4,3770	3,6479	-0,7291	0,0016	0,1430
HS3ST3B1	1,4066	0,6745	-0,7321	0,0011	0,1392
SKIL	3,1970	2,4647	-0,7323	0,0132	0,2860
STK17B	5,9109	5,1782	-0,7327	0,0126	0,2832
NECAP1	2,0052	1,2704	-0,7348	0,0391	0,4024
CREBRF	3,2564	2,5214	-0,7351	0,0044	0,2074
ZFX	3,4571	2,7220	-0,7352	0,0086	0,2589
KLF3	2,7262	1,9887	-0,7375	0,0036	0,1973
C18orf32	3,7402	2,9989	-0,7414	0,0001	0,0689
BRWD1	3,0829	2,3399	-0,7430	0,0006	0,1200
MAFF	1,3132	0,5668	-0,7464	0,0321	0,3838
PNRC2	4,5995	3,8522	-0,7473	0,0017	0,1440
SPTY2D1	2,1352	1,3849	-0,7503	0,0003	0,0951
CCNT1	1,8784	1,1266	-0,7518	0,0124	0,2800
SNHG14	1,4927	0,7395	-0,7532	0,0012	0,1399
ANKRD36	2,5235	1,7697	-0,7538	0,0099	0,2664
ASH1L	3,0124	2,2575	-0,7549	0,0005	0,1100
ZNF800	2,9735	2,2160	-0,7575	0,0026	0,1735
SERINC1	5,2036	4,4455	-0,7581	0,0026	0,1750
MTND2P28	4,1460	3,3871	-0,7588	0,0369	0,3972
YPEL5	5,2600	4,4993	-0,7607	0,0108	0,2741
ANKRD12	4,2667	3,5026	-0,7642	0,0010	0,1339
C16orf72	2,6839	1,9196	-0,7643	0,0147	0,2958
ZNF350	2,5928	1,8265	-0,7663	0,0380	0,3998
HBP1	4,3799	3,6120	-0,7680	0,0247	0,3496
CTSO	3,2343	2,4638	-0,7705	0,0047	0,2143
DOCK5	1,9784	1,2042	-0,7742	0,0025	0,1705
KMT2E	4,7671	3,9897	-0,7774	0,0007	0,1211
CNOT6L	4,4327	3,6521	-0,7806	0,0024	0,1664
CDC42SE2	6,4410	5,6590	-0,7820	0,0000	0,0457
ARL4C	5,8224	5,0403	-0,7821	0,0016	0,1430
MOB4	3,2180	2,4337	-0,7843	0,0095	0,2648
C1orf56	3,1293	2,3443	-0,7850	0,0157	0,3038
DNAJB1	3,6948	2,9059	-0,7889	0,0314	0,3824
ZNF91	3,6367	2,8467	-0,7900	0,0037	0,1989
BNC2	1,3486	0,5581	-0,7905	0,0013	0,1399
SERTAD3	1,9307	1,1389	-0,7918	0,0061	0,2316
ITK	3,6862	2,8938	-0,7924	0,0053	0,2188
REL	2,9446	2,1501	-0,7946	0,0259	0,3545
JOSD1	2,1075	1,3124	-0,7951	0,0084	0,2579
NFAT5	1,8613	1,0648	-0,7965	0,0003	0,0951
DCP1A	3,3506	2,5514	-0,7992	0,0209	0,3356
ZNF250	1,2514	0,4515	-0,8000	0,0001	0,0814
SLC15A4	2,2981	1,4953	-0,8028	0,0232	0,3458
ZNF430	2,6145	1,8072	-0,8073	0,0061	0,2316
PPP1R15B	2,3762	1,5658	-0,8105	0,0046	0,2127
PLEKHA3	2,2028	1,3873	-0,8155	0,0006	0,1194
USPL1	2,8152	1,9928	-0,8223	0,0176	0,3177
SELENOK	4,9475	4,1236	-0,8239	0,0068	0,2443
MYLIP	2,1019	1,2768	-0,8251	0,0044	0,2097
NR3C1	4,2544	3,4276	-0,8268	0,0004	0,0986
AC027290.2	2,3672	1,5388	-0,8283	0,0247	0,3496

SYNE2	5,4766	4,6466	-0,8300	0,0002	0,0868
TRAF6	2,8168	1,9782	-0,8386	0,0035	0,1929
RNF125	3,5626	2,7235	-0,8391	0,0377	0,3985
MT-ND2	7,9772	7,1309	-0,8463	0,0246	0,3496
SLC2A3	4,3453	3,4915	-0,8538	0,0152	0,3008
CCNL1	3,4799	2,6249	-0,8550	0,0095	0,2648
B4GALT1	3,8597	3,0014	-0,8583	0,0409	0,4079
ZFP36L2	5,5645	4,7054	-0,8591	0,0337	0,3892
CLK4	2,3283	1,4657	-0,8626	0,0041	0,2050
ARRDC3	3,9925	3,1293	-0,8632	0,0013	0,1399
SAMD8	1,7092	0,8370	-0,8722	0,0177	0,3177
IL7R	2,0715	1,1919	-0,8796	0,0120	0,2789
PCMTD1	3,2234	2,3334	-0,8900	0,0053	0,2179
FOSL2	2,6281	1,7380	-0,8902	0,0281	0,3657
CYTIP	4,8139	3,9228	-0,8912	0,0019	0,1527
TXNIP	7,7426	6,8494	-0,8933	0,0168	0,3129
DUSP1	6,2561	5,3609	-0,8953	0,0483	0,4260
MSL2	2,2809	1,3699	-0,9110	0,0069	0,2458
RNF38	2,2305	1,3108	-0,9198	0,0013	0,1399
TOB1	4,0710	3,1464	-0,9245	0,0000	0,0342
MED21	2,5347	1,6013	-0,9334	0,0206	0,3343
LYST	3,8976	2,9616	-0,9360	0,0024	0,1646
SBDS	3,7192	2,7728	-0,9465	0,0123	0,2789
TMCC3	1,7176	0,7614	-0,9561	0,0010	0,1339
DDIT3	2,3019	1,3383	-0,9636	0,0358	0,3949
DNAJB9	3,1422	2,1776	-0,9646	0,0024	0,1664
KIAA1551	4,6582	3,6891	-0,9691	0,0002	0,0839
NR1D2	2,0465	1,0584	-0,9882	0,0006	0,1161
ZBTB44	3,7619	2,7690	-0,9929	0,0006	0,1134
TIPARP	3,1703	2,1748	-0,9955	0,0077	0,2508
COQ10B	3,8345	2,8388	-0,9957	0,0075	0,2497
MGAT4A	4,1108	3,1105	-1,0003	0,0127	0,2832
FAM46C	3,7764	2,7663	-1,0101	0,0377	0,3986
CLK1	3,6055	2,5727	-1,0328	0,0110	0,2742
ZBTB1	3,7083	2,6715	-1,0367	0,0180	0,3205
ARID5B	4,1085	3,0573	-1,0512	0,0009	0,1339
METRNL	1,9481	0,8913	-1,0567	0,0398	0,4026
ZNF14	1,6056	0,5436	-1,0619	0,0058	0,2305
AC012615.1	1,8630	0,7774	-1,0856	0,0075	0,2497
FGFBP2	6,3915	5,3040	-1,0874	0,0004	0,0995
FCRL3	2,6712	1,5664	-1,1048	0,0086	0,2589
PRDM1	4,2697	3,1150	-1,1547	0,0048	0,2151
ENPP5	2,6878	1,5306	-1,1573	0,0010	0,1339
ZBTB20	2,5006	1,3374	-1,1631	0,0000	0,0487
MALAT1	9,7823	8,5624	-1,2199	0,0001	0,0803
PRSS23	4,4410	3,2055	-1,2355	0,0067	0,2428
MAP3K8	5,3190	4,0539	-1,2651	0,0085	0,2580
CD160	4,3997	3,1158	-1,2838	0,0025	0,1702
FCRL6	3,5831	2,2893	-1,2937	0,0002	0,0887
NFE2L2	3,9814	2,5823	-1,3991	0,0171	0,3148
PDE4D	3,3293	1,8846	-1,4447	0,0066	0,2420
PDE4B	2,8277	1,3123	-1,5154	0,0327	0,3863

B3GNT7	4,5325	2,9655	-1,5670	0,0365	0,3967
RGS1	5,6211	4,0309	-1,5902	0,0441	0,4189
RGS2	3,8224	1,8531	-1,9693	0,0005	0,1033

### Upregulated genes T2 over T1. Gene Ontology database: Biological Processes.

ID	Description	GeneRatio	BgRatio	pvalue	p.adjust
GO:0140014	mitotic nuclear division	22/188	309/21081	6,37E-14	1,63E-10
GO:0007059	chromosome segregation	23/188	352/21081	1,02E-13	1,63E-10
GO:0000280	nuclear division	25/188	469/21081	7,80E-13	8,30E-10
GO:0098813	nuclear chromosome segregation	18/188	287/21081	1,10E-10	5,88E-08
GO:0010965	regulation of mitotic sister chromatid separation	9/188	61/21081	3,42E-09	1,56E-06
GO:0051983	regulation of chromosome segregation	11/188	110/21081	4,19E-09	1,67E-06
GO:1905818	regulation of chromosome separation	9/188	67/21081	8,06E-09	2,34E-06
GO:0051783	regulation of nuclear division	13/188	201/21081	3,26E-08	6,93E-06
GO:0009116	nucleoside metabolic process	10/188	105/21081	3,47E-08	6,93E-06
GO:0045930	negative regulation of mitotic cell cycle	17/188	409/21081	1,66E-07	2,53E-05
GO:1902850	microtubule cytoskeleton organization involved in mitosis	11/188	163/21081	2,50E-07	3,63E-05
GO:1901657	glycosyl compound metabolic process	10/188	131/21081	2,84E-07	3,95E-05
GO:0042493	response to drug	17/188	434/21081	3,83E-07	4,62E-05
GO:0071103	DNA conformation change	16/188	385/21081	3,90E-07	4,62E-05
GO:0051383	kinetochore organization	5/188	23/21081	1,58E-06	1,58E-04
GO:0072522	purine-containing compound biosynthetic process	11/188	224/21081	5,67E-06	4,32E-04
GO:0009636	response to toxic substance	12/188	277/21081	7,64E-06	5,68E-04
GO:0065004	protein-DNA complex assembly	12/188	278/21081	7,93E-06	5,76E-04
GO:0009164	nucleoside catabolic process	5/188	33/21081	1,04E-05	7,36E-04
GO:0006268	DNA unwinding involved in DNA replication	4/188	17/21081	1,33E-05	8,03E-04
GO:0050000	chromosome localization	7/188	88/21081	1,38E-05	8,04E-04
GO:0051303	establishment of chromosome localization	7/188	88/21081	1,38E-05	8,04E-04
GO:0021766	hippocampus development	7/188	90/21081	1,61E-05	8,87E-04
GO:0000082	G1/S transition of mitotic cell cycle	12/188	306/21081	2,07E-05	1,08E-03
GO:0034109	homotypic cell-cell adhesion	7/188	95/21081	2,29E-05	1,16E-03
GO:0045091	regulation of single stranded viral RNA replication via double stranded DNA intermediate	4/188	20/21081	2,65E-05	1,30E-03
GO:0071824	protein-DNA complex subunit organization	12/188	319/21081	3,11E-05	1,48E-03
GO:1901659	glycosyl compound biosynthetic process	5/188	42/21081	3,48E-05	1,57E-03
GO:0070527	platelet aggregation	6/188	69/21081	3,49E-05	1,57E-03

GO:0031145	anaphase-promoting complex-dependent catabolic process	7/188	102/21081	3,63E-05	1,61E-03
GO:0008406	gonad development	10/188	227/21081	3,86E-05	1,64E-03
GO:0039692	single stranded viral RNA replication via double stranded DNA intermediate	4/188	22/21081	3,95E-05	1,64E-03
GO:1903322	positive regulation of protein modification by small protein conjugation or removal	8/188	142/21081	4,18E-05	1,71E-03
GO:1901658	glycosyl compound catabolic process	5/188	44/21081	4,38E-05	1,74E-03
GO:0044843	cell cycle G1/S phase transition	12/188	335/21081	4,99E-05	1,83E-03
GO:0019693	ribose phosphate metabolic process	14/188	452/21081	5,76E-05	2,04E-03
GO:0042063	gliogenesis	12/188	351/21081	7,79E-05	2,65E-03
GO:0000086	G2/M transition of mitotic cell cycle	11/188	298/21081	7,90E-05	2,65E-03
GO:0060326	cell chemotaxis	12/188	362/21081	1,04E-04	3,29E-03
GO:0045540	regulation of cholesterol biosynthetic process	5/188	53/21081	1,08E-04	3,29E-03
GO:0106118	regulation of sterol biosynthetic process	5/188	53/21081	1,08E-04	3,29E-03
GO:0070383	DNA cytosine deamination	3/188	11/21081	1,09E-04	3,29E-03
GO:0090151	establishment of protein localization to mitochondrial membrane	5/188	54/21081	1,19E-04	3,51E-03
GO:0044839	cell cycle G2/M phase transition	11/188	317/21081	1,36E-04	3,92E-03
GO:0050819	negative regulation of coagulation	5/188	56/21081	1,41E-04	4,00E-03
GO:1901028	regulation of mitochondrial outer membrane permeabilization involved in apoptotic signaling pathway	5/188	56/21081	1,41E-04	4,00E-03
GO:0000727	double-strand break repair via break-induced replication	3/188	12/21081	1,45E-04	4,02E-03
GO:0090331	negative regulation of platelet aggregation	3/188	12/21081	1,45E-04	4,02E-03
GO:0034110	regulation of homotypic cell-cell adhesion	4/188	32/21081	1,81E-04	4,98E-03
GO:0016554	cytidine to uridine editing	3/188	13/21081	1,87E-04	4,98E-03
GO:0033044	regulation of chromosome organization	12/188	389/21081	2,03E-04	5,36E-03
GO:0042744	hydrogen peroxide catabolic process	4/188	33/21081	2,05E-04	5,36E-03
GO:0001666	response to hypoxia	12/188	402/21081	2,75E-04	6,91E-03
GO:0008637	apoptotic mitochondrial changes	7/188	142/21081	2,90E-04	7,05E-03
GO:0051099	positive regulation of binding	8/188	189/21081	3,04E-04	7,19E-03
GO:0042100	B cell proliferation	6/188	102/21081	3,08E-04	7,23E-03
GO:0043281	regulation of cysteine-type endopeptidase activity involved in apoptotic process	9/188	240/21081	3,15E-04	7,35E-03
GO:0032355	response to estradiol	7/188	145/21081	3,29E-04	7,53E-03
GO:0010389	regulation of G2/M transition of mitotic cell cycle	9/188	243/21081	3,45E-04	7,83E-03
GO:1902969	mitotic DNA replication	3/188	16/21081	3,59E-04	7,96E-03

GO:0090181	regulation of cholesterol metabolic process	5/188	69/21081	3,79E-04	8,29E-03
GO:0140013	meiotic nuclear division	8/188	197/21081	4,01E-04	8,65E-03
GO:0045637	regulation of myeloid cell differentiation	10/188	304/21081	4,19E-04	8,89E-03
GO:0042542	response to hydrogen peroxide	7/188	151/21081	4,20E-04	8,89E-03
GO:0006270	DNA replication initiation	4/188	40/21081	4,36E-04	9,04E-03
GO:0043279	response to alkaloid	6/188	111/21081	4,84E-04	9,67E-03
GO:0007006	mitochondrial membrane organization	7/188	157/21081	5,31E-04	1,02E-02
GO:0061351	neural precursor cell proliferation	7/188	157/21081	5,31E-04	1,02E-02
GO:0072655	establishment of protein localization to mitochondrion	7/188	157/21081	5,31E-04	1,02E-02
GO:1902749	regulation of cell cycle G2/M phase transition	9/188	260/21081	5,64E-04	1,05E-02
GO:0000096	sulfur amino acid metabolic process	4/188	43/21081	5,76E-04	1,06E-02
GO:0051205	protein insertion into membrane	5/188	77/21081	6,29E-04	1,10E-02
GO:0007599	hemostasis	11/188	384/21081	6,93E-04	1,18E-02
GO:0050817	coagulation	11/188	384/21081	6,93E-04	1,18E-02
GO:1902653	secondary alcohol biosynthetic process	5/188	79/21081	7,07E-04	1,19E-02
GO:1905710	positive regulation of membrane permeability	5/188	80/21081	7,49E-04	1,25E-02
GO:0098869	cellular oxidant detoxification	6/188	123/21081	8,33E-04	1,38E-02
GO:0032496	response to lipopolysaccharide	11/188	396/21081	8,91E-04	1,45E-02
GO:0002478	antigen processing and presentation of exogenous peptide antigen	10/188	337/21081	9,26E-04	1,49E-02
GO:2001233	regulation of apoptotic signaling pathway	12/188	462/21081	9,39E-04	1,49E-02
GO:0006790	sulfur compound metabolic process	11/188	399/21081	9,47E-04	1,49E-02
GO:0018198	peptidyl-cysteine modification	4/188	49/21081	9,49E-04	1,49E-02
GO:0035722	interleukin-12-mediated signaling pathway	4/188	49/21081	9,49E-04	1,49E-02
GO:0070671	response to interleukin-12	4/188	52/21081	1,19E-03	1,79E-02
GO:1900047	negative regulation of hemostasis	4/188	52/21081	1,19E-03	1,79E-02
GO:0010951	negative regulation of endopeptidase activity	9/188	292/21081	1,28E-03	1,87E-02
GO:0044282	small molecule catabolic process	12/188	483/21081	1,37E-03	1,96E-02
GO:0043624	cellular protein complex disassembly	8/188	239/21081	1,41E-03	1,98E-02
GO:0006839	mitochondrial transport	9/188	300/21081	1,54E-03	2,13E-02
GO:0010528	regulation of transposition	3/188	26/21081	1,56E-03	2,13E-02
GO:0010529	negative regulation of transposition	3/188	26/21081	1,56E-03	2,13E-02
GO:0036297	interstrand cross-link repair	4/188	56/21081	1,57E-03	2,13E-02
GO:0048732	gland development	12/188	494/21081	1,66E-03	2,22E-02
GO:0062012	regulation of small molecule metabolic process	12/188	494/21081	1,66E-03	2,22E-02

GO:0006919	activation of cysteine-type endopeptidase activity involved in apoptotic process	5/188	96/21081	1,70E-03	2,27E-02
GO:1900740	positive regulation of protein insertion into mitochondrial membrane involved in apoptotic signaling pathway	3/188	27/21081	1,74E-03	2,29E-02
GO:0006890	retrograde vesicle-mediated transport, Golgi to endoplasmic reticulum	5/188	98/21081	1,86E-03	2,40E-02
GO:0070125	mitochondrial translational elongation	5/188	98/21081	1,86E-03	2,40E-02
GO:0019218	regulation of steroid metabolic process	6/188	144/21081	1,87E-03	2,40E-02
GO:0000302	response to reactive oxygen species	8/188	251/21081	1,91E-03	2,45E-02
GO:0042743	hydrogen peroxide metabolic process	4/188	61/21081	2,15E-03	2,66E-02
GO:0002573	myeloid leukocyte differentiation	8/188	257/21081	2,22E-03	2,74E-02
GO:0002833	positive regulation of response to biotic stimulus	10/188	383/21081	2,38E-03	2,89E-02
GO:0006636	unsaturated fatty acid biosynthetic process	4/188	63/21081	2,42E-03	2,92E-02
GO:0009743	response to carbohydrate	8/188	261/21081	2,44E-03	2,92E-02
GO:0097529	myeloid leukocyte migration	8/188	261/21081	2,44E-03	2,92E-02
GO:0090068	positive regulation of cell cycle process	9/188	323/21081	2,54E-03	3,02E-02
GO:0046148	pigment biosynthetic process	4/188	64/21081	2,56E-03	3,05E-02
GO:0032196	transposition	3/188	31/21081	2,61E-03	3,07E-02
GO:0043032	positive regulation of macrophage activation	3/188	31/21081	2,61E-03	3,07E-02
GO:0000079	regulation of cyclin-dependent protein serine/threonine kinase activity	5/188	106/21081	2,62E-03	3,07E-02
GO:0030888	regulation of B cell proliferation	4/188	66/21081	2,87E-03	3,30E-02
GO:0045023	G0 to G1 transition	4/188	67/21081	3,03E-03	3,47E-02
GO:0034446	substrate adhesion-dependent cell spreading	5/188	110/21081	3,08E-03	3,49E-02
GO:0034104	negative regulation of tissue remodeling	3/188	33/21081	3,13E-03	3,52E-02
GO:0035456	response to interferon-beta	3/188	33/21081	3,13E-03	3,52E-02
GO:0045089	positive regulation of innate immune response	9/188	334/21081	3,17E-03	3,54E-02
GO:0009396	folic acid-containing compound biosynthetic process	2/188	10/21081	3,40E-03	3,72E-02
GO:0070723	response to cholesterol	3/188	34/21081	3,41E-03	3,72E-02
GO:0070661	leukocyte proliferation	10/188	404/21081	3,49E-03	3,79E-02
GO:0031579	membrane raft organization	3/188	35/21081	3,70E-03	3,97E-02
GO:1901607	alpha-amino acid biosynthetic process	4/188	71/21081	3,74E-03	3,99E-02
GO:0051235	maintenance of location	9/188	344/21081	3,84E-03	4,07E-02
GO:0010821	regulation of mitochondrion organization	7/188	222/21081	3,86E-03	4,07E-02
GO:0033197	response to vitamin E	2/188	11/21081	4,13E-03	4,27E-02

GO:0006369	termination of RNA polymerase II transcription	3/188	37/21081	4,34E-03	4,40E-02
GO:0030262	apoptotic nuclear changes	3/188	37/21081	4,34E-03	4,40E-02
GO:0043094	cellular metabolic compound salvage	3/188	37/21081	4,34E-03	4,40E-02
GO:0071887	leukocyte apoptotic process	5/188	120/21081	4,46E-03	4,47E-02
GO:1901570	fatty acid derivative biosynthetic process	5/188	122/21081	4,78E-03	4,72E-02
GO:0035567	non-canonical Wnt signaling pathway	6/188	175/21081	4,91E-03	4,78E-02
GO:1902652	secondary alcohol metabolic process	6/188	175/21081	4,91E-03	4,78E-02
GO:0033632	regulation of cell-cell adhesion mediated by integrin	2/188	12/21081	4,92E-03	4,78E-02
GO:2000109	regulation of macrophage apoptotic process	2/188	12/21081	4,92E-03	4,78E-02

### Downregulated genes T2 over T1. Gene Ontology database: Biological Processes.

ID	Description	GeneRatio	BgRatio	pvalue	p.adjust
GO:0050851	antigen receptor-mediated signaling pathway	17/196	424/21081	5,00E-07	1,47E-03
GO:0030098	lymphocyte differentiation	15/196	398/21081	5,10E-06	7,50E-03
GO:0060021	roof of mouth development	7/196	100/21081	4,16E-05	2,14E-02
GO:0018210	peptidyl-threonine modification	8/196	137/21081	4,35E-05	2,14E-02
GO:0043405	regulation of MAP kinase activity	13/196	386/21081	7,01E-05	2,95E-02
GO:0060485	mesenchyme development	11/196	308/21081	1,53E-04	3,91E-02
GO:0061647	histone H3-K9 modification	5/196	56/21081	1,72E-04	3,91E-02
GO:0009791	post-embryonic development	6/196	88/21081	1,72E-04	3,91E-02
GO:0060317	cardiac epithelial to mesenchymal transition	4/196	32/21081	2,13E-04	4,18E-02
GO:0071875	adrenergic receptor signaling pathway	4/196	33/21081	2,40E-04	4,43E-02

### Upregulated genes T2 over T1. Reactome database.

ID	Description	GeneRatio	BgRatio	pvalue	p.adjust
R-HSA-69620	Cell Cycle Checkpoints	23/159	294/10704	5,68E-11	3,98E-08
R-HSA-68882	Mitotic Anaphase	19/159	236/10704	1,89E-09	4,73E-07
R-HSA-2555396	Mitotic Metaphase and Anaphase	19/159	237/10704	2,02E-09	4,73E-07
R-HSA-2467813	Separation of Sister Chromatids	16/159	191/10704	2,21E-08	3,87E-06
R-HSA-2500257	Resolution of Sister Chromatid Cohesion	13/159	126/10704	4,21E-08	5,61E-06
R-HSA-68886	M Phase	23/159	418/10704	5,13E-08	5,61E-06
R-HSA-68877	Mitotic Prometaphase	16/159	204/10704	5,60E-08	5,61E-06
R-HSA-69618	Mitotic Spindle Checkpoint	12/159	113/10704	1,03E-07	9,04E-06

R-HSA-141424	Amplification of signal from the kinetochores	11/159	96/10704	1,63E-07	1,15E-05
R-HSA-141444	Amplification of signal from unattached kinetochores via a MAD2 inhibitory signal	11/159	96/10704	1,63E-07	1,15E-05
R-HSA-453279	Mitotic G1 phase and G1/S transition	13/159	149/10704	3,07E-07	1,96E-05
R-HSA-9648025	EML4 and NUDC in mitotic spindle formation	11/159	117/10704	1,23E-06	7,18E-05
R-HSA-109581	Apoptosis	13/159	178/10704	2,34E-06	1,26E-04
R-HSA-5357801	Programmed Cell Death	13/159	190/10704	4,82E-06	2,42E-04
R-HSA-5663220	RHO GTPases Activate Formins	11/159	140/10704	7,17E-06	3,35E-04
R-HSA-2514853	Condensation of Prometaphase Chromosomes	4/159	11/10704	1,43E-05	6,25E-04
R-HSA-68867	Assembly of the pre-replicative complex	7/159	68/10704	6,34E-05	2,61E-03
R-HSA-195258	RHO GTPase Effectors	15/159	327/10704	1,04E-04	4,04E-03
R-HSA-15869	Metabolism of nucleotides	8/159	101/10704	1,25E-04	4,13E-03
R-HSA-109606	Intrinsic Pathway for Apoptosis	6/159	53/10704	1,26E-04	4,13E-03
R-HSA-176409	APC/C:Cdc20 mediated degradation of mitotic proteins	7/159	76/10704	1,29E-04	4,13E-03
R-HSA-194315	Signaling by Rho GTPases	18/159	455/10704	1,39E-04	4,13E-03
R-HSA-176814	Activation of APC/C and APC/C:Cdc20 mediated degradation of mitotic proteins	7/159	77/10704	1,41E-04	4,13E-03
R-HSA-69206	G1/S Transition	9/159	131/10704	1,42E-04	4,13E-03
R-HSA-69481	G2/M Checkpoints	10/159	168/10704	1,98E-04	5,56E-03
R-HSA-69002	DNA Replication Pre-Initiation	7/159	85/10704	2,61E-04	7,05E-03
R-HSA-174143	APC/C-mediated degradation of cell cycle proteins	7/159	88/10704	3,24E-04	8,11E-03
R-HSA-453276	Regulation of mitotic cell cycle	7/159	88/10704	3,24E-04	8,11E-03
R-HSA-69052	Switching of origins to a post-replicative state	7/159	91/10704	3,98E-04	9,62E-03
R-HSA-174154	APC/C:Cdc20 mediated degradation of Securin	6/159	68/10704	5,00E-04	1,17E-02
R-HSA-69306	DNA Replication	8/159	128/10704	6,29E-04	1,28E-02
R-HSA-68949	Orc1 removal from chromatin	6/159	71/10704	6,31E-04	1,28E-02
R-HSA-176974	Unwinding of DNA	3/159	12/10704	6,41E-04	1,28E-02
R-HSA-264870	Caspase-mediated cleavage of cytoskeletal proteins	3/159	12/10704	6,41E-04	1,28E-02
R-HSA-73817	Purine ribonucleoside monophosphate biosynthesis	3/159	12/10704	6,41E-04	1,28E-02
R-HSA-174178	APC/C:Cdh1 mediated degradation of Cdc20 and other APC/C:Cdh1 targeted proteins in late mitosis/early G1	6/159	74/10704	7,87E-04	1,53E-02



R-HSA-75205	Dissolution of Fibrin Clot	3/159	13/10704	8,25E-04	1,56E-02
R-HSA-2980766	Nuclear Envelope Breakdown	5/159	52/10704	1,01E-03	1,81E-02
R-HSA-75153	Apoptotic execution phase	5/159	52/10704	1,01E-03	1,81E-02
R-HSA-176408	Regulation of APC/C activators between G1/S and early anaphase	6/159	81/10704	1,27E-03	2,19E-02
R-HSA-8956320	Nucleobase biosynthesis	3/159	15/10704	1,28E-03	2,19E-02
R-HSA-2559585	Oncogene Induced Senescence	4/159	33/10704	1,37E-03	2,29E-02
R-HSA-156711	Polo-like kinase mediated events	3/159	16/10704	1,56E-03	2,55E-02
R-HSA-3301854	Nuclear Pore Complex (NPC) Disassembly	4/159	35/10704	1,71E-03	2,67E-02
R-HSA-8953750	Transcriptional Regulation by E2F6	4/159	35/10704	1,71E-03	2,67E-02
R-HSA-983189	Kinesins	5/159	59/10704	1,78E-03	2,67E-02
R-HSA-9659787	Aberrant regulation of mitotic G1/S transition in cancer due to RB1 defects	3/159	17/10704	1,88E-03	2,67E-02
R-HSA-9661069	Defective binding of RB1 mutants to E2F1,(E2F2, E2F3)	3/159	17/10704	1,88E-03	2,67E-02
R-HSA-9675126	Diseases of mitotic cell cycle	4/159	36/10704	1,91E-03	2,67E-02
R-HSA-9687139	Aberrant regulation of mitotic cell cycle due to RB1 defects	4/159	36/10704	1,91E-03	2,67E-02
R-HSA-69239	Synthesis of DNA	7/159	120/10704	2,05E-03	2,81E-02
R-HSA-111471	Apoptotic factor-mediated response	3/159	18/10704	2,23E-03	3,00E-02
R-HSA-111465	Apoptotic cleavage of cellular proteins	4/159	38/10704	2,34E-03	3,00E-02
R-HSA-8950505	Gene and protein expression by JAK-STAT signaling after Interleukin-12 stimulation	4/159	38/10704	2,34E-03	3,00E-02
R-HSA-2132295	MHC class II antigen presentation	7/159	123/10704	2,35E-03	3,00E-02
R-HSA-69275	G2/M Transition	9/159	196/10704	2,58E-03	3,22E-02
R-HSA-2995383	Initiation of Nuclear Envelope (NE) Reformation	3/159	19/10704	2,62E-03	3,22E-02
R-HSA-453274	Mitotic G2-G2/M phases	9/159	198/10704	2,77E-03	3,34E-02
R-HSA-69242	S Phase	8/159	162/10704	2,85E-03	3,38E-02
R-HSA-2426168	Activation of gene expression by SREBF (SREBP)	4/159	42/10704	3,38E-03	3,95E-02
R-HSA-449147	Signaling by Interleukins	15/159	461/10704	3,55E-03	4,02E-02
R-HSA-983231	Factors involved in megakaryocyte development and platelet production	8/159	168/10704	3,56E-03	4,02E-02
R-HSA-4615885	SUMOylation of DNA replication proteins	4/159	45/10704	4,35E-03	4,84E-02
R-HSA-174184	Cdc20:Phospho-APC/C mediated degradation of Cyclin A	5/159	73/10704	4,53E-03	4,96E-02

### Downregulated genes T2 over T1. Reactome database.

ID	Description	GeneRatio	BgRatio	pvalue	p.adjust
R-HSA-3899300	SUMOylation of transcription cofactors	5/112	45/10704	0,00	0,04

### GSEA performed with DEG T2 over T1. KEGG database

ID	Description	setSize	Enrichment Score	NES	pvalue	p.adjust
hsa01100	Metabolic pathways	214	0,421	2,760	1E-10	3E-10
hsa05014	Amyotrophic lateral sclerosis	57	0,588	2,962	1E-10	3E-10
hsa05168	Herpes simplex virus 1 infection	86	-0,422	-2,300	9,46E-07	1,89E-06
hsa05010	Alzheimer disease	53	0,460	2,273	2,17E-05	3,25E-05
hsa05022	Pathways of neurodegeneration - multiple diseases	58	0,455	2,302	3,58E-05	4,29E-05

### Upregulated genes T2 over T1. KEGG modules database.

ID	Description	GeneRatio	BgRatio	pvalue	p.adjust
M00095	C5 isoprenoid biosynthesis, mevalonate pathway	3/16	10/830	0,00	0,01
M00053	Pyrimidine deoxyribonucleotide biosynthesis, CDP => dCTP	3/16	11/830	0,00	0,01
M00938	Pyrimidine deoxyribonucleotide biosynthesis, UDP => dTTP	3/16	14/830	0,00	0,01
M00049	Adenine ribonucleotide biosynthesis, IMP => ADP,ATP	3/16	22/830	0,01	0,02
M00052	Pyrimidine ribonucleotide biosynthesis, UMP => UDP/UTP,CDP/CTP	2/16	12/830	0,02	0,05

### Downregulated genes T2 over T1. KEGG modules database.

ID	Description	GeneRatio	BgRatio	pvalue	p.adjust
M00075	N-glycan biosynthesis, complex type	2/4	16/830	0,002	0,004

### Upregulated genes T3 over T1. Gene Ontology database: Biological Processes

ID	Description	GeneRatio	BgRatio	pvalue	p.adjust
GO:0050777	negative regulation of immune response	6/37	263/21081	5,98E-06	6,29E-03
GO:0002698	negative regulation of immune effector process	5/37	220/21081	3,93E-05	2,06E-02
GO:0042088	T-helper 1 type immune response	3/37	53/21081	1,10E-04	3,05E-02
GO:0071104	response to interleukin-9	2/37	10/21081	1,34E-04	3,05E-02
GO:0007159	leukocyte cell-cell adhesion	6/37	465/21081	1,45E-04	3,05E-02

### Downregulated genes T3 over T1. Gene Ontology database: Biological Processes

ID	Description	GeneRatio	BgRatio	pvalue	p.adjust
GO:0030098	lymphocyte differentiation	6/21	398/21081	1,86E-06	1,76E-03
GO:0045577	regulation of B cell differentiation	3/21	30/21081	3,40E-06	1,76E-03
GO:0042113	B cell activation	5/21	325/21081	1,40E-05	4,84E-03
GO:0050864	regulation of B cell activation	4/21	189/21081	3,32E-05	7,73E-03
GO:0030888	regulation of B cell proliferation	3/21	66/21081	3,74E-05	7,73E-03
GO:0001768	establishment of T cell polarity	2/21	13/21081	7,32E-05	9,83E-03
GO:0007015	actin filament organization	5/21	467/21081	7,92E-05	9,83E-03
GO:0001767	establishment of lymphocyte polarity	2/21	14/21081	8,54E-05	9,83E-03
GO:0042100	B cell proliferation	3/21	102/21081	1,37E-04	1,42E-02
GO:0110053	regulation of actin filament organization	4/21	299/21081	1,96E-04	1,54E-02
GO:0043491	protein kinase B signaling	4/21	301/21081	2,01E-04	1,54E-02
GO:0032944	regulation of mononuclear cell proliferation	4/21	309/21081	2,23E-04	1,54E-02
GO:0051491	positive regulation of filopodium assembly	2/21	30/21081	4,04E-04	2,13E-02
GO:0030010	establishment of cell polarity	3/21	148/21081	4,11E-04	2,13E-02
GO:0032943	mononuclear cell proliferation	4/21	375/21081	4,64E-04	2,19E-02
GO:1902903	regulation of supramolecular fiber organization	4/21	409/21081	6,43E-04	2,56E-02
GO:0032970	regulation of actin filament-based process	4/21	430/21081	7,76E-04	2,87E-02
GO:0030835	negative regulation of actin filament depolymerization	2/21	45/21081	9,12E-04	3,08E-02
GO:2000785	regulation of autophagosome assembly	2/21	46/21081	9,53E-04	3,08E-02
GO:0002285	lymphocyte activation involved in immune response	3/21	208/21081	1,10E-03	3,27E-02
GO:0060976	coronary vasculature development	2/21	51/21081	1,17E-03	3,27E-02
GO:0002204	somatic recombination of immunoglobulin genes involved in immune response	2/21	53/21081	1,26E-03	3,27E-02
GO:0002208	somatic diversification of immunoglobulins involved in immune response	2/21	53/21081	1,26E-03	3,27E-02

GO:0045190	isotype switching	2/21	53/21081	1,26E-03	3,27E-02
GO:0048568	embryonic organ development	4/21	495/21081	1,31E-03	3,28E-02
GO:0032735	positive regulation of interleukin-12 production	2/21	55/21081	1,36E-03	3,28E-02
GO:0044088	regulation of vacuole organization	2/21	56/21081	1,41E-03	3,30E-02
GO:0002377	immunoglobulin production	3/21	232/21081	1,51E-03	3,30E-02
GO:0008037	cell recognition	3/21	237/21081	1,61E-03	3,33E-02
GO:0032233	positive regulation of actin filament bundle assembly	2/21	66/21081	1,95E-03	3,74E-02
GO:0046847	filopodium assembly	2/21	66/21081	1,95E-03	3,74E-02
GO:0051495	positive regulation of cytoskeleton organization	3/21	258/21081	2,05E-03	3,74E-02
GO:0097529	myeloid leukocyte migration	3/21	261/21081	2,12E-03	3,74E-02
GO:0031529	ruffle organization	2/21	69/21081	2,13E-03	3,74E-02
GO:1901880	negative regulation of protein depolymerization	2/21	73/21081	2,38E-03	4,11E-02
GO:0050854	regulation of antigen receptor-mediated signaling pathway	2/21	78/21081	2,71E-03	4,46E-02
GO:0042531	positive regulation of tyrosine phosphorylation of STAT protein	2/21	81/21081	2,92E-03	4,65E-02
GO:0002637	regulation of immunoglobulin production	2/21	84/21081	3,14E-03	4,85E-02
GO:0001822	kidney development	3/21	302/21081	3,20E-03	4,87E-02

### Upregulated genes T3 over T1. Reactome database

ID	Description	GeneRatio	BgRatio	pvalue	p.adjust
-	-	-	-	-	-

### Downregulated genes T3 over T1. Reactome database

ID	Description	GeneRatio	BgRatio	pvalue	p.adjust
R-HSA-198933	Immunoregulatory interactions between a Lymphoid and a non-Lymphoid cell	3/11	132/10704	0,00	0,01

### GSEA performed with DEG T3 over T1. KEGG database

ID	Description	setSize	Enrichment Score	NES	pvalue	p.adjust
-	-	-	-	-	-	-

### Upregulated genes T3 over T1. KEGG modules database.

ID	Description	GeneRatio	BgRatio	pvalue	p.adjust
hsa04612	Antigen processing and presentation	4/26	78/8093	0,00	0,01
hsa05332	Graft-versus-host disease	3/26	42/8093	0,00	0,01
hsa04650	Natural killer cell mediated cytotoxicity	4/26	131/8093	0,00	0,02

### Downregulated genes T3 over T1. KEGG modules database.

ID	Description	GeneRatio	BgRatio	pvalue	p.adjust
-	-	-	-	-	-

### Upregulated genes T2 over T3. Gene Ontology database: Biological Processes.

ID	Description	GeneRatio	BgRatio	pvalue	p.adjust
GO:0140014	mitotic nuclear division	23/191	309/21081	9,01E-15	1,80E-11
GO:0007059	chromosome segregation	24/191	352/21081	1,60E-14	1,80E-11
GO:0006260	DNA replication	22/191	288/21081	2,09E-14	1,80E-11
GO:0000819	sister chromatid segregation	19/191	200/21081	2,66E-14	1,80E-11
GO:0000280	nuclear division	26/191	469/21081	1,54E-13	8,33E-11
GO:0098813	nuclear chromosome segregation	20/191	287/21081	1,88E-12	7,24E-10
GO:0071103	DNA conformation change	22/191	385/21081	7,21E-12	2,44E-09
GO:0051983	regulation of chromosome segregation	13/191	110/21081	2,26E-11	6,79E-09
GO:0000082	G1/S transition of mitotic cell cycle	19/191	306/21081	5,12E-11	1,38E-08
GO:0065004	protein-DNA complex assembly	18/191	278/21081	8,52E-11	2,09E-08
GO:0010965	regulation of mitotic sister chromatid separation	10/191	61/21081	1,78E-10	4,00E-08
GO:0044843	cell cycle G1/S phase transition	19/191	335/21081	2,39E-10	4,97E-08
GO:0010948	negative regulation of cell cycle process	21/191	427/21081	3,55E-10	6,00E-08
GO:0000727	double-strand break repair via break-induced replication	6/191	12/21081	4,52E-10	7,00E-08
GO:0071824	protein-DNA complex subunit organization	18/191	319/21081	7,91E-10	1,12E-07
GO:0000086	G2/M transition of mitotic cell cycle	16/191	298/21081	1,45E-08	1,31E-06
GO:0031145	anaphase-promoting complex-dependent catabolic process	10/191	102/21081	3,05E-08	2,49E-06
GO:1902850	microtubule cytoskeleton organization involved in mitosis	12/191	163/21081	3,19E-08	2,53E-06
GO:0044839	cell cycle G2/M phase transition	16/191	317/21081	3,44E-08	2,66E-06
GO:0051783	regulation of nuclear division	13/191	201/21081	3,94E-08	2,87E-06
GO:0010389	regulation of G2/M transition of mitotic cell cycle	14/191	243/21081	5,00E-08	3,53E-06
GO:0033044	regulation of chromosome organization	17/191	389/21081	1,02E-07	6,58E-06

GO:0006760	folic acid-containing compound metabolic process	6/191	30/21081	2,53E-07	1,46E-05
GO:0000083	regulation of transcription involved in G1/S transition of mitotic cell cycle	6/191	34/21081	5,57E-07	3,13E-05
GO:0042558	pteridine-containing compound metabolic process	6/191	36/21081	7,94E-07	4,26E-05
GO:0051290	protein heterotetramerization	5/191	20/21081	8,04E-07	4,26E-05
GO:0051383	kinetochore organization	5/191	23/21081	1,71E-06	7,95E-05
GO:1901293	nucleoside phosphate biosynthetic process	13/191	287/21081	2,31E-06	1,04E-04
GO:0006520	cellular amino acid metabolic process	14/191	393/21081	1,49E-05	5,02E-04
GO:0034109	homotypic cell-cell adhesion	7/191	95/21081	2,53E-05	7,77E-04
GO:0045091	regulation of single stranded viral RNA replication via double stranded DNA intermediate	4/191	20/21081	2,82E-05	8,57E-04
GO:0016579	protein deubiquitination	12/191	320/21081	3,74E-05	1,10E-03
GO:0070527	platelet aggregation	6/191	69/21081	3,82E-05	1,11E-03
GO:0039692	single stranded viral RNA replication via double stranded DNA intermediate	4/191	22/21081	4,20E-05	1,18E-03
GO:0006338	chromatin remodeling	10/191	229/21081	4,75E-05	1,31E-03
GO:0032543	mitochondrial translation	8/191	146/21081	5,69E-05	1,55E-03
GO:0043624	cellular protein complex disassembly	10/191	239/21081	6,80E-05	1,82E-03
GO:0009396	folic acid-containing compound biosynthetic process	3/191	10/21081	8,38E-05	2,18E-03
GO:0061351	neural precursor cell proliferation	8/191	157/21081	9,48E-05	2,44E-03
GO:2000045	regulation of G1/S transition of mitotic cell cycle	9/191	202/21081	9,78E-05	2,49E-03
GO:0031124	mRNA 3'-end processing	7/191	119/21081	1,07E-04	2,70E-03
GO:0006575	cellular modified amino acid metabolic process	9/191	207/21081	1,18E-04	2,89E-03
GO:0044282	small molecule catabolic process	14/191	483/21081	1,37E-04	3,31E-03
GO:0050000	chromosome localization	6/191	88/21081	1,50E-04	3,50E-03
GO:0051303	establishment of chromosome localization	6/191	88/21081	1,50E-04	3,50E-03
GO:0006336	DNA replication-independent nucleosome assembly	5/191	57/21081	1,66E-04	3,79E-03
GO:0034502	protein localization to chromosome	6/191	92/21081	1,91E-04	4,23E-03
GO:0006216	cytidine catabolic process	3/191	13/21081	1,96E-04	4,23E-03
GO:0007077	mitotic nuclear envelope disassembly	3/191	13/21081	1,96E-04	4,23E-03
GO:0009972	cytidine deamination	3/191	13/21081	1,96E-04	4,23E-03
GO:0016554	cytidine to uridine editing	3/191	13/21081	1,96E-04	4,23E-03
GO:0140053	mitochondrial gene expression	8/191	178/21081	2,25E-04	4,79E-03
GO:0009636	response to toxic substance	10/191	277/21081	2,27E-04	4,80E-03
GO:1902806	regulation of cell cycle G1/S phase transition	9/191	229/21081	2,51E-04	5,21E-03

GO:0006890	retrograde vesicle-mediated transport, Golgi to endoplasmic reticulum	6/191	98/21081	2,70E-04	5,52E-03
GO:0045023	G0 to G1 transition	5/191	67/21081	3,55E-04	6,66E-03
GO:1904874	positive regulation of telomerase RNA localization to Cajal body	3/191	16/21081	3,76E-04	6,87E-03
GO:0042769	DNA damage response, detection of DNA damage	4/191	38/21081	3,79E-04	6,87E-03
GO:0030397	membrane disassembly	3/191	17/21081	4,53E-04	7,90E-03
GO:0006730	one-carbon metabolic process	4/191	41/21081	5,09E-04	8,75E-03
GO:0046390	ribose phosphate biosynthetic process	8/191	209/21081	6,57E-04	1,09E-02
GO:0006403	RNA localization	9/191	263/21081	6,85E-04	1,11E-02
GO:2000573	positive regulation of DNA biosynthetic process	5/191	81/21081	8,50E-04	1,29E-02
GO:1901570	fatty acid derivative biosynthetic process	6/191	122/21081	8,66E-04	1,29E-02
GO:0006275	regulation of DNA replication	6/191	123/21081	9,04E-04	1,34E-02
GO:0001738	morphogenesis of a polarized epithelium	7/191	170/21081	9,32E-04	1,38E-02
GO:0090263	positive regulation of canonical Wnt signaling pathway	7/191	172/21081	9,98E-04	1,45E-02
GO:0035722	interleukin-12-mediated signaling pathway	4/191	49/21081	1,01E-03	1,45E-02
GO:0007163	establishment or maintenance of cell polarity	8/191	230/21081	1,22E-03	1,71E-02
GO:0042398	cellular modified amino acid biosynthetic process	4/191	52/21081	1,26E-03	1,73E-02
GO:0070671	response to interleukin-12	4/191	52/21081	1,26E-03	1,73E-02
GO:0031396	regulation of protein ubiquitination	8/191	233/21081	1,32E-03	1,80E-02
GO:0051653	spindle localization	4/191	53/21081	1,35E-03	1,81E-02
GO:1990748	cellular detoxification	6/191	134/21081	1,41E-03	1,87E-02
GO:0010528	regulation of transposition	3/191	26/21081	1,63E-03	2,10E-02
GO:0010529	negative regulation of transposition	3/191	26/21081	1,63E-03	2,10E-02
GO:0032069	regulation of nuclease activity	3/191	26/21081	1,63E-03	2,10E-02
GO:0032201	telomere maintenance via semi-conservative replication	3/191	28/21081	2,03E-03	2,54E-02
GO:0042493	response to drug	11/191	434/21081	2,09E-03	2,60E-02
GO:0043648	dicarboxylic acid metabolic process	5/191	101/21081	2,27E-03	2,80E-02
GO:0043457	regulation of cellular respiration	3/191	30/21081	2,48E-03	3,01E-02
GO:0045333	cellular respiration	7/191	203/21081	2,57E-03	3,08E-02
GO:0046148	pigment biosynthetic process	4/191	64/21081	2,72E-03	3,17E-02
GO:0002082	regulation of oxidative phosphorylation	3/191	31/21081	2,73E-03	3,17E-02
GO:0032196	transposition	3/191	31/21081	2,73E-03	3,17E-02
GO:0051642	centrosome localization	3/191	31/21081	2,73E-03	3,17E-02
GO:0000079	regulation of cyclin-dependent protein serine/threonine kinase activity	5/191	106/21081	2,81E-03	3,24E-02

GO:0034110	regulation of homotypic cell-cell adhesion	3/191	32/21081	2,99E-03	3,38E-02
GO:0061842	microtubule organizing center localization	3/191	32/21081	2,99E-03	3,38E-02
GO:0031099	regeneration	7/191	210/21081	3,10E-03	3,49E-02
GO:0046394	carboxylic acid biosynthetic process	10/191	395/21081	3,33E-03	3,67E-02
GO:0019882	antigen processing and presentation	10/191	397/21081	3,45E-03	3,75E-02
GO:1904851	positive regulation of establishment of protein localization to telomere	2/191	10/21081	3,50E-03	3,75E-02
GO:0006119	oxidative phosphorylation	6/191	165/21081	3,98E-03	4,17E-02
GO:0051321	meiotic cell cycle	8/191	279/21081	4,03E-03	4,20E-02
GO:1904869	regulation of protein localization to Cajal body	2/191	11/21081	4,26E-03	4,32E-02
GO:1904871	positive regulation of protein localization to Cajal body	2/191	11/21081	4,26E-03	4,32E-02
GO:0031440	regulation of mRNA 3'-end processing	3/191	37/21081	4,54E-03	4,54E-02
GO:0040001	establishment of mitotic spindle localization	3/191	37/21081	4,54E-03	4,54E-02
GO:0015931	nucleobase-containing compound transport	8/191	285/21081	4,57E-03	4,56E-02
GO:0097421	liver regeneration	3/191	38/21081	4,89E-03	4,82E-02
GO:0006348	chromatin silencing at telomere	2/191	12/21081	5,08E-03	4,83E-02
GO:0055015	ventricular cardiac muscle cell development	2/191	12/21081	5,08E-03	4,83E-02
GO:0090331	negative regulation of platelet aggregation	2/191	12/21081	5,08E-03	4,83E-02
GO:0098974	postsynaptic actin cytoskeleton organization	2/191	12/21081	5,08E-03	4,83E-02
GO:1903405	protein localization to nuclear body	2/191	12/21081	5,08E-03	4,83E-02
GO:1904867	protein localization to Cajal body	2/191	12/21081	5,08E-03	4,83E-02
GO:0038061	NIK/NF-kappaB signaling	7/191	231/21081	5,21E-03	4,91E-02

#### Downregulated genes T2 over T3. Gene Ontology database: Biological Processes.

ID	Description	GeneRatio	BgRatio	pvalue	p.adjust
-	-	-	-	-	-

#### Upregulated genes T2 over T3. Reactome database.

ID	Description	GeneRatio	BgRatio	pvalue	p.adjust
R-HSA-69620	Cell Cycle Checkpoints	29/159	294/10704	2,86E-16	1,92E-13
R-HSA-453279	Mitotic G1 phase and G1/S transition	20/159	149/10704	5,01E-14	1,68E-11
R-HSA-69206	G1/S Transition	18/159	131/10704	6,60E-13	1,48E-10



R-HSA-69306	DNA Replication	17/159	128/10704	5,25E-12	8,81E-10
R-HSA-69481	G2/M Checkpoints	18/159	168/10704	4,81E-11	6,45E-09
R-HSA-69239	Synthesis of DNA	15/159	120/10704	2,40E-10	2,48E-08
R-HSA-68882	Mitotic Anaphase	20/159	236/10704	2,75E-10	2,48E-08
R-HSA-2555396	Mitotic Metaphase and Anaphase	20/159	237/10704	2,96E-10	2,48E-08
R-HSA-69190	DNA strand elongation	9/159	32/10704	5,88E-10	4,38E-08
R-HSA-176187	Activation of ATR in response to replication stress	9/159	37/10704	2,45E-09	1,64E-07
R-HSA-2467813	Separation of Sister Chromatids	17/159	191/10704	3,10E-09	1,89E-07
R-HSA-69002	DNA Replication Pre-Initiation	12/159	85/10704	3,93E-09	2,20E-07
R-HSA-2500257	Resolution of Sister Chromatid Cohesion	14/159	126/10704	4,70E-09	2,30E-07
R-HSA-69205	G1/S-Specific Transcription	8/159	28/10704	4,80E-09	2,30E-07
R-HSA-176974	Unwinding of DNA	6/159	12/10704	8,39E-09	3,54E-07
R-HSA-68877	Mitotic Prometaphase	17/159	204/10704	8,45E-09	3,54E-07
R-HSA-69242	S Phase	15/159	162/10704	1,62E-08	6,38E-07
R-HSA-68886	M Phase	23/159	418/10704	5,13E-08	1,91E-06
R-HSA-68867	Assembly of the pre-replicative complex	10/159	68/10704	5,46E-08	1,93E-06
R-HSA-5663220	RHO GTPases Activate Formins	13/159	140/10704	1,48E-07	4,96E-06
R-HSA-176409	APC/C:Cdc20 mediated degradation of mitotic proteins	10/159	76/10704	1,62E-07	5,18E-06
R-HSA-176814	Activation of APC/C and APC/C:Cdc20 mediated degradation of mitotic proteins	10/159	77/10704	1,84E-07	5,61E-06
R-HSA-2514853	Condensation of Prometaphase Chromosomes	5/159	11/10704	2,92E-07	8,52E-06
R-HSA-68962	Activation of the pre-replicative complex	7/159	33/10704	4,32E-07	1,21E-05
R-HSA-174143	APC/C-mediated degradation of cell cycle proteins	10/159	88/10704	6,58E-07	1,70E-05
R-HSA-453276	Regulation of mitotic cell cycle	10/159	88/10704	6,58E-07	1,70E-05
R-HSA-69618	Mitotic Spindle Checkpoint	11/159	113/10704	8,67E-07	2,15E-05
R-HSA-69052	Switching of origins to a post-replicative state	10/159	91/10704	9,02E-07	2,16E-05
R-HSA-68949	Orc1 removal from chromatin	9/159	71/10704	9,52E-07	2,20E-05
R-HSA-9648025	EML4 and NUDC in mitotic spindle formation	11/159	117/10704	1,23E-06	2,75E-05
R-HSA-141424	Amplification of signal from the kinetochores	10/159	96/10704	1,48E-06	3,11E-05
R-HSA-141444	Amplification of signal from unattached kinetochores via a MAD2 inhibitory signal	10/159	96/10704	1,48E-06	3,11E-05
R-HSA-176408	Regulation of APC/C activators between G1/S and early anaphase	9/159	81/10704	2,94E-06	5,97E-05
R-HSA-174184	Cdc20:Phospho-APC/C mediated degradation of Cyclin A	8/159	73/10704	1,18E-05	2,32E-04

R-HSA-179419	APC:Cdc20 mediated degradation of cell cycle proteins prior to satisfaction of the cell cycle checkpoint	8/159	74/10704	1,30E-05	2,50E-04
R-HSA-8852276	The role of GTSE1 in G2/M progression after G2 checkpoint	8/159	77/10704	1,75E-05	3,27E-04
R-HSA-69275	G2/M Transition	12/159	196/10704	3,44E-05	6,24E-04
R-HSA-453274	Mitotic G2-G2/M phases	12/159	198/10704	3,80E-05	6,72E-04
R-HSA-194315	Signaling by Rho GTPases	19/159	455/10704	4,36E-05	7,50E-04
R-HSA-174154	APC/C:Cdc20 mediated degradation of Securin	7/159	68/10704	6,34E-05	1,06E-03
R-HSA-195258	RHO GTPase Effectors	15/159	327/10704	1,04E-04	1,70E-03
R-HSA-174178	APC/C:Cdh1 mediated degradation of Cdc20 and other APC/C:Cdh1 targeted proteins in late mitosis/early G1	7/159	74/10704	1,09E-04	1,75E-03
R-HSA-446353	Cell-extracellular matrix interactions	4/159	18/10704	1,22E-04	1,90E-03
R-HSA-8953750	Transcriptional Regulation by E2F6	5/159	35/10704	1,54E-04	2,35E-03
R-HSA-109581	Apoptosis	10/159	178/10704	3,16E-04	4,72E-03
R-HSA-390450	Folding of actin by CCT/TriC	3/159	10/10704	3,57E-04	5,21E-03
R-HSA-174048	APC/C:Cdc20 mediated degradation of Cyclin B	4/159	24/10704	3,95E-04	5,64E-03
R-HSA-5357801	Programmed Cell Death	10/159	190/10704	5,31E-04	7,42E-03
R-HSA-1538133	G0 and Early G1	4/159	27/10704	6,30E-04	8,63E-03
R-HSA-6811434	COPI-dependent Golgi-to-ER retrograde traffic	7/159	99/10704	6,63E-04	8,90E-03
R-HSA-69017	CDK-mediated phosphorylation and removal of Cdc6	6/159	73/10704	7,32E-04	9,63E-03
R-HSA-15869	Metabolism of nucleotides	7/159	101/10704	7,47E-04	9,65E-03
R-HSA-5689603	UCH proteinases	7/159	102/10704	7,93E-04	1,00E-02
R-HSA-8856688	Golgi-to-ER retrograde transport	8/159	133/10704	8,10E-04	1,01E-02
R-HSA-75035	Chk1/Chk2(Cds1) mediated inactivation of Cyclin B:Cdk1 complex	3/159	13/10704	8,25E-04	1,01E-02
R-HSA-499943	Interconversion of nucleotide di- and triphosphates	4/159	30/10704	9,51E-04	1,14E-02
R-HSA-162658	Golgi Cisternae Pericentriolar Stack Reorganization	3/159	14/10704	1,04E-03	1,22E-02
R-HSA-73886	Chromosome Maintenance	8/159	141/10704	1,19E-03	1,36E-02
R-HSA-180585	Vif-mediated degradation of APOBEC3G	5/159	54/10704	1,19E-03	1,36E-02
R-HSA-389958	Cooperation of Prefoldin and TriC/CCT in actin and tubulin folding	4/159	32/10704	1,22E-03	1,36E-02
R-HSA-174113	SCF-beta-TrCP mediated degradation of Emi1	5/159	55/10704	1,30E-03	1,43E-02
R-HSA-73894	DNA Repair	13/159	334/10704	1,41E-03	1,53E-02

R-HSA-156711	Polo-like kinase mediated events	3/159	16/10704	1,56E-03	1,66E-02
R-HSA-72187	mRNA 3'-end processing	5/159	58/10704	1,65E-03	1,73E-02
R-HSA-68827	CDT1 association with the CDC6:ORC:origin complex	5/159	59/10704	1,78E-03	1,78E-02
R-HSA-983189	Kinesins	5/159	59/10704	1,78E-03	1,78E-02
R-HSA-5368286	Mitochondrial translation initiation	6/159	87/10704	1,83E-03	1,78E-02
R-HSA-5389840	Mitochondrial translation elongation	6/159	87/10704	1,83E-03	1,78E-02
R-HSA-5419276	Mitochondrial translation termination	6/159	87/10704	1,83E-03	1,78E-02
R-HSA-196757	Metabolism of folate and pterines	3/159	17/10704	1,88E-03	1,80E-02
R-HSA-6804114	TP53 Regulates Transcription of Genes Involved in G2 Cell Cycle Arrest	3/159	18/10704	2,23E-03	2,11E-02
R-HSA-8950505	Gene and protein expression by JAK-STAT signaling after Interleukin-12 stimulation	4/159	38/10704	2,34E-03	2,18E-02
R-HSA-174084	Autodegradation of Cdh1 by Cdh1:APC/C	5/159	64/10704	2,56E-03	2,31E-02
R-HSA-5368287	Mitochondrial translation	6/159	93/10704	2,57E-03	2,31E-02
R-HSA-1362277	Transcription of E2F targets under negative control by DREAM complex	3/159	19/10704	2,62E-03	2,31E-02
R-HSA-2995383	Initiation of Nuclear Envelope (NE) Reformation	3/159	19/10704	2,62E-03	2,31E-02
R-HSA-176412	Phosphorylation of the APC/C	3/159	20/10704	3,05E-03	2,62E-02
R-HSA-69186	Lagging Strand Synthesis	3/159	20/10704	3,05E-03	2,62E-02
R-HSA-73856	RNA Polymerase II Transcription Termination	5/159	67/10704	3,13E-03	2,65E-02
R-HSA-141405	Inhibition of the proteolytic activity of APC/C required for the onset of anaphase by mitotic spindle checkpoint components	3/159	21/10704	3,51E-03	2,88E-02
R-HSA-141430	Inactivation of APC/C via direct inhibition of the APC/C complex	3/159	21/10704	3,51E-03	2,88E-02
R-HSA-5651801	PCNA-Dependent Long Patch Base Excision Repair	3/159	21/10704	3,51E-03	2,88E-02
R-HSA-983231	Factors involved in megakaryocyte development and platelet production	8/159	168/10704	3,56E-03	2,88E-02
R-HSA-72766	Translation	11/159	291/10704	4,07E-03	3,25E-02
R-HSA-1445148	Translocation of SLC2A4 (GLUT4) to the plasma membrane	5/159	72/10704	4,27E-03	3,37E-02
R-HSA-5688426	Deubiquitination	11/159	297/10704	4,74E-03	3,70E-02
R-HSA-9020591	Interleukin-12 signaling	4/159	47/10704	5,09E-03	3,93E-02
R-HSA-379716	Cytosolic tRNA aminoacylation	3/159	24/10704	5,18E-03	3,95E-02
R-HSA-73893	DNA Damage Bypass	4/159	48/10704	5,49E-03	4,14E-02

R-HSA-389960	Formation of tubulin folding intermediates by CCT/TriC	3/159	25/10704	5,82E-03	4,29E-02
R-HSA-69273	Cyclin A/B1/B2 associated events during G2/M transition	3/159	25/10704	5,82E-03	4,29E-02
R-HSA-1236978	Cross-presentation of soluble exogenous antigens (endosomes)	4/159	49/10704	5,91E-03	4,31E-02
R-HSA-211733	Regulation of activated PAK-2p34 by proteasome mediated degradation	4/159	50/10704	6,35E-03	4,58E-02
R-HSA-110373	Resolution of AP sites via the multiple-nucleotide patch replacement pathway	3/159	26/10704	6,51E-03	4,60E-02
R-HSA-179409	APC-Cdc20 mediated degradation of Nek2A	3/159	26/10704	6,51E-03	4,60E-02
R-HSA-5610787	Hedgehog 'off' state	6/159	113/10704	6,70E-03	4,66E-02
R-HSA-180786	Extension of Telomeres	4/159	51/10704	6,81E-03	4,66E-02
R-HSA-350562	Regulation of ornithine decarboxylase (ODC)	4/159	51/10704	6,81E-03	4,66E-02
R-HSA-180534	Vpu mediated degradation of CD4	4/159	52/10704	7,30E-03	4,66E-02
R-HSA-349425	Autodegradation of the E3 ubiquitin ligase COP1	4/159	52/10704	7,30E-03	4,66E-02
R-HSA-69601	Ubiquitin Mediated Degradation of Phosphorylated Cdc25A	4/159	52/10704	7,30E-03	4,66E-02
R-HSA-69610	p53-Independent DNA Damage Response	4/159	52/10704	7,30E-03	4,66E-02
R-HSA-69613	p53-Independent G1/S DNA damage checkpoint	4/159	52/10704	7,30E-03	4,66E-02
R-HSA-75153	Apoptotic execution phase	4/159	52/10704	7,30E-03	4,66E-02
R-HSA-75815	Ubiquitin-dependent degradation of Cyclin D	4/159	52/10704	7,30E-03	4,66E-02
R-HSA-169911	Regulation of Apoptosis	4/159	53/10704	7,80E-03	4,94E-02

#### Downregulated genes T2 over T3. Reactome database.

ID	Description	GeneRatio	BgRatio	pvalue	p.adjust
-	-	-	-	-	-

#### GSEA performed with DEG T2 over T3. KEGG database

ID	Description	setSize	enrichment Score	NES	pvalue	p.adjust
hsa01100	Metabolic pathways	200	0,3580994	2,30595917	4,39E-09	2,64E-08
hsa05014	Amyotrophic lateral sclerosis	60	0,40546119	2,05939169	1,54E-04	4,62E-04
hsa05168	Herpes simplex virus 1 infection	71	-0,35107762	-1,79716554	8,67E-04	1,73E-03

hsa05022	Pathways of neurodegeneration - multiple diseases	65	0,29100538	1,48433456	2,49E-02	3,73E-02
hsa05010	Alzheimer disease	56	0,30517997	1,51653407	3,11E-02	3,73E-02

#### Upregulated genes T2 over T3. KEGG modules database.

ID	Description	GeneRatio	BgRatio	pvalue	p.adjust
M00938	Pyrimidine deoxyribonucleotide biosynthesis, UDP => dTTP	4/23	14/830	0,00	0,01
M00053	Pyrimidine deoxyribonucleotide biosynthesis, CDP => dCTP	3/23	11/830	0,00	0,02

#### Downregulated genes T2 over T3. KEGG modules database.

ID	Description	GeneRatio	BgRatio	pvalue	p.adjust
M00075	N-glycan biosynthesis, complex type	2/9	16/830	0,012	0,046